THE ASTROPHYSICAL JOURNAL

AN INTERNATIONAL REVIEW OF SPECTROSCOPY AND ASTRONOMICAL PHYSICS

MARCH 1951

RADIAL VELOCITIES DETERMINED BY RADIO OBSERVATIONS 238

A PHOTOELECTRIC MAP OF THE SOLAR SPECTRUM FROM $\lambda\lambda$ 3300 TO 8800 268
J. E. Hall, E. M. Gaddum, J. A. [illegible]

ELEMENTS AND ORBITS OF AR LACERTAE 279

A PROVISIONAL CLASSIFICATION OF STARS LISTED IN [illegible] 304

A PRELIMINARY LIST OF HIGH-LUMINOSITY STARS 309

THE VISUAL-INFRARED SPECTROSCOPIC BINARY BD +5°2500 317

THE IDENTIFICATION OF D'AGELET'S NOVA SAGITTARII OF 1752 328

RED AND INFRARED MAGNITUDES FOR 125 STARS IN THE [illegible] 334
Arne F. [illegible]

THE RED-BLUE-MAGNITUDE ARRAY FOR STARS IN THE CLUSTER [illegible] 344

PHOTOELECTRIC STUDIES. V. MAGNITUDES AND COLORS OF VARIABLE STARS 362

STELLAR POPULATIONS AND COLLISIONS OF GALAXIES 413

SOURCE FUNCTIONS BY AN EXTENSION OF CHANDRASEKHAR'S [illegible] 419

The Evolution of O Stars at High Galactic Latitudes 432
Donald A. Macrae, Sidney [illegible]

The Spectrum of BD +5°4231 435

A Search for Neutrinos. Observed in the Infrared Spectrum of [illegible] 439

Observations of the Infrared Spectrum of [illegible] 457

[illegible] Observations of [illegible] 469

Observations, Theoretical Probabilities, and the Q Star Problem 480

THE UNIVERSITY OF CHICAGO PRESS
CHICAGO, ILLINOIS, U.S.A.

March 1951 Vol. 113, No. 2

THE ASTROPHYSICAL JOURNAL

AN INTERNATIONAL REVIEW OF SPECTROSCOPY AND ASTRONOMICAL PHYSICS

Edited by

W. W. MORGAN
Managing Editor
Yerkes Observatory of the University of Chicago

PAUL W. MERRILL
Mount Wilson Observatory of the Carnegie Institution of Washington

S. CHANDRASEKHAR

MARSHALL H. WRUBEL

N. U. MAYALL
Lick Observatory
University of California

With the Collaboration of the American Astronomical Society

Collaborating Editors

1949-51

W. BAADE
Mount Wilson Observatory

LEO GOLDBERG
Observatory of the University of Michigan

O. HERZBERG
National Research Council, Ottawa

LYMAN SPITZER, JR.
Princeton University Observatory

L. H. ALLER
Lick Observatory

ALBERT E. WHITFORD
Washburn Observatory

The Astrophysical Journal is published bimonthly by the University of Chicago at The University of Chicago Press, 5750 Ellis Avenue, Chicago 37, Illinois, during July, September, November, January, March, and May. ¶Two volumes are published per year, one beginning with the January issue and the other beginning with the July issue. The subscription price is $6.00 per volume (two volumes per year); the price of single copies is $3.00. (Orders for service of less than a volume will be charged at the single copy rate.) ¶Postage is prepaid by the publishers on all orders from the United States and its possessions. No extra charge is made for postage to countries in the Pan American Postal Union. Orders to all other countries are as follows: for Canada, 50 cents per volume, 40 cents per year (total $6.40 per volume, $6.40 per year); for single copies 5 cents (total $3.05); for all other countries in the Postal Union, postage per volume $0.50 per year (total $6.50 per volume, $6.40 per year); on single copies 10 cents (total $3.10). Subscriptions are payable in advance. Please make all remittances payable to The University of Chicago Press. In United States currency or its equivalent by postal or express money orders or bank drafts.

The following is an authorized agent:

For the British Empire, except North America and Australasia: The Cambridge University Press, Bentley House, 200 Euston Road, London, N.W. 1, England. Prices of yearly subscriptions and of single copies may be had on application.

Claims for missing numbers should be made within the month following the month of publication. The publishers expect to supply missing numbers free only when claim is made within the month, and when the reserve stock will permit.

Business correspondence should be addressed to The University of Chicago Press, Chicago 37, Illinois.

Communications for the editors and manuscripts should be addressed to Dr. W. W. Morgan, Editor of The Astrophysical Journal, Yerkes Observatory, Williams Bay, Wisconsin.

Line drawings and photographs should be made by the author, and all necessary explanations, wave lengths, etc., should be included in the cuts. It will not be possible [illegible] prepared as type.

One copy of the corrected galley proof should be returned as soon as possible to the Editor, Yerkes Observatory, Williams Bay, Wisconsin. Authors should take notice that [illegible] are sent to them with the proof.

The cable address is "Observatory, Williamsbay, Wisconsin."

The articles in this journal are indexed in the *International Index to Periodicals*, New York, N.Y.

Applications for permission to quote from this journal should be addressed to the University of Chicago Press, and will be freely granted.

Microfilms of complete journal volumes are available to regular subscribers only and may be obtained at the end of the year. Orders and inquiries should be addressed to University Microfilms, 313 North First Street, Ann Arbor, Michigan.

Notice to subscribers: If you change your address, please notify us [illegible] immediately. The Post-Office does not forward second-class mail.

Entered as second-class matter July 31, 1906, at the Post-Office at Chicago, Illinois, under the Act of March 3, 1879. Acceptance for mailing at special rate of postage provided for in United States Postal Laws, paragraph [illegible], amended February 28, 1925.

[PRINTED IN U.S.A.]

THE ASTROPHYSICAL JOURNAL

AN INTERNATIONAL REVIEW OF SPECTROSCOPY AND ASTRONOMICAL PHYSICS

VOLUME 113 MARCH 1951 NUMBER 2

METEOR VELOCITIES DETERMINED BY RADIO OBSERVATIONS*

D. W. R. McKinley

National Research Council, Ottawa, Canada

Received October 25, 1950

ABSTRACT

The phenomenological theory of radio echoes from meteors is reviewed and extended to show how meteor velocities may be computed from amplitude-time records of meteor echoes. Observational data are presented for 10,933 meteors, based on 847 hours of operation from December, 1948, to March, 1950. The average error of a velocity determination was about 5 per cent, and there was no instrumental limitation on the measurement of velocities up to 150 km/sec.

A statistical analysis of the observations during the Geminid shower yielded a corrected geocentric Geminid velocity of 34.2 km/sec. An empirical probability function, expressing the rates of radio meteors in terms of the zenith angle of the radiant, is deduced from the Geminid shower data. Using this function, it is shown that reasonable agreement is obtained between the observed distributions of velocities and the distributions predicted by assuming all or nearly all the meteors to be moving in elliptical orbits, more being direct than retrograde, with heliocentric velocities up to 42 km/sec. All the observed geocentric velocities were in the range 10–79 km/sec, and only 32 lay in the interval 75–79 km/sec. The existence of any appreciable number of interstellar meteors down to the eighth visual magnitude is doubtful.

INTRODUCTION

Two radio methods of measuring the velocity of meteors have been developed, using radio frequencies in the band 10–100 megacycles per second to detect the ionized gas column left by the meteor. One of these techniques may be termed the "range-time method," because the distance to the meteoric target is continuously recorded as a graph of echo range versus time. To accomplish this, the energy is usually emitted in short pulses from a radar-type transmitter, and the time of flight of the pulses is measured. The other technique may be called the "amplitude-time method," since it is the echo amplitude, rather than echo range, that is recorded against time. For this purpose the radio-frequency energy may be emitted either in pulses or continuously.

Hey and Stewart[1] first used the radar range-time method during the Giacobinid shower of 1946. If the meteor is assumed to describe a straight-line path in space with constant velocity, the meteor echo will appear on the radar range-time record as a segment of a hyperbola. Usually only a very small part of the hyperbola near the point of minimum range is observed, but for some of the brighter meteors an appreciable length

* Presented in preliminary form at the Meteor Symposium, 81st Meeting of A.A.S., Ottawa, June, 1949 (*A.J.*, **54**, 179, 1949).

[1] *Proc. Phys. Soc. London*, **59**, 858, 1947.

of the path may be recorded, and the velocity may be computed by fitting an appropriate curve to the echo photograph. Not many meteor echoes are satisfactory for this purpose; though, when such records are obtained at three stations, not only can the velocity be measured, but the position of the path and the meteor orbit may be determined.[2]

The amplitude-time method has been employed by Davies and Ellyett,[3] using a pulse transmitter, and by Manning, Villard, and Peterson,[4] using a continuous-wave transmitter. The amplitude-time plot of a meteor echo is very similar to the optical diffraction fringes obtained at a straight-edge; and, if the output of the detector is applied to a loudspeaker, a characteristic "Doppler whistle" of varying pitch will be heard. The echo amplitude at a given instant is the summed effect of the echo from all parts of the meteor trail formed up to that instant. The pulse method samples the echo amplitude at short intervals of time (assuming the pulse length in kilometers to be greater than the total change in range observed, which is usually the case), while the continuous-wave (C.W.) record is smooth. The pulse and the C.W. records are similar, provided that the C.W. detecting receiver is completely shielded from the direct ground wave emitted by the C.W. transmitter. It is found, though, that, by judicious injection of the ground wave, one can increase both the accuracy of the velocity measurement and the number of measurable echoes. The actual computation of the velocity demands a knowledge of the minimum range of the meteor path; this information is intrinsic in the pulse method, but in the C.W. method it is usually derived from an auxiliary radar system.

The amplitude-time methods apply only over a short time interval near the instant at which the meteor is at the minimum distance from the observer. As the average faint meteor produces an echo near this point only, the amplitude-time method can be applied to many more echoes than can the range-time method, by a factor of about 1000. On the other hand, the range-time technique is capable of yielding the deceleration of the meteor in some cases, because of the long path length recorded.[5] We have made extensive use of both techniques, but all the observational material presented in this paper was obtained with the C.W. amplitude-time method.

PHENOMENOLOGICAL THEORY OF METEOR ECHOES

It should be emphasized that the physics of the problem is the same for all the observational techniques—radar range-time, pulse or C.W. amplitude-time, or audible Doppler whistles. One is treating the scattering, or reflection, of an electromagnetic wave from a dense column of ions and electrons formed by collision processes between the meteoric particle and the air molecules, although the information may appear in radically different forms as the result of stressing particular features of the data. There is no difference in the basic phenomena, regardless of the method of observation, but lack of appreciation of this point has led to some confusion in the literature. In an earlier paper McKinley and Millman[6] proposed a phenomenological theory of radar echoes from meteors based on an analysis of radar range-time records having a range resolution of the order of a kilometer. The introduction of the amplitude-time methods, with effective range resolution of the order of a meter, has permitted an extension of the theory in some details, leaving the basic hypotheses unaltered. As in the previous paper, attention will be confined to the phenomenological aspects of the meteor reflection processes, without investigating the microscopic theory of electron production and radio-wave scattering processes.

[2] D. W. R. McKinley and Peter M. Millman, *Canadian J. Res.*, **A27**, 53, 1949.

[3] *Phil. Mag.*, ser. 7, **40**, 614, 1949.

[4] *J. App. Phys.*, **20**, 475, 1949.

[5] D. W. R. McKinley, *J. App. Phys.*, **22**, 201, 1951.

[6] *Proc. I.R.E.*, **37**, 364, 1949.

Let us consider a meteor moving with velocity v along a straight-line path in space which may be described in a range-time co-ordinate system by the hyperbola,

$$R^2 = R_0^2 + s^2 = R_0^2 + v^2 (t - t_0)^2 , \tag{1}$$

where R is the range at time t, R_0 is the minimum range at time t_0, and s is the distance along the path measured from t_0. The assumption of constant velocity is valid for the short path length recorded for the vast majority of echoes. We have, furthermore, assumed in equation (1) that the transmitter and receiver are located at the same place. This is not a problem in the pulse methods, but the C.W. method requires some isolation between transmitter and receiver to attenuate the strong ground wave from the transmitter, for which a small correction will be made later. Let the radio wave length be λ, with angular velocity ω. For a given transmitter power and antenna gain, the phase and amplitude of the received electromagnetic wave scattered from a linear element, ds, of the line source of electrons created in the wake of the meteor is

$$dA = g(R, \alpha) \sin\left(\omega t - \frac{4\pi R}{\lambda}\right) ds . \tag{2}$$

The function $g(R, \alpha)$, where α is the linear density of the electrons, has been evaluated by Lovell[7] by adopting the classical scattering cross-section for free electrons. During the average observation, R varies but a fraction of 1 per cent, and α will be assumed constant. The records show that in the majority of cases α must be fairly constant, though there are a few cases in which α might be varying rapidly or discontinuously. In general, we shall treat $g(R, \alpha)$ as constant for a given meteor and integrate equation (2) over a finite segment of path, from the point s_1 at the instant the echo is first detected, to obtain the resultant instantaneous amplitude when the meteor is at the point s:

$$A_r = g(R, \alpha) \int_{s_1}^{s} \sin\left(\omega t - \frac{4\pi R}{\lambda}\right) ds . \tag{3}$$

This integral is difficult to evaluate in general, but near the t_0 point the approximation $R \doteq R_0 + s^2/2R_0$ may be used and can be shown to be valid over the average observed meteor path even if we adopt the criterion that the difference between the true and approximate ranges shall not exceed $\lambda/8$. Putting $\phi = \omega t - 4\pi R_0/\lambda$ and $\pi x^2/2 = 2\pi s^2/R_0\lambda$, we have

$$A_r = F_r \int_{x_1}^{x} \sin\left(\phi - \frac{\pi x^2}{2}\right) dx , \tag{4}$$

where F_r is a constant for a given meteor, having the dimensions of field strength.

Expanding equation (4), we have

$$A_r = F_r (C \sin\phi - S \cos\phi) , \tag{5}$$

where

$$C = \int_{x_1}^{x} \cos\frac{\pi x^2}{2}\, dx \quad \text{and} \quad S = \int_{x_1}^{x} \sin\frac{\pi x^2}{2}\, dx$$

are the conventional Fresnel integrals of optical diffraction theory. In our work $\omega \doteq 2 \times 10^8$ radians per second, whereas the functions C and S fluctuate at much lower frequencies, with an upper limit of approximately 10^4 c.p.s. Hence we are justified in treating C and S as slowly varying amplitude factors of the sinusoidal high-frequency wave. It may be shown from tables of C and S and by using typical numerical values of

[7] A. C. B. Lovell and J. A. Clegg, *Proc. Phys. Soc. London*, **60**, 491, 1948.

the parameters that the contribution from the lower limit, x_1, is usually negligible where the average observed path length is 10–15 km in the vicinity of t_0. Hence the lower limit may be considered to be effectively at minus infinity.

The intensity of the reflected wave follows from equation (5),

$$I_r = F_r^2 (C^2 + S^2) . \tag{6}$$

This expression is identical with the optical diffraction pattern produced at a straight-edge. It represents a steadily increasing intensity up to the t_0 point (corresponding to the region inside the geometrical shadow in optics), after which the intensity oscillates about a final mean value, the oscillations decreasing in intensity and increasing in frequency as

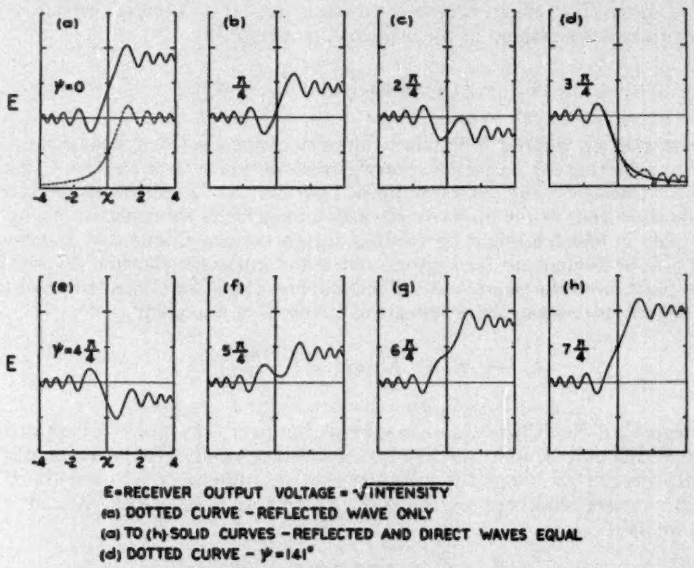

FIG. 1.—Theoretical amplitude-time, or "Doppler whistle," records. $2F_r^2 = F_d^2$

the meteor crosses the Fresnel zones in moving away from t_0 (corresponding to the diffraction fringes in the region outside the optical geometrical shadow) (see Fig. 1, *a*, *dotted curve*). Lovell and Clegg[7] first elucidated this diffraction theory of meteor echoes, based on a suggestion by Herlofson; and Davies and Ellyett[3] applied it to observations made with their pulsed amplitude-time method. If the ground wave is completely suppressed in the C.W. case, the expression indicates that the majority of the "Doppler whistles" should be of ascending pitch. The time resolution of conventional radar records is usually inadequate to show the fine structure of the oscillations, but the mean echo intensity will follow the sharp rise after t_0, indicated by the dotted curve in Figure 1, *a*. The echo from the ionized cloud will eventually fade away, of course, owing to diffusion and recombination, and will often show strong fluctuations which may be attributed to several causes. However, an examination of the phenomena occurring after the passage of the meteor has little or no bearing on the velocity measurement and will not be discussed here in detail.

Suppose that the detector receives a small fraction of the transmitted power directly. Let the amplitude of the direct ground wave be

$$A_d = F_d \sin\left(\omega t - \frac{2\pi D}{\lambda}\right), \tag{7}$$

where D is the distance between the transmitter and the receiver. By adding A_r and A_d and proceeding as above, we obtain the combined intensity of the direct and reflected waves:[8]

$$I_{r+d} = F_r^2 (C^2 + S^2) + F_d^2 + 2F_r F_d (C \cos\psi - S \sin\psi) \tag{8a}$$

$$= (F_r C + F_d \cos\psi)^2 + (F_r S - F_d \sin\psi)^2, \tag{8b}$$

where $\psi = 2\pi(2R_0 - D)/\lambda$ is the phase difference between the direct and the reflected paths at time t_0.

The voltage output, E, of a square-law detector will reproduce the intensities of equations (6) and (8a) and (8b) directly, while a linear detector, such as has been used in our

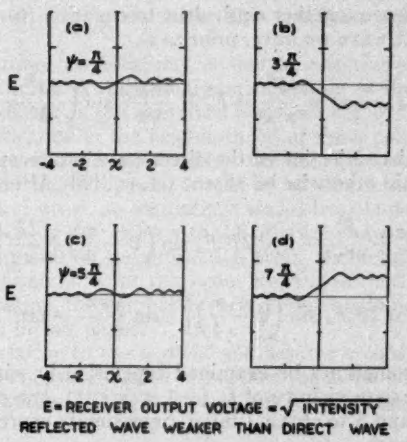

FIG. 2.—Theoretical amplitude-time records. $2F_r^2 < F_d^2$

work, will follow the square root of the intensity. A suitably adjusted balanced detector, with properly phased local injection of the direct ground wave, would eliminate the first two terms of equation (8a) and yield only the third, which would simplify some of the analysis. Tables of Fresnel integrals may be used to calculate the theoretical wave forms, using selected values of the angle ψ and selected ratios of the intensity of the direct wave, F_d^2, relative to $2F_r^2$, which is the effective ultimate intensity of the meteor echo. The solid curves of Figure 1, a–h, are plotted as output voltage against x, for selected phase angles from 0 to $7\pi/4$ and for equal intensities. Figure 2 shows a similar set of curves when the meteor echo intensity is less than that of the direct wave. All of them show a "Doppler whistle" of increasing amplitude and decreasing pitch, prior to t_0.

[8] The extension of the diffraction theory to include the case of the direct ground wave is due to E. L. R. Webb, National Research Council, Ottawa.

One can use Cauchy's approximations for the Fresnel integrals, excluding a region about the t_0 point, $(-1 > x > 1)$, to show the wave forms analytically in terms of ordinary trigonometrical functions. On the approach side of t_0, $(-s)$, these approximations are, assuming x_1 to be effectively at minus infinity,

$$C = \frac{1}{\pi x} \sin \frac{\pi x^2}{2}, \qquad S = -\frac{1}{\pi x} \cos \frac{\pi x^2}{2}.$$

On the receding side of t_0, $(+s)$, they become

$$C = 1 + \frac{1}{\pi x} \sin \frac{\pi x^2}{2}, \qquad S = 1 - \frac{1}{\pi x} \cos \frac{\pi x^2}{2}.$$

We then have

$$I_r(-s) = \frac{F_r^2}{\pi^2 x^2}, \tag{9}$$

$$I_r(+s) = 2F_r^2 + \frac{F_r^2}{\pi^2 x^2} + \frac{2\sqrt{2}}{\pi x} F_r^2 \sin\left(\frac{\pi x^2}{2} - \frac{\pi}{4}\right). \tag{10}$$

Equations (9) and (10) are together equivalent to equation (6). For the case of the reflected wave plus direct wave we have, prior to t_0,

$$I_{r+d}(-s) = \frac{F_r^2}{\pi^2 x^2} + F_d^2 + \frac{2F_rF_d}{\pi x} \sin\left(\frac{\pi x^2}{2} + \psi\right). \tag{11}$$

Equation (11) shows that injection of the direct wave produces a "whistle" on the approach side which would otherwise be absent (cf. eq. [9]). After t_0 we have

$$I_{r+d}(+s) = F_d^2 + 2F_r^2 + \frac{F_r^2}{\pi^2 x^2} - 2\sqrt{2F_rF_d} \sin\left(\psi - \frac{\pi}{4}\right) + \frac{2F_r}{\pi x}\left[F_d^2 + 2F_r^2 - 2\sqrt{2F_rF_d} \sin\left(\psi - \frac{\pi}{4}\right)\right]^{1/2} \sin\left\{\frac{\pi x^2}{2} - \tan^{-1}\left(\frac{F_r - F_d \sin\psi}{F_r + F_d \cos\psi}\right)\right\}. \tag{12}$$

Particular cases can sometimes be examined expeditiously with the aid of equations (9)–(12). In the immediate vicinity of t_0, $(-1 < x < 1)$, one can use Knochenhauer's approximations for C and S to obtain similar approximate expressions, though these are of little value in this work.

It has frequently been reported that the majority of audible meteor whistles appear to be of the approaching or descending-pitch type. The theoretical curves of Figure 1 do not suggest much difference in the amplitude of the whistle before and after t_0, with the single exception of the special case, $\psi = 3\pi/4$ (Fig. 1, *d*). This has no receding whistle (in fact, it is precisely the reverse of the curve that would be obtained if no ground wave were present, Fig. 1, *a*, *dotted line*), but small variations in the relative amplitudes or in the phase angle (cf. Fig. 1, *d*, *dotted line*, for $\psi = 141°$) will cause the receding whistle to reappear in strength. A far more practical explanation of the predominance of approach whistles follows as a consequence of the distribution of observed meteor paths. The angle of elongation from the radiant of a meteor path can vary from 0°, corresponding to a meteor moving directly toward the observer, to a maximum of about 165°, corresponding to the rare case of a meteor moving along a horizontal path away from the observer at the maximum recorded radar range of 260 km. It may be shown from a theoretical statistical analysis that the most probable angle of elongation of the center of an observed meteor path should be less than 90°; this has been confirmed for radar meteors.[6]

Not only will there be more meteors approaching than receding, but the approaching meteors will be somewhat closer to the observer, on the average, and hence will return stronger echoes. All the meteors considered in this paper reached the t_0 or 90° point, but an extension of the above discussion suggests that, in general, the observed path length prior to t_0 was greater than that after t_0.

Two other factors may contribute to the attenuation or loss of the receding whistle. First, the receiver may saturate on some of the strong echoes and thus limit the amplitude of the whistle oscillations after t_0 (see, for example, the upper left record of Fig. 3). Second, most of the meteor echoes show a low-frequency oscillation of large and frequently irregular amplitude, termed "body Doppler," immediately after the t_0 point, which may be due to radial expansion of the trail, to wind drift of the ionized column as a whole, or to movement of one part of the column relative to another. This low-frequency flutter, which is not connected with the velocity of the meteor, can obscure the high-frequency whistle very effectively when listening is done aurally. Some of the records of Figure 3 show this effect.

If the final intensity from the meteor is considerably less than that of the ground wave, the upward or downward shift in output level after the t_0 point is not so pronounced (see Fig. 2). On the other hand, if the ground wave is weak and the meteor echo is strong, a faint whistle should be heard on the approach side and a strong one on the receding side, provided that the receiver does not saturate. This condition approaches the I_r case, of course.

The theoretical conditions are idealized, in that an effectively infinite, though practically finite, path is assumed. A surprisingly large number of the meteor echoes agrees well with the curves predicted on this simplified basis (see Fig. 3). The experimental data show clearly that the reflection in the neighborhood of the t_0 point is the summed echo from a considerable length of the ionized trail rather than an echo from a "moving-ball" type of target. The "moving-ball" echo would be an interference effect, and, in the absence of a direct ground wave, no oscillations would be detected at all, which is contrary to general experience. In rare cases with the brighter meteors we do get a "moving-ball" type of echo superposed on the diffraction echo. A different physical mechanism appears to be required to account for this echo, and the subject has been treated elsewhere.[5] Statistically speaking, the number of such echoes is completely insignificant, and they will be disregarded in this paper.

If we let τ be time relative to the t_0 point and assume a constant velocity over the short duration of the whistle record, i.e., $s = v\tau$, then the instantaneous frequency of the oscillatory terms of equations (10), (11), and (12) is found to be

$$f = \frac{2v^2}{R_0\lambda}\tau . \tag{13}$$

The slope of a graph of f against τ is proportional to the square of the velocity. Manning[9] deduced the same expression, though his echoing mechanism more closely resembled the "moving-ball" assumption than the line-source diffraction hypothesis. Manning's theory does not explain the antisymmetrical characteristics of the amplitude-time plot as it passes through t_0, nor does it predict the observed amplitude variation of the oscillation envelope. The linear relationship between f and τ holds to a fraction of 1 per cent if one excludes the dozen or so oscillations near t_0. For some selected specimens several hundred oscillations prior to t_0 are resolvable on the records, and the technique of plotting f against τ yields the velocity with an error of about 1 per cent. Most of the small meteors produce only a few oscillations near t_0, however, and this method can lead to rather large errors if applied near t_0. Fortunately, the t_0 point can usually be located on the meteor record; and, with this as starting point, one can count the oscillations extending in either

[9] *J. App. Phys.*, 19, 689, 1948.

direction. If the measured time interval between the mth and the nth cycles is Δt, the meteor velocity can be deduced from equation (10), (11), or (12) to be

$$v = \sqrt{R_0 \lambda}\left(\frac{\sqrt{n} - \sqrt{m}}{\Delta t}\right). \tag{14}$$

The precise instant of t_0 is not required, merely the general vicinity, so that integral numbers of oscillations can be counted. The fourth and ninth oscillations were used in the bulk of the reduction work, and the probable error of an individual measurement by this method was of the order of 5 per cent, including contributions from all sources.

It should be noted that at points on the path remote from t_0 the instantaneous frequency approaches asymptotically to the value $2v/\lambda$, corresponding to the case of a meteor coming directly toward the observer. Only in very rare cases does the observed Doppler whistle extend beyond the linear part of the f, τ plot; and in any case the instantaneous frequency at the remote points would be higher than the resolution limit of the present experimental gear.

A more detailed theoretical analysis, in which the contribution of the lower limit, x_1, of the Fresnel integrals is not neglected, leads to sets of predicted whistle-curves which are analogous to the optical diffraction fringes due to a rectangular slit, the slit-width being variable with time. A comparison with the experimental records indicates that some of the meteor whistles are probably due to trails which begin or end fairly abruptly near the t_0 point. In other cases, and especially if the echo is weak, there is a suggestion that the ionization may be diffusing and recombining so rapidly that the lower limit, x_1, is not effectively fixed but is moving in the direction of the meteor. If the process is sufficiently rapid, the radio target might then be regarded as a short-line segment moving across the line of sight, yielding a combination of the diffraction and "moving-ball" echo types. These anomalous echoes require further investigation, but their number is insignificant for the purposes of the present discussion.

APPARATUS

The continuous-wave Doppler transmitter located at Ottawa has a C.W. output of about 1.5 kw on 30.02 mc/sec, feeding a half-wave dipole mounted a quarter-wave above ground. A similar dipole is used at the receiver, the axes of the two antennae being nearly collinear, to reduce the direct ground wave. The receiving site is located at South Gloucester, 7.5 km from the transmitter. Two types of recording have been used. In the first, or "slow Doppler" method, which has been employed for practically all the meteors reported in this paper, the output of the receiver is applied to a cathode-ray tube as vertical amplitude modulation of a horizontally moving trace and is photographed by a camera which moves the film in a vertical plane continuously past the lens at 4 inches per minute. This film speed is the same as that of the radar film, thus facilitating correlation of the two records. In the second, or "fast Doppler" method, the amplitude modulation is applied horizontally to a stationary spot on the cathode-ray tube, and the film is drawn past the lens at 4 inches per second.

Figure 4 illustrates two meteor echoes, *a* and *b*, that have been recorded on the radar range-time record (*top*), on the "slow Doppler" record (*center*), and on the "fast Doppler" record (*bottom*). The radar record is the conventional type, in which the echo signal appears as intensity modulation of a cathode-ray tube sweep, the time dimension being produced by drawing the film past the open camera lens at 4 inches per minute. In the center photos of Figure 4 the cathode-ray spot moves from the bottom to the top in $\frac{1}{4}$ second, flashes back in about a millisecond, and repeats while the record moves slowly to the right. The same seconds pulses appear on the Doppler record as on the radar photo (transmitted to the Doppler receiving site via separate radio link), but, while the time

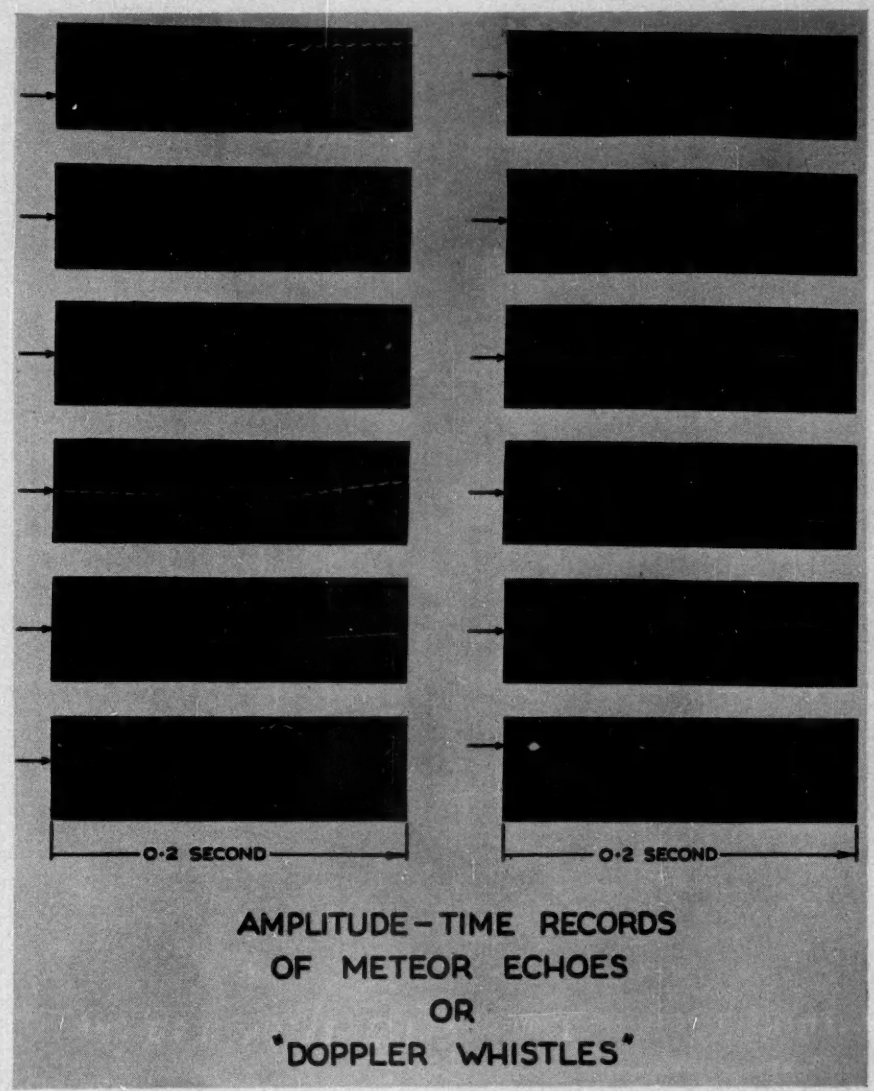

FIG. 3.—Some examples of observed amplitude-time meteor echo records taken with the "fast Doppler" system.

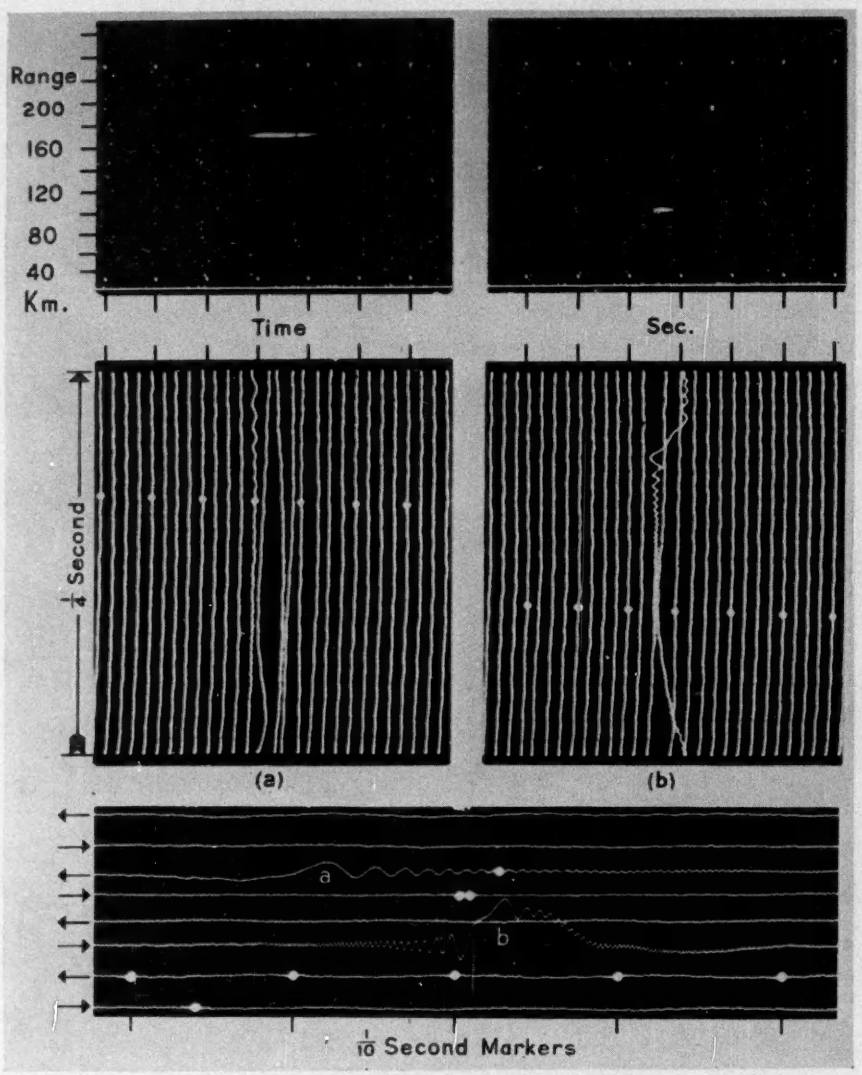

FIG. 4.—Two meteor echoes. Velocities: *a*, 28 km/sec; *b*, 47 km/sec. *Top*, radar range-time record; *center*, C.W. amplitude-time record, "slow Doppler" method; *bottom*, C.W. amplitude-time record, "fast Doppler" method.

resolution on the radar record is of the order of 0.02 second, that of the "slow Doppler" trace is 0.001 second. Instantaneous frequencies up to 800 cycles per second can be measured. The "slow Doppler" trace is calibrated at intervals by applying standard 100 c.p.s. calibration pips because the trace is not strictly linear and a detailed calibration of the sweep speed must be made before reducing the meteor whistle. The "fast Doppler" film is passed back and forth eight times to conserve film. The direction of film is indicated by the small arrows (Fig. 4, *bottom*). Every hour the time transmitter emits pips every 0.1 second for a few seconds, which happen to appear on the second line from the bottom of the "fast Doppler" record. The frequency resolution of the "fast Doppler" trace is of the order of 1500 c.p.s.

Referring to the linear relation between f and τ in equation (13), it follows that at any instant the total number of oscillations, counting from t_0, is given by $f\tau/2$. The limit of resolution for the "slow Doppler" is about 800 c.p.s., and, assuming $R_0 = 100$ km (the mean R_0 is actually about 130 km), it follows that the numbers of clearly resolvable oscillations for meteor velocities of 50, 100, and 150 km/sec are 64, 16, and 7, respectively. The numbers of oscillations resolvable by the "fast Doppler" method for the same velocities are 225, 55, and 25, respectively. The number of resolvable oscillations is directly proportional to the echo range, e.g., all the preceding values will be doubled if $R_0 = 200$ km. For reasons of film economy the "fast Doppler" system was operated only on special occasions, but the above figures indicate that even the "slow Doppler" record should yield good results for meteors at least as fast as 100 km/sec, using the simplified fourth- and ninth-cycle reduction method. Three or four oscillations near t_0 would suffice for a good velocity determination (cf. Davies and Ellyett[3]) if care were taken in the reduction. Thus there is no instrumental limitation on the measurement of velocities up to about 150 km/sec with the "slow Doppler," or up to 200 km/sec or more with the "fast Doppler." If the trend of observed velocities had warranted it, e.g., if a number of velocities had been found in the range 85–120 km/sec, the recording could easily have been improved to extend the range of resolution; alternatively, our present records could have been re-examined by more tedious reduction methods designed to yield velocities from the three or four oscillations next t_0. The resolution of the equipment used by Davies and Ellyett was somewhat lower than that of our "slow Doppler," since their pulse transmitter "sampled" the echo intensity about 800–900 times per second. Because at least three pulse-amplitude samples would be needed to outline a given instantaneous oscillation cycle, i.e., Fresnel zone, their effective maximum resolution frequency would be about 300 c.p.s. The mechanical recording technique used by Manning, Villard, and Peterson was limited to 120 c.p.s., but they also made use of magnetic tape recorders for frequencies up to 1500 c.p.s.

It should be mentioned that we use the Ottawa radar value of R_0 for the Doppler velocity computations, whereas the value that should actually be used is half the distance from the Doppler transmitter to the meteor and back to the Doppler receiver. The radar and Doppler transmitters and the radar receiver are located at the Ottawa site, but the Doppler receiver is 7.5 km southeast of Ottawa. Hence there will be a slight correction to be applied to the radar R_0, its sign and magnitude depending on the position of the meteor in the sky. In the worst cases this correction will have an effect of ± 1 per cent in the measured velocity. If the meteor position is known, the correction can easily be applied; otherwise the probable error of the velocity measurement must include the error due to the uncertainty in R_0. Where the meteor radiant is known, though not the positions of individual meteors, a statistical correction factor can be determined. If the radar receiver had been at South Gloucester, the radar and Doppler ranges would have coincided exactly, but this was not a practical procedure because the true Ottawa ranges are used in other phases of the meteor program.

OBSERVATIONS

Measurement of meteor velocities by the C.W. amplitude-time technique first commenced at Ottawa in September, 1948, using magnetic tape recorders. In December, 1948, the two photographic recording systems outlined in the preceding section were put into operation. For the next fifteen months an attempt was made to operate the equipment for at least one 48-hour period each month, in order to accumulate observational data on meteor velocities over a calendar year. Several of the well-established visual meteor showers were included in the program, and on these and some other occasions direct meteor cameras and spectrographs were in use, and a crew of visual meteor observers was on duty.[19] For technical reasons, some of the months are not so well represented as others, and the presence of summer assistants is reflected in the increased number of observations made in July and August, 1949.

Suitable presentation of the observational data has been a perplexing problem. Several hundred pages would be required to tabulate the fundamental data, which comprise, for each meteor, the date, hour, minute, and second of occurrence; the radar R_0 to the nearest km; the time interval Δt for the adopted cycle-counting technique; the velocity computed to the nearest km/sec; and any pertinent remarks. Some simplification of the information was obviously desirable. In view of the 5 per cent probable error of the average individual measurement, the velocity data have been arbitrarily grouped in steps of 5 km/sec, and only the velocity distributions per hour are given. Where an operating period extended to 48 or 72 hours, the data are added for the same hour on each of the days. Tables outlining this information from December, 1948, to March, 1950, are given in the appendix.

Only a small fraction of the total number of meteor echoes appearing on the records has been reduced. Since the numbers of echoes detected by either the radar or the C.W. system are roughly inversely proportional to their intensities, it follows that a large percentage of the echoes recorded on the Doppler films will make their presence known chiefly by the amplitude shift near the t_0 point, the whistle oscillations being too weak to show above the receiver noise level. On the other hand, there are also some strong meteor echoes that show little or no sign of whistle oscillations, although they do display the "body Doppler" effect. When these echoes can be correlated with visual observations or with three-station triangulation data, it often appears that the ionization was detected at a point on the path remote from t_0. Such echoes correspond to the brighter meteors, and their number is insignificant for statistical purposes. About 1 in 10 of the Doppler echoes shows an appreciable number of whistle oscillations suitable for reduction purposes. Of this number, about 3 out of 4, or the "cream of the crop," were actually reduced, the remainder either having fewer than the nine cycles used in the velocity formula or suffering other defects. Thus a rate of 20 meteors per hour in the tables in the appendix would correspond to an over-all rate of 200–250 detectable echoes, of which perhaps 5 or 6 more could be analyzed at the expense of a considerable increase in time and effort and with larger probable errors.

It would be well to emphasize that the hourly rates from a specific operating period can be compared with those of another period only qualitatively, as the performance of the equipment varied considerably throughout the year. Hourly rates within a given operating period are more likely to be consistent, although, again, care must be used in comparing diurnal rates, first, because the tables in the appendix give no indication of the time lost because of breakdowns or other causes and, second, because more radio interference was encountered in the daylight hours, with the result that fewer of the echoes were measurable. All this information is available in the records but is too voluminous to reproduce. The important point to note is that the velocity distributions are

[19] Peter M. Millman and D. W. R. McKinley, *Sky and Telescope*, 8, 114, 1949.

unaffected by the sensitivity of the equipment and are only slightly affected by the presence of interference.

Another factor influencing radio meteor rates which appears to have been overlooked in previous discussions is the presence of the galactic noise which is pronounced at these radio frequencies.[11] We have used a diode noise generator to show that there is a 2 to 1 diurnal variation in the noise level of our radio receivers operating in the 30–36 mc/sec band, the maximum corresponding to the time when the main region of general galactic noise and the intense source in Cygnus are highest in the sky. The maximum noise level occurs about midnight in August and about noon in December. The radio rate counts made during the hours of darkness of the Perseid shower period are appreciably lower than the counts made during the Geminid shower period, although the visual rates in each case are about equal. Loss of the weaker radio echoes in the higher noise level of the August observations may be a contributing factor. The analysis of the observations presented here will be based largely on a discussion of the velocity distributions, with only qualitative support from a consideration of the rates.

A particular effort was made to find examples of fast meteors, which could have had the effect of unduly weighting the distribution in the higher-velocity groups. Echoes that were obviously due to high-speed meteors were analyzed in some cases where the echo quality would have caused them to be rejected if they had occurred lower in the velocity range. On the other hand, this tendency might be counteracted by the fact that fast meteors were more difficult to measure than slow meteors when severe interference occurred on the record, usually caused in the daytime hours near noon by distant radio stations.

Of the total of 10,933 echoes measured, using the formula of equation (14), 9 fell in the class interval 80–84 km/sec, and not one was over 83 km/sec. From a purely statistical viewpoint, it would have been proper to retain the 9 high-speed meteors, especially as their contribution to the analysis was negligible. However, each was re-examined by more accurate methods, and, without exception, the revised velocities fell below 80 km/sec. The meteors in the class range 75–79 km/sec were reworked as well, and, although there were some minor changes, 32 velocities remain in this range. The average probable error of an individual velocity measurement in any of the velocity classes was about 5 per cent, including the uncertainty in R_0, though the errors were as high as 10 per cent for some of the whistles with poor definition. Because of the extra attention they received, the errors in the high-velocity classes are less than the over-all mean error.

Velocity distributions of the total number observed in each operating period have been plotted in Figure 5. The numbers in each histogram have been normalized to 100 per cent for more effective comparison of the over-all distributions throughout the year. Graph No. 1 in Figure 5 shows the distribution for all the velocities measured throughout the year. An annual trend in the monthly velocity distributions is apparent, with a decided shift to the higher velocities in the fall months compared to the spring months. The effects of the two strong visual showers are pronounced—the Geminids, graphs Nos. 2 and 16, and the Perseids, graph No. 11, and also the summer daylight showers,[12] graphs Nos. 6–10. Some of the less active showers, e.g., the η and δ Aquarids, show up in the hourly distributions given in the appendix tables but are not readily apparent in the over-all distributions. However, the radio meteor rates do not increase proportionally to the visual rates during the visual showers, as even at the peak of a strong shower, when the visual rates are four or five times the normal rates, the radio rates will have barely doubled. It follows that the radio systems detect meteors below the threshold of vision and that the proportion of large meteors to small ones is greater in the long-established

[11] J. W. Herbstreit, *Advances in Electronics* (New York: Academic Press, 1948), **1**, 347.

[12] A. Aspenall, J. A. Clegg, C. D. Ellyett, and A. C. B. Lovell, *M.N.*, **109**, 352, 1949.

visual showers than in the normal background of meteors.[6] Allowance will be made for the presence of the showers in analyzing the velocity distributions in a later section.

Without going into the details of the arguments, which will be put forward elsewhere, a few qualitative remarks may be made concerning the equivalent visual-magnitude range of the radio meteors. On a typical nonshower night, for example, when the visual

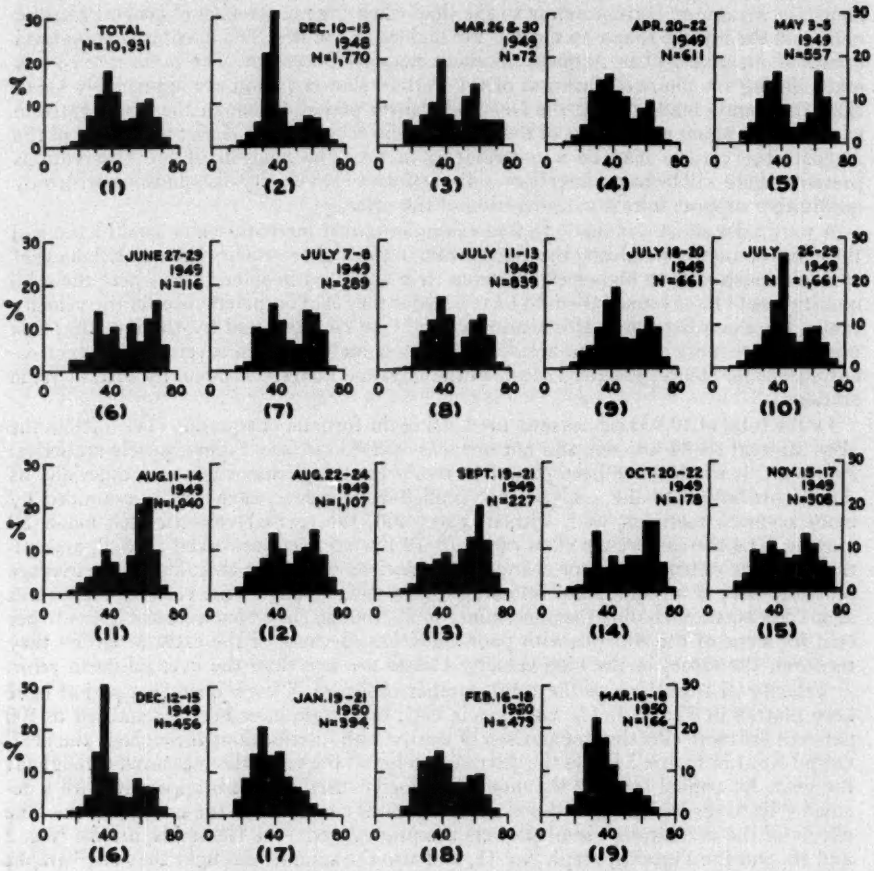

FIG. 5.—Velocity distributions from December, 1948, to March, 1950. These histograms represent the total distributions for the periods indicated, usually covering from 48 to 72 hours continuously, though with exceptions noted in the appendix tables. Histogram No. 1 is the sum total of all observations.

rates, corrected to a team of six observers, are about 20–30 per hour, the radio rates run about 400–600 per hour. The visual observer can detect a meteor in his field of view, regardless of its path orientation, but the radio echoes from the majority of the meteors can be obtained only when the path is normal to the line of sight. Assuming that both the radio and the visual meteors follow similar laws of numbers for a given size, it is possible to estimate the over-all rates of meteors seen by the radio equipment, although some of

the assumptions involved are doubtful. In qualitative terms it appears that, under circumstances when the average visual meteor is in the second- or third-magnitude range and the minimum detectable visual meteor about fifth magnitude, the average radio meteor lies in the sixth- to seventh-magnitude range, with the minimum detectable meteor being about ninth magnitude. Another approach to the problem, which leads to a similar conclusion, consists in measuring the echo strength of a number of radio meteors having simultaneous visual observations. These correlations usually extend from the brightest magnitudes down to about the third or fourth visual magnitude, and by extrapolation one can deduce the equivalent visual magnitude of the weakest detectable echo. It is difficult to determine this relation precisely, as a faint visual meteor often produces a striking radio echo and vice versa. These relations are mentioned here tentatively to indicate the general order of the magnitudes seen by our radio systems. More work is required on this matter before firm conclusions can be reached. With the selective method of velocity reduction employed in this paper, the average meteor in the appendix tables is probably of the order of fourth or fifth magnitude, with a limit of about seventh to eighth magnitude.

Before proceeding to a general statistical analysis of the observational data, a detailed examination will be made of the Geminid shower, first, to give an indication of the accuracy of the statistical analysis and, second, to deduce a probability function of general application.

THE GEMINID SHOWER

Tables A2 and A16 in the appendix list the available velocity data for the Geminid shower periods of 1948 and 1949. Operations were curtailed in the 1949 period, so the 1948 information will receive chief attention. Figure 6 shows the hourly normalized distribution of velocities from 1700 to 1200 E.S.T., the data from the corresponding hours of each of the three days being added. The area of each plot is normalized to 100 per cent to emphasize the trend of the velocities, which shows that the appearance of the Geminid meteors during the evening and morning hours is quite marked. The Geminids were not recorded for the hours around 0200 E.S.T., when the radiant was highest in the sky, because the R_0 distances were then beyond the maximum recorded radar range, which was arbitrarily cut off at 260 km to improve the range resolution. The small arrow on each graph indicates the maximum possible observed velocity for that hour, assuming the parabolic heliocentric velocity.

The velocity range between 30 and 40 km/sec was broken down into unit steps (see Fig. 7, where the data for 1948, 1949, and the totals are shown). These plots certainly contain some non-Geminid meteors, but the proportions are small during the peak Geminid hours and unlikely to exceed 15 or 20 per cent of the totals. If we assume, using information from other periods tabled in the appendix, that the distribution of non-Geminid velocities is reasonably uniform over the range 30–40 km/sec, the effect of the nonshower meteors on the general shape of the curves of Figure 7 should be smaller still. During the hours near transit of the radiant, it was possible to reject a small number of observations because the associated R_0 ranges were too short for them to be Geminids.

The mean velocities, shown by arrows in Figure 7, are as follows: for 851 meteors in the 1948 period, 35.2 km/sec; for 234 meteors in the 1949 period, 35.5 km/sec; mean of both periods, 35.25 km/sec. These velocities are mean apparent observed velocities of the Geminids. To obtain the geocentric velocity of the meteors, the observed velocities should be corrected for diurnal motion, for zenith attraction, and for resistance of the atmosphere. The diurnal-motion correction would tend to average out if equal numbers of meteors were taken at equal time intervals about the transit time, although the spread of velocities would be greater than if the correction were applied individually to each meteor. In Figure 8, *a*, the dotted curve shows the diurnal-motion correction at Ottawa. The dashed curve shows the average correction which should have been applied to the

observed velocities each hour to allow for the separation of the Doppler transmitter and receiver. This correction is fortuitously of the same magnitude as the diurnal correction but of different phase. The net correction is shown in solid line (Fig. 8, *a*), and, when averaged over the observational period, it amounts to −0.036 km/sec in the mean measured velocity, which is scarcely significant. We may therefore adopt the value 35.2 km/sec as

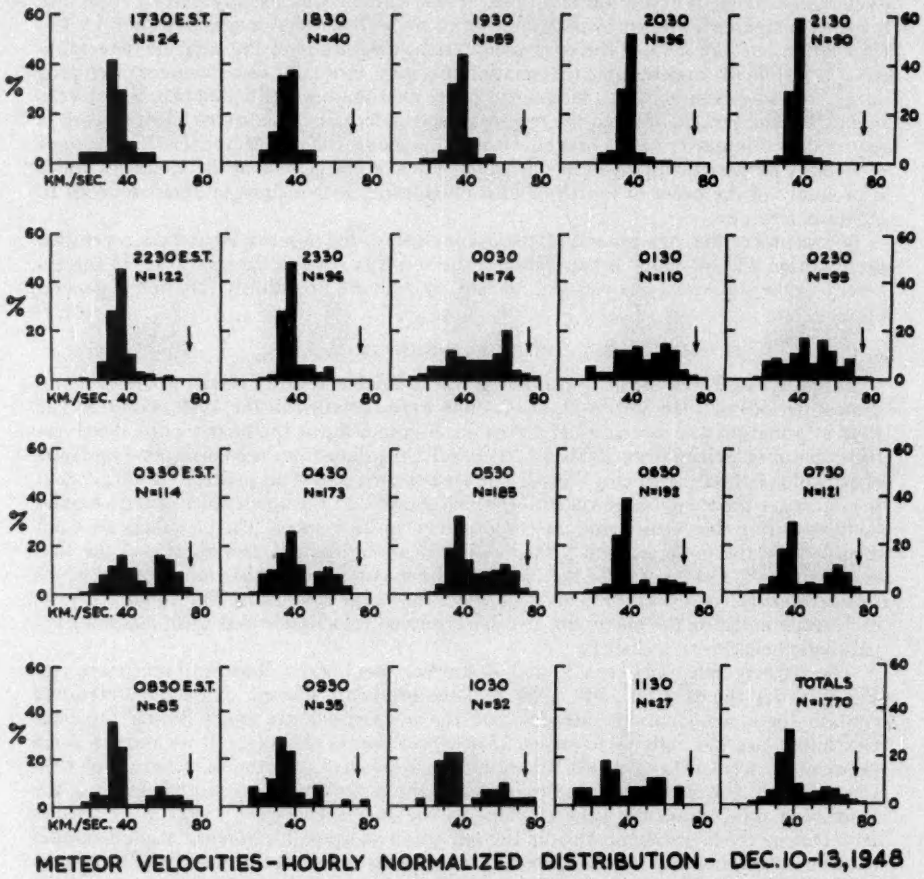

FIG. 6.—Velocity distributions for period December 10–13, 1948. The data for each hour have been normalized to make the areas of all the histograms equal.

the observed velocity of the Geminid shower, corrected for diurnal motion but not corrected for air resistance or zenith attraction. Whipple[13] obtained from his photographic work a mean value of 35.95 km/sec for the apparent relative velocity, before applying any of the corrections. Referring to the total distribution-curve of Figure 7, the formal standard deviation of an individual observation is found to be ±2.3 km/sec, and the

[13] *Proc. Amer. Phil. Soc.*, 91, 189, 1947.

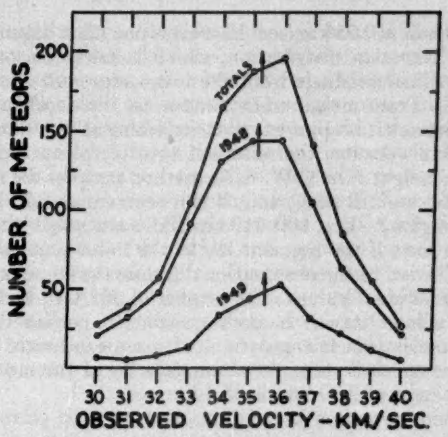

FIG. 7.—Velocity distribution of probable Geminid meteors. 1948 graph contains 851 observations, with mean velocity 35.2 km/sec. 1949 graph contains 234 observations, with mean velocity 35.5 km/sec. Totals graph contains 1085 observations, with mean velocity 35.25 km/sec.

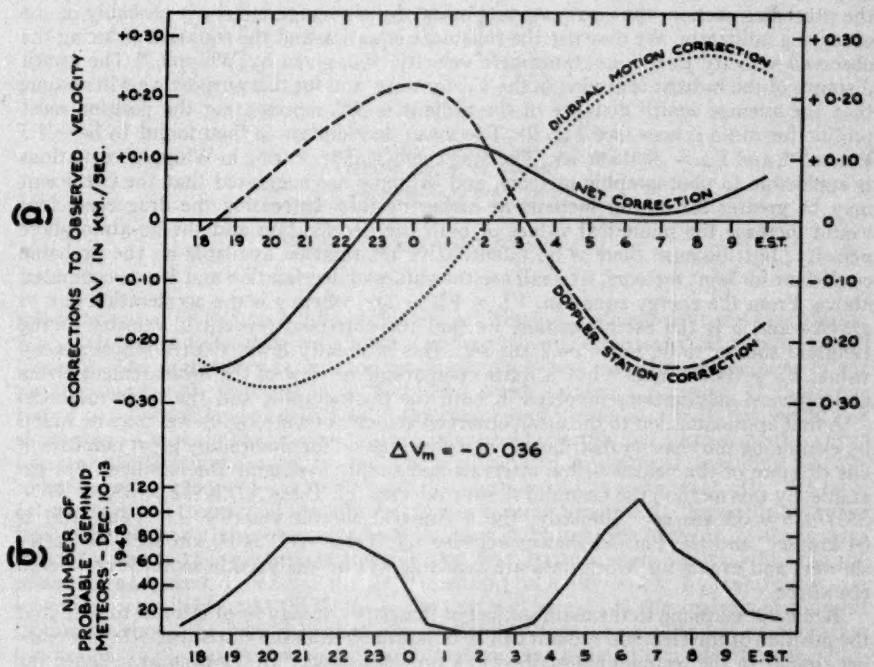

Fig. 8.—*a*, ***Dotted line***, diurnal motion correction for Geminid meteors; ***dashed line***, statistical correction for average position of Geminid meteors, due to spacing of Doppler transmitter and receiver; ***solid line***, net correction to be applied to observed velocities each hour. *b*, Observed hourly rates of probable Geminid meteors, 1948 data.

probable error of the mean is 0.05 km/sec. However, one must assume not only that the observations follow a Gaussian distribution, which is fairly reasonable, but that the deviations of the individual readings from the mean represent accidental errors only, which is very doubtful. From measurements made on the deceleration of both photographic[14] and radar[5] meteors it is apparent that, assuming all the shower meteors to have the same no-atmosphere velocity, the observed velocity of an individual meteor will depend on its mass and height. The C.W. radio method samples the meteor velocity only over a short part of the ionized path, and, if this segment should happen to lie in the upper parts of the M-region,[6]—say, 100–110 km above sea level—the measured velocity will be slightly higher than if the segment lay in the lower parts of the M-region, say 80–90 km. Thus, in addition to the observational errors, the standard deviation includes a true spread of the individual values. The heights of 302 Geminid meteors have been computed,[15] either by using Ottawa visual observations in conjunction with the Ottawa radar record or by three-station triangulation, with a mean height of 97.0 km. At this stage one can therefore conclude that the mean velocity of the radio Geminid meteors, measured at a mean height of 97.0 km, is 35.2 km/sec.

The zenith attraction correction is easily applied, but the correction for the air resistance, that is, for the mean deceleration of the meteors, is more difficult to evaluate because the deceleration is a function of the height and mass of the meteor as well as of the velocity, and some dubious assumptions may have to be made. If the average visual magnitude of the radio meteors is assumed to be about the fourth or fifth, as suggested in the preceding section, the corresponding mass of the average meteor is probably of the order of a milligram. We may use the resistance equation and the equation reducing the observed velocity to the no-atmosphere velocity, V_∞, given by Whipple.[16] The zenith distance of the radiant is needed in the V_∞ formula, and for this purpose we will assume that the average zenith distance of the radiant is 50°, representing the position most prolific for radio echoes (see Fig. 9). The mean deceleration is then found to be -2.5 km/sec^{-2}, and $V_\infty = 36.0$ km/sec. The drag coefficient appearing in Whipple's equations is applicable to photographic meteors, and Whipple has suggested that the coefficient may be greater for fainter meteors at higher heights. Increasing the drag coefficient would increase the numerical values of both the deceleration and the no-atmosphere velocity; but, because there is no quantitative information available on the probable coefficient for faint meteors, we shall use the values of deceleration and V_∞ as computed above. From the energy equation, $V_G^2 = V_\infty^2 - 2g\rho$, where g is the acceleration due to gravity and ρ is the earth's radius, we find the corrected geocentric velocity of the Geminid shower to be $V_G = 34.2$ km/sec. This is slightly lower than Whipple's mean value, $V_G = 34.7$ km/sec[13] but is quite comparable in view of the measurement errors and physical assumptions involved in both the photographic and the radio methods.

A first approximation to the mean observed velocity of a strong shower may be found by examining the velocity distribution of a given period for abnormally great numbers in one or more of the velocity-class intervals and simply averaging the numbers. For example, by this method the Geminid shower velocity (cf. Table A2) is $(32 \times 383 + 37 \times 552)/935 = 35$ km/sec. Similarly, the η Aquarid shower velocity (cf. Table A5) is 64 km/sec, and the Perseid shower velocity (cf. Table A11) is 60 km/sec. The latter showers and others for which data are available will be analyzed in more careful detail elsewhere.

While not germane to the main subject of this paper, it may be of interest to note that the position of the Geminid radiant can be determined from the statistical data in a manner similar to the technique described in a previous paper.[6] In the present instance the

[14] Fred L. Whipple, *Rev. Mod. Phys.*, **15**, 243, 1943.

[15] Peter M. Millman, *J.R.A.S. Canada*, **44**, 209, 1950.

[16] *Proc. Amer. Phil. Soc.*, **79**, 499, 1938.

criterion used to select the probable Geminids each hour is that the velocities shall lie between 30 and 40 km/sec. From the hourly range distributions of these selected meteors the most probable minimum range each hour is deduced, and that value is then used to determine the radiant elevation for that hour. No data are available for the hours when the radiant was highest because of the arbitrary cutoff of the range records, and these data would have been most helpful in determining the maximum radiant elevation accurately. However, the information available yielded a radiant transit time of 0200 E.S.T. and a maximum radiant elevation angle between 75° and 80°, corresponding to a radiant position at right ascension 112°, declination +30° to +35°, in reasonable agreement with our earlier radar determination and with the position given by Whipple.[13]

An empirical relation between radio meteor rates and zenith angle of the meteor radiant can be deduced from the information shown in Figure 8, *b*, together with similar data from the 1949 shower. The transit time of the radiant is 0210 E.S.T., and, by adding the numbers from the corresponding hours on either side of the transit and plotting these against the zenith angle of the radiant rather than against time, we obtain the

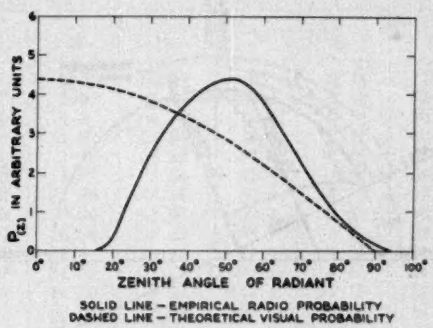

FIG. 9.—The probability function $P(z)$

solid-line curve of Figure 9. The ordinates (arbitrary units) represent the probability, $P(z)$, that the radio system will detect a meteor when the radiant is at a given zenith distance. The probability is zero for zenith distances less than 16°–18° because of the radar range cutoff, resulting in a "forbidden zone" around the zenith. If the range record had been extended indefinitely, the curve would begin at $z = 0°$ but would rise slowly, and the main shape would be unchanged. While this is an experimental curve based on the Geminid shower, it should be applicable to any radiant, assuming that the radiant emits meteors of a standard size distribution and at a constant rate. We have calculated some theoretical probability-curves, several of which fit the empirical curve fairly well. However, there seems to be little point in reproducing here the involved arguments leading to the synthesis of these curves, first, because there are weak links in the reasoning and, second, because the experimental probability-curve represents the best information available, and this is the curve that will be used in the analysis of the next section. It should be remarked that this probability function applies to our operating conditions. If the parameters of the radio system were to be altered significantly, particularly the antenna pattern, some changes in the curve would be expected, though the general trend should be similar.

The quantity $P(z) = \cos z$ is plotted as the dashed line in Figure 9 and represents, to a first order of approximation, the probability function for a visual observer.

COMPARISON OF OBSERVED AND HYPOTHETICAL VELOCITY DISTRIBUTIONS

For many years workers in the meteor field have investigated the observed distributions of meteor rates, radiants, and velocities with a view to interpreting them in terms of assumed celestial distributions. Depending on the data selected and on how they are treated, one school of thought has reached the conclusion that most of the meteors are moving in elliptical orbits, and the other school finds that the majority are hyperbolic meteors from interstellar space. An adequate review of these theses would be prohibitively long, and an attempt to analyze them critically would be beyond the scope of the present discussion. Instead, we shall try to draw conclusions from our own observations, using a similar method, it is true, but justifying the procedure on the grounds that the radio data embrace nearly eleven thousand meteor velocities of greater accuracy than has hitherto been available. Furthermore, the radio probability factor, $P(z)$, has intro-

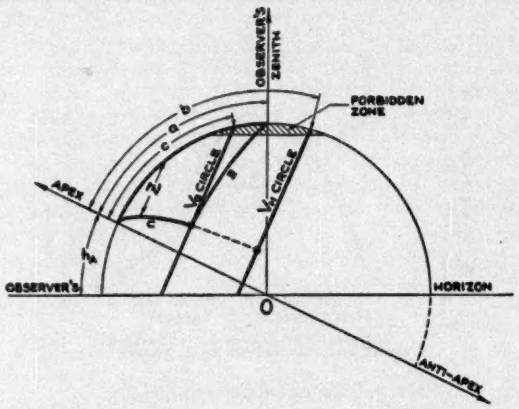

FIG. 10.—Geometry of problem of synthesizing theoretical distributions of meteor radiants and velocities for comparison with the observed distributions.

duced a new element into the problem that must be included in any attempt at synthesizing radio meteor distributions.

We shall tentatively assume that meteor radiants are uniformly spread over the celestial sphere. All these radiants emit meteors with the same distribution of velocities, sizes, and rates. Figure 10 shows the geometry of the problem, with the observer at O moving at 30 km/sec in the direction of the apex of the earth's way. The apex is at an elevation h_A relative to the observer's horizon or at a distance a from the observer's zenith. Small circles are drawn on the celestial sphere at distances b from the apex as pole, designated on the diagram as V_H circles, where V_H is the heliocentric velocity. True radiants on these circles will appear to the observer to be on the small circles at distances c from the apex, termed V_G circles, where V_G is the geocentric velocity. The transformation is effected by the following relations:

$$V_G^2 = V_H^2 + 900 + 60\, V_H \cos b \tag{15}$$

$$V_G \sin c = V_H \sin b\,. \tag{16}$$

Owing to the attraction of the earth, both the meteor velocity and the apparent direction of the radiant will be altered slightly, according to the following expressions:[17]

$$V_0^2 = V_G^2 + 125\,, \tag{17}$$

$$\tan\frac{\Delta z}{2} = \frac{V_0 - V_G}{V_0 + V_G}\tan\frac{z}{2}\,, \tag{18}$$

where V_0 is the observed or apparent velocity and Δz is a positive correction to be applied to the zenith angle, z, of the radiant.

We may regard V_H as a parameter and assign a selected value of V_H to all the radiants over the sphere. Table 1 shows typical values of V_0, c, and Δz (Δz here being the maximum correction when $z = 90°$), calculated for uniform values of b and for three values of the parameter, $V_H = 30$, 36, and 42 km/sec.

TABLE 1

b	$V_H = 30$			$V_H = 36$			$V_H = 42$		
	V_0	c	Δz	V_0	c	Δz	V_0	c	Δz
0°...	61.03	0°	0° 58′	66.94	0°	0° 48′	72.86	0°	0° 41′
15....	60.51	7.5	1 0	66.39	8.2	0 50	72.27	8.8	0 42
30....	59.02	15.0	1 2	64.75	16.4	0 52	70.50	17.1	0 44
45....	56.55	22.5	1 8	62.04	24.6	0 57	67.61	26.5	0 48
60....	53.15	30.0	1 18	58.32	33.0	1 4	63.63	35.5	0 54
75....	48.90	37.5	1 32	53.66	41.5	1 16	58.67	44.8	1 4
90....	43.88	45.0	1 56	48.18	50.2	1 35	52.81	54.5	1 19
105....	38.20	52.5	2 34	41.98	59.2	2 6	46.22	64.8	1 44
120....	32.02	60.0	3 44	35.23	68.9	3 2	39.11	76.1	2 27
135....	25.53	67.5	6 4	28.18	79.8	4 55	31.73	89.3	3 48
150....	19.14	75.0	11 54	21.22	93.8	9 16	24.63	106.9	6 35
165....	13.65	82.5	30 20	15.32	117.4	21 18	18.84	134.2	12 22
180....	11.18	90.0	90 0	12.69	180.0	39 24	16.40	180.0	17 36

The values of Δz have been included in Table 1 chiefly to show the order of magnitude of the maximum correction. It is most troublesome for low heliocentric velocities with radiants near the antapex. Inclusion of the correction would cause the V_G circles to become distorted in the direction of the zenith, but the effect is not serious for the majority of the radiants. In the simplified analysis that follows, this angular correction will be neglected, though the velocity correction will be included.

We have assumed a uniform surface density of V_H radiants over the sphere. It is possible to write down a surface integral representing the conversion of these radiants to the V_0 set of radiants. This would have to include a functional representation of the $P(z)$ probability-curve and would tend to become very intricate indeed if the original uniform distribution were to be modified. For the purposes of the present argument a form of numerical integration appears to be adequate. This could be done by setting up the problem on a model sphere, which is a method that is particularly well adapted to the inclusion of special conditions; for example, an assumed concentration of radiants near the plane of the ecliptic. The theoretical distributions in this paper were actually computed according to the following procedure:

1. A particular value of a is first selected. Uniform surface density of radiants may be represented by uniform and equal line density along each of the V_H circles at equal

[17] C. P. Olivier, *Meteors* (Baltimore: Williams & Wilkins Co., 1925), p. 165.

increments of the distance b. Rather than divide the V_H circles into equal linear elements, we divide the circles into equal angular elements so that the transformation of points on the V_H circles to the V_G circles is effected by drawing great circles through the apex at equal intervals of the angle Z. In this case the number of points (i.e., radiants) so selected on a given V_H circle should be multiplied by sin b.

2. The distance z is computed for each point on the V_G circles selected by 10° increments of the angle Z, by means of the spherical triangle defined by the apex, the zenith, and the selected point.

3. At this stage the density of points on a given V_G circle is uniform, although it may be greater or smaller than the density on the corresponding V_H circle, depending on the angles b and c. Each point on a V_G circle must now be multiplied by the probability value $P(z)$ corresponding to the zenith distance of the point, using Figure 9. (For convenience, a plot of $P(z)$ versus cos z was employed, and in the intermediate stages graphs of numbers versus angle b were found useful.)

4. The sum of the modified densities along a given V_G circle is the rate of meteors of velocity V_G that will be detected by the radio system, for the selected values of a and V_H. The curves of Figure 11 show the computed theoretical distributions of apparent radio velocities based on initial uniform distributions of heliocentric velocities. The

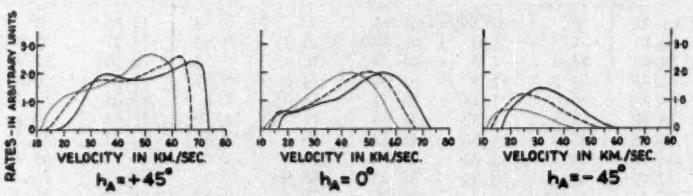

FIG. 11.—Theoretical radio meteor velocity distributions, based on uniform distribution of radiants. Computed for three elevations of the apex of the earth's way; $h_A = 45°$, 0°, and −45°. *Solid line*, V_H =42 km/sec; *dashed line*, $V_H = 36$ km/sec; *dotted line*, $V_H = 30$ km/sec.

selected values of the elevation of the apex, h_A, are +45°, 0°, and −45°. The solid curves are for $V_H = 42$ km/sec, the dashed curves for $V_H = 36$ km/sec, and the dotted curves for $V_H = 30$ km/sec.

In order to select the appropriate observational data for comparison with the theoretical distributions, the local times corresponding to the three chosen values of h_A were first determined for each of the operating periods. The apex is on the horizon twice daily all year round, but h_A reaches +45° only from June to December and −45° from December to June. Hourly velocity distributions were then selected from the tables in the appendix to correspond to these times. If the selected h_A time occurred near the hour—say, at 0310 or 0250 E.S.T.—then data for the hours 0200–0300 and 0300–0400 were used. If the h_A time occurred near the half-hour—say, 0320 or 0340—then data for the hours 0200–0300, 0300–0400, and 0400–0500 were used. Superscripts appended to the hour figures in the appendix tables indicate the data actually used: [1] referring to $h_A = +45°$, [2] to $h_A = 0°$, and [3] to $h_A = -45°$.

A considerable amount of information was necessarily rejected because the presence of the strong visual showers, e.g., Perseids, Geminids, η Aquarids, and the summer daylight showers,[12] was quite evident, and certain hours from observing periods known to contain appreciable numbers of shower meteors have not been used. All these showers have elliptical orbits, and their inclusion might unduly weight the results. The aim of this analysis is to account for the normal diurnal and annual observed distributions of meteor velocities and rates. The expression "normal distribution of meteors" corresponds to the terms "background meteors" or "sporadic meteors" appearing in the literature, but we

hesitate to use these latter designations, preferring, instead, to regard the strong showers as very active but isolated particular cases of the general radiant distribution. The effect of the strong showers, representing an abnormal phenomenon, should thus be removed before attacking the normal distribution problem.

The selected observational data are plotted in Figure 13 in the form of histograms (the curves of Fig. 13 will be considered later). Using the theoretical curves of Figure 11, one may now attempt to synthesize velocity distributions similarly shaped to the histograms of Figure 13, for example, by adding together equal numbers of $V_H = 30$, 36, and 42 km/sec meteors or by mixing them in various proportions. None of the combinations appeared to fit the observations very well, and in particular the double-humped distribution of the histogram of $h_A = 45°$ seemed difficult to match. The closest approximations were obtained by using equal numbers of 36 and 42 km/sec meteors but with few, or none, of 30 km/sec meteors.

We next consider a nonuniform radiant distribution. We will assume that there are more direct orbits than retrograde orbits, that is, the inclinations of the orbital planes favor the interval $0° \pm 90°$, and that the ellipticities are large, approaching the parabolic rather than the circular. These assumptions are to be regarded as purely *ad hoc* for our purposes, though there is considerable evidence in the general literature to give them

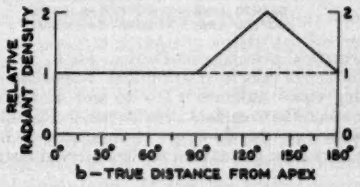

FIG. 12.—Assumed theoretical distribution of radiants as a function of the distance from the apex, b. *Dotted line*, uniform distribution; *solid line*, adopted nonuniform distribution.

support. Our analytical technique does not lend itself readily to a separate consideration of the orbital inclination and the ellipticity, but the parameter b is a measure of the combined effect of these factors, and, by postulating more radiants with $b > 90°$ than with $b < 90°$, we imply that more of the orbits will be direct. By eliminating $V_H = 30$ km/sec, we definitely remove the circular and slightly elliptical orbits. The adopted density distribution as a function of b is shown in Figure 12 by a solid line, with the original uniform distribution indicated as a dotted line. The densities on the V_H circles are modified according to this function, and the integration procedure is repeated. In practice it is necessary merely to multiply the ordinates of the curves in Figure 11 by the corresponding ordinates of Figure 12, using the link between b and V_0 in Table 1.

The dashed-line curves in Figure 13 show the theoretical distributions of the radio meteor velocities, computed on this basis, assuming equal numbers of $V_H = 36$ and $V_H = 42$ km/sec meteors, with no $V_H = 30$ km/sec meteors. The ordinate axis is marked in hourly rates per 5 km/sec class interval. The dotted-line curves in Figure 13 are the theoretical distributions of visual meteor velocities, calculated in the same manner but using the visual probability-curve of Figure 9 in place of the radio probability-curve. The visual meteor-curves are themselves of academic interest only, as there are no corresponding sets of visual velocity observations, but the areas under the curves are proportional to the hourly rates of visual meteors (all velocities), and a wealth of observational material exists on over-all visual meteor rates.

Before comparing the theoretical curves and the experimental histograms of Figure 13, the method of evaluating the relative heights of the curves will be mentioned. The total

number of observed radio meteors in each histogram, the number of hours of data, and the over-all hourly rates are listed in Table 2.

The relative theoretical hourly rates in Table 2 have been obtained by first integrating the curves of Figure 13 in arbitrary units. There is more observational material available for $h_A = 0°$ than for the other two apex positions; hence the theoretical over-all rates have been made equal to the observed over-all rate for this case, and the theoretical rates (Table 2) and the theoretical curves (Fig. 13) for the other two h_A cases have been nor-

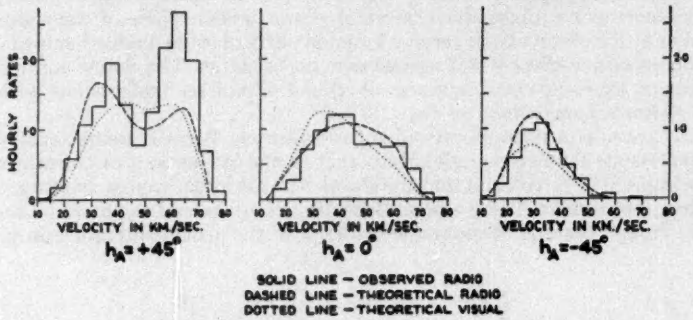

FIG. 13.—Observed and theoretical velocity distributions for $h_A = +45°$, 0°, and −45°. *Solid-line histograms*, actual observed radio meteor velocity distributions; *dashed-line curves*, theoretical radio meteor velocity distributions, assuming equal numbers $V_H = 36$ and 42 km/sec and no $V_H = 30$ km/sec, from Fig. 11, and applying the nonuniform radiant distribution in Fig. 12; *dotted-line curves*, theoretical visual meteor velocity distributions on the above set of assumptions. Both the theoretical radio and theoretical visual distributions have been normalized to the observed distribution for $h_A = 0°$.

TABLE 2

	$h_A = +45°$	$h_A = 0°$	$h_A = -45°$
Total number of radio observations	1157	975	250
Number of hours of operation	67	116	56
Observed radio hourly rates	17.26	8.41	4.46
Ratios of observed radio hourly rates	3.9	1.9	1
Theoretical radio hourly rates	12.9	8.41	5.4
Ratios	2.4	1.6	1
Theoretical visual hourly rates	11.7	8.41	3.7
Ratios	3.2	2.3	1

malized accordingly. On examining Figure 13, a reasonably good agreement is noted between the general trend of the theoretical radio-curves and the corresponding observational histograms, except that in the $h_A = +45°$ case the number of observed velocities in the high-velocity ranges exceeds the predicted numbers and in the lower ranges the ratio is reversed. The distribution of radiant density as a function of the angle b (Fig. 12) can be altered to make the curve and histogram for $h_A = +45°$ agree more closely by increasing the radiant density in the region $b = 0°$–$30°$. This would imply a slight increase in the number of highly retrograde orbits over the number with inclinations in the neighborhood of $\pm 90°$, though the number with inclinations smaller than $\pm 90°$ would still preponderate. Not much evidence could be found to support this premise, and alternative explanations may be sought. The most plausible explanation appears to be that, for a given size of meteoric particle, the faster meteor produces more ionization,

hence smaller particles, and therefore more of them will be detectable in the high-velocity ranges. The exact form of the dependence of ionization on velocity is a matter of conjecture at present. The production of visible light certainly increases with the speed of the meteor, and the ionization is thought to increase even more rapidly.

While not too much reliance should be put on the observed over-all rate figures of Table 2, the trend is in fair agreement with the predicted rates. As far as can be ascertained from an incomplete examination of visual meteor records, the theoretical visual ratio of 3.2 to 1, for $h_A = +45°$ to $h_A = -45°$, appears quite reasonable. The average observed visual ratio is somewhat higher, possibly because of the luminosity-velocity relationship. If the reliability of the radio meteor rates selected from periods six months apart had warranted the comparison, the theoretical annual variation in both radio and visual meteor rates could have been evaluated by a further integration over the diurnal ranges of h_A from selected days throughout the year.

The data in each of the appendix tables show clearly a decrease in maximum observed velocity as the apex descends below the horizon. As an alternative method of analysis the maximum V_0 corresponding to the parabolic heliocentric velocity may be computed for each hour of a selected period and compared with the observations, and it will be found that few, if any, of the observed velocities exceed this limiting velocity. This was done in the preliminary presentation of this paper at the 81st Meeting of the A.A.S., but in preparing the material for publication it was thought that it would be preferable to use all the observed velocities in selected periods for comparison with theoretical velocity distributions, rather than to confine attention solely to the marginal velocities.

The number of variables in the general problem of meteor orbits discussed here can be increased almost at will, and various corrections and modifications can be introduced to create a situation of fascinating complexity. It appears to the author, however, that not much is to be gained beyond the present stage of the statistical analysis. With so many parameters to adjust, a reasonable fit with the observational data might be expected from dissimilar theoretical postulates. If the treatment is confined to one part of the year, a fair case can be made for the presence of strongly hyperbolic heliocentric velocities, but the hyperbolic meteors must be assumed to be moving almost entirely in direct orbits of low inclinations. The analysis breaks down completely when applied to another time in the year, unless one can put forward convincing reasons why hyperbolic meteors coming from outside the solar system should have direct motions all year round and should lie close to the plane of the ecliptic.

The 32 meteors lying in the class interval 75–79 km/sec merit a remark. These meteors, representing 0.3 per cent of the total, are probably genuinely hyperbolic in the sense that they exceed the parabolic limit for V_0 (this limit is as great as 74 km/sec at times, when the true earth's orbital velocity is used instead of the assumed 30 km/sec). If they are interstellar meteors, it is difficult to see why an appreciable number has not been found over 80 km/sec. It might be preferable to regard them as interplanetary meteors, formerly moving in elliptical orbits, that have been thrown into slightly hyperbolic orbits by planetary perturbations. It can be shown that the influence of Jupiter, for example, may cause an effect of the right order of magnitude.

Of the thousands of meteor velocities in our records, we have not yet found one which we can definitely assert to be a meteor from interstellar space. The search for hyperbolic meteors will be continued. The limitation of the statistical analysis is fully realized; a knowledge of the path of every meteor and a conversion of the observed velocity to the heliocentric velocity in each case would be required to ascertain whether appreciable numbers of meteors with V_0 below 74 km/sec might be hyperbolic. However, there should certainly have been some meteors found with velocities well above 74 km/sec, especially if the velocity distributions were as highly hyperbolic as the ones which Öpik[18] and Hoffmeister[19] have deduced.

[18] *Tartu Obs. Pub.*, Vol. **30**, Nos. 5 and 6, 1940, 1941; *Observatory*, **68**, 226, 1948.

[19] *Meteorströme* (Weimar, 1948).

Öpik, furthermore, has suggested that the fraction of hyperbolic meteors increases in the fainter magnitudes until it includes nearly all meteors of the ninth magnitude. The range of our investigations extends from the brightest meteor down to about the eighth magnitude. We have not yet analyzed the velocity distribution directly in terms of the visual-magnitude ranges, this being feasible only in the comparatively few cases where simultaneous visual observations are available. On the other hand, on several occasions (usually inadvertently) we have depressed the over-all sensitivity of the radio system to reduce the echo rates by a factor of 10 or so, thus implying a loss of 2 or 3 mag. in the lower limit of detectability. Under these circumstances the velocity distributions have been indistinguishable from the distributions obtained when the equipment was operating at full efficiency. We conclude that no significant differences exist in the velocities of the normal meteor distributions down to the eighth magnitude and that the vast majority of meteors are moving in elliptical orbits, with little or no evidence of an interstellar component.

SUMMARY

The theory of meteor echoes has been reviewed briefly to indicate how the meteor velocity may be deduced from a record of the echo amplitude versus time. The limitations of the technique were discussed, and it was concluded that meteor velocities up to 150 km/sec could have been measured, if such meteors existed. The average probable error of the velocity-reduction method used in the statistical analysis was of the order of 5 per cent anywhere in the velocity range. A detailed discussion of the Geminid shower, together with preliminary results for other known showers, has shown that the statistical method of analysis yields velocities in good agreement with those obtained by the rotating-shutter photographic method.

Velocity data for 11,933 meteors, obtained from observations made over a 15-month period, have been presented. The diurnal and annual variations both in the meteor rates and in the general trend of velocity distributions are in broad agreement with observations made by other methods. However, a detailed examination of the velocity data does show significant disagreement with conclusions based on velocity measurements made visually.

A simplified theoretical analysis of the meteor orbit and radiant problem has been put forward to suggest that the radio observations may be satisfactorily explained by assuming all, or nearly all, meteors to be moving in elliptical orbits with more direct than retrograde motions.

E. L. R. Webb designed and supervised the construction of most of the equipment used in this project and also made some contributions on the theoretical side. Miss Blodwen Thomas set up the reduction procedure and for some time supervised the analysis of the film. Miss J. M. Connery later took over Miss Thomas' duties, assisted by the technical staff of the Radiophysics Section. Miss A. E. Puxley, Mrs. L. E. McManus, and D. Dingle were engaged in the velocity-measurement work for one summer. B. E. Bourne was responsible for much of the electronic circuit technique used throughout the system, and L. A. Petch planned and built the Doppler transmitter. D. K. Ritchie and J. R. Kenney collaborated on the design of receivers and displays. R. S. McClean was the senior technician of the group which built and operated the equipment and included R. L. Westby, W. T. Foster, S. M. Panagapko, H. W. Poapst, and J. D. Stewart. In the early days of the project the Doppler receiving station was located in L. T. Nolan's home at South Gloucester. Advice and guidance have been available from Peter M. Millman at all times, and Fred L. Whipple has offered helpful comments. The preparation of this paper has been greatly facilitated by the assistance of my wife, Barbara M. McKinley.

APPENDIX

The tables in this appendix have been drawn up to summarize the observational data as compactly as possible, consistent with the measurement errors involved and other considerations mentioned in the text. The velocity-class interval selected was 5 km/sec; for example, the column headed "30" contains meteors with measured velocities falling in the range 30–34 km/sec. As each velocity measurement has been previously rounded off to the nearest km/sec, this interval actually extends from 29.5 to 34.4 km/sec, with the mean of the interval at approximately 32.0 km/sec.

Data for corresponding hours within a continuous operating period are added, and the factor number appearing after the dates of the period indicates the number of hours so added. This procedure was generally followed, though there are many exceptions in which some hours or fractions of hours are missing from one or more days in the period, hence the over-all hourly rates are to be regarded as nominal uncorrected values. Whenever the equipment has been shut down deliberately within an operating period, the fact has been noted in the tables. The superscript [1] after an hour figure indicates data for that hour have been used for $h_A = 45°$, superscript [2] for $h_A = 0°$, and superscript [3] for $h_A = -45°$.

TABLE A1

TOTAL OF ALL PERIODS, DECEMBER, 1948, TO MARCH, 1950
(Total Observing Hours = 847)

	Velocity Class														Total
	10	15	20	25	30	35	40	45	50	55	60	65	70	75	
Total no.	9	171	434	793	1368	1945	1415	681	740	1104	1253	759	229	32	10,933

TABLE A2

DECEMBER 10–13, 1948—FACTOR 3

Hour E.S.T.	Velocity Class														To-tals
	10	15	20	25	30	35	40	45	50	55	60	65	70	75	
00–01	1	2	4	4	9	7	6	6	6	8	15	3	2	1	74
01–02	.....	6	3	3	13	13	15	9	12	16	13	4	2	1	110
02–03	.....	1	7	8	6	10	16	6	15	11	5	8	1	1	95
03–04	.....	1	5	9	13	18	12	6	3	18	16	10	3	.....	114
04–05	.....	1	7	10	29	45	21	5	16	19	14	6	3	.....	173
05–06	.....	.....	1	7	35	59	26	8	9	10	15	10	4	1	185
06–07	.....	3	5	7	46	75	7	10	5	11	10	8	5	.....	192
07–08	.....	1	4	8	22	36	4	5	4	10	14	10	3	.....	121
08–09	.....	2	5	4	30	21	1	1	4	7	4	4	2	.....	85
09–10	.....	3	2	4	10	8	2	1	3	.....	.....	1	.....	1	35
10–11	.....	1	.....	6	7	7	.....	1	2	2	3	1	1	1	32
11–12	2	2	1	5	4	1	2	2	3	3	.....	2	.....	.....	27
12–13	Equipment Shut Down from 1200 to 1700 Hours Each Day														
13–14															
14–15															
15–16															
16–17															
17–18	.....	1	1	1	10	7	2	1	1	.....	.....	.....	.....	.....	24
18–19	.....	.....	2	5	14	15	2	2	.....	.....	.....	.....	.....	.....	40
19–20	.....	1	1	3	19	26	6	1	2	.....	.....	.....	.....	.....	59
20–21	.....	.....	4	5	29	50	4	2	1	1	.....	.....	.....	.....	96
21–22	.....	1	1	3	26	53	3	2	1	.....	.....	.....	.....	.....	90
22–23	.....	1	.....	9	34	55	13	4	3	1	2	.....	.....	.....	122
23–24	.....	.....	1	2	27	46	6	6	3	5	.....	.....	.....	.....	96
Totals	3	27	54	103	383	552	148	78	93	122	111	67	23	6	1770

TABLE A3

MARCH 26 AND 30, 1949—FACTOR 2

Hour E.S.T.	Velocity Class														Totals
	10	15	20	25	30	35	40	45	50	55	60	65	70	75	
00–01[2]	.....	.....	1	.....	1	.....	2	.....	2	1	.....	.....	.....	.....	7
01–02[2]	.....	.....	1	2	1	4	1	.....	.....	1	.....	2	1	.....	13
02–03	.....	2	1	.....	2	.....	.....	1	1	1	.....	.....	1	.....	9
03–04	.....	.....	.....	.....	1	3	.....	1	1	1	.....	1	.....	.....	8
04–05	.....	.....	.....	2	1	3	1	.....	.....	.....	1	.....	.....	.....	8
05–06	.....	.....	.....	.....	.....	1	.....	1	.....	3	1	.....	.....	.....	6
06–07	.....	1	.....	.....	.....	3	1	.....	2	2	1	1	2	.....	13
07–08	.....	1	.....	1	1	.....	.....	1	2	1	1	.....	.....	.....	8
08–09															
09–10															
10–11															
11–12	Equipment Shut Down from 0800 to 2400 Hours														
12–13															
13–14															
14–15															
15–16															
16–17															
17–18															
18–19															
19–20															
20–21															
21–22															
22–23															
23–24															
Totals	0	4	3	5	7	14	5	4	8	10	4	4	4	0	72

TABLE A4

APRIL 20–22, 1949—FACTOR 2

Hour E.S.T.	Velocity Class														Totals
	10	15	20	25	30	35	40	45	50	55	60	65	70	75	
00–01	.....	.....	1	6	2	3	4	7	1	1	.....	.....	.....	.....	25
01–02	.....	.....	.....	4	3	6	8	5	1	2	2	2	.....	.....	33
02–03	.....	2	1	5	9	9	6	9	6	6	8	1	.....	.....	62
03–04	1	.....	.....	4	6	7	9	2	3	6	6	3	.....	.....	47
04–05	.....	1	1	6	10	8	7	1	9	3	6	1	2	.....	55
05–06	.....	.....	.....	2	6	7	4	.....	.....	5	12	1	1	1	39
06–07	.....	.....	2	6	4	3	3	.....	.....	5	9	5	.....	.....	37
07–08	.....	1	.....	3	2	7	2	2	.....	2	2	2	.....	.....	23
08–09	.....	1	1	3	3	5	5	4	3	5	4	3	.....	.....	37
09–10[2]	.....	.....	.....	1	1	2	2	2	2	4	8	4	.....	.....	26
10–11[2]	.....	.....	.....	.....	2	4	.....	2	2	1	1	.....	.....	.....	12
11–12[2]	.....	.....	1	2	5	4	1	4	1	4	1	.....	.....	.....	23
12–13	.....	.....	.....	3	5	6	3	2	1	3	1	.....	.....	.....	24
13–14	.....	1	1	3	6	5	1	2	.....	.....	.....	.....	.....	.....	19
14–15[3]	.....	1	1	3	5	3	3	1	.....	.....	.....	.....	.....	.....	17
15–16[2]	.....	.....	1	2	3	2	1	.....	.....	.....	.....	.....	.....	.....	9
16–17[2]	1	1	.....	2	.....	.....	.....	.....	.....	.....	.....	.....	.....	.....	4
17–18	.....	1	.....	.....	2	.....	.....	.....	.....	.....	.....	.....	.....	.....	3
18–19	.....	.....	2	2	.....	.....	1	.....	.....	.....	.....	.....	.....	.....	5
19–20[2]	1	1	4	.....	3	.....	1	.....	.....	.....	.....	.....	.....	.....	10
20–21[2]	.....	1	3	2	1	2	1	3	.....	.....	.....	.....	.....	.....	13
21–22[2]	.....	1	4	7	5	4	4	5	1	1	.....	.....	.....	.....	32
22–23	.....	.....	1	3	4	3	4	6	.....	1	.....	.....	.....	.....	22
23–24	.....	.....	1	6	2	7	4	10	4	.....	.....	.....	.....	.....	34
Totals	3	12	25	75	89	97	74	67	34	49	60	22	3	1	611

TABLE A5

MAY 3–5, 1949—FACTOR 2

HOUR E.S.T.	VELOCITY CLASS														TOTALS
	10	15	20	25	30	35	40	45	50	55	60	65	70	75	
00–01[2]	.....	.....	1	1	6	6	3	2	3	3	.....	.....	.....	.....	25
01–02[2]	.....	.....	1	2	3	2	2	1	3	2	.....	.....	.....	.....	16
02–03	.....	.....	.....	2	4	6	1	1	.....	1	.....	3	.....	.....	18
03–04	.....	2	.....	6	6	6	4	1	1	6	10	7	2	.....	51
04–05	.....	1	3	3	6	8	4	.....	4	3	11	11	1	.....	55
05–06	.....	1	.....	5	4	9	9	3	2	5	13	4	3	.....	58
06–07	.....	1	2	1	4	7	3	1	.....	4	8	10	2	.....	43
07–08	.....	.....	1	1	1	2	1	1	1	.....	.....	2	2	.....	12
08–09	.....	1	1	2	2	3	.....	.....	2	3	19	2	2	.....	37
09–10	.....	2	1	.....	7	3	2	1	1	4	13	9	1	.....	44
10–11	.....	.....	1	1	3	3	4	1	3	2	11	7	.....	.....	36
11–12	.....	.....	.....	.....	5	10	2	.....	4	.....	5	3	.....	.....	29
12–13	.....	.....	.....	.....	1	.....	1	.....	1	1	.....	.....	.....	.....	4
13–14	.....	.....	.....	3	6	5	1	.....	.....	1	1	.....	.....	.....	17
14–15[3]	.....	1	1	1	2	4	3	2	.....	1	.....	.....	.....	.....	15
15–16[2]	.....	.....	.....	2	1	4	2	.....	.....	.....	.....	.....	.....	.....	9
16–17	.....	.....	1	1	.....	.....	.....	.....	.....	.....	.....	.....	.....	.....	2
17–18	.....	.....	.....	2	1	1	1	.....	.....	.....	.....	.....	.....	.....	5
18–19	.....	1	1	3	.....	.....	.....	.....	.....	.....	.....	.....	.....	.....	5
19–20[2]	.....	1	2	3	3	1	.....	.....	.....	.....	.....	.....	.....	.....	10
20–21[2]	.....	.....	3	.....	2	1	.....	.....	.....	.....	.....	.....	.....	.....	6
21–22[2]	.....	1	3	5	2	2	2	.....	.....	.....	.....	.....	.....	.....	15
22–23	.....	1	.....	5	2	3	2	3	.....	1	.....	.....	.....	.....	17
23–24	.....	1	3	7	7	5	2	2	.....	1	.....	.....	.....	.....	28
Totals	0	14	25	56	78	91	49	19	25	38	91	58	13	0	557

TABLE A6

JUNE 27–29, 1949—FACTOR 2

HOUR E.S.T.	VELOCITY CLASS														TOTALS
	10	15	20	25	30	35	40	45	50	55	60	65	70	75	
00–01[2]						1	1	1	1						4
01–02				1	1										2
02–03						1									1
03–04									1		1				2
04–05					2						1	1			4
05–06						1	2					2			5
06–07					1		1		1		2	2	1		8
07–08					1		1	1		2	1	1	1		8
08–09							1	1			1	3			6
09–10						1		1	2	1	2	4	3		14
10–11									2	1		3	1		7
11–12[2]		1		1						1	2	1	1		7
12–13[2]					1				2	1	1	1			6
13–14[2]			1								1				2
14–15				1	2	1									4
15–16					1				1						2
16–17					1										1
17–18[2]				1	1										2
18–19															0
19–20			1			1		1							3
20–21		1	1		1	1	3			1					8
21–22		1			2	2	2	1	1			1			10
22–23					1	1				1					3
23–24[2]				1	1		1		2		2				7
Totals	0	3	3	5	16	10	12	6	13	8	14	19	7	0	116

TABLE A7

JULY 7–8, 1949—FACTOR 1

HOUR E.S.T.	VELOCITY CLASS														TOTALS
	10	15	20	25	30	35	40	45	50	55	60	65	70	75	
00–01[2]	.....	.....	1	.....	1	1	1	.....	.....	4	2	.....	.....	.....	10
01–02	.....	.....	.....	2	.....	5	2	2	4	5	4	4	.....	.....	28
02–03	.....	.....	.....	.....	.....	.....	.....	.....	.....	.....	.....	.....	.....	.....	.....
03–04[1]	.....	1	.....	1	1	6	2	1	1	4	3	3	.....	.....	23
04–05[1]	.....	.....	.....	2	4	3	2	.....	3	3	5	2	1	.....	25
05–06[1]	.....	.....	.....	.....	1	2	2	1	.....	2	2	.....	.....	.....	10
06–07	.....	.....	1	4	1	.....	2	3	1	2	5	5	.....	.....	24
07–08[1]	.....	1	.....	1	.....	1	.....	.....	1	5	5	3	1	.....	18
08–09[1]	.....	.....	.....	.....	.....	.....	.....	.....	.....	1	5	3	.....	.....	9
09–10	.....	.....	.....	1	.....	.....	1	.....	1	1	2	.....	1	.....	7
10–11	.....	.....	.....	.....	.....	.....	2	.....	.....	2	.....	.....	.....	.....	4
11–12	.....	.....	.....	1	1	.....	2	.....	.....	3	1	3	.....	.....	11
12–13	.....	.....	.....	1	.....	3	.....	.....	1	2	1	3	.....	.....	11
13–14	.....	.....	.....	2	.....	2	1	.....	.....	1	.....	.....	.....	.....	6
14–15[2]	.....	.....	.....	2	.....	3	.....	3	.....	.....	.....	.....	.....	.....	8
15–16[2]	.....	.....	1	1	2	2	1	.....	.....	1	.....	.....	.....	.....	8
16–17	.....	.....	.....	2	2	1	2	2	.....	.....	.....	.....	.....	.....	9
17–18	.....	.....	.....	2	1	1	2	.....	.....	.....	.....	.....	.....	.....	6
18–19	.....	.....	1	.....	2	2	2	1	.....	.....	.....	.....	.....	.....	8
19–20	.....	.....	.....	1	1	.....	1	.....	.....	.....	.....	.....	.....	.....	3
20–21	.....	1	.....	1	2	1	3	1	.....	1	.....	.....	.....	.....	10
21–22	.....	.....	2	.....	3	1	1	2	1	.....	.....	1	.....	.....	11
22–23	.....	.....	.....	2	5	5	1	1	2	.....	1	.....	.....	.....	17
23–24[2]	.....	.....	.....	3	1	6	3	3	2	3	2	.....	.....	.....	23
Totals	0	3	6	29	28	45	33	20	17	40	38	27	3	0	289

TABLE A8

JULY 11–13, 1949—FACTOR 2

HOUR E.S.T.	VELOCITY CLASS														TOTALS
	10	15	20	25	30	35	40	45	50	55	60	65	70	75	
00–01[3]	.....	1	1	4	2	11	4	3	2	2	6	6	.....	.....	42
01–02	.....	1	4	3	2	8	6	2	4	3	5	2	.....	.....	40
02–03	.....	.....	1	4	3	5	7	2	.....	10	6	3	1	.....	42
03–04[1]	.....	.....	2	6	6	10	6	2	4	5	7	7	2	.....	57
04–05[1]	.....	.....	3	5	12	11	2	1	4	8	11	.....	3	.....	60
05–06[1]	.....	.....	.....	4	9	8	8	6	5	7	9	9	.....	.....	64
06–07	.....	.....	3	3	11	5	8	3	5	6	7	11	2	.....	64
07–08[1]	.....	1	4	6	2	2	3	2	5	16	12	8	.....	.....	61
08–09[1]	.....	1	2	4	2	3	3	1	4	5	9	7	.....	.....	41
09–10[1]	.....	.....	.....	2	1	.....	.....	1	2	4	7	2	2	.....	21
10–11	1	.....	1	.....	.....	2	.....	1	3	3	9	5	.....	.....	25
11–12	.....	.....	.....	2	2	4	4	.....	1	5	4	2	.....	.....	24
12–13[3]	.....	.....	.....	.....	1	2	4	.....	4	5	1	2	1	1	21
13–14[2]	.....	.....	1	2	1	1	4	.....	1	2	2	1	1	.....	16
14–15	.....	.....	2	6	4	9	6	.....	1	2	1	.....	.....	.....	31
15–16	.....	.....	2	2	6	4	5	1	.....	2	.....	.....	.....	.....	22
16–17	.....	.....	2	.....	1	3	3	.....	.....	1	.....	.....	.....	.....	10
17–18	.....	.....	2	1	2	3	2	1	2	.....	.....	.....	.....	.....	13
18–19	.....	.....	1	3	2	4	5	.....	.....	.....	.....	.....	.....	.....	15
19–20	.....	1	2	.....	7	5	3	1	1	.....	.....	.....	.....	.....	20
20–21	.....	.....	2	4	3	6	4	1	1	.....	.....	.....	.....	.....	21
21–22	.....	.....	3	1	7	13	8	2	4	2	.....	.....	.....	.....	40
22–23	.....	.....	3	7	4	14	6	3	4	4	3	1	1	.....	50
23–24[2]	.....	.....	2	6	5	7	4	.....	5	3	7	.....	.....	.....	39
Totals	1	5	43	75	95	140	105	32	62	95	106	66	13	1	839

TABLE A9

JULY 18–20, 1949—FACTOR 2

HOUR E.S.T.	VELOCITY CLASS														TOTALS
	10	15	20	25	30	35	40	45	50	55	60	65	70	75	
00–01[2]	.....	.....	.....	1	8	7	11	2	3	4	7	1	.....	.....	44
01–02	.....	.....	3	4	6	6	10	1	4	7	11	9	3	1	65
02–03	.....	.....	2	2	5	10	8	3	1	4	4	12	3	.....	54
03–04[1]	.....	.....	3	4	7	21	13	6	2	3	6	7	2	.....	74
04–05[1]	.....	.....	1	1	5	9	6	2	5	3	2	3	.....	.....	37
05–06	.....	.....	1	.....	3	3	1	2	3	1	7	1	1	.....	23
06–07[1]	.....	1	1	4	5	4	5	3	4	3	7	3	1	.....	41
07–08[1]	.....	.....	2	.....	.....	5	3	1	4	3	5	5	1	.....	29
08–09[1]	.....	1	2	1	1	2	1	3	2	5	7	2	1	.....	28
09–10	1	.....	.....	1	.....	.....	2	1	3	5	4	5	1	.....	23
10–11	.....	.....	.....	.....	.....	.....	1	.....	1	3	1	3	.....	.....	9
11–12	.....	.....	.....	1	.....	1	3	.....	1	2	7	3	.....	.....	18
12–13[2]	.....	.....	.....	.....	.....	2	6	2	3	2	2	3	.....	.....	20
13–14[2]	.....	1	.....	.....	1	2	4	.....	2	1	1	1	.....	.....	13
14–15	.....	.....	1	.....	3	8	5	4	.....	1	.....	.....	.....	.....	22
15–16	.....	1	2	1	2	2	2	2	.....	.....	.....	.....	.....	.....	12
16–17	.....	.....	1	.....	2	3	3	1	.....	1	.....	.....	1	.....	12
17–18	.....	1	1	.....	2	1	1	1	.....	.....	.....	.....	.....	.....	7
18–19	.....	2	2	3	1	1	5	.....	.....	.....	.....	.....	.....	.....	14
19–20	.....	.....	.....	2	2	3	3	1	.....	.....	.....	.....	.....	.....	11
20–21	.....	.....	2	.....	1	1	3	.....	1	1	.....	.....	.....	.....	9
21–22	.....	.....	1	6	3	7	9	6	1	1	1	.....	.....	.....	35
22–23[2]	.....	1	1	2	3	1	8	4	3	5	1	3	.....	.....	32
23–24[2]	.....	1	.....	.....	2	5	9	1	1	3	5	1	1	.....	29
Totals	1	9	26	33	62	104	122	46	44	58	78	62	15	1	661

TABLE A10

JULY 26–29, 1949—FACTOR 3

HOUR E.S.T.	VELOCITY CLASS														TOTALS
	10	15	20	25	30	35	40	45	50	55	60	65	70	75	
00–01	.....	2	3	5	7	17	54	8	14	15	18	4	2	.....	149
01–02	.....	1	3	3	13	31	68	15	13	17	14	12	8	2	200
02–03	.....	.....	.....	6	6	20	50	8	2	12	9	12	3	.....	128
03–04	.....	3	5	5	14	24	37	15	7	10	7	7	3	1	138
04–05	.....	1	10	7	17	33	47	13	10	14	15	6	.....	.....	173
05–06	.....	2	3	4	10	27	41	14	12	12	10	9	2	2	148
06–07	.....	3	8	6	15	24	25	15	5	11	14	8	.....	.....	134
07–08	1	4	3	6	10	10	8	9	7	12	12	9	3	.....	94
08–09	.....	4	2	3	5	5	1	3	4	7	9	4	3	1	51
09–10	.....	1	3	1	1	1	.....	1	1	4	5	4	1	.....	23
10–11	.....	1	1	.....	.....	.....	5	1	4	4	6	1	.....	.....	23
11–12	.....	.....	.....	2	3	4	2	2	.....	9	7	3	1	.....	33
12–13	.....	.....	1	3	.....	2	2	1	3	3	6	4	1	.....	26
13–14	.....	.....	.....	1	.....	.....	.....	1	.....	.....	.....	2	.....	.....	4
14–15	.....	.....	.....	.....	.....	.....	1	.....	.....	1	1	.....	.....	.....	3
15–16	.....	.....	.....	.....	1	1	2	1	.....	1	1	.....	.....	.....	7
16–17	.....	1	1	1	.....	1	2	1	.....	.....	1	.....	.....	.....	8
17–18	.....	1	3	3	2	3	6	1	1	1	.....	.....	.....	.....	21
18–19	.....	.....	2	1	3	2	4	1	1	.....	1	.....	.....	.....	15
19–20	.....	.....	1	1	2	4	3	1	1	.....	.....	.....	.....	.....	13
20–21	.....	.....	4	4	9	7	5	2	1	1	3	.....	.....	.....	36
21–22	.....	.....	4	5	9	9	10	5	2	5	3	1	.....	.....	53
22–23	.....	.....	3	5	5	15	28	7	7	7	5	2	.....	.....	84
23–24	.....	.....	4	3	9	15	34	4	9	4	8	3	4	.....	97
Totals	1	24	64	85	141	255	435	129	94	150	155	91	31	6	1661

TABLE A11

AUGUST 11–14, 1949—FACTOR 3

HOUR E.S.T.	VELOCITY CLASS														TOTALS
	10	15	20	25	30	35	40	45	50	55	60	65	70	75	
00–01	.....	1	4	2	2	9	3	3	8	23	26	10	.....	.....	91
01–02	.....	.....	1	3	4	6	3	5	2	8	18	8	4	.....	62
02–03	.....	1	1	.....	7	12	6	4	5	19	22	8	4	.....	89
03–04	.....	1	2	7	5	13	7	6	3	12	8	11	2	.....	77
04–05	.....	1	1	2	7	15	7	4	12	11	15	6	.....	.....	81
05–06	.....	.....	1	3	1	7	2	1	4	6	5	5	1	.....	36
06–07	.....	.....	.....	1	4	4	5	2	4	5	6	1	1	.....	33
07–08	.....	.....	1	.....	4	.....	4	2	5	7	15	10	3	1	52
08–09	.....	.....	3	1	2	.....	1	6	10	9	10	11	.....	1	54
09–10	.....	1	.....	.....	1	3	2	2	5	14	23	6	1	.....	58
10–11	.....	1	.....	2	1	.....	.....	2	2	4	10	2	.....	.....	24
11–12	.....	.....	1	.....	1	.....	1	1	2	12	12	6	1	.....	37
12–13	.....	.....	.....	1	.....	1	.....	4	4	9	7	1	1	.....	28
13–14	.....	.....	2	.....	1	1	2	.....	2	7	7	1	1	.....	24
14–15	.....	.....	1	1	3	.....	1	.....	1	2	2	1	.....	.....	12
15–16	.....	1	1	1	.....	3	2	.....	2	1	1	.....	.....	.....	12
16–17	.....	.....	1	.....	2	3	2	3	.....	6	2	.....	.....	.....	19
17–18	.....	.....	.....	.....	1	.....	1	.....	2	4	2	1	.....	.....	11
18–19	.....	.....	.....	1	.....	2	1	.....	2	1	1	.....	.....	.....	8
19–20	.....	.....	1	2	1	2	2	2	2	6	4	.....	.....	.....	22
20–21	.....	.....	1	.....	1	1	2	.....	1	5	3	.....	.....	.....	14
21–22	.....	1	3	4	5	12	10	1	3	7	5	3	.....	.....	54
22–23	.....	.....	1	3	2	5	6	.....	4	10	14	2	.....	.....	47
23–24	.....	.....	1	7	10	7	6	3	6	28	13	13	1	.....	95
Totals	0	8	27	41	65	106	76	51	91	216	231	106	20	2	1040

TABLE A12

AUGUST 22–24, 1949—FACTOR 2

HOUR E.S.T.	VELOCITY CLASS														TOTALS
	10	15	20	25	30	35	40	45	50	55	60	65	70	75	
00–01	.....	.....	4	2	5	9	6	4	5	12	17	5	5	1	75
01–02	.....	.....	2	8	5	17	7	3	18	7	24	9	4	.....	104
02–03[1]	.....	1	3	10	10	14	8	5	13	15	17	20	8	.....	124
03–04[1]	.....	.....	5	3	11	16	13	6	1	12	10	14	6	4	101
04–05	.....	2	2	8	13	14	14	11	12	8	12	11	2	1	110
05–06	.....	.....	4	5	7	14	11	10	9	6	21	7	.....	.....	94
06–07	.....	.....	2	5	4	16	7	9	14	10	8	7	3	1	86
07–08	.....	2	1	2	.....	2	8	1	2	5	9	5	1	.....	38
08–09[1]	.....	.....	4	5	.....	2	2	1	4	5	10	5	2	.....	40
09–10[1]	.....	.....	2	.....	.....	1	1	1	3	4	5	5	3	.....	25
10–11[1]	.....	1	1	.....	2	2	2	.....	.....	5	6	2	1	1	23
11–12	.....	1	2	1	2	2	3	1	2	3	6	.....	2	.....	25
12–13	.....	.....	.....	.....	1	1	2	1	2	5	3	2	1	.....	18
13–14[2]	.....	1	2	1	3	1	3	1	2	2	1	.....	.....	.....	17
14–15[2]	.....	1	2	4	1	5	4	6	.....	.....	.....	1	.....	.....	24
15–16	.....	1	3	1	1	4	3	2	1	4	.....	.....	.....	.....	20
16–17	.....	2	4	2	1	3	1	1	4	1	.....	.....	.....	.....	19
17–18	.....	1	1	.....	2	3	2	2	1	.....	.....	.....	.....	.....	12
18–19	.....	1	4	3	2	3	4	.....	1	2	.....	.....	.....	.....	20
19–20	.....	.....	.....	1	3	6	1	3	2	2	1	.....	.....	.....	19
20–21	.....	.....	1	2	2	3	2	.....	.....	1	.....	.....	.....	.....	11
21–22	.....	.....	3	1	10	4	3	3	3	1	5	1	.....	.....	34
22–23[2]	.....	.....	.....	3	1	4	2	2	1	5	2	2	.....	.....	22
23–24[2]	.....	3	3	1	4	9	4	2	7	3	5	3	2	.....	46
Totals	0	17	55	68	90	155	113	75	107	118	162	99	40	8	1107

TABLE A13

SEPTEMBER 19–21, 1949—FACTOR 2

Hour E.S.T.	Velocity Class														Totals
	10	15	20	25	30	35	40	45	50	55	60	65	70	75	
00–01							2		3	3	4	2	1		15
01–02[1]			1	3	1	1	3	5	4	3	8	6	2		37
02–03[1]				4	2	1	1		2	1	5	1			17
03–04[1]				2	4	4	1			4	2	3	1		21
04–05			1	2	1	4	3	5	2	4	2	2	1		27
05–06		1			1	2	3			3	4	2	1	2	19
06–07				2			2		2	3	5	1			15
07–08			1			2		1		1	5		2		12
08–09[1]		1								3	1				5
09–10[1]						1						1			2
10–11												2	1		3
11–12					1	1					2	1			5
12–13[2]											1		1		2
13–14[2]					1			1				2			4
14–15[2]							1								1
15–16											1				1
16–17															0
17–18							1								1
18–19									1						1
19–20			1												1
20–21						2	3		1		1				7
21–22[2]					1					2					3
22–23[2]				1	1		1	2	3		3				11
23–24[2]			1	2	2			1	5	2	2	4			19
Totals	0	2	5	16	15	18	21	15	23	29	46	27	10	2	229

TABLE A14

OCTOBER 20–22, 1950—FACTOR 2

Hour E.S.T.	Velocity Class														Totals
	10	15	20	25	30	35	40	45	50	55	60	65	70	75	
00–01			1			1			1	1	5	9	4		22
01–02[1]					2					1	3	3	1		10
02–03[1]					2		4	2	4		2	2	2		18
03–04[1]		1	1	3	6	4	3	2	3	1	5	4		2	35
04–05			1	2	5		3	3	2	6	5	2	1		30
05–06					5	1	2			1	1	3	1		14
06–07[1]											1		1		2
07–08[1]						1				1					2
08–09[1]								1			2	1	1		5
09–10				1						1		1	1		4
10–11															
11–12															
12–13	Equipment Shut Down from 1000 to 1500 Hours Each Day														
13–14															
14–15															
15–16		1				1									2
16–17				1				1	1		1				4
17–18				1	1				1						3
18–19				1		1	1		1		1				5
19–20				1	2			1							4
20–21					1			1		1					3
21–22[2]					1				1						2
22–23[2]							2			2	3	1			8
23–24						1			1			3			5
Totals	0	2	3	10	25	10	15	11	15	15	29	29	12	2	178

TABLE A15

NOVEMBER 15–17, 1949—FACTOR 2

HOUR E.S.T.	VELOCITY CLASS														TOTALS
	10	15	20	25	30	35	40	45	50	55	60	65	70	75	
00–01	.....	.....	.....	2	.....	8	1	1	3	4	2	1	2	.....	24
01–02	.....	.....	1	2	2	1	5	1	4	4	3	3	3	.....	29
02–03[1]	.....	2	3	3	2	4	5	1	6	10	8	4	3	1	52
03–04[1]	.....	1	3	4	1	4	1	3	3	10	4	1	4	.....	39
04–05	.....	2	.....	4	5	1	3	.....	.....	2	2	4	1	.....	24
05–06	.....	1	2	1	1	2	3	2	.....	5	1	1	.....	.....	19
06–07	.....	.....	3	4	1	2	.....	3	2	2	3	2	.....	1	23
07–08[1]	.....	.....	.....	2	1	3	.....	2	.....	2	4	2	1	.....	17
08–09[1]	.....	.....	.....	.....	.....	.....	.....	.....	1	.....	1	1	.....	.....	3
09–10	.....	.....	.....	.....	.....	.....	.....	.....	.....	.....	.....	1	1	.....	2
10–11	.....	.....	.....	.....	1	.....	.....	.....	.....	.....	.....	.....	1	.....	2
11–12[2]	.....	.....	.....	.....	.....	.....	.....	.....	.....	.....	.....	.....	1	.....	1
12–13[2]	.....	.....	.....	.....	.....	.....	.....	.....	.....	.....	.....	.....	.....	.....	0
13–14[2]	.....	.....	.....	.....	1	.....	.....	.....	.....	.....	1	.....	.....	.....	2
14–15	.....	.....	.....	1	.....	.....	.....	.....	.....	.....	.....	.....	.....	.....	1
15–16	.....	.....	1	.....	.....	.....	.....	1	.....	.....	.....	.....	.....	.....	2
16–17	.....	1	.....	.....	.....	.....	1	1	.....	.....	.....	.....	.....	.....	3
17–18	.....	.....	.....	.....	2	.....	.....	.....	2	.....	.....	.....	.....	.....	4
18–19	.....	.....	.....	2	.....	.....	.....	.....	1	.....	.....	.....	.....	.....	3
19–20	.....	.....	.....	5	2	4	2	1	.....	.....	.....	1	.....	.....	15
20–21	.....	.....	.....	.....	1	1	1	3	.....	1	1	.....	.....	.....	8
21–22[2]	.....	.....	.....	.....	5	2	5	3	2	1	.....	.....	.....	.....	18
22–23[2]	.....	.....	.....	.....	.....	2	1	1	.....	.....	1	1	.....	.....	6
23–24[2]	.....	.....	.....	.....	2	1	2	1	2	.....	3	.....	.....	.....	11
Totals	0	7	13	30	27	35	30	24	26	41	34	22	17	2	308

TABLE A16

DECEMBER 12–15, 1949—FACTOR 3

HOUR E.S.T.	VELOCITY CLASS														TOTALS
	10	15	20	25	30	35	40	45	50	55	60	65	70	75	
00–01	.....	2	1	4	1	2	5	3	3	5	12	6	.....	.....	44
01–02	.....	.....	.....	1	5	4	9	3	5	6	10	13	4	1	61
02–03	.....	.....	3	.....	.....	3	4	3	3	9	5	8	5	.....	43
03–04															
04–05															
05–06															
06–07															
07–08															
08–09															
09–10	Equipment Shut Down from 0300 to 1700 Hours Each Day														
10–11															
11–12															
12–13															
13–14															
14–15															
15–16															
16–17															
17–18	.....	.....	1	1	3	2	1	.....	.....	1	.....	.....	.....	.....	9
18–19	.....	2	2	1	8	17	2	.....	1	.....	.....	.....	.....	.....	33
19–20	.....	.....	1	5	9	33	4	2	.....	1	.....	.....	.....	.....	55
20–21	.....	.....	1	3	14	30	3	1	1	2	.....	.....	.....	.....	55
21–22	.....	.....	.....	2	11	28	2	.....	.....	3	.....	.....	.....	.....	46
22–23	.....	1	.....	3	14	30	10	6	4	8	2	1	.....	.....	79
23–24	.....	.....	.....	1	2	11	5	2	2	4	2	2	.....	.....	31
Totals	0	5	9	21	67	160	45	20	19	39	31	30	9	1	456

TABLE A17

JANUARY 19–21, 1950—FACTOR 2

HOUR E.S.T.	VELOCITY CLASS														TOTALS
	10	15	20	25	30	35	40	45	50	55	60	65	70	75	
00–01[2]			1	1	4	4	2	3	1						16
01–02[2]		2	2	3	7	10	4	1	3	1	2				35
02–03			2	8	6	8	10	4	5						43
03–04			3	4	9	10	12	3	5	3	3	1			53
04–05			5	5	10	9	7	6	3	4	1	1			51
05–06		1	4	2	5	1	3	8		3	2	2			31
06–07				2	4	1		1		2			1		11
07–08		1	1	1	5	1		1	2	4	3	1			20
08–09		2	2	2	2				2						10
09–10		2	1		2	2	1			1					9
10–11		1	2	2	2	1	1			2					11
11–12[2]				3	3		4	1		1					12
12–13[2]		1	1	7	3		2	4							18
13–14			3	2	2			1	2						10
14–15			1				2								3
15–16[2]				3		1	1								5
16–17[2]				1	4										5
17–18			2	2	1										5
18–19		2	1		1		1								10
19–20[2]		2	1	3	3		1								7
20–21[2]			1	3	2	1									3
21–22					1	1		1							12
22–23		1	1		3	4	2		1						9
23–24				1	1		4	1	1	1					
Totals	0	15	34	55	80	54	57	35	25	22	11	5	1	0	394

TABLE A18

FEBRUARY 16–18, 1950—FACTOR 2

HOUR E.S.T.	VELOCITY CLASS														TOTALS
	10	15	20	25	30	35	40	45	50	55	60	65	70	75	
00–01		1		3	4	8	5	1	3	2					27
01–02[2]			2	4	5	6	2	6	5	3	1	2			36
02–03[2]			3	2	1	2	6	2	5	2	5	4	2		34
03–04				7	4	6	4	7	5	3	2	3			41
04–05			4	4	3	6	3	3	2	5	8	1			39
05–06			2	1	4	6	4	3	2	2	6	4	1		35
06–07		2	1	4	4	4	4	1	4	6	5	1	2		38
07–08		1		3	5	8	3	1	1	3	9	3	2		39
08–09			2	7	2	5	6	5	2	12	6	2			49
09–10		1	1	2	4	1	2	3	2	3	1	1	1		22
10–11			1	1		2	4				1				9
11–12[2]					1				2	1					4
12–13[2]					2		2				1				5
13–14			1	1	2	2	1								7
14–15[2]					1										1
15–16[2]		1	2	1	2	1						1			8
16–17[2]				1	2										3
17–18		1		1		1									3
18–19			2	2	1										5
19–20			1	1	3	1									6
20–21[2]		1	1	1	1	1		1							6
21–22[2]		1	5	3	5	3	2	1							20
22–23[2]		1	2	5	4	3	5	1	1	1					23
23–24				5	3	4	3	1	2	1					19
Totals	0	10	30	59	63	70	56	36	36	44	45	22	8	0	479

TABLE A19

MARCH 16–18, 1950—FACTOR 2

HOUR E.S.T.	VELOCITY CLASS														TOTALS
	10	15	20	25	30	35	40	45	50	55	60	65	70	75	
00–01[3]		1		2	1	2	3	1	1						11
01–02[3]		1		3		2			1						7
02–03				1		2	3	1			1				8
03–04				1	3	1	1				2				8
04–05				3	2	2	1	1	3	2	1				15
05–06			1	2	2	3	1	1							10
06–07			1	2	2	2	1	1			1				10
07–08					1	1		1	1	1		1			6
08–09		1		1	2		2	1		1		1			9
09–10[3]						2		1	2	2	1				8
10–11[3]						1	3	2		1					7
11–12[3]				2	3		1	2			1	1			10
12–13					4	4				2					10
13–14			3		4	1		1							9
14–15[3]				1	1										2
15–16[3]					1	2									3
16–17			3	1			1								5
17–18		1													1
18–19			1			1									2
19–20					1										1
20–21[3]				2	1	2									5
21–22[3]				2	5	1	1								9
22–23[3]				4	2		1			1					8
23–24[3]					2										2
Totals	0	4	9	27	37	29	19	13	8	10	7	3	0	0	166

A GRATING MAP OF THE SOLAR SPECTRUM FROM 3.0 TO 5.2 MICRONS*

J. H. SHAW, R. M. CHAPMAN,† J. N. HOWARD, AND M. L. OXHOLM
Mendenhall Laboratory of Physics, Ohio State University
Received August 9, 1950

ABSTRACT

An account is given of the infrared solar spectrum from 3.0 μ to 5.2 μ obtained at the Ohio State University with a high-resolution, Pfund-type grating spectrometer of 1 meter focal length and a relative aperture of $f/5$. A Perkin-Elmer thermocouple and thirteen-cycle-per-second amplifier were used in the detecting system. Many features of the spectrum are discussed, and a map is presented, together with a table of wave lengths, frequencies, and line identifications where possible. Among the bands and lines identified are those of H_2O, HDO, CO_2, CO, CH_4, and N_2O.

INTRODUCTION

The solar spectrum has been under investigation since Newton found in 1666 that a band of colors is produced when a prism is placed in a beam of sunlight and since the further discovery by Sir William Herschel[1] that energy existed beyond both the red and the violet ends of the visible spectrum. The spectrum from 0.29 μ to 1.3 μ, which is easily accessible with photographic techniques, has been studied under very high resolution by many investigators, and, with the increase in sensitivity of infrared detectors, there has recently been a renewed interest in the spectrum from 2 μ to 14 μ. Although few solar lines have been observed in this region, it is very rich in telluric lines, since the intense fundamental vibration-rotation bands of almost all polyatomic and polar diatomic gases occur here. Thus, an analysis of the solar spectrum can be used as a sensitive method of detecting small quantities of such gases in the earth's atmosphere.

Among early workers, S. P. Langley[2] published a map from the visible to 5.5 μ obtained with a rock-salt prism. A. Adel[3] repeated this work and extended the spectrum, first as far as 14 μ, where an intense carbon dioxide fundamental band gives complete absorption, and later as far as 24 μ.[4] Adel[5] has also published a map taken with a grating instrument of the region between 6.8 μ and 14.0 μ, together with a list of frequencies of the lines observed.

During the past few years a series of observations has been made at the McMath-Hulbert Observatory of the University of Michigan by R. R. McMath and his associates[6] on the solar spectrum from the visible region to 3.6 μ, with the use of lead sulphide cell detectors. They have obtained a resolution comparable with that in the visible region and have identified many new solar lines and atmospheric bands.

Although other workers have observed bands from 3.5 μ to 5.5 μ, no complete grating map of this region of the infrared solar spectrum has been published. It is the purpose of

* This work was supported in part by Contract No. AF19(122)65 between the U.S. Air Force and the Ohio State University Research Foundation, through the sponsorship of the Geophysical Research Directorate, Air Force Cambridge Research Laboratories.

† Now at the AF Geophysical Research Laboratory, Cambridge, Mass.

[1] *Phil. Trans. R. Soc. London, A*, **90**, 284, 1800.

[2] *Ann. Ap. Obs., Smithsonian Institution*, **1**, 1, 1900.

[3] *Ap. J.*, **87**, 198, 1938; **91**, 1, 481, 1940; **93**, 506, 1941.

[4] *Ap. J.*, **96**, 239, 1942; *J. Opt. Soc. America*, **37**, 769, 1947.

[5] *Ap. J.*, **94**, 451, 1941.

[6] R. R. McMath, O. C. Mohler, L. Goldberg, and A. K. Pierce. See series of papers in *Phys. Rev.*, *Ap. J.*, and *J. Opt. Soc. America*, beginning 1947.

this paper to present a map and frequency table, together with identifications of many of the lines observed in this region at Columbus, Ohio (latitude 40° N., elevation 800 feet above M.S.L.).

This work is a continuation of a program of investigation of atmospheric transmission in the infrared and of identification of atmospheric constituents, begun by Dr. M. V. Migeotte (now at the Institut d'Astrophysique de Cointe-Sclessin, Belgium) in 1947 at the Ohio State University, Columbus, Ohio. He used the apparatus described below to map the solar spectrum from 2 μ to 12 μ and identified many bands in the spectra he obtained, including a fundamental of methane at 3.3 μ,[7] three bands of nitrous oxide at 3.9 μ, 4.5 μ, and 8.6 μ,[8] and the fundamental of carbon monoxide at 4.7 μ.[9]

APPARATUS AND EXPERIMENTAL TECHNIQUE

A schematic drawing of the optical train is presented in Figure 1. The coelostat is patterned after one used at the University of Liége, Belgium, and, except for its two 12-inch-diameter plane mirrors, was constructed in our Physics Department machine shop. The lower of the two mirrors is rotated about an axis in its surface parallel to the earth's axis at the rate of one revolution in 48 hours, and so constantly directs solar radiation to the upper mirror for reflection down an 8-foot steel tube to the spectrometer room. Here the beam is reflected by another plane mirror to a 10-inch-diameter, off-axis paraboloid of 1 meter focal length. This produces an image of the sun about ½ inch in diameter on the entrance slit of the spectrometer after a further reflection by a small plane mirror.

The spectrometer was designed and built in 1946 by Dr. R. H. Noble under the supervision of Professor H. H. Nielsen. Inspection of Figure 1 will show that it is basically of conventional design with a *NaCl* prism monochromator for the isolation of various spectral regions preceding the Pfund-type grating section. The paraboloidal mirrors used for collimating and focusing in the grating section are 20 cm in diameter and have a focal length of 1 meter. Two gratings, placed back to back, can be put in the grating holder, which is mounted on a turntable with a very accurately centered conical bearing and divided circle. The maximum eccentricity of the divided circle is 30 seconds of arc, measured as the difference in reading, minus 180°, of two microscopes initially set on a line through the center of rotation and the center of calibration of the circle.

A reduced image of the exit slit is formed on the detector by an elliptical mirror with a 5½-to-1 reduction ratio. The detector used was a Perkin-Elmer thermocouple, and the signal was amplified with a Perkin-Elmer thirteen-cycle-per-second amplifier and chopping system. The grating and prism are rotated, and the slit widths changed, by Selsyn motors operated from a control panel outside the instrument housing.

A Brown recording potentiometer with a full-scale deflection of 10 millivolts and a paper speed of ½ inch per minute was used to map the spectrum. Fiduciary marks were made on the chart paper by a mechanical trigger device operated by an observer viewing coincidences of the grating circle markings with a graduated scale in the eyepiece of a microscope. Most of this work was done with a 7200-line-per-inch replica echelette grating (dimensions 5.5″ long × 4″ high). The conversion of angular rotation of the grating, as marked on the recording charts, to wave length was made by applying the formula

$$n\lambda = K \sin \theta ,$$

where n is the grating order, λ the wave length, K a constant of the grating, and θ the angular displacement of the grating from the central image. The value K was determined

[7] *Phys. Rev.*, **73**, 519, 1948; *Ap. J.*, **107**, 400, 1948.

[8] *A.J.*, **54**, 45, 1948.

[9] *Phys. Rev.*, **75**, 1108, 1949.

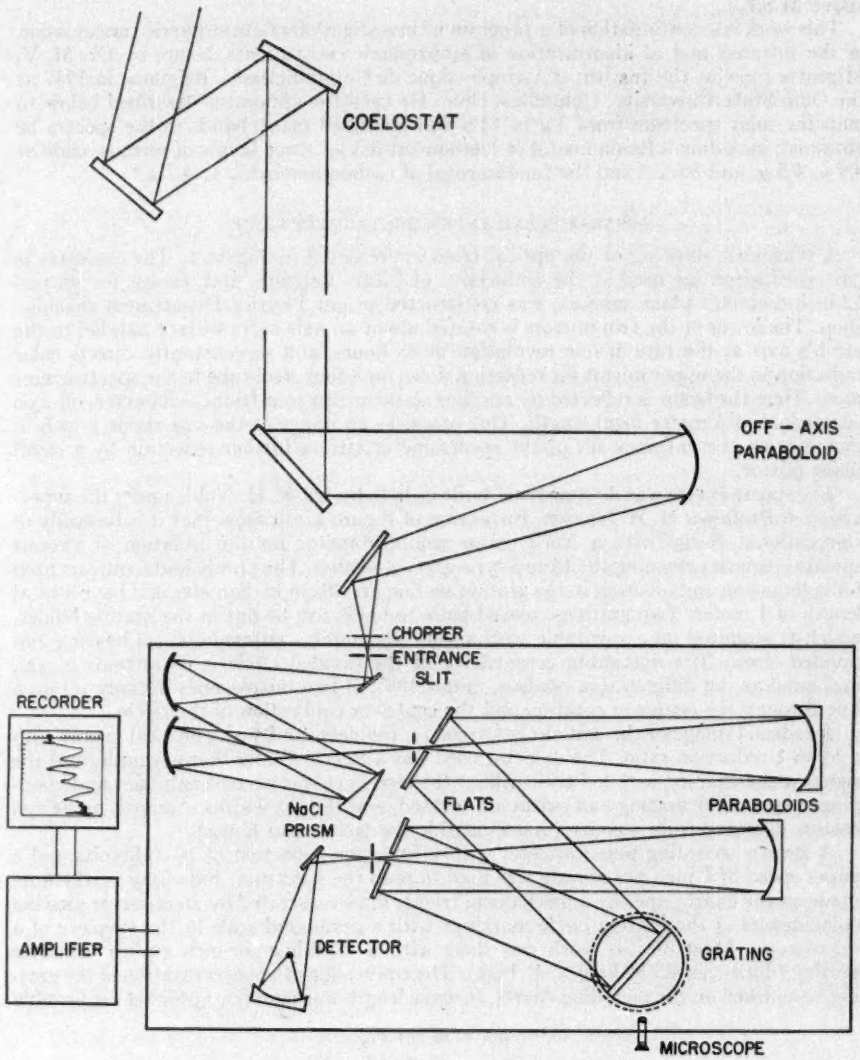

FIG. 1.—Schematic diagram of the apparatus

from measurements of the various higher orders of mercury-arc lines at 0.546073, 0.5769598, 0.5790659, and 1.013975 μ from both a low-pressure and a high-pressure mercury arc. Where the intensities of these lines were too small to measure with the thermocouple, a lead sulphide cell or a photomultiplier tube was used. The absolute accuracy of the value of the grating constant is believed to be one part in 60,000, giving an accuracy of one part in 30,000 for the wave lengths of lines measured.

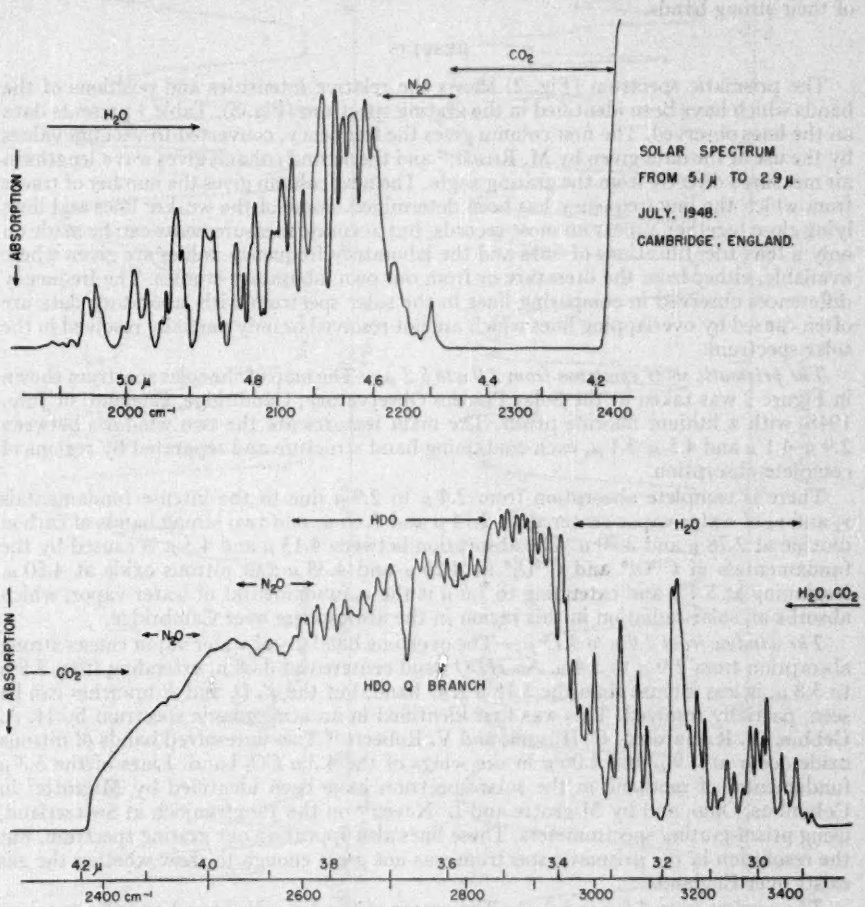

FIG. 2.—The prismatic solar spectrum

Laboratory spectra of weak bands have been obtained with a 1-meter, large-aperture, multiple-traversal absorption cell of the White type,[10] with a path length which can be varied in steps of 4 meters from 4 to 60 meters. The identifications of some of the lines in the solar spectrum have been made by comparison with spectra taken with this and other smaller absorption cells.

[10] J. U. White. *J. Opt. Soc. America*, **32**, 285, 1942.

In addition, we are fortunate in having a small-aperture, 22-meter, multiple-traversal absorption cell similar to that described by H. J. Bernstein and G. Herzberg.[11] The construction and design of the cell was started by M. V. Migeotte in 1948 and recently finished by R. B. Murray. The cell can be completely evacuated and is to be used for obtaining low-dispersion spectra of weak bands of gases in the infrared and also to detect small quantities of gases in the atmosphere near ground level by measuring the intensities of their strong bands.

RESULTS

The prismatic spectrum (Fig. 2) shows the relative intensities and positions of the bands which have been identified in the grating spectrum (Fig. 3). Table 1 presents data on the lines observed. The first column gives the frequency, converted to vacuum values by the use of the data given by M. Rusch,[12] and the second column gives wave lengths in air measured directly from the grating angle. The next column gives the number of traces from which the line frequency has been determined. Some of the weaker lines and lines lying close together appear on most records, but accurate measurements can be made on only a few. Identifications of lines and the laboratory frequency values are given where available, either from the literature or from our own laboratory studies. The frequency differences observed in comparing lines in the solar spectrum with laboratory data are often caused by overlapping lines which are not resolved or only partially resolved in the solar spectrum.

The prismatic solar spectrum from 2.9 μ to 5.2 μ.—The map of the solar spectrum shown in Figure 2 was taken at the Solar Physics Observatory, Cambridge, England, in July, 1948, with a lithium fluoride prism. The main features are the two windows between 2.9 μ–4.1 μ and 4.5 μ–5.1 μ, each containing band structure and separated by regions of complete absorption.

There is complete absorption from 2.4 μ to 2.9 μ due to the intense fundamentals ν_1 and ν_3 of water vapor centered at 2.74 μ and 2.66 μ, and two strong bands of carbon dioxide at 2.78 μ and 2.70 μ. The absorption between 4.15 μ and 4.5 μ is caused by the fundamentals of $C^{12}O_2^{16}$ and $C^{13}O_2^{16}$ at 4.26 μ and 4.38 μ and nitrous oxide at 4.50 μ. Beginning at 5.1 μ and extending to 7.6 μ is the ν_2 fundamental of water vapor, which absorbs all solar radiation in this region in the atmosphere over Cambridge.

The window from 2.9 μ to 4.15 μ.—The overtone band $2\nu_2$ of water vapor causes strong absorption from 2.9 μ to 3.4 μ. An *HDO* band centered at 3.68 μ, extending from 3.5 μ to 3.8 μ, is less intense than the 3.18 μ H_2O band, but the *P*, *Q*, and *R* branches can be seen, partially resolved. This was first identified in an atmospheric spectrum by H. A. Gebbie, W. R. Harding, C. Hilsum, and V. Roberts.[13] Two unresolved bands of nitrous oxide occur at 3.9 μ and 4.06 μ in the wings of the 4.3 μ CO_2 band. Lines of the 3.3 μ fundamental of methane in the solar spectrum have been identified by Migeotte[7] in Columbus, Ohio, and by Migeotte and L. Neven[14] on the Jungfraujoch in Switzerland, using prism-grating spectrometers. These lines also appear on our grating spectrum, but the resolution in the prismatic spectrum was not great enough to show whether the gas exists over England.

The window from 4.5 μ to 5.2 μ.—The center of the 4.5 μ N_2O band and the envelope of the *P* branch can be seen on the short-wave-length side. The structure in the window consists partly of some lines of water vapor, and there is a weak band of CO_2 near 4.8 μ.

Lines of the 4.7 μ fundamental of carbon monoxide have been observed by Migeotte in Columbus, Ohio,[9] and by Migeotte and Neven in Switzerland,[15] and also appear in the

[11] *J. Chem. Phys.*, **16**, 30, 1948.

[12] *Ann. d. Phys.*, **70**, 373, 1923.

[13] *Phys. Rev.*, **76**, 1534, 1949.

[14] Private communication.

[15] *Physica*, Vol. **16**, June, 1950.

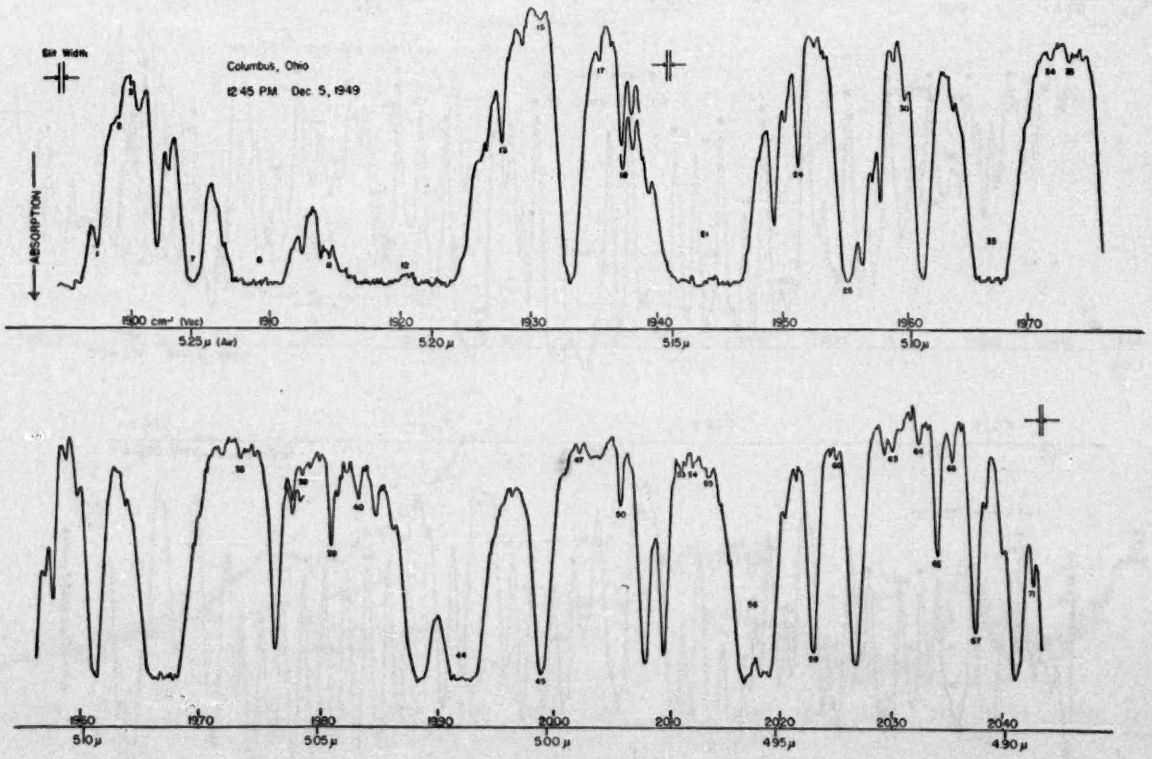

FIG. 3*a*.—The grating map

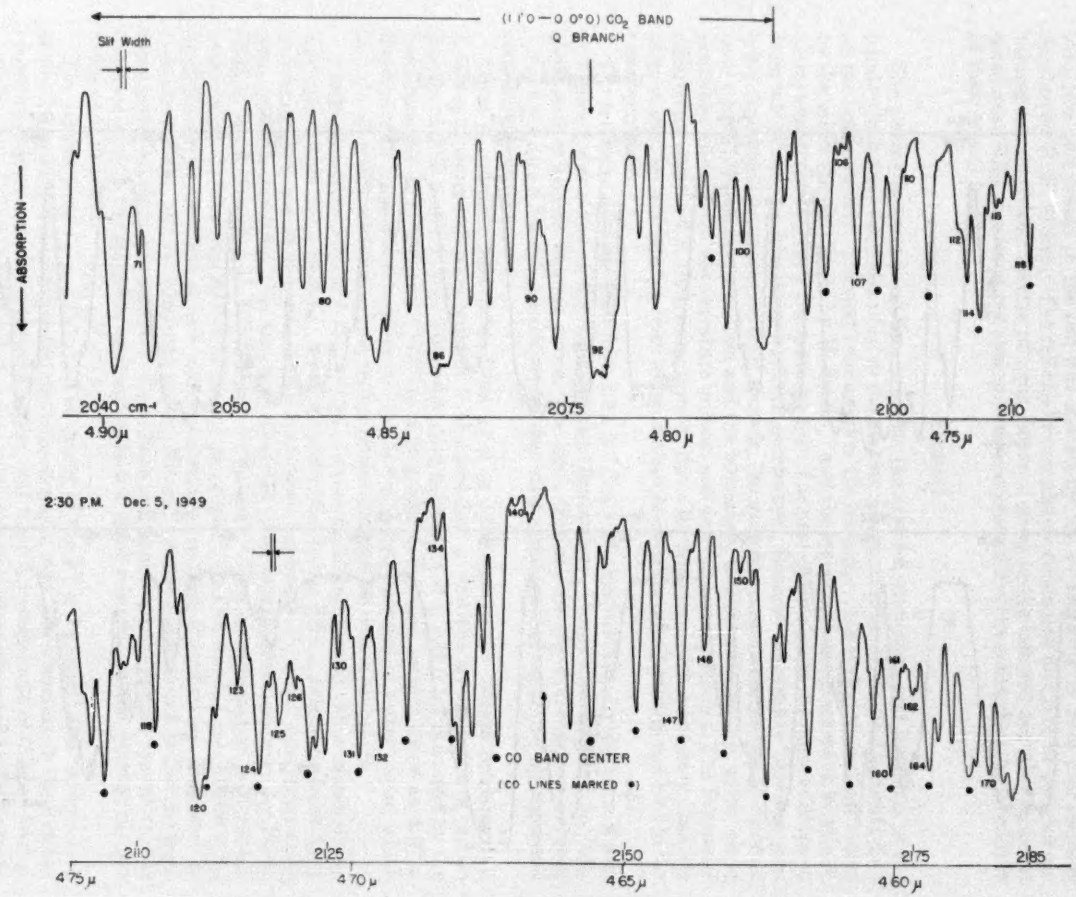
(1 1° 0 — 0 0° 0) CO_2 BAND
Q BRANCH
Slit Width
ABSORPTION
2040 cm-1
2050
2075
2100
2110
4.90 μ
4.85 μ
4.80 μ
4.75 μ
2:30 P.M. Dec. 5, 1949
CO BAND CENTER
(CO LINES MARKED •)
2110
2125
2150
2175
2185
4.75 μ
4.70 μ
4.65 μ
4.60 μ

FIG. 3*b*

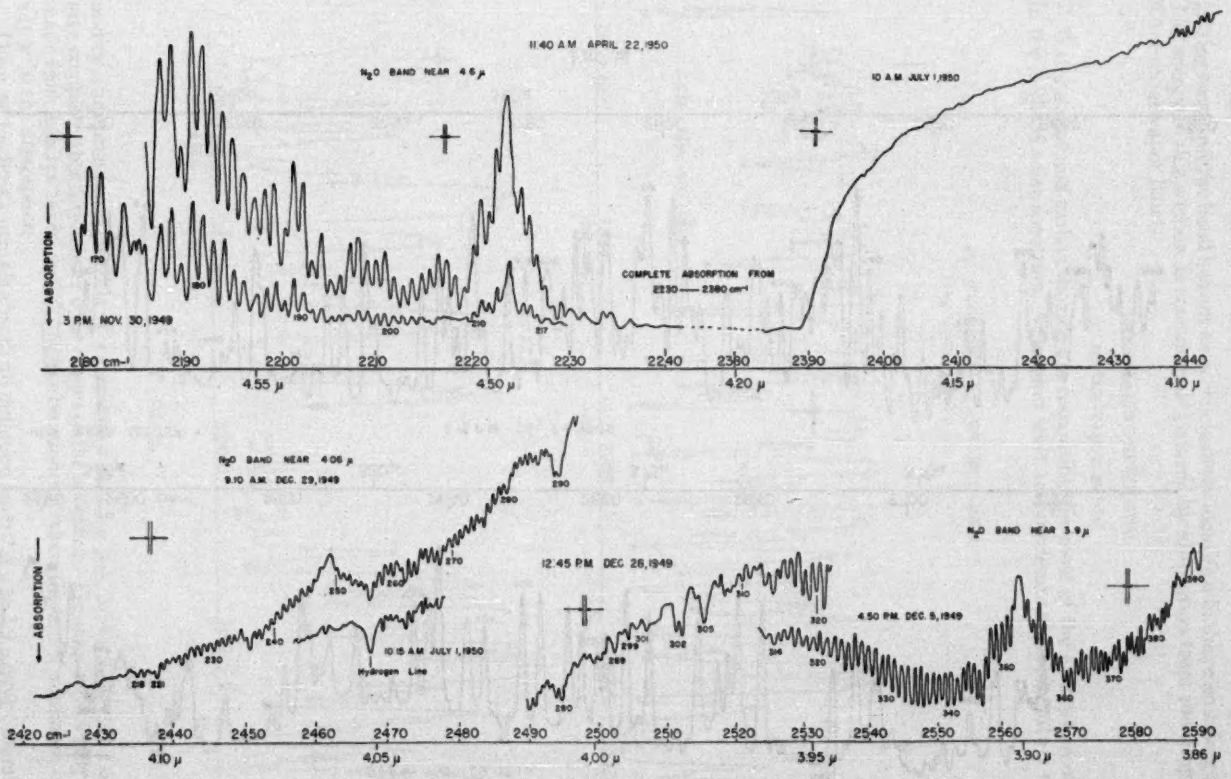
11:40 A.M. APRIL 22, 1950
H_2O BAND NEAR 4.6 μ
10 A.M. JULY 1, 1950
COMPLETE ABSORPTION FROM 2230 — 2380 cm⁻¹
3 P.M. NOV. 30, 1949
ABSORPTION
2180 cm⁻¹ 2190 2200 2210 2220 2230 2240 2380 2390 2400 2410 2420 2430 2440
4.55 μ 4.50 μ 4.20 μ 4.15 μ 4.10 μ
H_2O BAND NEAR 4.05 μ
9.10 A.M. DEC. 29, 1949
12:45 P.M. DEC. 26, 1949
H_2O BAND NEAR 3.9 μ
10:15 A.M. JULY 1, 1950
Hydrogen Line
4:50 P.M. DEC. 5, 1949
2420 cm⁻¹ 2430 2440 2450 2460 2470 2480 2490 2500 2510 2520 2530 2540 2550 2560 2570 2580 2590
4.10 μ 4.05 μ 4.00 μ 3.95 μ 3.90 μ 3.86 μ

FIG. 3c

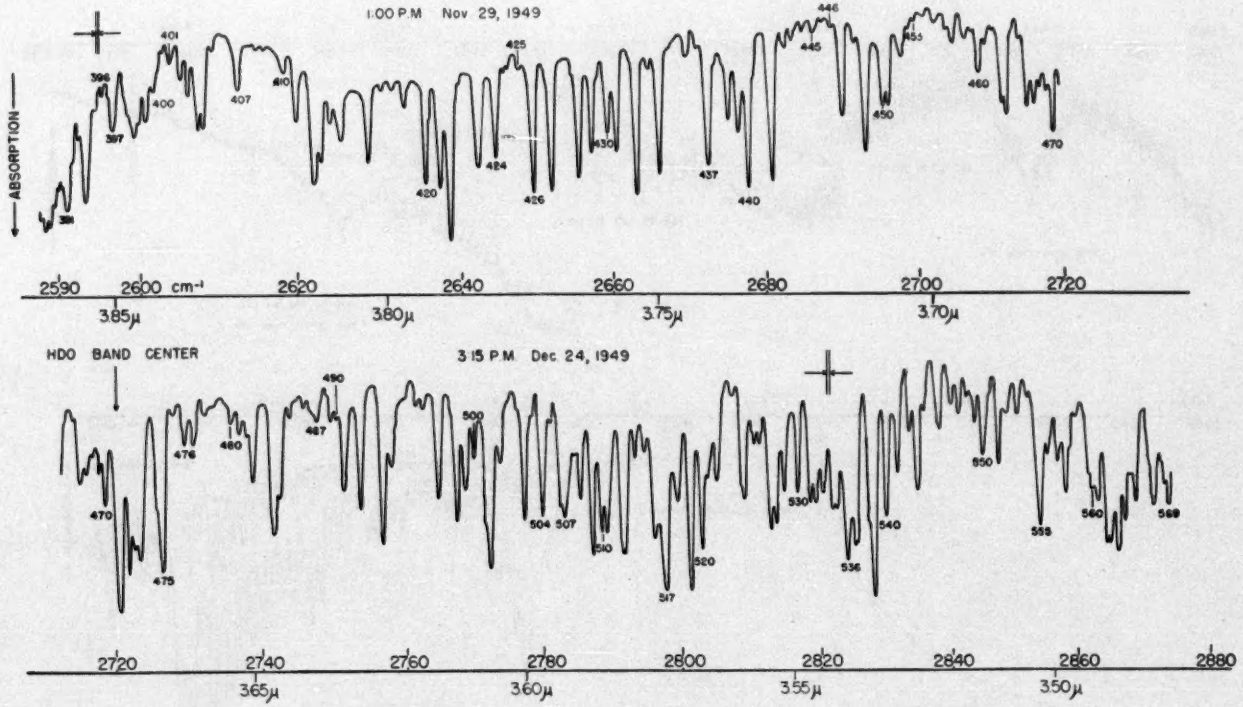
1:00 P.M. Nov 29, 1949
ABSORPTION
401
396
400
397
407
410
425
420
424
426
430
437
440
446
445
455
450
460
470
2590
2600 cm⁻¹
2620
2640
2660
2680
2700
2720
3.85μ
3.80μ
3.75μ
3.70μ
HDO BAND CENTER
3:15 P.M. Dec 24, 1949
490
487
500
476
480
470
475
504 507
510
520
517
530
536
540
550
555
560
569
2720
2740
2760
2780
2800
2820
2840
2860
2880
3.65μ
3.60μ
3.55μ
3.50μ

FIG. 3*d*

grating map; but the band has not been conclusively identified in the prismatic spectrum. The energy in this window is considerably reduced by absorption from the wings of the 6.3 μ water-vapor band.

THE GRATING SPECTRUM

I. WATER-VAPOR BANDS

Water vapor and carbon dioxide are responsible for most of the absorption observed in the infrared solar spectrum. At ground level and moderate air temperature and hu-

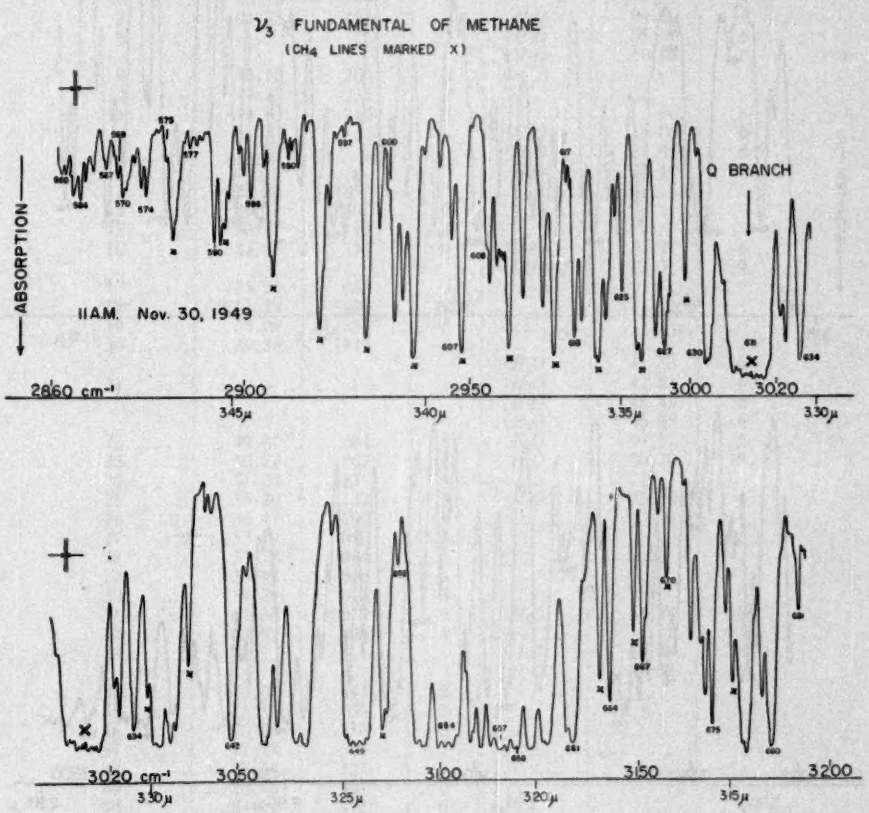

FIG. 3e

midity, the three fundamentals of water vapor at 6.3 μ (ν_2), 2.74 μ (ν_1), and 2.66 μ (ν_3) give complete absorption over wide ranges of the spectrum. The map shown (Fig. 3) was made from spectra taken during the winter months, when there is a minimum of water vapor in the atmosphere.

The ν_1 and ν_3 fundamentals absorb all radiation from 2.4 μ to 2.9 μ over Columbus and limit this end of the map. The overtone band $2\nu_2$ centered at 3.18 μ produces most of the intense lines between 3.0 μ and 3.3 μ, but in the frequency table only those lines measured

by H. H. Nielsen[16] are identified. This band covers the region where the fundamental *C-H* vibration of many hydrocarbons occurs and masks the lines of such molecules which may exist in the earth's atmosphere. Mohler and Pierce[17] and McMath and Goldberg[18] have mapped the solar spectrum from 3.0 μ to 3.6 μ, using a lead sulphide cell detector, and have described much of the structure obtained.

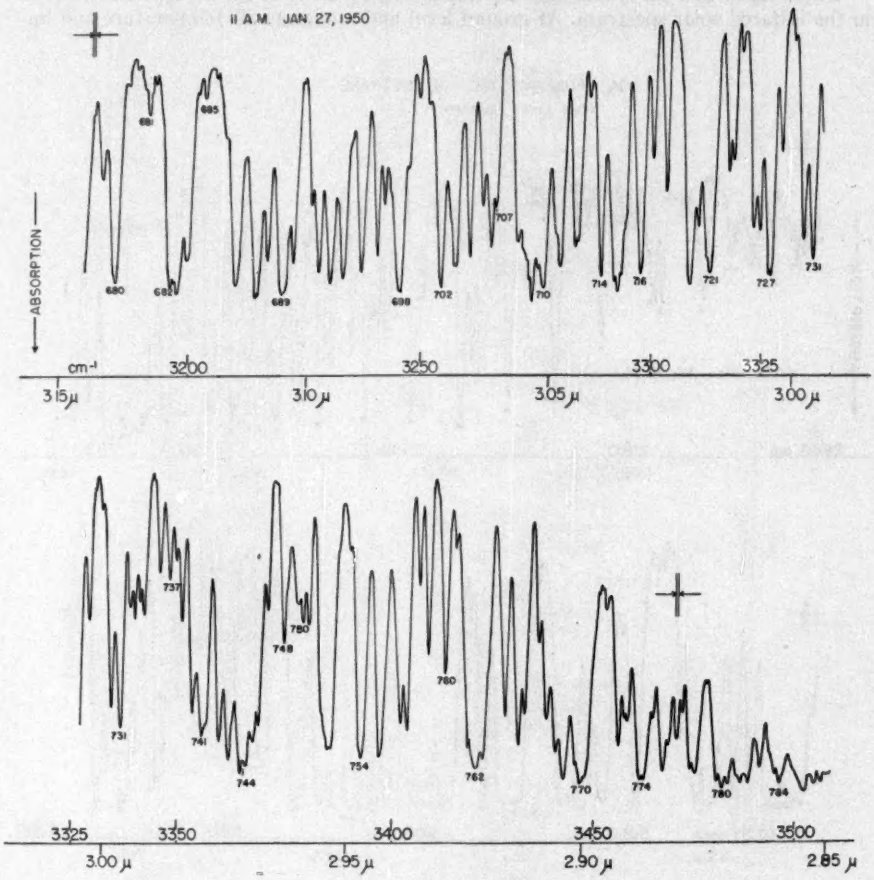

FIG. 3*f*

The ν_2 fundamental prevents any solar radiation from being detected at wave lengths greater than 5.3 μ during most of the year in Columbus and is responsible for some of the strong lines from 4.6 μ to 5.2 μ. Many of these water-vapor lines have been identified by comparison with our own laboratory spectra.

[16] *Phys. Rev.*, **59**, 565, 1941.

[17] *Pub. A.S.P.*, **61**, 221, 1949.

[18] *Proc. Amer. Phil. Soc.*, **93**, 362, 1949.

TABLE 1

TABLE OF LINE FREQUENCIES AND IDENTIFICATIONS

Line No.	Frequency [Cm^{-1}(Vac)]	Wave Length A(Air)	No. of Measurements	Identification	Laboratory Value [Cm^{-1}(Vac)]	Source*
1	1897.61	52683	3	.....	.....	
2	98.86	649	2	.....	.....	
3	1900.25	610	2	.....	.....	
4	00.75	596	4	.....	.....	
5	02.04	561	8	H_2O	1902.01	6
6	02.78	540	4	.....	.....	
7	04.55	492	7	H_2O	04.50	6
8	.....	.....	.....	H_2O	08.06	6
				H_2O	10.08	6
9	12.75	266	2	.....	.....	
10	14.27	225	2	.....	.....	
11	14.83	210	2	.....	.....	
12	.....	.....	.....	H_2O	18.06	6
				H_2O	22.45	6
				H_2O	23.15	6
13	27.86	51857	7	.....	.....	
14	29.71	807	6	.....	.....	
15	30.97	773	4	.....	.....	
16	33.21	713	9	H_2O	33.27	6
				CO_2 (Q)	32.5	9
17	35.50	652	6	.....	.....	
18	37.29	604	10	.....	.....	
19	38.09	583	6	.....	.....	
20	39.36	549	2	.....	.....	
21	.....	.....	.....	H_2O	41.73	6
				H_2O	42.61	6
				H_2O	45.41	6
				H_2O	46.45	6
22	49.41	284	8	H_2O	49.57	6
23	50.22	262	4	H_2O	50.30	6
24	51.25	235	9	.....	.....	
25	55.20	132	2	H_2O	55.08	6
26	56.42	100	4	.....	.....	
27	57.19	080	4	.....	.....	
28	57.78	064	5	.....	.....	
29	58.91	035	4	.....	.....	
30	59.79	012	5	.....	.....	
31	61.30	50973	9	H_2O	61.28	6
32	63.92	905	4	.....	.....	
33	.....	.....	.....	H_2O	66.45	6
				H_2O	67.58	6
34	72.06	695	2	.....	.....	
35	73.59	655	2	.....	.....	
36	76.28	586	6	.....	.....	
37	77.75	549	7	.....	.....	
38	78.61	527	2	.....	.....	
39	80.96	467	6	.....	.....	
40	83.12	412	6	.....	.....	
41	84.65	373	6	.....	.....	
42	86.19	334	2	.....	.....	
43	88.42	278	3	H_2O	88.50	6
44	.....	.....	.....	H_2O	92.05	6
45	99.10	009	5	H_2O	99.07	6
46	2000.96	49962	2	.....	.....	
47	02.18	932	3	.....	.....	
48	03.18	907	2	.....	.....	
49	04.06	885	2	.....	.....	

* See list of references at end of table.

TABLE 1—*Continued*

Line No.	Frequency [Cm^{-1}(Vac)]	Wave Length A(Air)	No. of Measurements	Identification	Laboratory Value [Cm^{-1}(Vac)]	Source*
50	2005.75	49843	5			
51	07.78	793	3	H_2O	2007.79	6
52	09.41	752	3	H_2O	09.38	6
53	10.89	716	3			
54	12.23	682	2			
55	13.60	649	2			
56				H_2O	16.93	6
				H_2O	18.46	6
				H_2O	19.21	6
57	20.69	475	3			
58	21.76	448	2			
59	23.16	414	4	H_2O	23.16	6
60	25.34	361	3			
61	26.93	322	3	H_2O	26.79	6
62	29.52	259	2			
63	30.21	242	4			
64	32.55	186	5			
65	34.26	144	4			
66	35.57	113	5	CO_2	35.33	5
67	37.59	064	4			
68	38.51	042	4	CO_2	38.36	5
69	40.24	000	5	CO_2	39.83	5
70	41.40	48973	5	CO_2	41.42	5
				H_2O	41.43	6
71	43.13	931	5	CO_2	42.99	5
72	44.05	909	5	H_2O	44.04	6
				CO_2	44.35	5
73	46.44	852	4	CO_2	46.02	5
74	47.55	826	5	CO_2	47.54	5
75	49.10	789	5	CO_2	49.08	5
76	50.70	750	4	CO_2	50.57	5
77	52.22	714	4	CO_2	52.14	5
78	53.77	678	4	CO_2	53.66	5
79	55.29	642	4	CO_2	55.19	5
80	56.79	606	4	CO_2	56.77	5
81	58.35	569	3	CO_2	58.30	5
82	59.98	531	3	CO_2	59.80	5
				CO	60.03	1
83	60.61	516	3	H_2O	60.42	6
84	61.33	499	3	CO_2	61.33	5
85	62.99	460	3	CO_2	62.93	5
86				CO_2	64.79	5
				H_2O	64.95	6
				H_2O	65.98	6
				CO_2	66.02	5
87	67.62	351	5	CO_2	67.53	5
88	69.18	315	4	CO	68.96	1
				CO_2	69.53	5
89	70.79	278	3	CO_2	70.61	5
90	72.49	238	5	CO_2	72.05	5
91	74.25	197	5	CO	73.38	1
				CO_2	74.09	5
92				CO	77.76	1
				CO_2 (Q)	77.60	5
93	80.89	043	6	CO_2	80.75	5
94	82.08	016	6	CO	82.11	1
				CO_2	82.25	5
95	83.95	47973	7	CO_2	83.95	5
96	85.04	948	4	$C^{12}O^{16}$	84.85	12
97	85.57	935	7	CO_2	85.45	5

TABLE 1—*Continued*

Line No.	Frequency [Cm^{-1}(Vac)]	Wave Length A(Air)	No. of Measurements	Identification	Laboratory Value [Cm^{-1}(Vac)]	Source*
98	2086.44	47915	7	CO	2086.43	1
99	87.43	893	7	CO_2	87.23	5
				H_2O	87.44	6
100	88.68	864	7	CO_2	88.55	5
				H_2O	90.12	6
101	90.19	830	7	CO_2	90.13	5
				CO	90.72	1
102	91.83	792	6	CO_2	91.86	5
103	92.30	781	4	$C^{13}O^{16}$	92.35	12
104	93.67	750	6	CO_2 (Q)	93.63	5
105	95.01	720	6	CO	94.97	1
106	96.18	693	3	.....	.....	
107	97.52	662	7	.....	.....	
108	99.24	623	7	CO	99.19	1
109	2100.55	593	7	.....	.....	
110	01.47	573	3	.....	.....	
111	03.40	529	7	CO	2103.38	1
112	05.93	472	3	.....	.....	
113	06.45	460	7	.....	.....	
114	07.51	436	6	CO	07.53	1
115	08.76	408	3	.....	.....	
116	09.16	399	3	.....	.....	
117	10.22	375	6	$C^{13}O^{16}$	10.44	12
118	11.64	344	6	CO	11.65	1
119	13.41	304	6	.....	.....	
120	15.06	267	6	.....	.....	
121	15.59	255	3	CO	15.74	1
122	16.35	238	5	.....	.....	
123	18.08	200	6	.....	.....	
124	19.72	163	7	CO	19.79	1
125	21.41	126	7	.....	.....	
126	22.73	096	4	.....	.....	
127	23.82	072	7	CO	23.81	1
128	24.29	062	6	.....	.....	
129	25.00	046	7	.....	.....	
130	26.16	020	7	.....	.....	
131	27.79	46984	7	CO	27.79	1
132	29.63	944	7	.....	.....	
133	31.74	897	7	CO	31.74	1
134	34.42	838	7	$C^{13}O^{16}$	34.30	12
135	35.77	809	3	CO	35.65	1
136	36.18	800	7	.....	.....	
137	37.27	776	7	.....	.....	
138	38.29	754	7	.....	.....	
139	39.47	728	8	CO	39.53	1
140	41.02	694	5	$C^{13}O^{16}$	40.83	12
141	41.32	666	8	.....	.....	
142	45.60	594	8	.....	.....	
143	47.38	556	9	CO	47.19	1
144	48.46	532	8	.....	.....	
145	50.95	478	7	CO	50.97	1
146	52.62	442	7	.....	.....	
147	54.71	397	7	CO	54.71	1
148	56.66	355	7	.....	.....	
149	58.35	319	6	CO	58.41	1
150	59.83	287	6	$C^{13}O^{16}$	59.43	12
151	60.72	268	5	.....	.....	
152	61.88	243	10	CO	62.08	1
153	62.90	222	8	.....	.....	
154	63.46	210	10	.....	.....	

TABLE 1—*Continued*

Line No.	Frequency [Cm^{-1}(Vac)]	Wave Length A(Air)	No. of Measurements	Identification	Laboratory Value [Cm^{-1}(Vac)]	Source*
155	2164.35	46191	4	.....	.....	
156	65.70	162	9	*CO*	2165.71	1
157	67.46	124	10	N_2O	67.36	7
				N_2O	68.53†	7
158	69.33	085	10	*CO*	69.31	1
				N_2O	69.73†	7
				N_2O	70.86†	7
159	71.42	040	10	.....	.....	
160	72.86	010	10	*CO*	72.87	1
				N_2O	72.49	7
161	73.48	45997	5	N_2O	73.71	7
162	74.69	971	2	N_2O	74.79	7
163	75.06	963	9	.....	.....	
164	76.32	937	9	*CO*	76.39	1
				N_2O	76.00	7
165	77.10	920	9	N_2O	77.09	7
166	78.29	895	9	N_2O	78.14	7
167	79.44	871	4	N_2O	79.22	7
168	79.81	863	9	*CO*	79.88	1
169	80.43	850	8	N_2O	80.34	7
170	81.55	827	9	N_2O	81.39	7
171	82.81	800	9	N_2O	82.49	7
172	83.54	785	9	*CO*	83.33	1
				N_2O	83.57	7
173	85.12	752	8	.....	.....	
174	85.56	742	2	.....	.....	
175	86.07	732	3	N_2O	86.07	7
176	86.99	713	11	*CO*	86.75	1
				N_2O	87.19	7
177	88.44	682	12	N_2O	88.31	7
178	89.59	658	10	N_2O	89.48	7
179	90.35	642	10	*CO*	90.13	1
				N_2O	90.40	7
180	91.55	618	10	N_2O	91.45	7
181	92.59	596	9	N_2O	92.48	7
182	93.56	576	9	*CO*	93.47	1
				N_2O	93.52	7
183	94.60	554	9	N_2O	94.65	7
184	95.67	532	9	N_2O	95.55	7
185	96.78	509	9	*CO*	96.77	1
				N_2O	96.72	7
186	97.83	487	9	N_2O	97.86	7
187	98.90	465	9	N_2O	98.85	7
188	99.91	444	7	N_2O	99.81	7
				CO	2200.04	1
189	2200.69	428	7	N_2O	00.75	7
190	01.80	405	8	N_2O	01.78	7
191	02.93	382	6	*CO*	03.27	1
				N_2O	02.76	7
192	03.66	367	4	N_2O	03.69	7
193	04.73	345	4	N_2O	04.67	7
194	05.67	325	4	N_2O	05.54	7
195	06.56	307	4	*CO*	06.46	1
				N_2O	06.72	7
196	07.63	285	4	N_2O	07.62	7
197	08.67	264	4	N_2O	08.61	7
198	09.59	245	4	*CO*	09.61	1
				N_2O	09.46	7
199	10.48	227	4	N_2O	10.50	7

† Indicates line frequency observed in laboratory, but the line is not numbered.

TABLE 1—*Continued*

Line No.	Frequency [Cm^{-1}(Vac)]	Wave Length A(Air)	No. of Measurements	Identification	Laboratory Value [Cm^{-1}(Vac)]	Source*
200	2211.46	45207	4	N_2O	2211.47	7
201	12.45	186	4	CO	12.73	1
				N_2O	12.37	7
202	13.29	169	4	N_2O	13.38	7
203	14.26	150	4	N_2O	14.21	7
204	15.09	133	3	N_2O	15.16	7
205	16.00	114	3	N_2O	16.02	7
206	16.92	095	3	N_2O	16.83	7
207	17.85	076	3	N_2O	17.72	7
208	18.70	059	3	N_2O	18.54	7
209	19.69	039	4	N_2O	19.49	7
210	20.45	024	4	N_2O	20.46	7
211	21.35	006	5	N_2O	21.27	7
212	22.09	44990	5	N_2O	22.09	7
213	22.93	974	5	N_2O	22.86	7
				N_2O	Band center	
214	24.76	936	5	N_2O	24.73	7
215	25.59	920	5	N_2O	25.40	7
216	26.42	903	4	N_2O	26.53	7
217	2227.20	44887	3	N_2O	2226.99	7
218	2435.27	41052.0	4	N_2O	2435.27	7
219	36.19	036.5	9	N_2O	36.16	7
220	37.12	021.0	5	N_2O	37.03	7
221	37.88	008.0	7	N_2O	37.96	7
222	38.80	40992.5	7	N_2O	38.81	7
223	39.71	977.0	6	N_2O	39.72	7
224	40.52	963.5	7	N_2O	40.62	7
225	41.49	947.5	8	N_2O	41.46	7
				CH_4	41.65†	8
226	42.24	935.0	7	N_2O	42.36	7
227	43.12	920.0	9	N_2O	43.23	7
228	44.05	904.5	10	N_2O	44.13	7
229	44.88	890.5	9	N_2O	44.97	7
230	45.79	875.5	9	N_2O	45.85	7
231	46.67	860.5	9	N_2O	46.71	7
232	47.55	846.0	8	N_2O	47.57	7
233	48.42	831.5	9	N_2O	48.49	7
234	49.24	818.0	9	N_2O	49.33	7
235	50.17	802.0	10	N_2O	50.17	7
236	50.97	789.0	10	CH_4	51.03	8
				N_2O	51.04	7
237	51.87	774.0	10	N_2O	51.88	7
				CH_4	52.64†	8
238	52.72	760.0	10	N_2O	52.78	7
239	53.54	746.0	11	N_2O	53.64	7
240	54.42	731.5	11	N_2O	54.46	7
241	55.25	718.0	12	N_2O	55.35	7
242	56.09	704.0	12	N_2O	56.16	7
243	56.96	689.5	12	N_2O	57.06	7
244	57.72	677.0	8	N_2O	57.84	7
245	58.65	661.5	9	N_2O	58.71	7
				CH_4	59.71†	8
246	.....	.....	.....	N_2O	59.63	7
247	.....	.....	.....	N_2O	60.45	7
248	.....	.....	.....	N_2O	61.19	7
249	N_2O band center		.....	.....	62.12	7
250	63.22	586.0	1	N_2O	62.82	7
251	63.54	581.0	5	N_2O	63.88	7
252	64.57	564.0	6	N_2O	64.56	7
253	65.38	550.5	7	N_2O	65.43	7

TABLE 1—*Continued*

Line No.	Frequency [Cm^{-1}(Vac)]	Wave Length A(Air)	No. of Measurements	Identification	Laboratory Value [Cm^{-1}(Vac)]	Source*
254.....	2466.18	40537.5	8	N_2O	2466.28	7
255.....	67.07	522.5	6	N_2O	67.11	7
256.....	67.80	511.0	13	H	67.75	10
				N_2O	67.94	7
257.....	68.58	498.0	11	N_2O	68.74	7
258.....	69.49	483.0	11	N_2O	69.54	7
259.....	70.41	468.0	11	N_2O	70.30	7
260.....	71.20	455.0	11	N_2O	71.10	7
261.....	72.06	441.0	11	N_2O	71.94	7
				CH_4	72.52†	8
262.....	72.77	429.5	11	N_2O	72.75	7
263.....	73.67	414.5	11	N_2O	73.54	7
				CH_4	73.63†	8
264.....	74.38	403.0	10	N_2O	74.38	7
265.....	75.32	387.5	11	N_2O	75.18	7
266.....	76.07	375.5	11	N_2O	76.00	7
267.....	76.88	362.5	11	N_2O	76.79	7
268.....	77.66	349.5	11	N_2O	77.60	7
				CH_4	77.68†	8
269.....	78.40	337.5	8	N_2O	78.44	7
270.....	79.26	323.5	9	N_2O	79.21	7
271.....	80.07	310.5	8	N_2O	79.98	7
272.....	80.78	299.0	8	N_2O	80.87	7
273.....	81.62	285.0	8	N_2O	81.64	7
274.....	82.38	273.0	9	N_2O	82.44	7
275.....	83.20	259.5	9	N_2O	83.22	7
276.....	83.98	247.0	9	N_2O	84.02	7
277.....	84.67	236.0	6	N_2O	84.76	7
278.....	85.51	222.0	10	N_2O	85.51	7
279.....	86.35	208.5	9	N_2O	86.35	7
280.....	87.09	196.5	8	N_2O	87.12	7
281.....	87.65	187.5	4	N_2O	87.88	7
282.....	88.40	175.5	3	N_2O	88.70	7
283.....	89.29	161.0	5	N_2O	89.36	7
284.....	90.09	148.0	7	N_2O	90.20	7
285.....	90.85	136.0	7	N_2O	90.98	7
286.....	91.66	123.0	7	N_2O	91.74	7
287.....	92.38	111.5	3	N_2O	92.47	7
288.....	93.18	098.5	4	N_2O	93.20	7
289.....	93.98	085.5	9	N_2O	93.98	7
				CH_4	94.09	8
290.....	94.80	072.5	8	N_2O	94.78	7
				CH_4	94.71	8
291.....	95.29	064.5	1	N_2O	95.36	7
292.....	97.22	033.5	5	.....	.....	
293.....	98.45	014.0	3	.....	.....	
294.....	99.32	000.0	5	.....	.....	
295.....	2500.50	39981.0	2	.....	.....	
296.....	02.25	953.0	2	.....	.....	
297.....	02.62	947.0	4	.....	.....	
298.....	03.68	930.0	1	.....	.....	
299.....	04.66	914.5	2	.....	.....	
300.....	05.79	896.5	2	.....	.....	
301.....	07.00	877.5	2	.....	.....	
302.....	11.67	803.0	7	CH_4	2511.72	8
303.....	12.45	791.0	7	CH_4	12.51	8
304.....	14.41	760.0	3	.....	.....	
305.....	15.62	740.5	6	CH_4	15.53	8
306.....	17.76	707.0	4	.....	.....	
307.....	18.72	692.0	4	.....	.....	

TABLE 1—*Continued*

Line No.	Frequency [Cm^{-1}(Vac)]	Wave Length A(Air)	No. of Measurements	Identification	Laboratory Value [Cm^{-1}(Vac)]	Source*
308	2519.77	39675.5	6	.....	.....	
309	20.56	663.0	2	.....	.....	
310	21.25	652.0	7	N_2O	2521.09	7
311	22.40	634.0	6	N_2O	22.27	7
312	23.52	616.5	6	N_2O	23.40	7
313	24.68	598.0	8	N_2O	24.64	7
314	25.78	581.0	7	N_2O	25.72	7
				CH_4	25.92†	8
315	26.75	565.5	6	N_2O	26.59	7
316	27.95	547.0	8	N_2O	27.89	7
317	28.98	531.0	9	N_2O	28.86	7
318	30.13	513.0	9	N_2O	30.09	7
319	31.12	497.5	10	N_2O	31.00	7
320	32.22	480.5	9	N_2O	32.18	7
321	33.32	463.0	9	N_2O	33.31	7
322	34.41	446.0	8	N_2O	34.49	7
323	35.47	429.5	8	N_2O	35.57	7
324	36.49	414.0	8	N_2O	36.55	7
				CH_4	36.63†	8
325	37.46	399.0	8	N_2O	37.45	7
326	38.47	383.0	8	N_2O	38.48	7
327	39.53	366.5	8	N_2O	39.58	7
328	40.50	351.5	8	N_2O	40.52	7
329	41.50	336.0	8	N_2O	41.54	7
330	42.47	321.0	8	N_2O	42.49	7
331	43.47	305.5	8	N_2O	43.51	7
332	44.46	290.5	8	N_2O	44.47	7
333	45.41	276.0	8	N_2O	45.42	7
334	46.38	261.0	8	N_2O	46.39	7
335	47.33	246.0	8	N_2O	47.34	7
336	48.30	231.0	8	N_2O	48.32	7
337	49.24	217.0	8	N_2O	49.20	7
338	50.23	201.5	9	N_2O	50.27	7
339	51.18	187.0	9	N_2O	51.18	7
340	52.13	172.0	9	N_2O	52.09	7
341	53.06	158.0	9	N_2O	53.05	7
342	53.95	144.5	9	N_2O	53.91	7
343	54.84	130.5	9	N_2O	54.80	7
344	55.78	116.5	9	N_2O	55.89	7
345	56.64	103.0	9	N_2O	56.72	7
				CH_4	57.32†	8
346	57.53	089.5	9	N_2O	57.58	7
347	58.34	077.0	9	N_2O	58.32	7
348	59.27	063.0	9	N_2O	59.25	7
349	60.11	050.0	9	N_2O	60.07	7
350	60.98	037.0	9	N_2O	60.90	7
351	61.94	022.0	9	N_2O	61.98	7
352	62.59	012.5	5	N_2O	62.35	7
	N_2O band center					
353	64.16	38988.5	8	N_2O	64.05	7
354	65.15	973.5	8	N_2O	65.23	7
355	65.85	963.0	8	N_2O	65.74	7
356	66.78	948.5	8	N_2O	66.72	7
357	67.65	935.5	8	N_2O	67.55	7
358	68.41	924.0	8	N_2O	68.25	7
359	69.19	912.0	8	N_2O	68.97	7
360	70.02	899.5	8	N_2O	69.97	7
361	70.72	889.0	8	N_2O	70.57	7
362	71.46	878.0	8	N_2O	71.35	7
363	72.24	866.0	8	N_2O	72.04	7

TABLE 1—*Continued*

Line No.	Frequency [Cm⁻¹(Vac)]	Wave Length A(Air)	No. of Measurements	Identification	Laboratory Value [Cm⁻¹(Vac)]	Source*
364	2573.01	38854.5	8	N_2O	2572.73	7
365	73.73	843.5	8	N_2O	73.46	7
366	74.49	832.0	8	N_2O	74.28	7
367	75.18	821.5	8	N_2O	74.98	7
368	75.96	810.0	8	N_2O	75.84	7
369	76.65	799.5	8	N_2O	76.44	7
370	77.31	789.5	8	N_2O	77.13	7
371	78.05	778.5	8	N_2O	77.82	7
372	78.73	768.0	8	N_2O	78.52	7
373	79.48	757.0	7	N_2O	79.28	7
374	80.04	748.5	7	N_2O	79.70	7
375	80.81	737.0	8	N_2O	79.65	7
376	81.35	729.0	7	N_2O	81.15	7
377	82.24	715.5	8	N_2O	82.19	7
378	82.56	711.0	5	N_2O	.....	
379	83.33	699.0	5	N_2O	.....	
380	84.11	687.5	6	N_2O	.....	
381	84.64	679.5	5	N_2O	.....	
382	85.37	668.5	4	N_2O	.....	
383	86.05	658.5	6	N_2O	.....	
384	86.61	650.0	5	N_2O	.....	
385	87.15	642.0	3	N_2O	.....	
386	87.94	630.5	2	N_2O	.....	
387	88.46	622.5	5	N_2O	.....	
388	88.94	615.5	4	N_2O	.....	
389	89.51	607.0	5	N_2O	.....	
390	90.05	598.5	2	N_2O	.....	
391	91.20	581.5	7	.....	.....	
392	91.65	575.0	1	.....	.....	
393	92.80	558.0	2	.....	.....	
394	93.55	547.0	7	.....	.....	
395	94.45	533.5	3	.....	.....	
396	95.25	521.5	3	.....	.....	
397	96.85	498.0	8	.....	.....	
				CH_4	99.00†	8
398	99.40	460.0	4	.....	.....	
399	2600.95	437.5	7	.....	.....	
400	01.80	424.5	3	.....	.....	
401	03.85	394.0	4	.....	.....	
402	05.30	372.5	5	.....	.....	
403	06.40	356.5	4	.....	.....	
404	07.65	338.5	4	.....	.....	
405	08.35	328.5	4	.....	.....	
406	09.20	315.0	2	.....	.....	
407	12.65	265.0	6	.....	.....	
408	13.85	248.0	2	CH_4	2614.00	8
409	14.70	235.5	2	CH_4	14.80	8
410	18.45	180.5	9	.....	.....	
411	19.90	159.0	10	.....	.....	
412	22.25	125.0	10	.....	.....	
413	23.00	114.0	10	.....	.....	
414	24.25	095.5	10	*HDO*	.....	
415	25.50	077.5	11	*HDO*	.....	
416	28.75	030.5	9	*HDO*	.....	
417	30.20	009.0	2	CH_4	30.30	8
418	31.60	37989.5	5	CH_4	31.35	8
419	33.05	968.5	7	CH_4	32.95	8
420	35.65	931.0	9	*HDO*	.....	
421	37.50	904.5	9	*HDO*	.....	

TABLE 1—*Continued*

Line No.	Frequency [Cm^{-1}(Vac)]	Wave Length A(Air)	No. of Measurements	Identification	Laboratory Value [Cm^{-1}(Vac)]	Source*
422	2638.75	37886.5	9	*HDO*	.....	
				CH_4	2639.35†	8
				CH_4	41.75†	8
423	42.25	836.0	9	*HDO*	.....	
424	44.55	803.5	8	*HDO*	.....	
425	47.55	760.0	4	CH_4	47.60	8
426	49.45	733.5	8	*HDO*	.....	
				CH_4	49.80†	8
427	51.90	698.5	8	*HDO*	.....	
				CH_4	54.80†	8
428	55.60	646.0	8	*HDO*	.....	
				CH_4	56.40†	8
429	57.50	619.5	8	*HDO*	.....	
430	59.55	590.5	7	*HDO*	.....	
431	60.60	575.0	8	*HDO*	.....	
432	63.30	537.0	8	*HDO*	.....	
433	65.20	510.5	4	CH_4	65.10	8
434	66.40	493.5	8	*HDO*	.....	
435	69.90	444.5	6	*HDO*	.....	
				CH_4	70.20	8
436	71.45	422.5	3	.....	.....	
437	72.75	404.5	8	*HDO*	.....	
				CH_4	73.85†	8
438	75.40	367.5	8	*HDO*	.....	
439	76.65	349.5	8	*HDO*	.....	
440	77.95	332.0	8	*HDO*	.....	
				CH_4	78.45†	8
441	80.85	291.5	6	*HDO*	.....	
442	82.60	267.0	5	CH_4	82.50	8
443	83.75	251.0	4	CH_4	83.55	8
444	84.85	235.5	4	CH_4	84.75	8
445	86.35	215.0	4	.....	.....	
				CH_4	86.50†	8
446	88.85	180.5	2	.....	.....	
447	90.05	164.0	6	*HDO*	.....	
448	91.85	139.0	4	CH_4	91.50	8
449	93.05	122.5	7	*HDO*	.....	
450	95.50	088.5	7	*HDO*	.....	
451	96.10	080.5	6	CH_4	96.00	8
452	97.60	060.0	3	CH_4	97.75	8
453	99.10	039.5	2	.....	.....	
454	2701.10	012.0	2	.....	.....	
455	02.55	36992.0	5	CH_4	2702.50	8
456	04.20	969.5	2	.....	.....	
457	04.80	961.0	6	CH_4	04.70	8
458	06.60	936.5	6	CH_4	06.55	8
459	07.55	924.0	4	.....	.....	
460	08.25	914.5	8	*HDO*	.....	
461	09.45	897.5	3	CH_4	09.20	8
462	10.70	880.5	3	.....	.....	
463	11.80	866.0	4	CH_4	12.05	8
464	12.30	859.0	4	.....	.....	
465	14.30	832.0	3	.....	.....	
466	15.35	817.5	5	*HDO*	.....	
467	16.35	804.0	5	*HDO*	.....	
468	17.25	792.0	2	.....	.....	
469	18.10	780.5	4	.....	.....	
470	18.85	770.5	6	*HDO*	.....	
471	20.70	745.5	7	*HDO*	.....	
472	22.15	725.5	5	*HDO*	.....	

TABLE 1—*Continued*

Line No.	Frequency [Cm^{-1}(Vac)]	Wave Length A(Air)	No. of Measurements	Identification	Laboratory Value [Cm^{-1}(Vac)]	Source*
473	2722.90	36715.5	5	.....	.....	
474	23.60	706.0	6	*HDO*	.....	
475	26.55	666.5	8	*HDO*	.....	
				CH_4	2726.70	8
476	29.90	621.5	6	*HDO*	.....	
477	31.05	606.0	6	*HDO*	.....	
478	32.75	583.0	5	.....	.....	
479	33.95	567.0	2	.....	.....	
480	36.10	538.0	5	CH_4	36.05	8
481	37.40	521.5	6	CH_4	37.30	8
482	38.30	509.0	3	.....	.....	
483	38.90	500.5	9	*HDO*	.....	
484	41.80	462.5	7	CH_4	41.70	8
485	42.85	448.5	4	.....	.....	
486	44.30	429.5	5	.....	.....	
487	46.20	404.0	3	.....	.....	
488	47.80	383.0	5	.....	.....	
489	50.00	353.5	5	.....	.....	
490	50.90	341.5	3	.....	.....	
491	51.55	333.0	6	*HDO*	.....	
492	53.75	304.0	7	*HDO*	.....	
493	56.90	262.5	7	CH_4	56.75	8
				CH_4	57.85†	8
494	58.20	245.5	6	.....	.....	
				CH_4	59.65†	8
495	61.65	200.0	3	CH_4	61.45	8
496	62.80	185.5	5	CH_4	62.60	8
497	64.75	159.5	7	*HDO*	.....	
498	67.45	124.5	7	*HDO*	.....	
499	68.80	107.0	6	.....	.....	
500	70.10	090.0	6	*HDO*	.....	
				CH_4	71.95†	8
501	72.40	059.5	7	.....	.....	
502	74.00	039.5	7	*HDO*	.....	
				CH_4	77.30†	8
503	77.45	35994.5	8	*HDO*	.....	
504	80.15	959.0	7	*HDO*	.....	
				CH_4	81.20†	8
505	81.60	941.0	3	.....	.....	
506	83.10	921.5	2	.....	.....	
507	83.30	918.5	3	*HDO*	.....	
				CH_4	84.30†	8
508	85.85	885.5	7	*HDO*	.....	
				CH_4	85.75	8
509	87.50	864.5	8	.....	.....	
510	88.90	847.0	6	CH_4	89.10	8
511	89.70	836.5	6	*HDO*	.....	
512	92.00	807.0	2	*HDO*	.....	
513	92.25	804.0	5	CH_4	92.45	8
514	93.65	785.5	6	CH_4	93.75	8
515	94.80	771.0	3	CH_4	94.95	8
516	96.45	749.5	4	*HDO*	.....	
517	97.90	731.0	6	*HDO*	.....	
518	99.75	707.5	5	CH_4	99.60	8
519	2801.60	684.0	7	*HDO*	.....	
520	03.15	664.0	7	*HDO*	.....	
				CH_4	2803.30	8
521	04.25	650.0	3	.....	.....	
522	05.40	635.5	6	*HDO*	.....	
523	07.85	604.5	4	.....	.....	

TABLE 1—*Continued*

Line No.	Frequency [Cm^{-1}(Vac)]	Wave Length A(Air)	No. of Measurements	Identification	Laboratory Value [Cm^{-1}(Vac)]	Source*
				CH_4	2808.90†	8
524	2809.20	35587.0	7	.....	.....	
525	10.80	567.0	6	*HDO*	.....	
526	11.55	557.5	6	*HDO*	.....	
527	12.90	540.5	6	*HDO*	.....	
528	13.80	529.0	5	CH_4	13.60	8
529	15.00	514.0	5	*HDO*	.....	
				CH_4	14.70	8
530	17.00	488.5	5	*HDO*	.....	
531	18.85	466.0	5	.....	.....	
532	19.75	454.0	4	.....	.....	
533	20.80	441.5	4	.....	.....	
534	22.15	424.0	3	.....	.....	
535	22.75	416.5	3	CH_4	22.55	8
536	24.30	397.0	5	*HDO*	.....	
537	25.50	382.0	3	CH_4	25.40	8
538	25.85	378.0	3	.....	.....	
539	28.20	348.5	6	*HDO*	.....	
				CH_4	28.30	8
540	30.15	324.5	7	CH_4	30.10	8
541	31.90	302.0	6	CH_4	31.95	8
542	33.85	278.0	5	CH_4	33.80	8
543	34.95	264.5	7	*HDO*	.....	
				CH_4	34.90	8
544	36.05	250.5	3	CH_4	36.00	8
545	38.30	222.5	6	*HDO*	.....	
				CH_4	38.05†	8
546	40.25	198.5	5	*HDO*	.....	
				CH_4	40.30	8
547	41.40	184.5	6	*HDO*	.....	
				CH_4	41.55	8
548	42.70	168.0	2	.....	.....	
549	44.00	152.0	4	.....	.....	
550	45.30	136.0	5	.....	.....	
551	47.90	104.0	5	CH_4	47.70	8
					47.59	2
552	49.05	089.5	3	.....	.....	
553	50.90	067.0	5	CH_4	51.00	8
554	52.75	044.0	2	CH_4	52.55	8
555	54.30	025.0	6	CH_4	53.80	8
					53.9	4
556	55.55	010.0	4	CH_4	55.35	8
					55.40	2
557	57.05	34991.5	7	CH_4	56.95	8
558	58.20	977.5	7	.....	.....	
559	60.05	954.5	3	.....	.....	
				CH_4	61.85†	8
560	62.45	925.5	4	.....	.....	
561	63.05	918.0	6	CH_4	63.00	8
562	64.80	897.0	2	CH_4	64.80	8
563	65.00	894.5	2	.....	.....	
564	66.10	881.0	5	CH_4	66.10	8
					65.7	4
565	67.05	869.0	5	.....	66.95	2
566	68.80	848.0	5	.....	.....	
567	71.35	817.5	6	CH_4	71.35	8
					71.3	4
568	73.20	795.0	2	.....	.....	
569	73.80	787.5	4	.....	.....	
570	74.90	774.5	6	CH_4	74.7	4

TABLE 1—*Continued*

Line No.	Frequency [Cm⁻¹(Vac)]	Wave Length A(Air)	No. of Measurements	Identification	Laboratory Value [Cm⁻¹(Vac)]	Source*
571	2875.60	34766.0	2	.....	.....	
572	77.20	746.5	4	.....	.....	
573	78.40	732.0	6	.....	.....	
574	79.65	717.0	6	.....	.....	
575	83.60	669.0	5	.....	.....	
576	85.20	650.0	6	CH_4	2885.3	3
					85.0	4
577	88.70	608.0	5	.....	.....	
578	90.30	589.0	4	.....	.....	
579	91.40	576.0	2	.....	.....	
580	93.70	548.5	6	.....	93.75	2
					93.9	4
581	95.20	530.5	6	.....	95.3	4
582	96.10	520.0	5	CH_4	95.9	3
583	97.00	509.0	5	.....	.....	
584	99.75	476.5	2	.....	.....	
585	2900.25	470.5	5	.....	.....	
586	01.80	452.0	7	.....	.....	
587	04.55	419.0	6	.....	.....	
588	05.95	402.5	3	.....	2905.65	2
589	06.65	394.5	6	CH_4	06.2	3
					06.3	4
590	09.70	358.5	5	.....	.....	
591	10.60	347.5	5	.....	.....	
592	12.00	331.0	6	.....	.....	
593	14.00	308.0	3	.....	.....	
594	16.60	277.5	6	CH_4	16.9	3
					16.5	4
595	18.90	250.5	6	.....	.....	
596	20.70	229.0	2	.....	.....	
597	22.50	208.0	2	.....	.....	
598	27.20	153.0	6	CH_4	27.0	3
					27.4	4
599	30.20	118.0	6	.....	30.00	2
					30.2	4
600	32.20	094.5	3	.....	.....	
601	33.60	079.0	7	.....	.....	
602	35.35	058.5	7	.....	.....	
603	37.75	030.5	7	CH_4	37.3	3
					37.5	4
604	40.15	003.0	6	.....	.....	
605	43.55	33963.0	7	.....	42.37	2
606	46.15	933.5	6	.....	45.64	2
607	48.20	910.0	6	CH_4	47.9	4
					47.5	3
608	53.80	845.0	3	.....	.....	
609	54.30	839.5	7	.....	54.2	4
610	55.75	823.0	7	.....	55.55	2
611	56.55	813.5	3	.....	.....	
612	57.15	807.0	5	.....	.....	
613	58.40	793.0	7	CH_4	57.8	3
					58.0	4
614	61.55	757.0	6	.....	61.3	4
615	66.05	706.0	5	.....	65.92	2
					65.7	4
616	68.50	678.0	5	CH_4	68.0	3
					68.5	4
617	71.15	648.0	4	.....	70.60	2
618	73.20	624.5	5	.....	.....	
619	74.85	606.0	5	.....	75.09	2

TABLE 1—*Continued*

Line No.	Frequency [Cm^{-1}(Vac)]	Wave Length A(Air)	No. of Measurements	Identification	Laboratory Value [Cm^{-1}(Vac)]	Source*
620	2978.45	33565.0	4	CH_4	2978.3	3
					78.5	4
621	80.05	547.0	5			
622	82.40	521.0	4		82.50	2
623	84.10	502.0	5			
624	87.50	463.5	4			
625	88.55	452.0	6	CH_4	88.4	3
626	92.05	413.0	6		92.4	4
627	94.10	390.0	6		94.0	4
					99.15	2
628	99.05	335.0	5	CH_4	98.9	3
					98.8	4
629	3001.60	306.5	3			
630	04.20	277.5	5		3004.5	4
				H_2O	10.7	11
				H_2O	13.0	11
631				H_2O	13.8	11
				H_2O	16.0	11
				H_2O	16.9	11
	CH_4 (Q branch)			H_2O	18.7	11
				CH_4	18.8	3
632	21.35	089.0	5			
633	22.20	079.5	5			
634	25.75	040.5	5		25.7	4
635	28.90	006.5	4	CH_4	28.3	3
636	31.20	32981.0	4	H_2O	31.4	11
				H_2O	33.1	11
637	34.40	946.5	4			
638	35.60	933.5	3			
639	38.70	900.0	6	CH_4	38.2	3
				H_2O	38.2	11
					38.63	2
640	42.75	856.5	3			
641	44.20	840.0	4			
642	48.90	790.0	5	CH_4	47.8	3
				H_2O	48.9	11
643	52.35	752.5	4			
644				CH_4	57.3	3
				H_2O	56.7	11
645	60.00	670.5	4	H_2O	59.8	11
646	64.60	621.5	3	H_2O	64.4	11
647	66.60	600.5	3	CH_4	66.7	3
				H_2O	66.9	11
648	73.40	528.5	3		73.43	2
				CH_4	76.2	3
				H_2O	76.8	11
649				H_2O	78.0	11
				H_2O	80.1	11
				H_2O	81.4	11
				H_2O	83.1	11
650	86.15	394.0	4	CH_4	85.5	3
				H_2O	86.1	11
651	87.15	383.5	2			
652	89.95	354.0	4			
				H_2O	94.0	11
653				CH_4	94.6	3
				H_2O	95.4	11
				H_2O	96.1	11

TABLE 1—*Continued*

Line No.	Frequency [Cm^{-1}(Vac)]	Wave Length A(Air)	No. of Measurements	Identification	Laboratory Value [Cm^{-1}(Vac)]	Source*
				H_2O	3100.1	11
				H_2O	01.5	11
654				H_2O	03.1	11
				CH_4	03.8	3
				H_2O	04.8	11
655	3107.70	32169.5	4	H_2O	07.4	11
656	10.10	144.5	4			
				CH_4	12.7	3
657				H_2O	14.2	11
				H_2O	16.1	11
658				H_2O	18.2	11
				H_2O	19.0	11
				CH_4	21.7	3
659	22.50	017.0	3	H_2O	22.4	11
660				H_2O	26.9	11
				CH_4	30.7	3
661	33.00	31909.5	6	H_2O	31.7	11
				H_2O	33.2	11
662	36.40	874.5	4	H_2O	36.5	11
663	40.55	832.5	6	H_2O	40.4	11
				CH_4	39.4	3
					40.14	2
664	43.00	808.0	6	H_2O	42.6	11
665	46.65	771.0	5			
666	49.20	745.5	6	CH_4	48.3	3
				H_2O	48.9	11
667	51.50	722.0	6			
668	52.30	714.0	2			
669	55.45	682.5	5			
670	57.65	660.5	5	CH_4	56.9	3
					57.51	2
671	62.15	615.5	2			
672	64.00	596.5	5			
673	66.35	573.5	2			
674	68.05	556.5	5			
675	69.60	541.0	5			
676	73.15	505.0	5		73.15	2
677	75.05	487.0	5			
678				H_2O	77.9	11
679	82.75	411.0	5			
680	85.15	387.0	5	H_2O	85.6	11
681	92.10	318.5	5		92.06	2
682	96.45	276.5	2	H_2O	96.6	11
683	97.80	263.0	5	H_2O	98.1	11
684	99.85	243.0	2			
685	3203.60	206.5	5			
686	09.85	145.5	5	H_2O	3210.2	11
687	14.15	104.0	5	H_2O	14.4	11
688	16.55	080.5	5			
689	19.80	049.0	5	H_2O	19.8	11
690	22.00	028.0	4	H_2O	22.6	11
691	26.20	30987.5	5			
692	27.70	973.5	5	H_2O	27.6	11
693	30.00	951.0	5	H_2O	29.9	11
				H_2O	30.2	11
694	32.80	924.5	5	H_2O	33.3	11
695	36.85	886.0	5	H_2O	36.9	11
696	40.45	851.5	5	H_2O	40.5	11
697	42.00	836.5	5			

TABLE 1—*Continued*

Line No.	Frequency [Cm^{-1}(Vac)]	Wave Length A(Air)	No. of Measurements	Identification	Laboratory Value [Cm^{-1}(Vac)]	Source*
698	3245.20	30806.0	5	H_2O	3245.1	11
699	47.45	785.0	2	.....	.....	
700	49.70	763.5	6	.....	.....	
701	51.90	743.0	3	.....	.....	
702	54.55	717.5	5	H_2O	54.2	11
703	57.50	690.0	6	H_2O	57.3	11
704	60.80	658.5	5	H_2O	60.7	11
705	63.65	632.0	5	.....	.....	
706	65.40	615.5	5	.....	.....	
707	66.40	606.0	3	.....	.....	
708	71.15	562.0	3	.....	.....	
709	74.15	534.0	2	H_2O	74.0	11
710	76.40	513.0	4	H_2O	77.6	11
711	80.00	479.5	5	H_2O	78.8	11
				H_2O	80.6	11
712	83.55	446.5	5	H_2O	83.2	11
713	86.30	421.5	5	.....	.....	
714	88.95	396.5	5	H_2O	89.1	11
715	92.55	363.0	4	H_2O	91.7	11
				H_2O	93.3	11
716	97.60	317.0	6	H_2O	98.1	11
717	3300.42	291.0	6	.....	.....	
718	03.25	264.5	5	.....	.....	
719	08.90	213.5	5	H_2O	3308.8	11
720	10.65	197.5	5	H_2O	10.7	11
721	13.10	175.0	5	H_2O	12.3	11
				H_2O	13.4	11
722	17.65	133.5	6	.....	.....	
723	18.70	124.0	6	.....	.....	
724	20.70	106.0	6	.....	.....	
725	23.35	082.0	3	H_2O	23.1	11
726	24.75	069.5	3	H_2O	25.0	11
727	27.05	048.5	5	.....	.....	
728	29.80	023.5	5	.....	.....	
729	32.70	29997.5	4	.....	.....	
730	35.00	977.0	5	H_2O	35.1	11
731	37.00	959.0	5	H_2O	37.3	11
732	39.35	937.5	5	.....	.....	
733	40.45	928.0	5	.....	.....	
734	41.65	917.5	3	.....	.....	
735	42.50	909.5	5	.....	.....	
736	46.30	875.5	6	.....	.....	
737	48.50	856.0	6	.....	.....	
738	50.15	841.0	4	.....	.....	
739	51.60	828.5	6	.....	.....	
740	54.00	807.0	5	.....	.....	
741	56.40	785.5	5	.....	.....	
742	60.25	751.5	4	.....	.....	
743	62.40	732.5	4	.....	.....	
744	65.75	703.0	3	.....	.....	
745	67.60	686.5	3	.....	.....	
746	69.30	671.5	3	.....	.....	
747	71.40	653.5	5	.....	.....	
748	75.15	620.0	6	.....	.....	
749	78.35	592.0	2	.....	.....	
750	79.45	582.5	6	.....	.....	
751	80.80	570.5	6	.....	.....	
752	84.90	535.0	6	.....	.....	
753	90.20	489.0	2	.....	.....	
754	92.80	466.0	4	.....	.....	

TABLE 1—*Continued*

Line No.	Frequency [Cm^{-1}(Vac)]	Wave Length A(Air)	No. of Measurements	Identification	Laboratory Value [Cm^{-1}(Vac)]	Source*
755	3397.45	29425.5	4			
756	3402.05	386.0	3			
757	03.65	372.0	3			
758	06.80	345.0	4			
759	09.00	326.0	4			
760	13.15	290.5	4			
761	15.75	268.0	4			
762	21.15	222.0	3			
763	28.00	163.5	4			
764	31.40	134.5	4			
765	32.70	123.5	3			
766	36.45	091.5	4			
767	38.50	074.5	3			
768	40.70	055.5	3			
769	42.75	038.5	3			
770	47.10	002.0	3			
771	53.40	28949.0	3			
772	56.10	926.5	4			
773	57.95	911.0	4			
774	62.00	877.0	4			
775	64.75	854.0	2			
776	67.05	835.0	3			
777	70.50	806.5	3			
778	71.75	796.0	3			
779	74.30	774.5	3			
780	81.80	713.0	3			
781	83.30	700.5	2			
782	88.30	659.0	3			
783	91.30	634.5	3			
784	96.45	592.5	3			

SOURCES OF LABORATORY VALUES

1. K. Narahari Rao, *J. Chem. Phys.*, **18**, 213, 1950.
2. O. C. Mohler and A. K. Pierce, *Pub. A.S.P.*, **61**, 221, 1949.
3. A. H. Nielsen and H. H. Nielsen, *Phys. Rev.*, **48**, 864, 1935.
4. M. V. Migeotte, *Final Report* (Ohio State University Research Foundation, 1948).
5. Our laboratory measurements on CO_2.
6. Our laboratory measurements on atmospheric H_2O.
7. Our laboratory measurements on N_2O, 3600-line-per-inch grating.
8. Our laboratory measurements on CH_4.
9. G. Herzberg, *Molecular Spectra and Molecular Structure*, Vol. 2: *Infrared and Raman Spectra of Polyatomic Molecules* (New York: D. Van Nostrand Co., Inc., 1945), p. 274.
10. Hydrogen line (see text).
11. H. H. Nielsen, *Phys. Rev.*, **59**, 565, 1941.
12. R. T. Lagemann, A. H. Nielsen, and F. P. Dickey, *Phys. Rev.*, **72**, 284, 1947.

Lines of this band give strong absorption in the region of 4.5 μ–5.2 μ. Preliminary estimates with the 22-meter multiple-traversal absorption cell with a prism spectrometer at a path length of 1 mile show that the transmission of the evacuated cell in the 4.5 μ–5.2 μ region is reduced about 50 per cent when air, at a temperature of 10° C. and about 80 per cent humidity, is admitted at atmospheric pressure. This estimate is based on the energy at 3.8 μ being 100 per cent in both cases.

II. ISOTOPIC BANDS

In addition to bands of H_2O^{16}, there is a sufficient amount of *HDO* present in the atmosphere to produce strong absorptions in the more intense bands of this molecule, although the amount of D_2O^{16} present appears to be negligible. The relative abundance of O^{18}:O^{16} is 1:500, while that of D:H is 1:5000, so that lines of the isotopic molecule H_2O^{18} should also appear in solar spectra, but no laboratory data are available on the absorption bands of this molecule for comparison. It is unlikely that lines of this molecule will be observed, since the bands will lie very close to those of H_2O^{16} and will be masked by the more intense lines of this molecule. This is also true for the molecule H_2O^{17}, which will be five times less abundant than H_2O^{18}.

III. *HDO*

Since the amount of H_2O in the atmosphere is the equivalent of 2–4 cm of liquid water, there should be several atmo-mm of *HDO* in the atmosphere. The presence of this gas in the atmosphere was first suggested by Adel,[3] who identified the ν_2 fundamental in the 7.2 μ region of a prismatic solar spectrum. Recently the 3.68 μ fundamental ν_1 has been observed by Gebbie, Harding, Hilsum, and Roberts[13] in a *LiF* prismatic spectrum of about $1\frac{1}{4}$ miles of air at sea level. Many lines of this band in the solar spectrum have been identified by some of the present writers[19] by comparison with laboratory spectra of a 50-50 mixture of H_2O and D_2O. The interfering lines of D_2O in the laboratory spectrum were identified by comparison with a pure D_2O spectrum.

For the present work the identification of *HDO* lines has been extended by comparison with laboratory spectra taken in the multiple-traversal absorption cell fitted with *AgCl* windows, using a path length of 8 meters and a mixture of ten parts of H_2O to one part of D_2O. Compared with the previous laboratory spectra, the *HDO* lines were of the same intensity, but the D_2O lines were much weaker. In addition to the lines of *HDO* in this region of the solar spectrum, there are also some weak lines which have been identified with methane.

IV. CARBON DIOXIDE

Carbon dioxide occupies 0.03 per cent of the atmosphere by volume or gives an equivalent thickness of 2.4 atmo-meters of gas in a vertical column of the atmosphere. Consequently, all except very weak bands appear in the solar spectrum, as well as bands of the isotopic molecules.

The opaque region from 4.15 μ to 4.5 μ is caused by the fundamental ν_3 of the molecule $C^{12}O_2^{16}$ at 4.26 μ and of the molecule $C^{13}O_2^{16}$ at 4.37 μ. In addition to this complete absorption, the wings of these bands extend into the portion of the window lying between 3.7 μ and 4.15 μ. The two strong bands of carbon dioxide at 2.785 μ and 2.70 μ, together with the water-vapor bands in this region, give complete absorption at this end of the spectrum.

Four weaker bands at 5.17 μ, 4.84 μ, 4.77 μ, and 4.68 μ have also been observed, although they are partially overlapped by lines of water vapor and carbon monoxide. These bands are very intense on spectra taken during the winter months, but recent observations in May, 1950, with a shorter atmospheric path show a much reduced intensity. Laboratory spectra of these bands have been reported by E. F. Barker and Ta-Yuo Wu,[20]

[19] R. M. Chapman and J. H. Shaw, *Phys. Rev.*, **78**, 71, 1950.

[20] *Phys. Rev.*, **45**, 1, 1934.

who resolved the rotational structure of the band at 4.84 μ but did not give the frequencies of the individual lines. To find these frequencies, the spectrum of a 4-meter path of carbon dioxide at 60 cm pressure was taken, and the values obtained are shown in Table 1.

V. CARBON MONOXIDE

The fundamental band of carbon monoxide at 4.7 μ in the solar spectrum was first reported by Migeotte,[9] who identified more than 20 lines of the band by comparison with the laboratory spectrum published by R. T. Lagemann, A. H. Nielsen, and F. P. Dickey.[21] Later Adel[22] reported that there was no indication of this band in spectra taken at Flagstaff, Arizona, in 1941. Recently, however, Migeotte and Neven[15] have observed lines of the band in spectra taken on the Jungfraujoch in Switzerland at an altitude of about 11,730 feet, which indicates that at least part of the *CO* is of world-wide distribution.

The present spectra, recorded during the winter 1949–1950, all show intense *CO* lines. Migeotte observed that the line called R_3 by Lagemann, Nielsen, and Dickey varied from 50 per cent maximum absorption in April to 15 per cent on June 16 and 17, 1948; but on our traces, taken between December, 1949, and March, 1950, the peak absorption of this line was never less than 45 per cent. Because of overlapping bands of other gases, not all the lines of this band are completely resolved. At shorter wave lengths the 4.5 μ N_2O band is the main obscuring agent, and at longer wave lengths CO_2 and water vapor.

Recently K. N. Rao[23] has calculated line frequencies for the *CO* fundamental from constants obtained from the ultraviolet bands of the molecule and has proposed these line frequencies as standards for infrared calibration purposes. The values are about 0.2 cm^{-1} higher than those observed by Lagemann, Nielsen, and Dickey but agree to ± 0.07 cm^{-1} with frequencies for the *CO* lines as observed in the solar spectrum.

VI. METHANE

Methane was discovered in the solar spectrum by Migeotte[7] at Columbus, Ohio, in January, 1948, when he observed 13 lines of the ν_3 fundamental at 3.3 μ. The gas cannot be a local impurity, since Migeotte[24] has identified lines near 7.8 μ in the solar spectrum, taken at Flagstaff, Arizona, by Adel,[5] with lines of the ν_4 fundamental of CH_4, and the methane lines at 3.3 μ also appear on solar spectra taken at the Jungfraujoch, Switzerland, by Migeotte and Neven.[14] Recently McMath, Mohler, and Goldberg[25] have identified some weak bands of the gas between 1 μ and 2 μ, and Mohler and Pierce[17] have observed lines of the ν_3 fundamental in the solar spectrum taken at Michigan. McMath, Mohler, and Goldberg have estimated that there is probably about 1.2 p.p.m. of methane in the earth's atmosphere and suggest an average temperature of $-37°$ C. for the atmospheric column in which the methane absorption takes place, a temperature which occurs at a height of 8 km.

The present map (Fig. 3) shows the intense *Q* branch and some lines in the *P* and *R* branches, but many are obscured by overlapping lines of the 3.18 μ water-vapor band. The frequencies obtained by A. H. Nielsen and H. H. Nielsen[26] are shown in the table.

In addition to the strong lines of this band, many weaker lines of this gas occur in the 3.5 μ–4.0 μ region. Laboratory spectra of 15 atmo-cm of methane have been taken and used to identify some of these lines, many of which occur in the region occupied by the *HDO* band. There are also a few weak lines in the 3.9 μ and 4.06 μ bands of N_2O. The laboratory frequencies of these lines are given in Table 1, although not all of them are resolved in the solar spectrum.

[21] *Phys. Rev.*, **72**, 284, 1947.

[22] *Phys. Rev.*, **75**, 1766, 1949.

[23] *J. Chem. Phys.*, **18**, 213, 1950.

[24] *Phys. Rev.*, **74**, 112, 1948.

[25] *Phys. Rev.*, **73**, 1203, 1948; **74**, 623, 1948.

[26] *Phys. Rev.*, **48**, 864, 1935.

VII. NITROUS OXIDE

Adel[3] first suggested the existence of nitrous oxide in the atmosphere in 1939 to explain an absorption observed at 7.8 μ in his solar spectra taken at Flagstaff, Arizona. Its existence was confirmed in 1948 by Migeotte[8] at Columbus, Ohio, and by J. H. Shaw, G. B. B. M. Sutherland, and T. W. Wormell[27] in England, who independently found bands of N_2O at 3.9 μ and 4.5 μ in the solar spectrum. Recently, other bands of nitrous oxide have been observed by McMath and Goldberg[18] in the 1 μ–2 μ region of the solar spectrum, and they have observed a band at 2.97 μ. Migeotte and Neven[14] have obtained spectra of the 3.9 μ and 4.06 μ bands of the gas from the Jungfraujoch in Switzerland, and W. Benesch[28] has observed the 3.9 μ band and a weak band at 3.57 μ at Johns Hopkins University, Maryland. The envelopes of the 3.9 μ band, the 4.06 μ band, and part of the 4.5 μ band of N_2O stand out clearly in the solar spectra recorded by Langley[2] in 1900. The permanent character and world-wide distribution of N_2O have now been definitely established, and various writers have suggested that there is from 0.5 to 1.0 p.p.m. in the atmosphere, from comparison with laboratory spectra.

An accurate estimate of the amount in the atmosphere cannot be made from the intensity of the bands until the average height and pressure of the gas are known, since the bands are very susceptible to pressure broadening. Measurements made with the long multiple-traversal absorption cell with low dispersion show that, in a path length of 1 mile of air at atmospheric pressure containing 5 p.p.m. of N_2O, there is a maximum absorption of 30 per cent for the 3.9 μ band. For the same amount of gas plus 1 mm *Hg* pressure of air, the absorption falls to less than 10 per cent.

Three bands of N_2O are shown in the grating map—the fundamental ν_3 at 4.5 μ, the overtone $2\nu_1$ at 3.9 μ, and the weak combination band (00°0–12°0) at 4.06 μ. The band at 3.57 μ has not yet been identified in our solar spectrum, probably because it is too weak.

3.9 μ band (00°0–20°0).—Over seventy rotational lines of this band, lying between 3.85 μ and 3.95 μ have been resolved. There are few other interfering lines in this region, and most of these are weak lines of methane. It has been found that the line frequencies of the N_2O lines can be represented by the formula

$$\nu = 2563.50 + 0.8324m - 0.00350m^2 \text{ (cm}^{-1} \text{ vac)},$$

where $\nu_0 = 2563.50$ cm^{-1} is the center of the band which agrees with the value obtained by E. K. Plyler and E. F. Barker[29] and m can take the values $m = \pm 1, \pm 2, \pm 3$, etc. Our laboratory-determined frequencies of the individual lines are shown in Table 1.

The apparent intensity of the band varies with the season of the year. During the winter months the maximum absorption of the strongest lines was almost 35 per cent, but recent records in May, 1950, show only 10 per cent absorption for these lines.

4.06 μ band (00°0–12°0).—This is a weak band lying in the wings of the 4.26 μ CO_2 band, and the fine structure of the band has been obtained only when very long atmospheric path lengths could be used. The maximum absorption was never more than 10 per cent. Weak absorption lines of methane occur in this region, but they cause little interference with the band; the first line of the Brackett series of hydrogen is found at 2467.8 cm^{-1}.

The rotational lines of this N_2O band can be fitted to an equation similar to that given above:

$$\nu = 2462.00 + 0.8378m - 0.00075m^2 \text{ (cm}^{-1} \text{ vac)}.$$

[27] *Phys. Rev.*, **74**, 978, 1948.

[28] Paper presented at the Symposium on Molecular Structure and Spectroscopy, Ohio State University, June, 1950.

[29] *Phys. Rev.*, **38**, 1827, 1931.

The value observed for the band center is in good agreement with that obtained by Plyler and Barker.[29] The individual lines have been resolved in the laboratory, and measurements are given for comparison.

4.5 μ band (00°0–001).—This fundamental is the strongest of the three bands described and gives 100 per cent absorption in the strongest lines. It is overlapped by the band of $C^{13}O_2^{16}$ on the short-wave-length side, and only a few lines of the *R* branch have been observed. Two spectra are shown, one with a long atmospheric path length taken during the winter and the other taken with high sun in May, to show the variation of transmission of this band. On the long-wave-length side, lines of carbon monoxide interfere with the N_2O lines. Some of the N_2O lines have been identified by comparison with our own laboratory spectra.

VIII. OZONE

The equivalent thickness of the ozone layer in the atmosphere varies with the season between 2 and 4 atmo-mm, and the gas lies at an average height of about 25–30 km. Ozone bands occur at 4.7 μ, 9.6 μ, and 14.1 μ; but, as yet, only the 9.6 μ band has been found in the solar spectrum by Adel.[5] Recently H. S. Gutowsky and E. M. Petersen[30] have shown that the 4.7 μ band has a maximum absorption of 30 per cent for a concentration of gas several times that present in the atmosphere. Thus this atmospheric band will be weak, and, since it occurs in a region occupied by other strong bands, it has not yet been observed.

IX. NITRIC OXIDE

Although the presence of this gas in the atmosphere has been suggested, no definite evidence of its existence has been produced. Since the fundamental lies in the region covered by Figure 3, it was hoped that an upper limit could be set to the amount present. However, A. H. Nielsen and W. Gordy[31] and R. H. Gillette and E. H. Eyster[32] have reported that the fundamental occurs near 1875 cm^{-1}, where the water-vapor absorption is beginning to be intense. Spectra were taken on the coldest days of the winter to discover lines of the gas in the few windows which exist, but no lines could be positively identified. The lines, if present, are weak.

X. OTHER ATMOSPHERIC GASES

Sutherland and G. S. Callender[33] give a list of gases which may exist in the atmosphere and the evidence available for their presence. Of these gases, methane and nitrous oxide have been identified. The present writers have not obtained any evidence for the existence of any of the other oxides of nitrogen, and no other hydrocarbon bands have been observed in our solar spectra.

XI. SOLAR LINES

The intensity of line number 256 at 2467.8 cm^{-1} does not change appreciably from winter to summer or with solar altitude and hence must be of solar, and not telluric, origin. It has been identified as the first member of the Brackett series of the hydrogen spectrum. Benesch[28] has also made the same identification of this line. The authors have not identified any other solar lines in this region.

The authors wish to acknowledge the interest and encouragement of Professors H. H. Nielsen and Dudley Williams in this work.

[30] *J. Chem. Phys.*, **18**, 564, 1950.

[31] *Phys. Rev.*, **56**, 781, 1939.

[32] *Phys. Rev.*, **56**, 1113, 1939.

[33] *Rep. Prog. Phys.*, **9**, 18, 1943.

THE SPECTRA AND ORBITS OF AR LACERTAE

ROSCOE F. SANFORD
Mount Wilson and Palomar Observatories, Carnegie Institution of Washington,
California Institute of Technology
Received December 15, 1950

ABSTRACT

New elements of the spectroscopic binary AR Lacertae differ but slightly from Harper's. The *absorption lines* of the secondary star are wide and shallow directly preceding and following primary minimum. At other phases the profiles more nearly resemble those of the primary. The absorption lines of the primary are deeper than those of the secondary except in the phase interval 0.289–0.637 day. These variations of width and of percentage absorption preceding and following primary eclipse point to the importance of photometric observations for a considerable interval before and after primary eclipse as well as within it. Both stars have H and K in emission. These lines are not monochromatic, being 168 and 78 km/sec wide for secondary and primary, respectively. These widths give radii for the two stars that are 85 per cent of the values found photometrically with strong limb darkening. The average intensity of the emission H and K lines of the secondary, relative to those of the primary, is 3.8. Velocities from these emission lines average 6.4 km/sec less algebraically than the velocities from the absorption lines.

Photoelectric observations of the eclipsing binary AR Lacertae by F. B. Wood[1] showed that it varies from magnitude 7.31 at maximum to 8.20 when the primary star is totally eclipsed. He concluded also that the primary star was itself a variable. The spectral class of the primary is G5, that of the secondary K0, according to A. B. Wyse,[2] who found the H and K lines to be bright at primary minimum (total eclipse). G. E. Kron, in discussing his photoelectric observations,[3] commented as follows on the variability of the G5 component:

> The peculiar variations in the light curves can be explained on the hypothesis that the surface of the G5 star has upon it huge light and dark patches. . . . The patches must be of such size that a projected hemisphere at times has as much as 20 percent of its area covered, while the individual patches cover as much as 3 to 5 percent of the area. The data not only indicate that the patches are eclipsed by the K0 star but that they move, and that they form and dissolve. Furthermore, they appear and disappear around the limb, with rotation of the binary. Clearly, the phenomena are exceedingly complicated, and difficult to analyze precisely, particularly in view of the unfavorable period of rotation of the binary.

W. E. Harper[4] has derived orbital elements from spectrograms obtained at the Dominion Astrophysical Observatory.

In 1945 I began to observe this variable with the coudé spectrograph (10 A/mm), at first, primarily, for the bright H and K lines at total eclipse. It was soon evident, however, that these emission lines were always present outside, as well as within, eclipse; moreover, two components were observed, one belonging to the primary star, the other to the secondary. Table 1 is the journal of the 22 spectrograms obtained from 1945 to 1949 inclusive. The phases in Table 1 are derived from the formula

$$\text{Primary min.} = \text{JD } 2426624.338 + 1.98321525E \text{ (G.M.T.)}.$$

The epoch is Wood's and the period is Kron's, which he was kind enough to send me by letter.

The absorption lines of both components are present, well separated between eclipses but, of course, blended during eclipse. The lines are shallow and wide for stars of such advanced spectra, undoubtedly being widened by axial rotation of the same period as the orbital revolution. This fuzziness of the lines prevents the usual accuracy of measurement

[1] *Contr. Princeton. U. Obs.*, No. 21, 1946.
[2] *Lick Obs. Bull.*, **17**, 37, 1934.
[3] *Pub. A.S.P.*, **59**, 264, 1947.
[4] *J.R.A.S. Canada*, **27**, 146, 1933.

for stars of such late spectral type. Nevertheless, as will be seen later, velocities from the mean of several lines are quite consistent. They indicate essentially circular orbits, and therefore only γ, K1, and K2 were adjusted by the method of least squares. My corrected elements and the corresponding ones previously derived by Harper are given in Table 2. Although the lack of agreement in the values of γ, K1, and K2 is somewhat disappointing, it can be accounted for in part at least by the probable errors of these quantities. In any event, my values of $a \sin i$ and $m \sin^3 i$ and of the mass ratios differ but slightly from those found by Harper. The absorption velocities of Table 2 and the velocity-curves from my elements are shown in Figure 1.

TABLE 1

JOURNAL OF OBSERVATIONS

Plate No. Ce	Date	JD 243	Phase (Days)	Radial Velocity (Km/Sec)					
				Primary		Blended		Secondary	
				Abs.	Em.	Abs.	Em.	Abs.	Em.
3825	1945 June 16	1623.964	1.924	− 0.1	.....	.....	.....	− 59.8	− 58.8
3831	17	1624.975	0.951	.....	.....	−48.4	−18.4	.....	.....
3865	July 18	1655.906	0.151	− 86.5	− 98.7	.....	.....	+ 30.4	+ 21.0
3871	19	1656.905	1.150	+ 16.7	+ 7.7	.....	.....	− 88.9	− 95.0
3904	Aug. 19	1687.969	0.482	−151.8	−152.2	.....	.....	+ 66.4	+ 69.6
3970	Sept. 17	1716.818	1.566	+ 82.2	.....	.....	.....	−142.8	−145.0
3978	18	1717.860	0.625	−143.0	−144.9	.....	.....	+ 75.3	+ 53.2
4285	1946 June 11	1983.903	0.917	.....	.....	−52.2	−22.9	.....	.....
4343	July 20	2022.981	0.331	−134.4	−144.3	.....	.....	+ 69.6	+ 56.0
4351	Aug. 9	2042.889	0.407	−142.1	−149.3	.....	.....	+ 74.4	+ 64.8
4357	10	2043.988	1.506	+ 83.7	+ 81.8	.....	.....	−145.4	−142.7
4501	Dec. 13	2168.647	1.222	+ 38.8	+ 43.7	.....	.....	−110.2	−104.6
4504	14	2169.650	0.242	−121.7	−119.5	.....	.....	+ 51.2	+ 33.8
4871	1947 Sept. 26	2455.858	0.867	.....	.....	−72.6	.....	.....	.....
4876	27	2456.840	1.849	+ 13.6	− 10.8	.....	.....	− 84.7	− 80.6
4961	Nov. 2	2492.683	0.011	.....	.....	−31.5	−22.6	.....	.....
4983	Dec. 2	2522.683	0.263	−120.6	.....	.....	.....	+ 51.3	.....
5282	1948 Aug. 17	2781.882	1.644	+ 68.8	+ 67.8	.....	.....	−123.2	−130.6
5286	18	2782.858	0.636	−141.4	−141.5	.....	.....	+ 73.1	+ 58.4
5404	Oct. 24	2849.702	0.051	.....	.....	−29.8	−18.3	.....	.....
5408	25	2850.715	1.064	.....	.....	−42.1	.....	.....	.....
5453	Nov. 23	2879.688	0.289	−123.4	−131.7	.....	.....	+ 58.7	+ 49.2

Although the absorption lines of the two stellar components of AR Lac are much broadened by axial rotation and their equivalent widths consequently difficult to measure, the mean percentage absorption at the line centers should have significance in determining the relation between the absorption lines of the two stellar components. The three *Fe* I lines λλ 4045, 4063, and 4071 were chosen for this mean because they are so much stronger than near-by lines that blends would not be serious. Those spectrograms with the absorption lines of both components well separated have been traced with the microphotometer and the mean percentage absorption obtained for the three *Fe* I lines. These means were then corrected to the continuous spectrum to which each belonged, by assuming that 54.3 per cent of the total light of this variable is furnished by the primary and 45.7 per cent by the secondary, as given by Wood.[1] The density of the continuous spectrum to which these measures are referred can affect the accuracy of the percentage absorption on the various spectrograms much more than it can the ratios of these percentage absorptions. Hence only these ratios are given in Table 3.

It is apparent that the ratios average less for the interval between primary and secondary minimum (0.242–0.673 day) than for the interval between secondary and primary minimum (1.151–1.849 days). Moreover, these ratios have a somewhat orderly progression, with a minimum near phase 0.5 day and a maximum near phase 1.5 days. The lines of the primary have, therefore, their relatively strongest absorption when the primary is receding fastest and their relatively weakest absorption when the primary is approaching fastest.

Since the widths of the absorption lines of AR Lac are primarily caused by axial rotation, the ratios of the widths of the lines of the primary to those of the secondary

TABLE 2

ORBITAL ELEMENTS OF AR LACERTAE

Element	Sanford	Harper
P	1.98321525 days	1.983244 days
T(Prim. min.)	JD 2426624.338 G.M.T.	JD 2426624.377 G.M.T.
K_1	116.1 km/sec	120.0 km/sec
K_2	115.6 km/sec	119.2 km/sec
γ	− 33.7 km/sec	− 36.25 km/sec
$a_1 \sin i$	3.167×10^6 km	3.263×10^6 km
$a_2 \sin i$	3.151×10^6 km	3.247×10^6 km
$m_1 \sin^3 i$	1.29⊙	1.39⊙
$m_2 \sin^3 i$	1.30⊙	1.40⊙
m_1/m_2	0.995	0.993

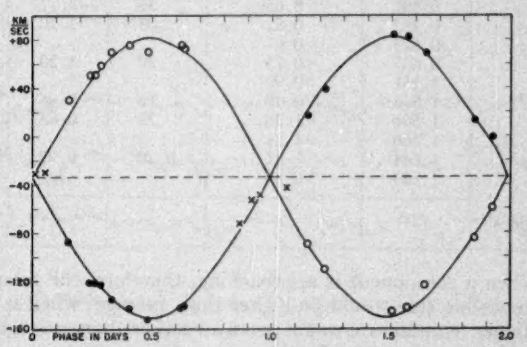

FIG. 1.—Velocity-curves of AR Lacertae. Dots represent the velocities of the primary component; circles, those of the secondary; crosses, velocities derived from blended lines. See Table 1. The velocity-curves and the γ-line are from the elements in Table 2.

should be close to the ratio of the respective radii, or, according to Wood, 1.82/2.99 = 0.61. Therefore, the ratios of the mean equivalent widths of the three *Fe* I lines should be roughly 61 per cent of the ratios in the third column of Table 3. This equivalent-width ratio varies from 0.40 to 0.80, approximately.

Six sample tracings are reproduced in Figure 2. The spectral region contains the three *Fe* I lines λλ 4045, 4063, and 4071. The first tracing has the profiles of the secondary star only, since the primary is in total eclipse. The second and third tracings belong to the first half-period, i.e., when the primary is approaching. The fourth is a tracing of a spectrogram obtained near annular eclipse of the secondary star. The last two tracings have the profiles of the lines of the two stellar components when the primary is receding.

The profiles of the secondary's lines on Ce 4504 are in strong contrast with profiles on Ce 3904. There is a similar contrast of flat, shallow profiles against relatively deep, sharp-bottomed ones between Ce 4357 and Ce 4501. An examination of all suitable tracings shows that flat, shallow profiles characterize the two intervals 1.506–1.849 and 0.152–0.242 days, i.e., preceding and following primary minimum. Kron[5] has called attention to "low portions of the curve just preceding and following primary minimum" in his light-curve for 1946. Kron's curve is for 1946 only; my spectrograms extend from 1945 to 1948, inclusive. Hence it would be important to obtain more observations of both light and spectrum within phases 1.5–0.25 days.

The heating of the stellar atmospheres by bombardment of interstellar or circumstellar particles might account in part for the foregoing observations. Whichever star is approaching would be overtaking these particles and hence would be hit by more than the average number of particles and with higher-than-average velocities of impact than

TABLE 3

PHOTOMETRIC DATA OF ABSORPTION AND EMISSION LINES OF AR LAC

PLATE Ce	PHASE (DAYS)	RATIO OF PER CENT ABSORPTION PRIM.: SEC. (MEAN FOR λλ 4045, 4063, 4071)	E.W. OF EMIS. (H+K)		
			Prim. (A)	Sec. (A)	Ratio Sec.: Prim.
4504	0.242	1.00	.....	.....	.....
4983	0.263	1.00	.....	.....	.....
5453	0.289	0.83	0.40	0.98	2.45
4343	0.331	0.71	.....	.....	.....
4351	0.407	0.85	.33	1.12	3.40
3904	0.483	0.82	.28	1.20	4.30
3978	0.625	0.67	.....	.....	.....
5286	0.637	0.75	.29	1.20	4.10
3871	1.151	0.90	.....	.....	.....
4501	1.223	0.90	.16	0.86	5.40
4357	1.506	1.38	.22	0.88	4.00
3970	1.566	1.21	.....	.....	.....
5282	1.644	1.37	0.29	0.92	3.20
4876	1.849	0.86	.....	.....	.....
Mean	.....	.....	.....	.....	3.84

for recession. When a component is approaching, therefore, the temperature of its atmosphere on the visible side would be higher than average; when it is receding, lower than average. Higher temperature would mean an earlier-than-average spectral type and consequently weaker-than-average *Fe* I lines.

Each component of AR Lac has emission lines H and K of *Ca* II. Their equivalent widths were measured upon microphotometer tracings of seven spectrograms of AR Lac which have complete separation of the lines of the two component stars. The fourth and fifth columns of Table 3 give the sums of the equivalent widths of H and K for primary and secondary, respectively, and the sixth column gives their ratio. The mean of these ratios is 3.8. The ratios increase progressively for the four spectrograms in the first half-period and decrease for the three in the second half-period. Four tracings of the H and K region (top of Fig. 2) illustrate the profiles of these emission lines. The first and third typify primary and secondary minimum, respectively; the second tracing shows the profiles of these lines when the primary is approaching, the fourth when it is receding. These emission lines are not monochromatic, the average width being 168 and 78 km/sec for secondary and primary, respectively. If it is assumed that emission H and K

[5] *Op. cit.*, p. 262.

lines come from all parts of the stellar surfaces or at least from complete equatorial zones, then the half-widths of these emission lines should be a simple function of the respective rotational velocities. The radii of primary and secondary stars are 1.54 and 2.52 solar radii, upon the assumption that the periods of axial and orbital rotation are the same. These radii are about 85 per cent of those obtained by Wood, who assumed heavy limb darkening.

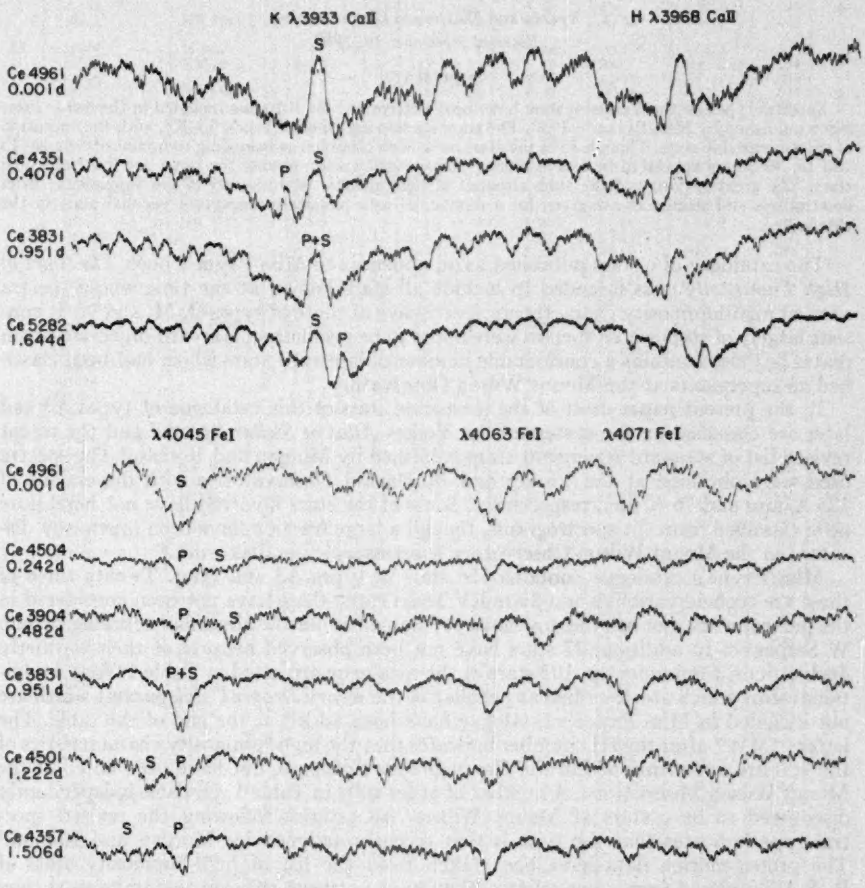

FIG. 2.—Microphotometer tracings of four spectrograms of AR Lacertae in the H and K region are at the top. The K emissions of the primary and secondary stars are identified by *P* and *S*; the H emissions have the same pattern. The six tracings in the lower group cover the region of the strong absorption *Fe* I lines λλ 4045, 4063, and 4071.

The velocities derived from the emission lines of H and K are, in the mean (28 comparisons), algebraically less by 6.4 km/sec than the velocities from all measured absorption lines of the corresponding components. This velocity difference may, of course, result from an outward flow of the source of the emission H and K lines.

SPECTRAL CLASSIFICATION OF STARS LISTED IN MISS PAYNE'S CATALOGUE OF c STARS*

WILLIAM P. BIDELMAN
Yerkes and McDonald Observatories
Received November 10, 1950

ABSTRACT

Spectral types on the Yerkes system have been determined for 102 stars included in the c-star catalogue published by Miss Payne in 1930. The stars studied are those of types A3–K5, with the exception of certain variable stars. Though 36 of the stars have been classified as belonging to luminosity classes I*a* and I*b*, 30 others appear to be less luminous than normal giants; among the latter are 9 metallic-line stars. The great majority of the stars situated at high galactic latitudes are of low luminosity. Brief descriptions and references are given for a number of astrophysically important peculiar stars in the catalogue.

The catalogue of c stars published as an appendix to Miss Payne's book *The Stars of High Luminosity*[1] was intended to include all stars known at the time whose spectra showed high-luminosity characteristics, exclusive of those of types O, M, and N. It consists largely of stars whose spectra were noted to be peculiar on Harvard objective-prism plates but also contains a considerable number of late-type stars which had been classified as supergiants at the Mount Wilson Observatory.

In the present paper most of the accessible stars of this catalogue of types A3 and later are classified on the system of the Yerkes *Atlas of Stellar Spectra*[2] and the recent revised list of standard supergiant stars published by Morgan and Roman.[3] The spectra used were obtained at the Yerkes and McDonald Observatories with dispersions of 125 A/mm and 76 A/mm, respectively. Some of the stars involved have not heretofore been classified from slit spectrograms, though a large fraction have been previously discussed in the Mount Wilson Observatory spectroscopic parallax work.[4]

Miss Payne's catalogue contains 156 stars of types A3 and later. Twenty-three of these are cepheid variables and 2 are RV Tauri stars; these have not been considered in the present work, nor has the slow nova RT Serpentis nor the abnormal eclipsing system W Serpentis. In addition, 27 stars have not been observed because of their southerly declinations. Consequently, 102 stars of the catalogue are listed in Table 1. Also 3 additional stars which are described as peculiar in the *Henry Draper Catalogue* but which are not included in Miss Payne's catalogue have been added at the end of the table. The letters "MW" after the HD number indicates that the high-luminosity characteristics of the star are not mentioned in the *Henry Draper Catalogue*, but have been noted at the Mount Wilson Observatory. A number of other stars in Table 1 were also independently discovered to be c stars at Mount Wilson. An asterisk following the revised spectral type indicates that the type is that recently assigned by Morgan and Roman.[3] The proper-motion data have been taken from the list of high-luminosity stars of R. E. Wilson[5] and from other sources; they have not been reduced to a uniform system

* *Contributions from the McDonald Observatory, University of Texas*, No. 199.

[1] "Harvard Observatory Monographs," No. 3 (New York: McGraw-Hill Book Co., 1930).

[2] W. W. Morgan, P. C. Keenan, and E. Kellman, "Astrophysical Monographs" (Chicago: University of Chicago Press, 1943).

[3] *Ap. J.*, 112, 362, 1950. The writer is greatly indebted to these authors for access to this list prior to publication.

[4] *Mt. W. Contr.*, No. 511; *Ap. J.*, 81, 187, 1935.

[5] *Mt. W. Contr.*, No. 643; *Ap. J.*, 93, 212, 1941.

TABLE 1

DATA ON THE STARS CLASSIFIED IN THE PRESENT INVESTIGATION

HD Type	HD Number	Name	α(1900)	δ(1900)	l	b	m_v	Revised Type	V	μ	Remarks
A3..	13929	.....	2h10m5	+57° 34′	102°	− 2°	8.0	Fm	− 9	0".022	1
	17093	38 Ari	2 39.5	+12 1	130	−41	5.16	A7 IV	− 2.2	.146	
	27628	60 Tau	4 16.4	+13 50	149	−23	5.76	Fm	+43 V	.117	2
	59612	HR 2874	7 25.6	−22 49	205	− 1	4.80	A5 Ib*	+36.3	.005	
	84123	.....	9 37.8	+42 31	146	+51	6.82	F0p	+15.3 V	.104	3
	125335	.....	14 13.7	+10 58	327	+62	7.13	Fm	−29.0 O	.049	4
	210221	HR 8443	22 3.8	+52 49	68	− 2	6.50	A3 Ib*	−26.5	.015	
A5..	34578	19 Aur	5 13.4	+33 52	141	− 1	5.16	A5 II*	− 4.2	.012	
	40536	2 Mon	5 54.3	− 9 34	183	−15	5.10	Fm	+22.2 O	.054	5
	142846	.....	15 51.7	+15 2	354	+44	8.07	F2 IV	.....	.036	
	148743	HR 6144	16 25.1	− 7 17	336	+25	6.39	A7 Ib	+ 2.1 V	.025	6
	218393	.....	23 2.6	+49 40	74	− 9	6.85	Bpe	var.	.015	7
F0..	571	22 And	0 5.1	+45 31	84	−16	5.08	F2 II*	− 4.8	.005	
	1778	.....	0 17.0	+53 3	86	− 9	8.0	F3 II	.....	.011	
	24550	.....	3 49.2	+ 4 53	152	−34	7.65	F3 II–III	+15	.027	
	33054	14 Ori	5 2.5	+ 8 22	160	−17	5.47	Fm	+ 4.3 V	.069	8
	36673(MW)	α Lep	5 28.3	−17 54	188	−24	2.69	F0 Ib*	+24.7	.011	
	40535	1 Mon	5 54.3	− 9 24	182	−14	6.28	F2 II	+16 V	.018	9
	70761	HR 3291	8 18.6	−26 1	215	+ 7	5.86	F2 Ib	+64.0	.009	10
	70825	.....	8 19.0	+24 17	167	+32	7.27	F2 IV	− 2	.058	
	75276	HR 3496	8 43.9	−45 48	233	− 1	5.83	F0 Ib	+32.0	.008	
	105702	11 Vir	12 5.0	+ 6 22	247	+67	5.74	Fm	− 9.2	.161	11
	110628	.....	12 38.4	+26 40	256	+89	6.71	F2n III	.....	.022	
	116108	.....	13 16.4	+61 46	82	+56	9.1	F3 IV	.....	.....	
	137052	ϵ Lib	15 18.8	− 9 57	321	+36	5.08	F5 V	− 9.7 O	.175	
	143584	HR 5964	15 56.2	+50 10	45	+47	5.90	F0 IV	+ 4.0	.061	
	149748	.....	16 31.7	+63 2	60	+39	7.22	Fm	−21.7	.050	12
	164136	ν Her	17 54.7	+30 11	23	+22	4.48	F2 II*	−22.0	.006	
	194943(MW)	ρ Cap	20 23.2	−18 9	355	−31	4.96	F2 III	+19.5	.028	13
	201638	.....	21 5.8	+35 5	48	− 9	8.72	B0.5 Ib	.....	.020	
	201700	.....	21 6.2	+46 0	56	− 2	8.1	B3 IV	.....	.....	
	214470	31 Cep	22 33.3	+73 7	81	+13	5.22	F4 II–III	+ 0.7	.172	
F2..	13824	.....	2 9.6	+57 45	102	− 2	8.60	F2 IV	.....	.055	
	43382	.....	6 10.8	+35 10	145	+10	6.62	F6 V	.....	.066	
	90089	HR 4084	10 18.9	+83 4	95	+34	5.34	F2 V	+ 7.0	.085	
	102942–3	HR 4545	11 46.0	+33 56	149	+77	6.14	Fm	+ 0.8	.024	14
	130818	RY Boo	14 45.2	+23 27	358	+62	7.0–7.4	F6 IV	+ 1.9	.051	15
	178524	π Sgr	19 3.8	−21 11	343	−15	3.02	F2 II	− 9.8	.043	16
	181615–6	υ Sgr	19 16.0	−16 8	350	−15	4.35–4.44pe	Ape	+ 8.2 O	.005	17
	187258	.....	19 44.0	+18 24	24	− 5	7.6	Fm	.....	.026	18
	207826	.....	21 46.8	+66 20	74	+10	6.51	F3 IV	−15.2 O	.061	
F5..	7927	ϕ Cas	1 13.8	+57 42	95	− 4	5.25	F0 Ia*	−24.7 V	.002	19
	20902	α Per	3 17.2	+49 30	115	− 5	1.90	F5 Ib*	− 2.4	.035	
	24546	43 Per	3 49.2	+50 24	118	− 1	5.47	F5 IV	+25.7 O	.160	
	31964	ϵ Aur	4 54.8	+43 40	130	+ 2	3.7–4.5pg	A8 Ia	− 2.5 O	.006	20
	50058	.....	6 46.4	+29 34	154	+15	7.66	F5 V	.....	.083	
	61715	HR 2957	7 35.5	−48 22	229	−12	5.65	F4 Iab	+11.0	.009	
	67523(MW)	ρ Pup	8 3.3	−24 1	211	+ 6	2.88	F6 II	+46.6 V	.097	21
	74180	HR 3445	8 37.3	−46 18	233	− 2	4.06	F2 Ia	+25.3 V	.008	22
	83808–9(MW)	o Leo	9 35.8	+10 21	193	+43	3.76	Comp.	+27.1 O	.143	23
	161471	ι^1 Sco	17 40.6	−40 5	318	− 7	3.14	F2 Ia*	−27.6 V	.006	24
	163506	89 Her	17 51.4	+26 4	19	+22	5.48	F2 Ia*	−29.4 V	.005	25
	195295	41 Cyg	20 25.3	+30 2	39	− 6	4.09	F5 II*	−18.8	.011	
	196524	β Del	20 32.9	+14 15	27	−17	3.72	F5 III	−21.0 O	.111	26
F8..	54605	δ CMa	7 4.3	−26 14	206	− 7	1.98	F8 Ia*	+34.3 V	.006	27
	65228(MW)	11 Pup	7 52.6	−22 37	208	+ 4	4.35	F8 II	+13.8	.026	
	128027	.....	14 29.5	− 4 13	314	+48	7.6	F8 V	.....	.025	
	161796	.....	17 42.5	+50 5	44	+30	7.27	F3 Ib	.....	.022	28
	171620	.....	18 30.8	+34 20	30	+17	7.8	F6p	−32.8	.268	29
	171635	45 Dra	18 30.9	+56 58	53	+24	4.95	F7 Ib*	−11.7	.011	
	172052	.....	18 32.9	−23 16	338	− 9	6.79	F5 Ib	.....	.018	
	180028	.....	19 9.8	+ 5 52	9	− 4	7.24	F6 Ib	− 5.9	.022	
	194093	γ Cyg	20 18.6	+39 56	46	+ 1	2.32	F8 Ib*	− 7.6	.006	
	224014	ρ Cas	23 49.4	+56 57	83	− 4	4.1–6.2	Pec.	−42.6 V	.005	30
G0..	14662	HR 690	2 16.9	+54 55	104	− 4	6.46	F7 Ib*	−26.2	.032	
	26673–4(MW)	52 Per	4 8.1	+40 14	127	− 7	4.89	Comp.	+ 3 V	.030	31
	30353	.....	4 41.8	+43 6	129	0	7.7	Ape	var.	.014	32
	31910	β Cam	4 54.5	+60 18	117	+12	4.22	G0 Ib*	− 1.7	.015	
	57146	HR 2786	7 14.8	−26 25	207	− 5	5.40	G0 II	+33.1	.016	
	62058	R Pup	7 37.0	−31 25	214	− 3	6.64 V	G0 Ia*	.....	.020	33
	63700	ξ Pup	7 45.1	−24 37	209	+ 2	3.47	G3 Ib*	+ 3.7 V	.002	34
	67594(MW)	ζ Mon	8 3.6	− 2 41	193	+17	4.41	G2 Ib*	+29.6	.016	
	97334	HR 4345	11 7.1	+36 21	151	+69	6.32	G0 V	− 2.6	0.324	

* Type by Morgan and Roman, *Ap. J.*, **112**, 362, 1950.

TABLE 1—*Continued*

HD Type	HD Number	Name	α(1900)	δ(1900)	l	b	m_v	Revised Type	V	μ	Remarks
G0..	108134	.....	12h20m3	+61°14′	94°	+57°	7.41	G0p	−46.7	0".142	35
	159181(MW)	β Dra	17 28.2	+52 23	46	+32	2.99	G2 Ib	−20.1 V	.013	36
	.....(MW)	RZ Oph	18 40.9	+ 7 7	6	+ 3	10.0–10.9pg	F3 Ib	+ 0.7 V	.....	37
	187203	HR 7542	19 43.7	+10 26	17	− 9	6.38	F8 Ib–II	− 4.9	.012	38
	192876	α^1 Cap	20 12.1	−12 49	359	−26	4.55	G3 Ib*	−25.9	.019	
	209750	α Aqr	22 0.6	− 0 48	28	−43	3.19	G2 Ib*	+ 7.6	.021	
	217476	HR 8752	22 55.9	+56 24	76	− 3	5.48	G0 Ia*	−58.4 V	.005	39
	222574(MW)	104 Aqr	23 36.6	−18 23	30	−72	4.95	G0 II*	+ 4.8	.016	
G5..	16901(MW)	14 Per	2 37.5	+43 52	111	−13	5.58	G0 Ib	− 3.5	.008	
	18474	HR 885	2 53.1	+46 49	113	− 9	5.61	Gp	+ 6.4	.032	40
	25056	.....	3 53.8	+53 35	116	+ 2	7.35	F9 Ib	− 6.3	.004	
	86728	20 LMi	9 55.3	+32 26	162	+54	5.60	G2 V	+54.6	.680	
	101501	61 UMa	11 35.7	+34 46	149	+75	5.46	B8 V	− 5.4	.390	
	180262	HR 7300	19 10.8	+14 54	17	0	5.69	G5p	−22.9	.014	41
K0..	25878(MW)	XX Cam	4 0.9	+53 6	118	+ 2	8.7–10.3pg	Fp	+15.9	.006	42
	29094–5(MW)	58 Per	4 29.7	+41 4	130	− 3	4.46	Comp.	+ 4.2 O	.021	43
	52497(MW)	ω Gem	6 56.4	+24 21	160	+14	5.21	G5 II*	− 8.8	.002	
	78004	HR 3614	9 0.7	−46 42	236	0	3.69	K2 III	+24.3	.058	
	192577–8(MW)	σ^1 Cyg	20 10.5	+46 26	50	+ 6	3.95	Comp.	− 6.9 O	.006	44
	192909–10(MW)	σ^2 Cyg	20 12.3	+47 24	51	+ 6	4.16 V	Comp.	−14.4 O	.001	45
	205114–5(MW)	HR 8242	21 28.1	+52 11	63	+ 1	6.20	Comp.	−24.0 V	.009	46
	213310–1(MW)	5 Lac	22 25.4	+47 11	68	− 9	4.61	Comp.	var.	.011	47
K2..	44537(MW)	ψ^1 Aur	6 17.2	+49 20	133	+17	6.6–7.2pe	K5 Iab*	+ 4.2 V	.006	48
	50877	σ^1 CMa	6 49.9	−24 4	202	− 9	4.12	K3 Iab*	+36.3	.013	
	184398–9	HR 7428	19 29.2	+55 31	54	+16	6.52	Comp.	− 5.2 O	.018	49
K5..	106690	2 CVn	12 11.1	+41 13	112	+75	5.80	M1 III	−15.2	.042	
	192410	.....	20 9.6	−17 9	354	−27	7.76	K5 III	.....	.044	
	196725(MW)	θ Del	20 34.1	+12 58	26	−18	6.06	K3 Ib	−14.2	.008	
	200905(MW)	ξ Cyg	21 1.3	+43 32	54	− 3	3.92	K5 Ib*	−19.9 V	.008	50
	6474	.....	1 0.7	+63 15	92	+ 1	8.4	G0 Iab	.....	.027	51
	172365	HR 7008	18 34.7	+ 5 10	4	+ 4	6.30	F8 Ib–II	−18.5	.017	52
	180583	HR 7308	19 12.0	+27 45	28	+ 6	6.06	F6 II	−13.4	0.021	

NOTES TO TABLE 1

1. K-line A3, metallic spectrum F2 III.
2. Classified by Roman, Morgan, and Eggen (*Ap. J.*, **107**, 107, 1948) as K-line A5, metallic spectrum F2. Velocity range 39 km/sec (*Pub. Dom. Ap. Obs. Victoria*, **7**, 337, 1945).
3. All lines are abnormally weak, as in the early-type subdwarfs. Velocity range 20 km/sec (*Pub. David Dunlap Obs.*, **1**, 251, 1942).
4. K-line A5, metallic spectrum F2 III.
5. K-line A5, metallic spectrum F0 III.
6. Velocity range 12 km/sec (*Pub. Dom. Ap. Obs. Victoria*, **7**, 1, 1937).
7. This well-known shell star has been recently studied by Merrill (*Ap. J.*, **110**, 420, 1949), and by Halliday (*J.R.A.S. Canada*, **44**, 149, 1950).
8. K-line A3, metallic spectrum F5 II–III. Velocity range 14 km/sec (*Pub. Dom. Ap. Obs. Victoria*, **1**, 287, 1921). Visual binary: $d = 1".0$, $\Delta m = 0.8$.
9. Velocity range 25 km/sec (*Mt. W. Contr.*, No. 593; *Ap. J.*, **88**, 34, 1938).
10. Visual binary: $d = 0".1$, $\Delta m = 0.3$.
11. K-line F0, metallic spectrum F5 III.
12. K-line A3, metallic spectrum F3 II.
13. Visual binary: $d = 2".2$, $\Delta m = 5.0$.
14. K-line A5, metallic spectrum F5 II.
15. This star was once considered to be a cepheid but was later shown to be an irregular variable. The spectrum appears quite normal.
16. Visual triple system: $d = 0".1$, $\Delta m = 0.1$, and $d = 0".4$, $\Delta m = 2.3$. The close pair should eventually give a good absolute magnitude and mass for this rather luminous system.
17. This apparently hydrogen-poor star has been extensively studied by Greenstein (*Ap. J.*, **91**, 438, 1940, and later) and many others. The light-variability found by S. Gaposchkin has been recently confirmed by Eggen and Kron (*Pub. A.S.P.*, **62**, 171, 1950).
18. K-line F0, metallic spectrum F5 III.
19. Velocity range 10 km/sec (*Pub. A.S.P.*, **36**, 137, 1924).
20. The type given is from a spectrogram taken December 12, 1949. $H\beta$ is weaker than normal for this type, and the spectrum is probably slightly variable, even outside eclipse. The primary of this well-known system shows semiregular variations in radial velocity and light which have been discussed by McLaughlin (*Ap. J.*, **79**, 235, 1934).
21. Velocity range 11 km/sec (*Ann. Cape Obs.*, Vol. **10**, Part 8, 1928). The *Ca* II lines are rather weak for the type given (cf. *Harvard Ann.*, **28**, 96, remark 82, 1897).
22. Velocity range 14 km/sec (*Pub. Lick Obs.*, Vol. **16**, 1928).
23. Primary F6 II, secondary about A2.
24. Velocity range 16 km/sec (*Ann. Cape Obs.*, Vol. **10**, Part 8, 1928).
25. Velocity range 8 km/sec (*Pub. Lick Obs.*, Vol. **16**, 1928).
26. Visual binary: $d = 0".5$, $\Delta m = 1.0$.
27. Velocity range 6 km/sec (*Pub. Lick Obs.*, Vol. **16**, 1928).
28. The lines are very strong, and some may have an unusual intensity. This high-latitude supergiant deserves further study.
29. The lines, especially of hydrogen, are weak, as in the subdwarfs.
30. The remarkably variable spectrum of this very luminous star has not yet returned to its "normal" type of F8 Ia. The spectrum has been described in recent years by Keenan (*Ap. J.*, **106**, 295, 1947), Thackeray (*M.N.*, **108**, 276, 1948), Greenstein (*Ap. J.*, **108**, 78, 1948), and others.

NOTES TO TABLE 1—*Continued*

31. Primary G5 II, secondary A or B. Velocity range 33 km/sec (*Pub. A.S.P.*, **30**, 352, 1918).
32. This star, which appears to be a somewhat later-type analogue to υ Sagittarii, has been studied by the writer (*Ap. J.*, **111**, 333, 1950). The proper motion given was determined by Dr. G. Van Biesbroeck. A photometric study of this object would be very desirable.
33. R Puppis is the brightest star in the galactic cluster NGC 2439; the writer has obtained a visual absolute magnitude of −7.2 for it (*A.J.*, **55**, 165, 1950). Gould discovered this star to be variable visually, and subsequently a photographic variation of 0.6 mag. was found at Harvard (*Harvard Ann.*, **45**, 315, 1901), but other observers have not found the star to be variable. The radial velocity is near +70 km/sec.
34. Velocity range 8 km/sec (*Ann. Cape Obs.*, Vol. **10**, Part 8, 1928).
35. The spectrum of this star has been found by Dr. N. G. Roman to resemble that of a subdwarf (*Ap. J.*, in press).
36. Velocity range 10 km/sec (*Pub. A.A.S.*, **6**, 105, 1927).
37. A velocity range of 24 km/sec has been published for this eclipsing system by Adams, Joy, and Sanford (*Pub. A.S.P.*, **36**, 139, 1924), but Hiltner found no orbital variation on low-dispersion spectrograms (*Ap. J.*, **104**, 396, 1946). The value of the velocity given in the table is the average of Hiltner's determinations. The type given is that of the primary and is taken from a plate obtained on April 17, 1948. The spectroscopic luminosity of this system is considerably greater than that derived by Lohmann (*Zs. f. Ap.*, **27**, 161, 1950).
38. The G band is considerably stronger than in γ Cygni, F8 *Ib*, and the luminosity is probably somewhat lower. The strength of *CH* may be slightly abnormal.
39. Velocity range 7 km/sec (*Pub. Lick Obs.*, Vol. **16**, 1928).
40. The spectrum is extraordinarily peculiar, with the line spectrum matching fairly well G5 III but with no trace of *CN* or *CH* absorption. This star may be a unique case of *low* carbon abundance (see *Harvard Ann.*, **56**, 104, remark 15, 1912).
41. In general, the spectrum is similar to G5 II, but the hydrogen lines are definitely weaker than normal for this type. The *CH* band is probably of slightly abnormal strength. The common proper-motion companion, HD 180243, m_v = 7.8, is of type A1 V. Its radial velocity agrees well with that of the brighter star (*Ap. J.*, **111**, 221, 1950).
42. This recently discovered variable star was shown to be spectroscopically similar to R CrB by the writer (*Ap. J.*, **107**, 413, 1948).
43. Primary G8 II, secondary A or B.
44. Primary K2 II, secondary about B3 V. R. H. Wilson, Jr., has interferometrically found this system to have a separation of 0".06, and McLaughlin has observed an atmospheric eclipse (*A.J.*, **55**, 153, 1950).
45. Primary K3 *Ib*–II, secondary A or B. McLaughlin has recently discussed the variation of the spectrum of this system during eclipse (*Ap. J.*, **111**, 449, 1950).
46. Primary G0 II, secondary A. Velocity range 11 km/sec (*Pub. Dom. Ap. Obs., Victoria*, **3**, 209, 1925).
47. Primary M0 *Ib*–II, secondary A. Velocity range 33 km/sec (*Ap. J.*, **88**, 201, 1938).
48. Velocity range 7 km/sec (*Pub. Lick Obs.*, Vol. **16**, 1928).
49. Primary K2 II–III, secondary A. The spectrum shows strong emission lines of *Ca* II.
50. Velocity range 11 km/sec (*Pub. Lick Obs.*, Vol. **16**, 1928).
51. The G band is slightly stronger than in R Puppis.
52. See remark 38.

and are thus of indicative value only. Variable radial velocity or the existence of a spectrographic orbit is indicated by a "V" or "O" in the radial-velocity column. Remarks concerning individual stars follow the table.

An enumeration of the number of stars which have been classified into various categories is given in Table 2. The listing is subdivided according to whether the star was

TABLE 2

NUMBERS OF STARS IN VARIOUS GROUPS

Type of Object	Included because of Harvard Objective-Prism Observation	Included because of Mount Wilson Slit-Spectra Observation
Lum. classes *Ia* and *Iab*	10	1
Lum. classes *Ib* and *Ib*–II	19	7
Lum. classes II, II–III, and III	15	5
Lum. classes IV and V	18	0
Composite spectra (primary more luminous than class III)	1	7
Metallic-line stars (dwarfs)	9	0
Subdwarfs	3	0
Peculiar stars	6	1

noted to be a c star at the Harvard Observatory or solely at the Mount Wilson Observatory. It is seen in Table 2 that 30 stars, of a total of 102, have been classified as less luminous than normal giants; but no star included in the catalogue on the basis of observation by slit spectra is among these. On the other hand, the great majority of the

stars which have been classified as of high luminosity were noted as such on the Harvard objective-prism plates. This is especially true of stars resembling δ CMa and γ Cygni.

It was one of the purposes of the program to determine whether an appreciable number of the many high-latitude stars listed in the c-star catalogue are actually supergiant stars. As might have been expected, most of these objects proved to be of low or intermediate luminosity, among them being several metallic-line stars which are known to be dwarf stars, despite the fact that in many ways their spectra resemble F-type stars of

TABLE 3

HIGH-LUMINOSITY STARS AT MODERATELY HIGH GALACTIC LATITUDE

Star	m_v	Type	l	b
HR 6144	6.39	A7 Ib	336	+25°
89 Her	5.48	F2 Ia	19	+22°
HD 161796	7.27	F3 Ib	44	+30°

luminosity classes II or III. The only high-luminosity stars found fainter than 5th magnitude with a galactic latitude greater than 20° are the three objects listed in Table 3.

Although this investigation has, on the one hand, confirmed the statement of Wilson[5] that a considerable number of stars included in the c-star catalogue are not actually of high luminosity, it has also resulted in the discovery of several stars of considerable astrophysical interest. Peculiar objects to which attention has been directed as a result of their inclusion in Miss Payne's catalogue are the following: two stars showing subdwarf spectral characteristics, HD 84123 and HD 171620; the apparently hydrogen-poor star, HD 30353; the "hot" carbon star, XX Cam; and the unusual object which appears to show a deficiency of carbon, HR 885. In addition, a number of southern high-luminosity stars have been classified on slit spectra for the first time.

A FINDING LIST OF HIGH-LUMINOSITY STARS

LUIS MÜNCH
Observatorio Astrofisico Nacional, Tonanzintla, Puebla, Mexico
Received October 15, 1950

ABSTRACT

A catalogue is given of 199 stars classified on objective-prism plates as belonging to the group OB or to the supergiant classes between A0 and F8.

A spectral survey of the Milky Way is being carried out at the Tonanzintla Observatory, to photographic magnitude 11.5, by means of the 26–30-inch Schmidt telescope and a 4° objective prism.[1] A detailed account of the results of the survey will be published at a later date; however, at the suggestion of Dr. W. W. Morgan, we are publishing a list of the most luminous stars found so far. The great importance of these relatively rare objects for studying the structural features of the galactic system would seem to warrant this separate announcement of their discovery.

The stars included in the present list were found on plates taken by Guillermo Haro and Luis Rivera Terrazas; they cover a belt of approximately 5° in width, centered along the galactic equator, with pole at $\alpha = 12^h40^m$, $\delta = +28^\circ$ (1900), and extending in galactic longitude from 180° to 240°. The objects listed in Tables 1 and 2 have been tentatively classified as belonging either to the natural group OB as defined by Morgan[2] or to the supergiant classes in spectral types A and F. The present list is similar to the one recently prepared by J. J. Nassau and W. W. Morgan;[3] for a description of the objects included in the group we therefore refer to their paper. It should be mentioned that we cannot be entirely certain of having eliminated all stars with peculiar spectra, showing, with the low dispersion used, spectral characteristics resembling those of c stars (shell stars and peculiar stars of the γ Equ type). We have excluded from the list bright stars long recognized as c stars and also objects known to be highly luminous from their light-variations. The identification of most of the stars has been referred directly to the *Durchmusterung* catalogues, from which we have taken the equatorial co-ordinates and the magnitudes given in Tables 1 and 2. For objects not recorded in those catalogues we have used the spectral plates to estimate their approximate co-ordinates and to draw charts showing their relative positions to neighboring brighter stars. The charts thus obtained, reproduced in Figure 1, together with the identification of the reference BD or CD stars given in Table 3, should facilitate the location of the objects concerned, some of which have photographic magnitudes as faint as 11.5.

I am greatly indebted to Dr. W. W. Morgan for his guidance and advice in the problems of spectral classification. My thanks are also due to my brother, Dr. Guido Münch, for his help in the preparation of this list.

[1] A short description of the observational program and of the instruments used has been given recently by Luis Rivera Terrazas in *A.J.*, **55**, 65, 1950.

[2] See papers presented at the symposium held at the University of Michigan, June, 1950.

[3] *Ap. J.*, **113**, 141, 1951.

TABLE 1

STARS REFERRED TO THE BD

No.	BD	HD	α_{1855}	δ_{1855}	m	Sp.	HD Type
1	1472	.....	6^h25^m8	+ 0° 48′	9.3	OB	.....
2	1441	.....	30.9	+ 1 26	9.3	OB	.....
3	.....	.....	32.7	+ 1 01	.....	OB	.....
4	1385	.....	32.9	− 0 14	9.5	OB	.....
5	.....	.....	35.1	+ 0 10	.....	OB	.....
6	1726	.....	35.1	− 2 55	9.2	cF8	.....
7	1576	.....	37.4	+ 0 45	9.2	OB	.....
8	1517	.....	40.6	+ 1 52	9.3	cF0	.....
9	1595	.....	40.6	+ 0 52	9.5	OB	.....
10	1624	49585	41.7	+ 0 15	9.1	OB	B8
11	.....	.....	42.1	− 0 05	.....	OB	.....
12	1638	.....	42.8	+ 0 37	9.5	OB	.....
13	1827	49992	43.8	− 5 10	9.1	OB	B
14	1651	50064	44.1	+ 0 28	8.5	OBe	B
15	1560	.....	44.5	+ 1 33	9.3	OB	.....
16	1471	.....	49.7	− 1 34	9.3	OB	.....
17	1856	51756	51.2	− 2 50	7.8	OB	B3
18	.....	.....	51.9	− 4 23	.....	cF5	.....
19	1912	52266	53.2	− 5 37	7.3	OB	B2
20	1667	52382	53.7	− 9 00	6.8	OB	B0
21	1885	52533	54.2	− 2 55	8.0	OB	B3
22	1790	52537	54.6	− 9 16	9.0	cF2	F0
23	.....	.....	56.6	−11 30	.....	OB	.....
24	1848	53367	57.6	−10 14	7.3	OB	B0
25	1733	53649	58.5	− 8 48	9.0	OB	B
26	1734	53667	58.7	− 8 30	7.9	OB	Oe5
27	1737	53754	58.9	− 8 35	8.4	OB	B5
28	1862	53755	59.0	−10 27	7.0	OB	B3
29	1790	53974	59.9	−11 04	5.8	OB	B3
30	1745	54024	7 0.0	− 7 31	8.8	OB	B5
31	1825	.....	0.3	−13 27	9.0	OBe	.....
32	1892	54662	2.5	−10 07	6.8	OB	Oe5
33	1814	54727	2.7	−12 19	9.8	OB	B
34	1672	54786	3.1	−15 52	9.1	OBe	B
35	1750	.....	4.2	−14 13	9.6	OB	.....
36	1916	55420	5.6	−10 42	8.8	OB	B
37	1768	55493	5.9	−14 15	8.2	OB	F8
38	1933	55879	7.6	−10 04	6.4	OB	B1
39	1885	56952	12.0	−16 56	9.0	OB	B3
40	1866	.....	14.3	−20 57	9.2	OB	.....
41	1890	.....	16.2	−20 34	9.2	OB	.....
42	1871	.....	18.6	−19 08	9.5	OBe	.....
43	1916	.....	18.8	−20 53	8.5	OB	.....
44	1920	58509	18.9	−20 44	8.5	OB	B5
45	1919	58510	18.9	−20 53	7.3	OB	B2
46	1894	58720	19.6	−14 48	9.0	OB	B
47	1874	58978	20.8	−22 48	5.7	OB	B2p
48	1847	59075	21.2	−18 12	8.5	cA2	B9
49	1839	59114	21.3	−15 06	9.0	OB	B
50	1962	.....	22.5	−20 31	9.4	OB	.....

TABLE 1—*Continued*

No.	BD	HD	α_{1855}	δ_{1855}	m	Sp.	HD Type
51	.....	.....	7^h23^m0	−15°01′	.....	OB	.....
52	1873	59813	24.6	−18 38	9.0	OB	B3
53	1892	60308	26.6	−15 08	8.0	OB	B
54	1975	.....	27.4	−14 26	9.4	OB	.....
55	2007	60532	27.8	−21 59	5.4	cA5	F8
56	1909	.....	28.4	−15 56	9.6	OB	.....
57	1920	.....	28.8	−18 29	9.4	OB	.....
58	.....	.....	28.9	−21 45	.....	OB	.....
59	2021	.....	29.2	−21 16	9.5	OB	.....
60	2026	60831	29.4	−21 10	8.7	cA0	B9
61	1959	60859	29.4	−19 28	9.0	OB	B3
62	1927	.....	30.4	−18 40	9.5	OB	.....
63	1948	.....	33.0	−18 29	9.5	OBe	.....

TABLE 2

STARS REFERRED TO THE CD

No.	CD	HD	α_{1875}	δ_{1875}	m	Sp.	HD Type
64	4761	.....	7^h30^m5	−22° 37′	9.9	OBe	.....
65	5814	.....	32.6	−23 38	10.	OB	.....
66	5721	.....	33.9	−24 28	9.8	OBe	.....
67	4363	.....	34.2	−27 20	9.4	OB	.....
68	4899	.....	34.5	−22 13	9.5	OB	.....
69	5917	.....	35.4	−23 11	9.8	OB	.....
70	4390	.....	35.6	−27 22	9.5	OB	.....
71	4849	.....	38.5	−29 02	9.3	OB	.....
72	4775	.....	38.8	−28 41	10.	OB	.....
73	4881	.....	39.5	−26 39	9.1	OBe	.....
74	6114	.....	39.8	−23 01	9.6	OB	.....
75	4925	63005	40.6	−26 11	8.9	OB	B0
76	6178	63170	41.3	−23 50	8.6	cF2	G0
77	4955	.....	41.4	−26 23	9.7	OB	.....
78	4533	63290	42.0	−27 37	8.3	OB	B
79	4982	.....	42.4	−26 23	9.2	OBe	.....
80	5098	63423	42.7	−30 15	7.5	OB	B0
81	6017	.....	43.6	−24 14	9.5	OB	.....
82	5040	63735	44.3	−26 02	9.2	OB	B8
83	4186	63804	44.5	−33 01	8.0	OB	B
84	.....	.....	45.2	−26 54	.....	.....	.....
85	.....	.....	45.3	−27 06	.....	OB	.....
86	4950	63964	45.4	−28 44	8.2	cF6	F8
87	4985	.....	46.7	−28 04	9.6	OB	.....
88	.....	.....	47.0	−27 20	.....	OB	.....
89	4649	.....	47.0	−27 01	9.6	cF2	.....
90	5191	.....	47.0	−25 11	9.9	OB	.....
91	5115	64315	47.2	−26 06	8.4	OB	B
92	6101	64399	47.5	−24 47	8.6	OB	B2
93	5126	.....	47.6	−26 09	10.	OB	.....
94	5220	.....	47.8	−30 25	10.	OB	.....
95	5136	.....	47.9	−26 48	9.3	OB	.....
96	5228	64568	48.4	−25 54	9.1	OB	B
97	5034	.....	48.5	−28 25	9.5	OB	.....
98	4053	64571	48.5	−34 36	7.3	cF8	G0
99	.....	.....	49.7	−27 27	.....	OB	.....
100	.....	.....	50.4	−27 28	.....	OB	.....
101	5159	.....	50.7	−29 14	9.7	OB	.....
102	4743	.....	50.7	−27 49	9.7	OBe	.....
103	5107	65087	50.9	−28 12	9.0	OB	B5
104	5114	.....	51.1	−28 09	9.6	OB	.....
105	5191	.....	51.4	−29 05	9.4	OB	.....
106	5307	65232	51.5	−30 08	8.7	cF2	F8
107	5156	.....	52.4	−28 50	9.0	OB	.....
108	5309	.....	53.2	−31 46	8.0	OB	.....
109	5286	.....	53.4	−26 17	10.	OB	.....
110	5287	.....	53.4	−26 13	9.5	OB	.....

TABLE 2—*Continued*

No.	CD	HD	α_{1875}	δ_{1875}	m	Sp.	HD Type
111	5218	.....	7^h53^m9	−28°03′	9.7	OB	.....
112	5235	.....	54.3	−28 34	9.7	OB	.....
113	4835	.....	54.7	−27 54	9.6	OB	.....
114	5382	.....	54.8	−30 22	9.9	OBe	.....
115	4877	.....	56.7	−27 35	9.7	OB	.....
116	4114	66334	57.0	−36 51	8.5	OB	B
117	5365	.....	58.4	−28 20	10.	OB	.....
118	4933	66788	59.0	−27 08	9.3	OB	B2
119	5482	.....	8 2.6	−28 24	9.7	OB	.....
120	4291	68450	6.4	−36 55	6.8	OB	B0
121	4967	.....	7.3	−32 11	8.9	OB	.....
122	4168	.....	7.5	−38 46	9.0	OB	.....
123	4322	68761	7.8	−36 37	6.9	OB	B0
124	4326	.....	8.0	−36 19	9.5	OB	.....
125	4496	.....	8.8	−34 06	9.2	OB	.....
126	4359	.....	9.3	−35 08	9.7	OB	.....
127	4359	69106	9.4	−36 34	7.5	OB	Oe5
128	4384	.....	10.5	−35 22	9.4	OB	.....
129	4390	69425	10.9	−36 44	9.0	OB	B
130	4396	69464	11.1	−35 15	9.0	OB	B
131	4412	.....	11.7	−35 22	9.5	OB	.....
132	4191	.....	13.5	−39 19	9.8	OB	.....
133	4469	.....	14.2	−35 44	9.4	OB	.....
134	4471	.....	14.3	−35 45	9.1	OB	.....
135	4408	.....	19.5	−38 59	9.6	cF5	.....
136	4445	.....	20.7	−38 22	10.	OB	.....
137	4126	71528	21.9	−41 44	8.0	OB	B3
138	4649	71649	22.5	−36 14	8.8	OB	B3
139	4290	72014	24.5	−42 10	6.8	OB	B3
140	4420	.....	30.2	−43 03	9.4	cF5	.....
141	.....	.....	30.5	−43 53	.....	OB	.....
142	4569	.....	31.5	−44 28	10.	OB	.....
143	4580	.....	32.0	−44 16	9.9	OB	.....
144	4467	.....	32.3	−43 39	9.4	OB	.....
145	4602	73568	33.1	−44 46	8.5	OB	B3
146	4634	.....	34.2	−44 36	9.8	OB	.....
147	4338	73831	34.4	−45 30	8.3	OB	B8
148	4631	.....	34.6	−39 58	8.1	OB	.....
149	4683	74194	36.5	−44 37	8.1	OB	B2
150	4691	.....	37.0	−44 50	9.2	OB	.....
151	4705	.....	37.8	−44 21	10.	OB	.....
152	4570	.....	38.3	−43 42	9.9	OB	.....
153	4717	.....	38.3	−44 34	10.	OB	.....
154	.....	.....	38.9	−43 55	.....	OB	.....
155	4588	.....	39.9	−43 32	9.7	OB	.....
156	4496	74920	40.9	−45 35	8.5	OB	B3
157	4498	74936	41.0	−45 27	8.6	OB	B8
158	4794	.....	41.6	−44 50	10.	OB	.....
159	4810	.....	42.3	−44 57	9.6	OB	.....
160	4635	75211	42.6	−43 37	8.3	OB	B

TABLE 2—*Continued*

No.	CD	HD	α_{1875}	δ_{1875}	m	Sp.	HD Type
161	4541	75276	8^h43^m1	−45°42′	6.4	cF0	F0p
162	4547	75309	43.3	−46 00	8.2	OB	B2
163	4653	.....	43.5	−43.30	10.	OB	.....
164	4834	.....	43.9	−44 25	10.	OBe	.....
165	4605	.....	44.2	−46 27	9.3	OB	.....
166	4842	.....	44.4	−44 38	10.	OB	.....
167	4381	75534	44.6	−47 18	8.2	OB	B5
168	4669	.....	44.8	−43 50	10.	OB	.....
169	4549	75655	45.2	−41 16	8.5	OB	B8
170	4393	75658	45.3	−47 01	8.7	OB	B3
171	4591	.....	45.4	−45 04	9.8	OB	.....
172	4401	.....	45.4	−47 32	9.9	OB	.....
173	4554	75724	45.6	−41 38	8.0	OB	B3
174	4865	.....	45.7	−44 07	9.6	OB	.....
175	4694	.....	45.7	−42 42	10.	OB	.....
176	4560	75759	45.8	−41 38	6.5	OB	B2
177	4606	.....	45.9	−45 04	9.4	OB	.....
178	4615	.....	46.3	−45 05	9.8	OB	.....
179	4661	75821	46.3	−46 04	5.6	OB	B0
180	4690	.....	46.4	−43 22	9.5	OB	.....
181	4691	75860	46.5	−43 17	7.6	OB	B0
182	4639	.....	47.1	−45 16	10.	OB	.....
183	4901	.....	47.6	−44 33	10.	OB	.....
184	4716	76031	47.6	−43 33	9.1	OB	B
185	4721	.....	48.1	−43 44	10.	OB	.....
186	4333	.....	48.9	−43 52	10.	OB	.....
187	4676	.....	49.1	−45 34	9.2	OB	.....
188	4762	76341	49.5	−42 01	7.4	OB	B2
189	4490	.....	50.1	−47 01	9.9	OB	.....
190	4743	.....	50.4	−46 53	9.8	OB	.....
191	4750	76535	50.8	−46 56	8.9	OB	B2
192	4505	76556	50.9	−47 08	8.7	OB	B3
193	4719	.....	52.4	−45 25	9.8	OB	.....
194	4826	.....	59.7	−45 11	9.9	OB	.....
195	5113	.....	9 1.1	−44 28	10.	OB	.....
196	5305	80057	11.5	−44 23	6.7	OB	B5
197	4273	80210	12.4	−49 03	7.3	cF8	F8
198	3693	80558	14.6	−51 02	6.7	OB	B3p
199	3767	81471	19.8	−51 12	6.6	cA5	F0p

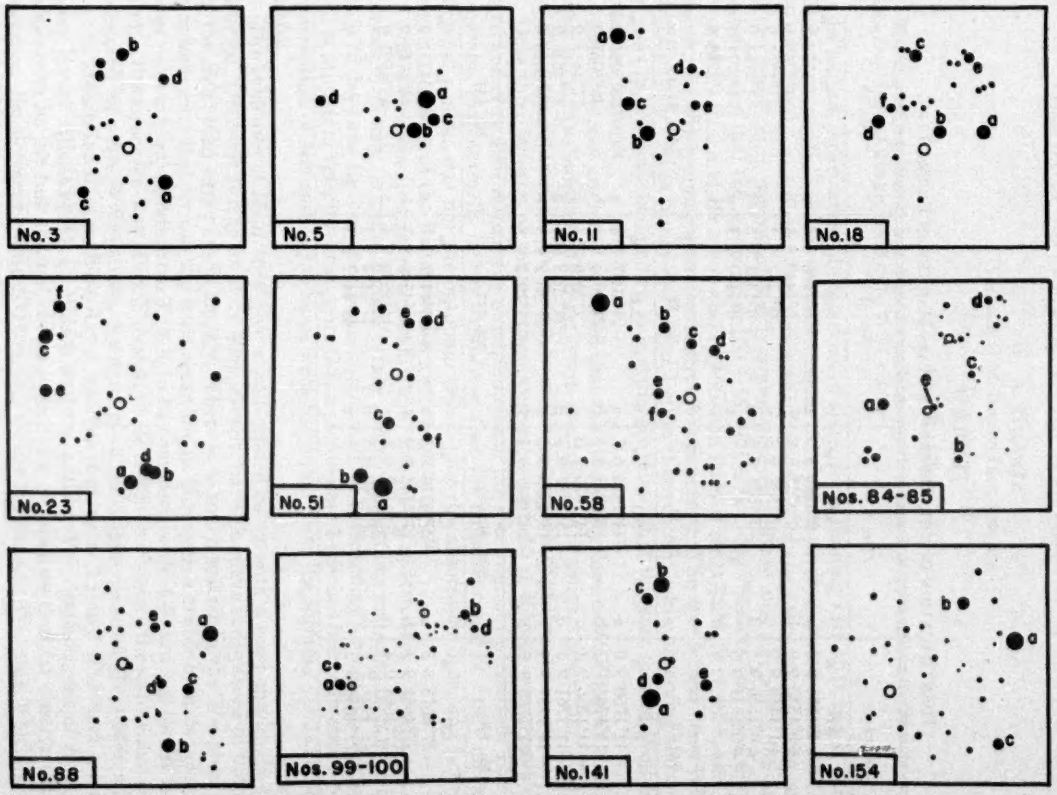

FIG. 1.—Identification charts for stars not contained in the *Durchmusterung* catalogues. The stars to be identified have been indicated by a circle and the field stars by dots of varying sizes according to their brightness. In all cases the south direction is at the top and west to the left. The angular dimensions of the squares drawn are 33′×33′.

TABLE 3

IDENTIFICATION OF THE REFERENCE STARS MARKED IN FIGURE 1

No. 3			No. 5			No. 11			No. 18		
	BD	m		BD	m		BD	m		BD	m
a	+1°1455	8.8	a	+0°1556	8.0	a	−0°1446	8.5	a	−4°1772	8.8
b	+0°1532	9.0	b	+0°1555	8.8	b	−0°1449	8.8	b	−4°1769	9.0
c	+1°1449	9.2	c	+0°1557	9.3	c	−0°1447	9.3	c	−4°1766	9.0
d	+0°1536	9.5	d	+0°1551	9.5	d	−0°1451	9.5	d	−4°1763	9.0
e	+0°1531	9.5				e	−0°1452	9.5	e	−4°1771	9.4
									f	−4°1765	9.5
No. 23			**No. 51**			**No. 58**			**Nos. 84–85**		
	BD	m		BD	m		BD	m		CD	m
a	−11°1760	9.0	a	−14°1925	6.7	a	−21°2007	5.4	a	−26°5055	9.0
b	−11°1763	9.2	b	−14°1923	8.7	b	−21°2014	9.3	b	−26°5077	9.3
c	−11°1756	9.2	c	−14°1926	9.0	c	−21°2016	9.4	c	−27°4615	9.3
d	−11°1761	9.3	d	−15°1857	9.3	d	−21°2018	9.4	d	−27°4620	9.4
e	−11°1757	9.4	e	−15°1855	9.5	e	−21°2012	9.5	e	−26°5070	9.5
f	−11°1758	9.5	f	−14°1927	9.5	f	−21°2013	9.8			
No. 88			**Nos. 99–100**			**No. 141**			**No. 154**		
	CD	m		CD	m		CD	m		CD	m
a	−27°4675	8.5	a	−27°4710	8.3	a	−43°4422	7.7	a	−44°4771	7.2
b	−27°4661	9.3	b	−27°4746	8.9	b	−44°4548	8.3	b	−44°4748	9.1
c	−27°4668	9.4	c	−27°4709	9.4	c	−44°4544	9.4	c	−43°4597	9.4
d	−27°4657	9.5	d	−27°4749	9.5	d	−43°4424	9.4			
e	−27°4648	9.5				e	−43°4437	9.5			

THE WOLF-RAYET SPECTROSCOPIC BINARY BD+36°3991*

W. A. HILTNER
Yerkes and McDonald Observatories
Received December 4, 1950

ABSTRACT

The star BD + 36°3991 is a Wolf-Rayet binary with a period of approximately 10.6 days and a semi-amplitude of 240 km/sec for the WN7 star.

In routine polarization observations of stars in "A Finding List of O and B Stars of High Luminosity"[1] in a selected region of Cygnus it was noted that one star, BD+36°3991,[2] was distinctively different from most of the other stars in the region. When opportunity permitted, spectrograms were obtained of this star and a few others. It was found that the spectrum of BD+36°3991 is not only characterized by absorption lines of *H*, *He* I, and *He* II but also by emission lines of *He* II 4686, *N* IV 4058, and emission in the 4640 region, where some structure is present. The star is near class WN7 or slightly earlier. Miss Nancy Roman at Yerkes Observatory, while observing the spectra of stars in this same finding list, independently found that this star showed Wolf-Rayet emission features.

Since it is now generally accepted that the absorption lines in Wolf-Rayet stars have their origin in a companion O–B-type star, spectrograms of a higher dispersion (75 A/mm at $H\gamma$) were obtained for the detection of the binary nature of this star.

Only three features of the spectrum were measured. *He* II 4685.68 was always measured and *N* IV 4057.80 and $H\gamma$ absorption when the spectrograms permitted. The spectrograms were normally lightly exposed so that the emission could be easily measured. This, of course, was not the optimum density for the absorption lines, and hence the higher members of the Balmer series were not attempted.

The radial velocities are recorded in Table 1. A period of 10.6 days was adopted. This period, obviously, is not of high accuracy, since observations extended over a period of only 25 days and the two spectrograms obtained for determining a more accurate period fell at minimum velocity. It appears that a period near 1 day has been eliminated by the observation of November 2. Phases were computed from the formula JD 2433585.5 + 10.6*E*.

The velocities of *He* II 4686 give a well-defined curve with a semi-amplitude of 240 km/sec. The same is true for *N* IV 4058, except that this curve is displaced to the violet of the *He* II 4686 curve by 53 km/sec. There is so much scatter in the $H\gamma$ absorption measurements that we can say little regarding it. However, a center of mass velocity of near −50 km/sec is indicated. This is to be compared with +40 km/sec for *He* II 4686 and −10 km/sec for *N* IV 4058. This shift of *He* II 4686 is of nearly the same value as that observed for other WN systems. A summary of the displacement of *He* II 4686 relative to the absorption lines in Wolf-Rayet binaries is given in Table 2. The data are taken from investigations by O. C. Wilson and the author. The displacement of *He* II 4686 appears to be the rule and not the exception; for all binaries thus far observed show a common displacement—near 100 km/sec, except for the one WC star, which shows a shift of 190 km/sec.

The orbital elements of BD+36°3991 are given in Table 3.

* *Contributions from the McDonald Observatory, University of Texas*, No. 200.

[1] J. J. Nassau and W. W. Morgan, *Ap. J.*, 113, 141, 1951. I am grateful to Drs. Nassau and Morgan for permission to use this list in advance of publication.

[2] HD 228766; MWC 1010; (1900) $\alpha = 20^h13^m8$; $\delta = +37°0'$.

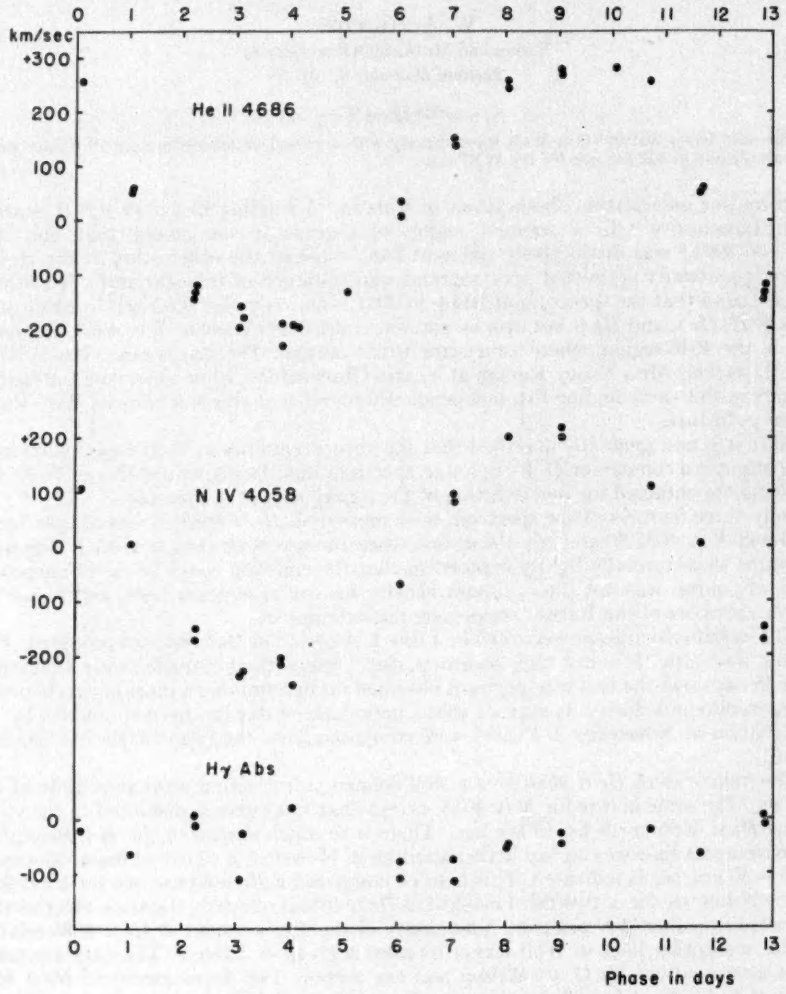

FIG. 1.—Velocity-curves of BD+36°3991

TABLE 1

RADIAL VELOCITIES OF BD+36°3991

PLATE f/2G	DATE (U.T.) 1950	PHASE (DAYS)	RADIAL VELOCITY (KM/SEC).		
			He II 4686	*N* IV 4058	*Hγ* Abs.
12674	Oct. 31.108	0.108	+256	+108	− 21
12678	Nov. 1.049	1.049	+ 52	+ 4	− 63
12679	1.066	1.066	+ 58	.....	.....
12710	2.203	2.203	−146	−171	+. 5
12711	2.223	2.223	−133	.....	− 11
12712	2.249	2.249	−120	−150	.....
12735	3.050	3.050	−199	.....	.....
12736	3.089	3.089	−159	−237	−110
12737	3.134	3.134	−179	−229	− 26
12738	4.053	4.053	−192	−254	+ 21
12742	4.119	4.119	−199	.....	.....
12766	5.057	5.057	−133	.....	.....
12771	6.040	6.040	+ 5	− 71	−110
12772	6.053	6.053	+ 32	.....	− 79
12776	7.037	7.037	+150	+ 95	− 73
12777	7.049	7.049	+137	+ 79	−114
12781	8.034	8.034	+256	.....	− 52
12782	8.047	8.047	+243	+199	− 47
12786	9.037	9.037	+276	+216	− 26
12787	9.050	9.050	+269	+199	− 47
12788	10.060	10.060	+282	.....	.....
12911	25.044	3.844	−192	−204	.....
12912	25.056	3.856	−232	−212	.....

TABLE 2

SHIFT OF *He* II 4686 IN WR BINARIES

STAR	TYPE	VELOCITY (KM/SEC)		SHIFT OF *He* II 4686 (KM/SEC)
		He II 4686	Abs.	
HD 168206	WC7	+200	+10	+190
HD 186943	WN5	+115	+10	+105
HD 190918	WN5	+ 88	−22	+110
BD+36°3991	WN7	+ 40	−50	+ 90
HD 193576	WN6	+ 56	−33	+ 89
HD 211853	WN6	+ 50	−55	+105

TABLE 3

ORBITAL ELEMENTS OF BD+36°3991

P	10.6 days	$a_B \sin i$	7.3×10^6 km
K_W	240 km/sec	$m_W \sin^3 i$	$4.6\odot$
K_{O-B}	50 km/sec (upper limit)	$m_B \sin^3 i$	$22.3\odot$
$a_W \sin i$	35×10^6 km	$\gamma_{He\,II}$	+40 km/sec
		γ_{abs}	−50 km/sec

THE IDENTIFICATION OF D'AGELET'S NOVA SAGITTAE OF 1783*

HAROLD F. WEAVER
Lick Observatory, University of California
Received November 15, 1950

ABSTRACT

On the basis of relative blueness, apparent magnitude, position, lack of proper motion, and present irregular fluctuations in brightness, N Sge 1783 is tentatively identified as a faint blue star with $m_{pg} = 18.9$.

I. INTRODUCTION

Among the oldest authentic galactic novae that are now known or for which there is some hope of rediscovery are: (1) P Cygni, discovered by Blaeu[1] in 1600; (2) a nova found by Hevelius in 1667 "between χ^1 and χ^3 Orionis," later observed by Bevis[2] during the period 1738–45 and possibly by Shackleton[3] in 1894; and (3) a star observed in July, 1783, by the French astronomer D'Agelet[4] in the course of his mural quadrant observations, and subsequently lost.

P Cygni is, of course, well known today; Hevelius' star is at present unknown but, with a proper search, might be identified. The present observations indicate that D'Agelet's star has now probably been found.

II. D'AGELET'S OBSERVATIONS AND EARLY SEARCHES FOR THE STAR

Gould's results for D'Agelet's position observations of N Sge 1783 are given in Table 1. A calibration of D'Agelet's magnitude estimates against modern measurements shows that the brightness of the nova, which we may reasonably assume was at or near maximum light when D'Agelet observed it, was magnitude 5.4 ± 0.4 on the Harvard visual scale. The uncertainty listed, ± 0.4, has been estimated from D'Agelet's results for constant stars of approximately the same brightness.

In the period 1882 to about 1908, Chandler, Gore, Eddie, Parkhurst, Orr, and others[5] made numerous unsuccessful attempts to find D'Agelet's star and identify it either as a variable or as a nova. Their failure to discover the star is not surprising. If D'Agelet's star is assigned to the nova class, we may assume that it had a light-amplitude of between 9.5 and 13 mag. This would imply that in its postnova state the star would have an apparent magnitude between 14.9 and 18.4, probably rather beyond the range of these earlier observers.

* *Contributions from the Lick Observatory*, Ser. II, No. 33. This investigation is based on observations made at the Mount Wilson and Palomar Observatories.

[1] Quoted by Stratton in *Handb. d. Ap.* **6/2**, 252, 1928.

[2] *J. British Astr. Assoc.*, **4**, 96, 1893.

[3] *J. British Astr. Assoc.*, **4**, 215, 1894.

[4] D'Agelet's observations have been discussed and published by B. A. Gould, *Washington Nat. Acad. Mem.*, Vol. 1, 1866. The star referred to is entered as "anonyma" on p. 237 of Gould's catalogue.

[5] References are given by E. Zinner in Müller and Hartwig's *Gesch. u. Lit. der Lichtwechsels*, **2**, 443, 1920.

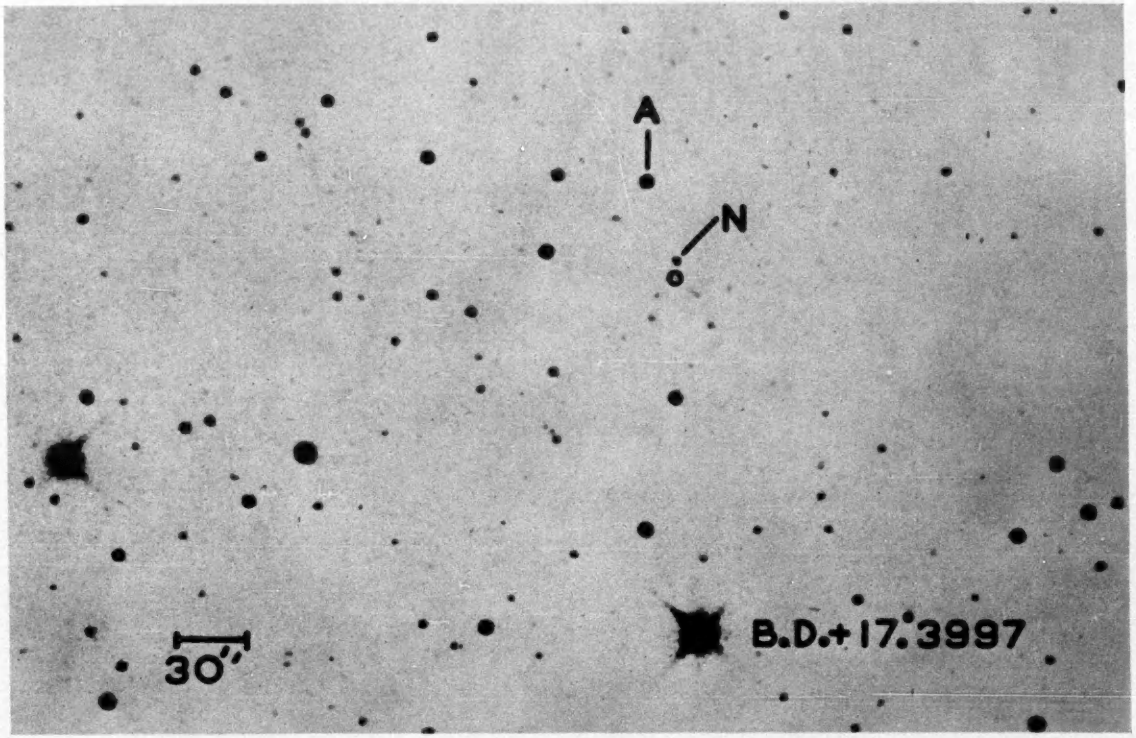

FIG. 1.—Field of N Sge 1783; 60-inch plate taken July 21, 1942. North is toward top; west is toward right

III. THE PRESENT SEARCH FOR THE NOVA

A photographic search for N Sge 1783 was made in 1942 with the 60-inch reflector at the Mount Wilson Observatory. Three main criteria were considered useful in the identification of the nova: (1) it should be relatively blue; (2) in view of the considerable accuracy of D'Agelet's observations, it should lie within a few seconds of arc of D'Agelet's measured position;[6] and (3) it should probably lie in the fainter portion of the rather broad magnitude range 14–20.

The first of these criteria is an important one in a search for old novae. Humason[7] has examined the spectral characteristics of 16 old novae observed from 3 to 88 years after outburst and has found that these stars show continuous spectra extending far into the ultraviolet. Temperatures resembling those of early B-type stars are indicated. We might thus assume that an average old nova would have a color index on the International System of the general order of -0.4 mag.

In actual application, however, the color criterion for an old nova is somewhat complicated by the effects of interstellar extinction. Fortunately, we can form some estimate of the amount of color extinction likely to be suffered by D'Agelet's star. If we assume

TABLE 1

D'AGELET'S OBSERVATIONS OF N SGE 1783

Date 1783	α_{1800}	δ_{1800}	Magnitude Estimate
July 26	$19^h23^m47^s.3$	$+17°19'43''.1$	6
27	19 23 47.6	17 19 43.4	6
29	19 23 47.8	17 19 42.0	6.7
Mean*	$19^h23^m47^s.6 \pm 0^s.2$	$17°19'42''.8 \pm 1''.3$	6

* The mean errors quoted for the mean α and δ have been computed from Gould's determination of the mean error of a single observation made by D'Agelet in the declination zone $+17°$.

that the absolute magnitudes of galactic novae at maximum light lie in the range -6 to -8, then for $m_{max} = 5.4$ the distance modulus of N Sge 1783 is between 11.4 and 13.4. From an analysis of the photoelectric colors of B stars measured by Stebbins, Huffer, and Whitford,[8] we find that stars in the direction of N Sge 1783 and at distance moduli of 11.4–13.4 possess average color excesses of the order of 0.30–0.40 mag., measured on the International System. We should thus expect the present apparent color index of N Sge 1783 to be essentially zero.

Relative color indices of stars in the region of N Sge 1783 were determined by blinking a matched pair of plates, one taken in red light, the other in blue light.[9] Figure 1 is an enlargement of the blue plate of the nova field. D'Agelet's position of the nova is at the center of the circle drawn with radius equal to the mean error of his mean place. The two bluest stars found by the comparison of the red and blue plates are marked *A* and *N*. The fainter of these, star *N*, is the bluer of the two by possibly 0.25 mag.

[6] Provided, of course, that D'Agelet's star is not an object of large proper motion.

[7] *Ap. J.*, **88**, 228, 1938; *Mt. W. Contr.*, No. 596.

[8] *Ap. J.*, **91**, 20, 1940; *Mt. W. Contr.*, No. 621.

[9] The red plate was taken on Eastman 103*a*-E emulsion behind a Schott RG2 filter; the blue plate was taken on a Cramer Hi Speed emulsion without filter. The red plates, we might remark, show no nebulosity around any stars in the nova field, though the exposures are not long enough to rule out completely the possible existence of such nebulosity.

Magnitudes of stars A and N were determined by photographic comparison with SA 61[10] on July 21.3, 1942. For star A, $m_{pg} = 16.56$; for star N, $m_{pg} = 18.72$. Both fall within the range of our magnitude criterion for N Sge 1783.

A very low-dispersion spectrogram of star A, obtained on September 16/17, 1942, shows the star to be approximately of type A3–A5, with broad hydrogen absorption lines. It is therefore unlikely that star A could be the nova. It has, unfortunately, not been possible to obtain a spectrogram of star N.

A knowledge of the spectral type of star A affords some check on the general consistency of the apparent color of star N, if it is identified as N Sge 1783, and the expected color of the nova. If A is an A3–A5 star, it has a distance modulus of about 15 and a true color index of approximately zero. If we extrapolate Stebbins, Huffer, and Whitford's color-excess–distance-modulus relationships rather considerably (4.5 mag.), we would expect a color excess and an observed color of somewhat more than +0.45 mag. for star A. Since, as mentioned above, star N is about 0.25 mag. bluer than star A, star N would have an estimated observed color index of the order of +0.2. In view of the great extrapolation of the color-excess relationship and our lack of knowledge about the true color of N, the value +0.2 would seem to be as close a check as could be expected for our former estimate of "essentially zero" for the expected color of N Sge 1783.

TABLE 2

POSITIONS OF STARS A AND N

Star	α_{1800}	δ_{1800}	Telescope	Epoch
A	$19^h23^m48^s.27$	+17° 20′ 18″.1	60-inch	1942.5
A	19 23 48.26	+17 20 18.0	100-inch	1950.5
N*	19 23 47.63	+17 19 49.2	60-inch	1942.5
N	19 23 47.62	+17 19 49.1	100-inch	1950.5
D'Agelet†	19 23 47.6±0.2	+17 19 42.8±1.3	Mural quadrant	1783.6

* For star N, $\alpha_{1950} = 19^h30^m29^s.77$; $\delta_{1950} = +17°38'25''.2$.
† No modern information on the systematic errors of D'Agelet's positions is available.

The positions of stars A and N indicate that it is very unlikely that A could be the nova, and they give considerable weight to the suggestion that N is D'Agelet's star. Positions of A and N determined from plates taken in 1942 and 1950 are given in Table 2.

The 1942 and 1950 positions of stars A and N have been obtained with respect to four reference stars found in both the Bordeaux and the Paris zones of the astrographic catalogue. There is a systematic difference of 1″.0 in the declinations of the four stars in the two zones. The declinations given in Table 2 are the means of the values computed separately from the positions given in each of the two zones. The tabulated declinations are thus uncertain by an amount of at least 0″.5–1″.0.

The small differences in the 1942.5 and 1950.5 positions of both A and N rule out the possibility that either star is an object of large proper motion. Thus star A cannot have moved from D'Agelet's observed position of 1783 to its present position. To do so, it would have had to possess a proper motion of more than 0″.20 per year. Such a large proper motion is incompatible with the observed positions for 1942.5 and 1950.5. Likewise, star N cannot be an extraneous object that has moved into the field of D'Agelet's nova. The close agreement of the two modern positions of star N indicate that its position cannot have changed by more than 2 or 3 seconds of arc during the 167 years that have elapsed since D'Agelet's observations were made.

[10] The magnitude scale in SA 61 was determined by the writer from half-filter plates taken by Dr. W. Baade. The zero point of the half-filter scale was established by reference to photoelectric measurements made by Stebbins, Whitford, and Johnson (*Ap. J.*, **112**, 469, 1950).

IV. OBSERVATIONS OF D'AGELET'S STAR MADE IN 1950

In June and July, 1950, the color observations made in 1942 and described above were repeated, with the same results. The more numerous 1950 observations give the additional information that star *N* is a rapidly fluctuating irregular variable of appreciable range. Magnitudes of star *N* measured in 1942 and in 1950 are collected in Table 3. These magnitudes were derived from measurements made with a Ross photometer and are referred to a magnitude sequence established in the immediate vicinity of the nova by transfer from SA 61.[10] The mean error of a magnitude in Table 3 is ± 0.07 mag.

TABLE 3

MEASURED MAGNITUDES OF STAR *N*

Date	m_{pg}	Date	m_{pg}
1942 July 21.3	18.72	1950 July 15.3	18.63
1950 June 14.4	19.47	July 17.4	18.86
July 14.4	18.96		

The marked brightness fluctuations of star *N*, which amount to 0.83 mag., offer strong supporting evidence to the hypothesis that it is, indeed, N Sge 1783. The rapidity of these fluctuations in a nova that flared more than a century and a half ago is of considerable interest, and they indicate that regular observations of star *N* are called for in the future. It will likewise be of considerable interest to attempt to obtain a spectrum of star *N* when it is at one of its light-maxima.

V. CONCLUSIONS

On the basis of color, apparent magnitude, position, and lack of proper motion, star *N* in Figure 1 can probably be identified as N Sge 1783. Additional evidence to support this identification is afforded by the fact that star *N* is fluctuating over a considerable range in magnitude in a rapid and irregular manner. Because of the rapidity and amplitude of the fluctuations and the great length of time that has elapsed since the nova's outburst in 1783, it is a matter of some interest to follow the course of the light-variations of star *N* as regularly as possible in the future.

It is a pleasure to express my thanks to Mrs. Beverly Franklin and Dr. S. Vasilevskis for their aid in measuring and reducing the positions of stars *A* and *N*, and to Mrs. Amelia Wehlau for making the photometric measurements and reductions.

RED AND INFRARED MAGNITUDES FOR 125 STARS IN TEN AREAS*

GERALD E. KRON AND J. LYNN SMITH
Lick Observatory, University of California
Received November 27, 1950

ABSTRACT

Magnitudes in the red and infrared spectral regions are tabulated for stars of the Polar Sequence, Harvard Standard Regions C 4, C 6, and C 12, and Kapteyn Selected Areas 51, 57, 61, 64, 68, and 71. The methods employed for calibrating the photelectric photometer are described in detail. An effort has been made to reduce systematic errors to a minimum. Not less than five stars were measured in each area. Stars in Areas 57 and 61 were observed to magnitude 16 with the photometer on the Mount Wilson 100-inch reflector. The limiting magnitudes in the remaining areas are from 8 to 12. The zero point of the new system is fixed by reference to magnitudes on the International System of the Polar Sequence.

I. INTRODUCTION

During the last decade the need for magnitudes of stars in red light has become increasingly apparent to observational astronomers. Very few red magnitudes are available at all, and those that are available are of a precision insufficient for use in some astrophysical problems. A program for determining, at this observatory during the last two years, red and infrared magnitudes for late-type dwarf stars has sharpened our interest in red magnitudes. When Dr. Baade, of the Mount Wilson and Palomar Observatories, suggested the desirability of experimenting with the determination of photoelectric red standards, the problem seemed important enough for initiation of a small program at the Lick Observatory. The first useful observations of this program, of which this paper is a report, were made on September 1, 1949.

Photoelectric methods always imply attempts at precision results, otherwise the use of methods so demanding on telescope time would not be justified. It has long been apparent to photoelectric observers, as Stebbins has often emphasized, that precision magnitudes cannot be determined unless colors are measured along with the magnitudes. In the present program, therefore, two colors were used, and they will be identified qualitatively as red and infrared. The program resulted in magnitudes in these two colors, each distinct and reasonably remote from the colors of the International System. Thus all stars for which magnitudes have also been determined on the International System will have four available magnitudes: photographic, photovisual, red, and infrared.

II. THE PHOTOMETER

Observations were made with two Continental Electric type CE25A/B photocells; cell *j* was used from September 1, 1949, until February 17, 1950, after which cell *e* was used. Cell *j* was selected because it had the highest cathode efficiency of all our infrared-sensitive photocells. It eventually had to be abandoned, however, because its sensitivity was erratic. Cell *e* was substituted because it was the next most-efficient cell and because its spectral sensitivity was almost identical with that of cell *j*. Cell *e* proved satisfactory in service, and it was used for the remainder of the program. Both cells were used with a gas-multiplying factor of 24. The electrical circuit was of the d.c. feedback type,[1] and it employed a Victoreen 2.5×10^{13} ohm load resistor. Photocell, amplifying tube, and resistor were inclosed in a small evacuated tank refrigerated with dry ice. The feedback amplifier, used under 100 per cent inverse feedback conditions, was of the chopper type;[2]

* *Contributions from the Lick Observatory*, Ser. II, No. 34.

[1] Developed under ONR Contract N7 onr 348.

[2] R. Gunn, *Rev. Sci. Instr.*, 9, 267, 1938.

a loop gain of 40 was sufficient to give an effective response time of 10 seconds to the circuit. The output from this feedback amplifier was fed to a balanced power amplifier[3] that provided some of the gain control and sufficient power output to drive a 0–1 milliammeter. The meter employed was a Brown strip chart millivoltmeter shunted to become a 0–1 milliammeter. A block diagram of the system is shown in Figure 1.

III. CALIBRATION

The ability of a photometer to compare two objects differing by any brightness ratio within the limits of the photometer and to within specified limits of precision will be called its "scale accuracy." The scale accuracy is affected chiefly by sensitivity-control errors, by linearity errors in any part of the photometer, and by scale errors of the indicating meter.

The process of insuring the scale accuracy of a photometer having multiple sensitivity controls and more than one amplifier is complicated and very important. It has seemed worth while to describe our methods in considerable detail in the following paragraphs.

The photometer has two sensitivity controls—a coarse control, giving a range of $2\frac{1}{2}$ mag. in one step, and a fine control, allowing an additional $2\frac{1}{2}$ mag. in steps of $\frac{1}{4}$ mag. Most of the investigation of the properties of the amplifiers was accomplished with the

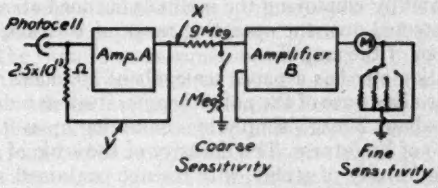

FIG. 1.—Schematic diagram of the photoelectric photometer

use of a Leeds and Northrup type 7651 Students' Potentiometer as a device for furnishing known voltage ratios. The resistors of this potentiometer are accurate to within 0.04 per cent of their nominal values, according to the manufacturer. A Weston Model 271 0–1 milliammeter, inserted at *M* (Fig. 1), was found to have such a finely calibrated scale and such good sensitivity that it gave reproducible readings to within 0.1 per cent of its full scale. This meter was employed as a null instrument with the potentiometer for calibration of the values of the steps of the fine sensitivity control. For each step of the latter a voltage was supplied from the potentiometer to give a nominal (usually full-scale) reading on the meter; the ratios of the voltages then gave the sensitivity steps. These steps were adjusted to within 0.1 per cent of their nominal values by trimming the wire-wound resistors of which the sensitivity control was made. Amplifier *B* had a loop voltage gain of 15,000 and a current inverse feedback. Extensive tests with several precision meters inserted at *M* indicated that there was no detectable nonlinearity of the amplifier over twice its service current range with either polarity of input—a result that is to be expected from the design of the amplifier. It is safe to conclude that amplifier *B* is entirely satisfactory up to the limits of precision of the test equipment.

The coarse sensitivity control was obtained by loading a 9-megohm resistor with a 1-megohm resistor. The resistors were both of the metallic-film type on ceramic tubes, manufactured by the Continental Carbon Company. These resistors have a temperature coefficient of only -0.06 per cent per °C.; however, inasmuch as both resistors are at the same temperature and only their ratio is required to be constant, the temperature

[3] Similar to that described in *Electronics*, August, 1948, p. 98.

coefficient is not important, provided that it is the same for both resistors. The ratio of the resistors was evaluated by inserting the potentiometer at X (Fig. 1) and by trimming the 1-megohm resistor until the sensitivity ratio of the control was 10/1, or 2.50 mag., to within 0.1 per cent of the nominal voltage values supplied by the potentiometer. A check of both factor-of-ten controls contained in the amplifier was obtained by constructing ten resistors of 200 ohms each, as measured by a General Radio impedance bridge. When this impedance bridge is operated on the particular decade required to measure 200 ohms, its absolute accuracy is only 1 per cent, but it will give reproducible results to about 0.2 per cent of the values of the resistors being measured. By measuring ten resistors, nominally of equal value, it was possible to construct with these a simple resistance attenuator of 10/1, each element of which was accurate to within 0.2 per cent of a mean value. This attenuator checked, within the precision of the methods, the ratios of 10 set up by means of the potentiometer as a standard, and thus it provided a good overall check. The input impedance of amplifier B is more than 10^{11} ohms, so this amplifier may be driven through a 9-megohm resistor with no appreciable loading effects.

Amplifier A is connected to have 100 per cent inverse voltage feedback, and thus its effective voltage gain is very close to unity. It is required to furnish an output of 10 volts maximum, and it is constructed to be able to give an output of 75 volts before serious lack of linearity occurs. The amplifier was tested for electrical linearity by inserting the potentiometer at Y and by employing the methods outlined above. No departure from linearity could be detected over the operating range of 10 volts, which is a result consistent with the design of the amplifier.

The Brown potentiometer has a paper scale, about 10 inches wide, divided into 100 units. This large scale allows use of the potentiometer itself as a device for extending the sensitivity range by about 2 mag., simply by containing upon its scale any deflections differing by this ratio of brightness. The linearity of the scale of the Brown instrument depends upon the uniformity of a slide-wire resistor contained within the instrument. The slide wire is made by winding a long, closely spaced helix of resistance wire on a very small cylindrical form. The manufacturers make no claims about the scale uniformity of their instrument, but our tests indicated that it is extremely good. The potentiometer was inserted at X, and the Brown potentiometer was placed at M; its scale was investigated at ten equally spaced places by known voltages provided by the potentiometer. The meter deflections were proportional to the applied voltages to within the width of the ink line, again approximately 0.1 per cent of full scale. Possibly larger errors could be found in spots, but it is improbable that serious errors in ratios can be made by depending upon the linearity of the scale of the particular Brown potentiometer that was used.

The above tests cover the electrical properties of both amplifiers and the meter, and they indicate that this assembly of instruments can measure relative voltages with a precision of a fraction of 1 per cent. It probably is safe to assume that the total accumulated errors of all kinds will allow the comparison of two voltages to within 0.4 per cent of the smaller voltage, which is equivalent to comparing the brightness of two stars with a systematic error of less than 0.004 mag. The total range in magnitudes is about 7, which can be extended by an additional 2.5 mag. to nearly 10 mag. by employing a screen over the telescope objective.

The voltage generated by the photocurrent appears across the 2.5×10^{13}-ohm resistor; the inverse feedback has no correcting influence on the properties of this resistor. The manufacturers of the resistor assert that it is ohmic up to 50 volts applied voltage; however, they do not recommend operating their resistors at temperatures below $-40°$ C. Because our technique requires the resistor to be at $-80°$ C., a test of its properties as a linear element becomes necessary. Such a test can be made either in the laboratory or on the telescope. A telescope test involves such disturbing factors as seeing effects and those from varying extinction. The precision of the results will therefore suffer. Results obtained on the telescope, however, are always more convincing than any other kind; and

we already know from laboratory tests that the remainder of the equipment operates with satisfactory linearity. It seemed advisable to make this last over-all linearity test under actual field conditions, just as the instrument is used on the telescope.

The final over-all linearity test was made on the principle that the whole must equal the sum of its parts. The Crossley reflector was diaphragmed with an opaque disk having four holes, each about 10 inches in diameter. The light from a star was measured through each of the four holes separately, and then through two, three, and all four. Failure of the measured sums to equal the calculated sums would be an indication of nonlinearity, since effects from variations in reflectivity over the mirror, differences in the sizes of the holes, and variations in sensitivity over the photocell cathode are all eliminated. The photometer was investigated over four voltage ranges, from 40 millivolts to its maximum of 10 volts, by choosing stars of different magnitudes. As expected, the precision of the results was reduced by seeing and extinction, but there was no indication of a linearity failure within the precision of the method, which was between 1 and 2 per cent. Inasmuch as voltage coefficient effects in a high resistor are large when they exist, it is safe to infer that the instrument is better than the limiting precision of the test. Our tests indicate that the photometer will not make a scale error greater than 0.01 mag., or 1 per cent, over its self-contained range of 7 mag. The $2\frac{1}{2}$-mag. screen has been calibrated to about 1 per cent, so the maximum systematic error over $9\frac{1}{2}$ mag. should be no greater than 2 per cent, or 0.02 mag. The screen was used on only three stars—NPS 1, 1r, and 2r.

Soon after the photometer was placed in service, it was found that the sensitivity did not remain constant. The variation was sometimes as much as 1 per cent per hour. Study of the sensitivity variations was complicated by varying extinction, and, of course, the wandering sensitivity made an accurate determination of the extinction impossible. Effective use could be made of the photometer, however, by employing mean extinction coefficients, which was found to be a permissible practice in the red and infrared, and by making frequent references to standard stars during the course of the work. On February 17, 1950, a satisfactory radium-light standard suitable for the red photometer was obtained. Use of this standard[4] permitted direct calibration of the sensitivity of the photometer and the direct determination of extinction coefficients. Furthermore, it permitted study of the sensitivity variations, which were traced to variations in the temperature of the photometer. After steps were taken to insure uniformity of temperature of the photometer, the sensitivity did not deviate more than 0.5 per cent from the mean during prolonged operation.

IV. COLOR SYSTEMS

During the course of this work the infrared magnitude determinations were obtained with a cemented gelatin Wratten 88A filter. The effective response to light as a function of wave length of this filter plus the photocell is shown in Figure 2. Up to October 16, 1949, the red magnitudes were obtained by a difference method. Deflections were taken through 2 mm of Schott OG2 glass and, of course, through the 88A filter. The OG2 glass transmits all infrared to which the photocell is sensitive, and therefore the difference between the two deflections is equal to the deflection that would be obtained by light from the spectral region included by the OG2 filter but excluded by the 88A filter. This region is shown by the dashed line in Figure 2, in which the photocell spectral response has been included. The effective wave length to light of uniform spectral distribution is λ 6700. As experience was gained with the method, it became apparent that the precision of the red magnitudes was lower than it should be, particularly for the red stars. This result was, of course, due to the fact that the observed error was that for the difference between two quantities. If the red deflection is only 30 per cent larger than the infra deflection, and if the infra deflection has a 1 per cent error, then the error in the difference

[4] V. K. Nikonov, Abastumani Observatory, private communication.

will be 3 per cent, not even counting the possibility of an error in the red deflection itself, which may add several more per cent to the total. The best results are obtained for the bluest stars, for which the difference will be a maximum. Even for such stars, however, the difference will be about equal to the infra, and the maximum error in a particular case will be twice that which one would get if the conventional method employing a single filter were used.

The difference method has two additional disadvantages of lesser importance. First, the deflection through the red filter is always the sum of the two desired deflections, and this results, generally speaking, in a limitation on the size of deflections that can be used

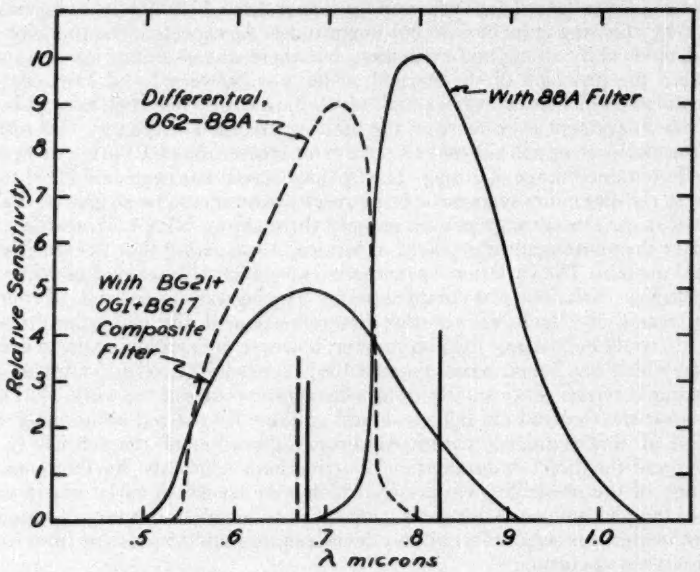

FIG. 2.—Response to equi-energy source of the photometer with various filters. The vertical lines mark wave lengths, which divide the response-curves into two equal areas. The heights of the vertical lines are proportional to the areas under the respective curves.

without going off-scale. Second, the records do not portray directly the data in a form for quick qualitative appraisal by the observer as the data are being taken.

The disadvantage of the conventional, simple two-filter method in the present work lies in the low efficiency of filters in the region of the spectrum around λ 6500. We know of no single-element filter that will satisfactorily isolate, by transmission, a region in this part of the spectrum; and compound filters, such as the red filter used in the Stebbins and Whitford six-color system, always have low maximum transmission and are therefore inefficient. The disadvantages of a band-isolation filter seemed to be less important than the disadvantages of the difference method, however, and the change was therefore made. The red filter used for the remainder of the work was cemented from 2-mm Schott OG1, 2-mm Schott BG21, and 1-mm Schott BG17. The spectral characteristics of this filter-plus-cell combination are shown in Figure 2. The effective wave lengths of the photometer to light of uniform spectral distribution were λ 8250 for the infrared and λ 6800 for the red, the latter only 100 A removed from the "difference" system. Color transformation was made between the two systems by observing stars of a wide range in color with both

systems and by constructing a transformation-curve with which all colors were converted to the new system. The change from cell *j* to cell *e* resulted in shifting the entire color system by −0.04 mag., regardless of the color of the star.

During the course of the work, four telescopes, including one refractor, were used. It is of interest that the change from one telescope to another did not result in appreciable changes in the color system, so that no corrections to the data from the several telescopes were necessary to obtain a homogeneous color system. Moreover, the small size of the color corrections required by the changes in cells and filters made very simple the process of placing the photoelectric colors on a homogeneous basis.

V. OBSERVING TECHNIQUE

A paper speed of $\frac{1}{8}$ inch per minute was used on the Brown recorder. Deflection times (exposures) of 30 seconds were used. Two deflections were made for each color for the difference-color system and one for each color for the absorption-filter system. Near the end of the program three deflections were usually taken, according to the pattern red-infrared-red. The last red deflection acts as a check on the guiding, a technique used by Eggen.

The photometer was constructed with a slide motion having adjustable stops that allowed the entire photometer to be shifted quickly from the star by approximately 1.5 times the diameter of the focal-plane aperture. Thus the stars were measured from the sky-brightness level instead of from dark. This process increased the efficiency of the work and the precision of the faint-star measurements, particularly in the infrared, where the sky is unusually bright and sometimes variable.[5]

The focal-plane aperture was 30″ (seconds of arc) in diameter on the 36-inch refractor and on the Crossley reflector. An aperture of 18″ was used with the 60-inch reflector, and one of 12″ with the 100-inch. The large aperture employed with the Lick telescopes did not result in a prohibitive amount of light from the sky because of the modest limiting magnitude, 13 to 14 photographic, accessible with these smaller telescopes. The large aperture, which makes the guiding relatively uncritical, is necessary in the case of the 36-inch refractor, to give clearance to the color aberrations of the lens. The 12″ aperture was required with the 100-inch telescope in order to reach stars as faint as the sixteenth photographic magnitude.

The 36-inch refractor was focused by means of the knife-edge method through the red filter. The focal aperture of the photometer was then moved outside this red focus by 15 mm, an amount that was found by experiment to be a good compromise between the effective red and infrared foci of the objective. The 36-inch telescope was found to be a valuable and useful instrument for the determination of red magnitudes, and its use greatly facilitated the work, owing to the heavy demands on the Crossley reflector. The refractor, however, is difficult to use near the pole, so all work on the North Polar Sequence was done with the Crossley.

In general, the photometer was always focused through the red filter by means of a knife-edge test, with the edge of the focal-plane aperture as the knife edge. It is necessary to focus through a filter, because the filters are placed inside the focus. The focus of the 100-inch reflector varied greatly during the night, and the focus was checked and corrected about once per hour.

During observing, about an hour usually was devoted to measurements of stars within an area. After the lapse of this much time, a transfer was made to another area, and stars within the new area were then measured. The series was usually completed by returning to the first area and making measures on four or five stars as a check. Within each area, two or three stars were used as standards of color and magnitude, and frequent reference was made to these stars, especially before the radium standard was placed in service. As

[5] J. Stebbins, A. E. Whitford, and P. Swings, *Ap. J.*, **101**, 40, 1945.

a rule, a star was not regarded as measured until consistent results had been obtained on three nights. A few of the published results, however, depend on less than three nights' observations. Almost all the faintest stars were measured on four nights.

The Polar Sequence was employed as a primary standard, partly because all other areas could be compared directly with it. In practice, however, all areas were not compared directly with the Polar Sequence. Instead, it was found more economical of time to set up a number of secondary standards in intermediate areas by direct comparison with the pole. These areas are the Harvard Standard Regions C 6 and C 12 and the Kapteyn Selected Areas 68, 61, and 64. The mean zero point of the brightest four or five stars in these areas is very close to the polar standard, probably within 0.01 mag.

VI. REDUCTIONS

The reductions were performed by the method used by Eggen,[6] with some simplification of the treatment of extinction. After it became possible to measure extinction, attempts were made to correct the red extinction as a function of the color of the star, thus taking into account the variation of effective wave length with the color of the star. The extinction was so small, however, that no significant change with star color was found, and thus all stars were treated alike in making extinction corrections. Before it became possible to determine extinction, mean extinction coefficients were taken from a compilation of Mount Hamilton extinction data that have been gathered from some years of photoelectric observations of variable stars. The values 0.12 and 0.07 mag. zenith extinction were adopted for the red and infrared, respectively, of the Mount Hamilton results. Later measurements checked these values, save for a few exceptional nights. All reductions were made to outside the atmosphere.

The extinction in the red and infrared was found to be remarkably constant from night to night, a result that probably is due to the small values of the coefficients. Owing to the small extinction, the precision of its determination is a small percentage of the quantity itself; by the same token, however, great refinement in its treatment is unnecessary.

On two nights, April 19 and May 19, 1950 (Table 1), the extinction was found to be very large, about three times normal. Curiously enough, the color was not affected; that is, both extinction coefficients were higher by the same increment in magnitudes. This is the effect that one would expect if some kind of nonselective absorption had been superimposed upon the normal atmospheric selective absorption. It is possible that this effect has not been noticed by other observers because it may be masked by the relatively large size of the selective absorption in the photographic and visual regions of the spectrum. One night, October 8, 1949, when the extinction could not be measured, gave results that could be explained on the assumption of large extinction; the results from this night were discarded.

No influence of atmospheric water vapor was noted on the extinction. This is not surprising, for only two very feeble water-vapor bands are included completely, and only a small portion of the great ρ band is included in the infrared. In addition, the altitudes of Mount Hamilton and of Mount Wilson are favorable factors, together with the usually dry air at these sites.

In making the reductions of the data, the red magnitude was carried as an actual magnitude, whereas the infrared was carried as a color index to be subtracted from the red magnitude for determination of the infrared magnitude. After the reductions of the original data had been completed, the results comprised a consistent set of red magnitudes referred to an arbitrary zero point, with each magnitude accompanied by a color on the natural photoelectric system. These colors and magnitudes will be called the "photoelectric colors and magnitudes."

[6] *Ap. J.*, 111, 68, 1950.

VII. THE ZERO POINTS

Figure 3 is a schematic diagram portraying roughly the positions of the areas dealt with in this paper and showing the scheme of magnitude transfers from one area to another. The principal feature of these transfers lies in the large number of intercomparisons available for independent checks of the zero points of the various areas. This

TABLE 1

SCHEDULE OF OBSERVATIONS

Date	Photocell	Filters	Telescope	Areas
1949 Sept. 1....	*j*	OG2-88A	Crossley	68, 64
Sept. 13....	*j*	OG2-88A	Crossley	68, 64, pole
Sept. 19....	*j*	OG2-88A	Crossley	68, pole
Sept. 20....	*j*	OG2-88A	Crossley	68, 64, pole
Sept. 27....	*e*	OG2-88A	Crossley	Tests only
Oct. 1....	*j*	OG2-88A	Crossley	Pole
Oct. 8....	*j*	OG2-88A	Crossley	Pole (discarded)
Oct. 16....	*j*	OG2-88A	Crossley	Pole
Oct. 20....	*j*	Red*-OG2-88A	36-inch	68, C 12
Oct. 22....	*j*	Red-OG2-88A	36-inch	64, C 12
Oct. 24....	*j*	Red-88A	36-inch	64, 68, C 12
Nov. 17....	*j*	Red-88A	36-inch	64, C 12
Nov. 27....	*j*	Red-88A	36-inch	68, 64, C 12
Nov. 28....	*j*	Red-88A	36-inch	51, 68, C 4, C 12
Dec. 8....	*j*	Red-88A	36-inch	51, 71
Dec. 12....	*j*	Red-88A	36-inch	71, 68, 51
1950 Feb. 17....	*j*	Red-88A	36-inch	51, C 4
Apr. 19....	*e*	Red-88A	36-inch	51, C 4 (discarded)
May 7....	*e*	Red-88A	36-inch	57, C 6, C 4
May 19....	*e*	Red-88A	36-inch	57, 51, C 6
June 7....	*e*	Red-88A	Crossley	61, C 6, pole
June 14....	*e*	Red-88A	60-inch	64, 61, 57
June 15....	*e*	Red-88A	100-inch	61, 57
June 16....	*e*	Red-88A	100-inch	61, 57
June 17....	*e*	Red-88A	100-inch	64, 61
June 18....	*e*	Red-88A	100-inch	64, 61, 57
Aug. 2....	*e*	Red-88A	Crossley	68, 64, C 12
Aug. 8....	*e*	Red-88A	Crossley	C 12, pole
Aug. 23....	*e*	Red-88A	Crossley	64, 61, C 12, pole
Aug. 30....	*e*	Red-88A	Crossley	64, 61, C 12, pole
Oct. 12....	*e*	Red-88A	36-inch	C 12, 71
Oct. 17....	*e*	Red-88A	36-inch	C 12, 71

* Red = OG1 + BG21 + BG17

technique was adopted in order to minimize systematic errors from inaccuracies in extinction corrections and from cumulative systematic errors caused by too remote a dependence of the zero point of any given area on the primary standard. It is unlikely that the present system contains any area with a systematic error in its mean zero point greater than 0.02 mag. Individual measurements for a few of the brightest stars of most of the areas are given in Table 2. This table contains most of the data (though not all) on

which the zero-point transfers from area to area are based. The magnitudes contained in Table 2 aid in an appraisal of the precision of the zero points of the areas.

Until a new system of magnitudes is established,[7] the zero point can, of course, be left perfectly arbitrary. In the case of the photographic system the zero point has been linked with the zero of the photovisual by definition of zero color index at spectral type A0. Because of this precedent, it is appropriate to fix zero points of red and infrared magnitude systems by a similar definition. But, before zero points can be fixed, one must have a clear understanding of just what is a photographic magnitude within the standards of

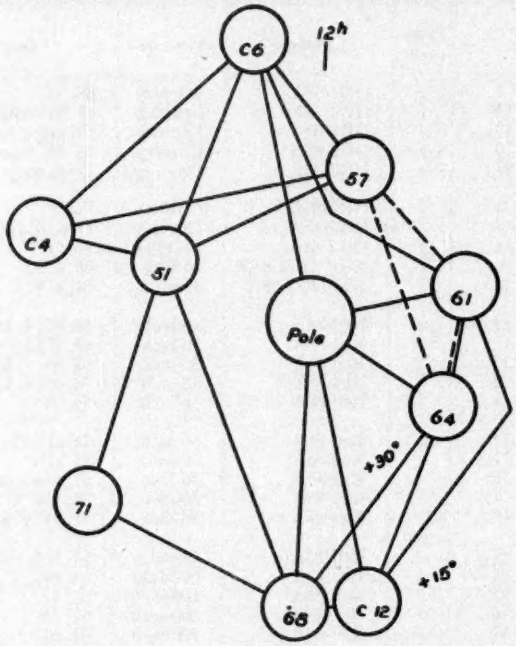

FIG. 3.—Diagram of the areas measured. Solid lines indicate intercomparisons made at Lick; dashed lines indicate Mount Wilson intercomparisons.

precision set by our photoelectric data. Certain stars of the Polar Sequence represent the only group of standards for which there is good agreement between accepted photoelectric magnitudes and colors and traditional photographic and photovisual magnitudes on the International System. These magnitudes, both photographic and photoelectric, therefore merit confidence, and our zero points of the red and infrared magnitudes have been fixed by reference to such stars. Our modified magnitudes and the colors resulting from differencing these magnitudes will be referred to as "standard" magnitudes and colors, to distinguish them from the "photoelectric" values.

Photoelectrically determined magnitudes and colors, after having been brought fairly close to the International System, have usually been designated by the symbols Pg_p and C_p, after a tradition started by Seares. At the present time there exist several lists of magnitudes, all designated by these symbols but differing somewhat in zero point and color

[7] C. P. Gaposchkin and S. Gaposchkin, *Harvard Ann.*, 89, 96, 1935.

TABLE 2

MAGNITUDE TRANSFERS—FROM POLE

To Area	Star	1949			1950			
		Sept. 13	Sept. 19	Sept. 20	June 7	Aug. 8	Aug. 23	Aug. 30
C 12	A	.....	.....	.....	.....	$6^m.99$	$6^m.94$	$6^m.98$
	D	.....	.....	.....	.....	5.99	5.98	5.99
	F	.....	.....	.....	.....	8.21	8.21	8.18
	+15°4733	.....	.....	.....	.....	7.57	7.57	7.58
C 6	A	.....	.....	.....	$7^m.06$	.....	.....	.....
	D	.....	.....	.....	7.17	.....	.....	.....
	F	.....	.....	.....	7.91	.....	.....	.....
	G	.....	.....	.....	7.30	.....	.....	.....
	K	.....	.....	.....	6.46	.....	.....	.....
61	80	.....	.....	.....	8.80	.....	8.73	8.77
	4s	.....	.....	.....	9.63	.....	9.58	9.62
	34s	.....	.....	.....	10.08	.....	10.09	10.09
	52s	.....	.....	.....	10.89	.....	.....	.....
64	239	$7^m.05$	.....	$7^m.06$	.....	.....	7.06	7.04
	383	.....	.....	.....	.....	.....	.....	10.14
	834	7.35	.....	7.36	.....	.....	7.39	7.39
	936	9.48	.....	9.49	.....	.....	9.45	9.45
68	197	8.21	$8^m.24$	8.21	.....	.....	.....	.....
	292	8.55	.....	.....	.....	.....	.....	.....
	371	7.97	.....	.....	.....	.....	.....	.....
	384	.....	.....	9.81	.....	.....	.....	.....
	398	7.06	7.06	.....	.....	.....	.....	.....

FROM C 12

To Area	Star	1949						1950		
		Oct. 20	Oct. 22	Oct. 24	Nov. 17	Nov. 27	Nov. 28	Aug. 2	Oct. 12	Oct. 17
68	197	$8^m.23$	.....	$8^m.23$	.....	$8^m.23$	$8^m.23$	$8^m.20$	.....	.....
	292	.....	.....	8.55	.....	.....	8.50	.....	.....	.....
	371	7.99	.....	8.03	.....	8.00	.....	7.95	.....	.....
	384	.....	.....	9.85	.....	.....	9.87	.....	.....	.....
	398	7.13	.....	7.08	.....	.....	7.12	7.11	.....	.....
64	239	.....	$7^m.03$	7.04	.....	7.04	.....	7.03	.....	.....
	383	.....	.....	10.19	.....	.....	.....	.....	.....	.....
	834	.....	7.35	7.37	$7^m.38$	7.39	.....	7.37	.....	.....
	936	.....	9.43	9.45	.....	.....	.....	9.43	.....	.....
C 4	B	.....	.....	.....	.....	.....	7.52	.....	.....	.....
	D	.....	.....	.....	.....	.....	6.60	.....	.....	.....
	E	.....	.....	.....	.....	.....	7.57	.....	.....	.....
	G	.....	.....	.....	.....	.....	8.94	.....	.....	.....
	K	.....	.....	.....	.....	.....	8.02	.....	.....	.....
	O	.....	.....	.....	.....	.....	9.12	.....	.....	.....
51	57	.....	.....	.....	.....	.....	8.99	.....	.....	.....
	177	.....	.....	.....	.....	.....	9.94	.....	.....	.....
	301	.....	.....	.....	.....	.....	9.70	.....	.....	.....
	438	.....	.....	.....	.....	.....	9.05	.....	.....	.....
71	90	.....	.....	.....	.....	.....	.....	.....	$9^m.55$	$9^m.48$
	205	.....	.....	.....	.....	.....	.....	.....	8.00	7.95
	257	.....	.....	.....	.....	.....	.....	.....	8.54	8.48
	347	.....	.....	.....	.....	.....	.....	.....	10.23	10.21

TABLE 2—*Continued*

FROM C 6

To Area	Star	1950 May 7	1950 May 19	To Area	Star	1950 May 7	1950 May 19
C 4	B	7^m54	.....	51	301	.....	9^m70
	D	6.58	.....		438	.....	9.03
	K	8.02	.....				
				57	192	.....	8.28
51	57	.....	8^m92		204	.....	7.98

FROM 68

To Area	Star	1949 Sept. 1	1949 Dec. 12	To Area	Star	1949 Sept. 1	1949 Dec. 12
64	239	7^m06	.....	71	90	.....	9^m57
	834	7.36	.....		205	.....	7.99
	936	9.43	.....		257	.....	8.53
					347	.....	10.22
51	57	.....	9^m00				

FROM 64

To Area	Star	1950 June 14	1950 June 17	1950 June 18	To Area	Star	1950 June 14	1950 June 17	1950 June 18
61	80	8^m82	8^m79	8^m77	57	192	8^m29	.....	8^m30
	4s	9.61	.....	.....		204	7.97	.....	.....
	34s	10.07	.....	.....		225	8.80	.....	.....
	52s	10.80	.....	.....					

system. When several of these systems are referred to in one place, they must be distinguished from one another by the use of unwieldy subscripts and by considerable verbal description. We feel that, as far as the present paper is concerned, we can contribute to simplification by dropping the traditional nomenclature and by starting a new one. We shall designate the photographic magnitudes of the standard list by ***P***, and the visual magnitudes by ***V***. Because of the confusion that would be caused by attempting to use *C* symbols to designate colors based on magnitudes in four wave lengths, color symbols will be abandoned, and colors will be expressed by magnitude differences. Thus C_p on our standard system will be expressed as $(P-V)$. The red and infrared magnitudes will be called ***R*** and ***I***, respectively. In this paper the symbols ***P***, ***V***, ***R***, and ***I*** refer only to magnitudes on the adopted standard system; where other symbols are used, they refer to other systems.

The specific primary standard used here, on which the zero points of our red and infrared magnitudes are based, is a list of magnitudes and colors set up by Stebbins, Whitford, and Johnson[8] for nine stars of the Polar Sequence. The stars of this list (Nos. 6, 2r,

[8] *Ap. J.*, 112, 469, 1950.

10, 4r, 13, 8r, 16, 19, and 12r) were not observed on this program, as some of them are too faint for precision observation at this observatory without expenditure of a disproportionate amount of time, and also because the list was not available until after the red and infrared Polar Sequence observations had been finished. Eggen,[9] however, has published a list of magnitudes of bright Polar Sequence stars on a system nearly the same as that of the above-mentioned nine-star sequence, and recently he has extended his observations to include seven of the nine stars.[10] These new observations allow derivation of

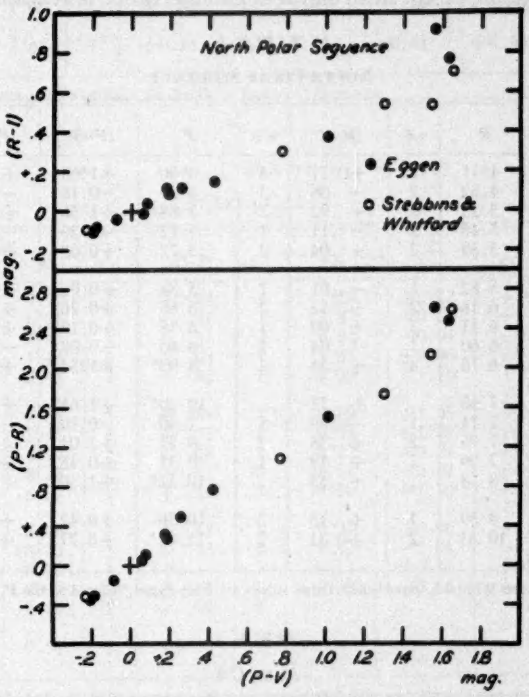

FIG. 4.—Relationship between the P, V and the R, I magnitude systems for stars of Polar Sequence. P and V are symbols used in this paper to designate photographic and photovisual magnitudes on the International System, while R and I designate red and infrared magnitudes determined as described in the text.

magnitude and color equations for reducing all of Eggen's Polar Sequence magnitudes to the new primary standard of the nine-star list. The reduction equations are:

$$P - V = -0^m.10 + 1^m.10\, C_p\,,$$

$$P = Pg_p\,,$$

where the values of Pg_p and C_p are Eggen's for his polar stars. The zero points of our R and I magnitudes have been fixed by equating our magnitudes to the P magnitudes at color $(P-V) = 0$. The standards R and I are plotted in Figure 4 to show their relationship with the P, V system for Polar Sequence stars.

[9] *Ap. J.*, 111, 67, 1950. [10] Unpublished.

VIII. THE OBSERVATIONS

The observations are given in Tables 3–12. In these tables the star designation is given in italics when it is a number from the *Mount Wilson Catalogue of Selected Areas*[11] and in roman when it is from *Harvard Annals*, Volume **101.** The C-region designations are from *Harvard Annals*, Volume **89,** No. 8, except for BD+15°4733, which, by chance, lies in Area C 12. This star is a red dwarf with known parallax, and it is included as a valuable red standard. Columns headed "a.d." contain the average deviation of the value given in the preceding column, except when only a single observation is available. The values for

TABLE 3

NORTH POLAR SEQUENCE

Star	*R*	a.d.	(*R*−*I*)	a.d.	*P*	(*P*−*V*)	(*P*−*R*)	No.
1r	4^{m}11	3	+0^{m}77	3	6^{m}60	+1^{m}63	+2^{m}49	2
1	4.52	2	− .08	3	4.23	−0.18	−0.29	7
2r	5.25	3	+ .92	3	7.88	+1.56	+2.63	5
2	5.45	2	− .11	1	5.12	−0.20	−0.33	4
3	5.59	2	+ .04	2	5.72	+0.08	+0.13	5
4	5.82	1	− .01	1	5.88	+0.06	+0.06	8
3s	6.16	2	+ .12	2	6.66	+0.26	+0.50	3
2s	6.21	3	+ .09	1	6.48	+0.19	+0.27	6
5	6.60	1	− .04	1	6.46	−0.08	−0.14	8
3r	6.76	4	+ .54	2	8.90*	+1.54*	+2.14	8
5r	7.60	.....	+ .71	.....	10.20*	+1.65*	+2.60	1
7	7.71	1	− .09	1	7.40	−0.19	−0.31	2
4r	7.75	2	+ .38	2	9.27	+1.01	+1.52	4
8	7.99	2	+ .12	1	8.31	+0.18	+0.32	3
6r	8.58	.....	+ .55	.....	10.32*	+1.30*	+1.74	1
4s	9.59	1	+ .15	2	10.36	+0.42	+0.77	3
6s	10.33	2	+0.31	2	11.42*	+0.77*	+1.09	2

* Stebbins and Whitford, unpublished. Other values are from Eggen, reduced to the *P*, *V* system as described in text.

TABLE 4

AREA C 4

Star	*R*	a.d.	(*R*−*I*)	a.d.	Pg_p^*	C_p^*	(Pg_p-R)	No.
D	6^{m}58	1	+0^{m}33	2	7^{m}72	+0^{m}88	+1^{m}14	4
F	6.90	1	+ .36	2	.....	.....	.....	3
A	7.22	1	− .14	1	6.74	−0.15	−0.48	5
B	7.50	1	− .03	1	7.27	+0.08	−0.23	5
E	7.58	1	+ .19	2	8.04	+0.43	+0.46	2
K	8.01	1	+ .38	1	9.40	+1.04	+1.39	5
G	8.95	.....	− .13	.....	8.49	−0.08	−0.46	1
O	9.14	2	+ .43	2	.....	.....	.....	4
L	9.19	2	+ .17	2	9.63	+0.40	+0.44	2
M	9.85	.....	+0.15	.....	.....	.....	.....	1

* Unpublished values from Eggen.

[11] *Pub. Carnegie Inst. Washington*, No. 402: *Papers of the Mt. W. Obs.*, Vol. 4.

TABLE 5

AREA C 6

Star	R	a.d.	$(R-I)$	a.d.	Pg_p^*	C_p^*	(Pg_p-R)	No.
K.....	6^m39	1	$+0^m78$	1	8^m94	$+1^m51$	$+2^m55$	6
A.....	7.02	1	− .09	1	6.65	−0.02	−0.37	6
D.....	7.10	1	+ .16	1	7.67	+0.51	+0.57	6
G.....	7.24	1	+ .33	1	8.56	+0.96	+1.32	6
M.....	7.68	1	+ .44	1	9.48	+1.19	+1.80	6
F.....	7.85	1	+0.14	1	8.25	+0.44	+0.40	6

* Values determined by Kron and Smith on Eggen's C 12 system.

TABLE 6

AREA C 12

Star	R	a.d.	$(R-I)$	a.d.	Pg_p^*	C_p^*	(Pg_p-R)	No.
D.....	5^m99	1	$+0^m45$	1	7^m59	$+1^m12$	$+1^m60$	7
E.....	6.67	1	+ .37	1	7.87	+0.86	+1.20	4
A.....	6.97	2	− .11	2	6.54	−0.04	−0.43	7
C.....	7.43	1	− .03	1	7.33	+0.06	−0.10	3
I.....	7.48	1	+ .45	1	9.09	+1.16	+1.61	3
+15°4733....	7.58	1	+ .88	1	9.89	+1.28	+2.31	7
M.....	7.85	1	+ .55	1	9.65	+1.20	+1.80	3
F.....	8.19	1	+ .08	1	8.27	+0.24	+0.08	6
G.....	8.29	2	+ .07	3	8.37	+0.23	+0.08	2
P.....	8.59	1	+ .46	1	10.10	+1.10	+1.51	3
O.....	8.62	1	+ .42	1	9.97	+0.96	+1.35	7
H.....	8.74	1	− .05	1	8.42	−0.01	−0.32	4
K.....	8.76	1	+ .17	3	9.13	+0.40	+0.37	2
L.....	8.99	1	+ .15	1	9.38	+0.36	+0.39	2
S.....	9.12	1	+ .59	1	.....	.....	.....	2
N.....	9.54	2	+0.20	1	.....	.....	.....	3

* Eggen, *Ap. J.*, **112**, 142, 1950, except star K, from unpublished data, and star G, a new revised value. Internal accuracy checked on two nights by Kron and Smith except for star N, which failed to check and may be variable.

TABLE 7

AREA 51

Star	R	a.d.	$(R-I)$	a.d.	No.	Star	R	a.d.	$(R-I)$	a.d.	No.
57.....	8^m94	2	$+0^m30$	2	3	303.....	10^m59	3	$+0^m26$	2	3
438.....	9.04	1	+ .36	4	3						
301.....	9.70	1	+ .02	1	3	386.....	11.35	3	+ .12	3	3
177.....	9.91	2	+0.18	1	3	428.....	11.86	2	+0.53	2	3

TABLE 8

AREA 57

Star	Lick				Mount Wilson				Mount Wilson			No.
	R	a.d.	(*R*−*I*)	a.d.	*R*	a.d.	(*R*−*I*)	a.d.	*P**	(*P*−*V*)*	(*P*−*R*)	
204	7^{m}96	1	+0^{m}35	1	7^{m}97	1	+0^{m}35	1				3, 2
192	8.29	1	+ .21	1	8.30	1	+ .21	1				2, 3
225	8.79	2	+ .30	1	8.79	1	+ .31	1				2, 2
178	9.40	1	+ .15	3	9.40	1	+ .15	1				2, 2
268	11.00	4	+ .31	2	10.99	....	+ .36	....				2, 1
96	11.14	....	+ .27	....	11.12	....	+ .22	....				1, 1
158	11.26	1	+0.41	1	11.21	....	+ .35	....				2, 1
167					11.23	....	+ .05	....				1
29					11.23	1	+ .28	1	12^{m}44	+0^{m}75	+1^{m}21	3
52					11.68	3	+ .46	3	13.48	+1.18	+1.80	5
11					12.63	1	+ .18	3	13.33	+0.40	+0.70	3
8					12.81	3	+ .23	6	13.60	+0.47	+0.79	3
16					12.90	2	+ .31	4	14.38	+0.90	+1.48	3
58					13.56	3	+ .29	2	14.78	+0.71	+1.22	4
54					13.70	3	+ .26	6	14.52	+0.51	+0.82	4
36					14.46	3	+ .29	4	15.87	+0.81	+1.41	4
7					14.52	2	+ .27	4	15.21	+0.44	+0.69	3
25					14.60	3	+ .16	3	15.69	+0.65	+1.09	4
40					14.61	2	+ .24	2	15.26	+0.28	+0.65	4
63					15.17	....	+0.61	....	16.58	+0.87	+1.41	1

* Stebbins, Whitford, and Johnson, *Ap. J.*, **112**, 469, 1050.

TABLE 9

AREA 61

Star	Lick				Mount Wilson				Lick and Mount Wilson			No.
	R	a.d.	(*R*−*I*)	a.d.	*R*	a.d.	(*R*−*I*)	a.d.	*P**	(*P*−*V*)*	(*P*−*R*)	
80	8^{m}78	4	+0^{m}15	1	8^{m}79	1	+0^{m}15	1	9^{m}27	+0^{m}29	+0^{m}49	3, 5
4s	9.61	3	+ .15	2	9.62	1	+ .15	1	10.07	+0.27	+0.45	3, 3
34s	10.09	2	+ .18	2	10.08	1	+ .19	1	10.76	+0.43	+0.68	3, 2
52s	10.89	....	+0.12	....	10.80	1	+ .12	2	11.16	+0.24	+0.34	1, 3
108s					10.52	1	+ .63	1	12.87	+1.51	+2.35	3
129s					10.56	1	+ .73	2	13.00	+1.54	+2.44	3
19					10.56	1	+ .34	2	12.02	+0.93	+1.46	3
123s					11.17	1	+ .22	1	11.97	+0.47	+0.80	3
23s					12.80	1	+ .31	1	13.66	+0.54	+0.86	2
32					12.81	1	+ .25	2	13.96	+0.74	+1.15	3
11					12.87	2	+ .30	1	14.02	+0.68	+1.15	4
66					13.08	1	+ .29	2	14.46	+0.85	+1.38	4
88					13.21	4	+ .36	3	14.69	+0.92	+1.48	4
100					13.60	2	+ .22	3	14.43	+0.50	+0.83	4
7					14.08	4	+ .25	2	15.09	+0.57	+1.01	3
130					14.12	1	+ .22	4	15.58	+0.85	+1.46	4
20					14.50	4	+ .43	4	15.87	+0.84	+1.37	4
63					14.81	2	+0.30	3	16.00	+0.71	+1.19	3

* Stebbins, Whitford, and Johnson, *Ap. J.*, **112**, 469, 1950.

TABLE 10

AREA 64

Star	Lick				Mount Wilson				No.
	R	a.d.	(*R*−*I*)	a.d.	*R*	a.d.	(*R*−*I*)	a.d.	
239.....	7^{m}05	1	+0^{m}81	1	7^{m}04	.....	*	.....	6, 1
834.....	7.38	2	+ .32	2	7.38	1	+0^{m}30	1	4, 3
936.....	9.44	2	− .08	2	9.47	1	− .09	2	6, 3
204.....	9.45	2	− .03	2	9.47	.....	− .05	.....	4, 1
383.....	10.14	.....	+ .41	.....	10.15	.....	+ .44	.....	1, 1
225.....	10.48	2	+0.04	2	10.48	2	.00	1	3, 3
347.....	.....	.....	.....	.....	11.33	1	+ .25	1	2
344.....	.....	.....	.....	.....	12.72	1	+0.14	2	2

* Infrared too bright for measurement with 100-inch telescope.

TABLE 11

AREA 68

Star	*R*	a.d.	(*R*−*I*)	a.d.	No.	Star	*R*	a.d.	(*R*−*I*)	a.d.	No.
398.....	7^{m}06	1	+0^{m}16	1	6	332.....	10^{m}26	2	+0^{m}19	2	5
371.....	8.01	1	+ .42	2	6	280.....	10.95	6	+ .36	4	4
197.....	8.23	1	+ .12	1	6	380.....	10.97	4	+ .34	5	4
174.....	8.49	3	+ .41	2	4	400.....	11.08	2	+ .32	4	4
292.....	8.53	1	+ .18	2	6	265.....	11.70	8	+ .36	6	4
335.....	8.70	1	+ .38	1	4	334.....	12.37	6	+ .46	6	4
218.....	9.07	2	+ .43	2	5	401.....	12.42	9	+ .07	7	5
327.....	9.25	2	+ .17	2	5	278.....	12.45	4	+0.38	6	4
391.....	9.29	1	+ .38	2	5						
384.....	9.89	2	+0.30	2	5						

TABLE 12

AREA 71

Star	*R*	a.d.	(*R*−*I*)	a.d.	No.	Star	*R*	a.d.	(*R*−*I*)	a.d.	No.
205.....	7^{m}99	2	+0^{m}40	1	4	137.....	10^{m}58	4	+0^{m}06	3	4
257.....	8.52	2	+ .22	1	4						
90.....	9.54	3	+ .19	1	4	89.....	11.88	3	+0.35	8	3
347.....	10.22	1	+0.43	2	4						

a.d. are in units of 0.01 mag.; when a.d. was less than 1.5, it was entered in the tables as "1," which accounts for the absence of zero values. Some of the tables contain values of magnitudes on other systems by other investigators. The meanings of these are indicated by the headings of the columns and by text in later pages in the discussion of the diagrams. The last column, headed "No.," refers to the number of nights on which the given star was observed, and the number in this column may therefore be taken as a weight. Some tables include a column headed "$(P-R)$"; these quantities are included whenever P, V data are available. The values are useful checks and in all cases are plotted in the accompanying diagrams.

Values of Pg_p and C_p on a system in current use by Eggen are available for Regions C 12[12] and C 4.[13] Values for Pg_p and C_p on this system were determined by us for stars in Region C 6 with a C-7073B multiplier on the 36-inch refractor. Observations were made

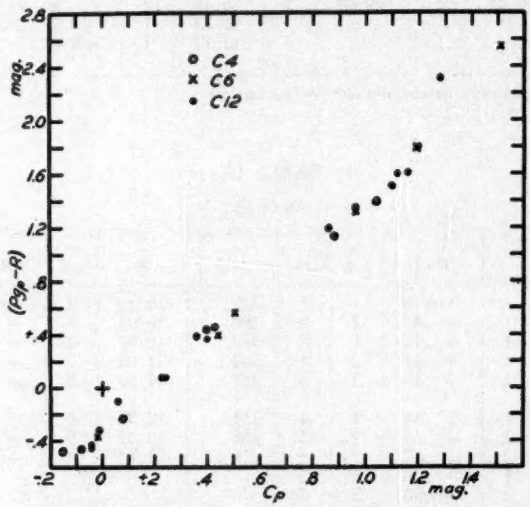

FIG. 5.—Relationship between the R system of magnitudes and Eggen's Pg_p, C_p system for three areas

on two nights according to Eggen's technique.[14] Correlations between the red magnitudes and the Pg_p and C_p values are shown in Figure 5. This diagram demonstrates a high degree of correlation between these two independent, carefully determined sets of photoelectric data. The conspicuous zero displacement is a property of the C 12 magnitude system, which will be discussed in detail by Eggen in a forthcoming publication.

In Figure 6 are plotted values like those for Figure 4, but for Selected Areas 57 and 61. The P and $(P-V)$ values are from Stebbins, Whitford, and Johnson.[15] There is satisfactory agreement between the sets of data shown in Figures 4 and 6. This is good evidence that the present red system and the Stebbins, Whitford, and Johnson P and V system are all on consistent zero points for the pole, Area 57, and Area 61. Inasmuch as the data from the two systems used in these areas are entirely independent, the agreement should be a source of comfort to anyone contemplating the use of either set.

[12] *Ap. J.*, 112, 142, 1950. [13] Unpublished.

[14] The internal consistency of the measurements in Eggen's C 12 list was also checked by us on two nights, with good agreement.

[15] *Ap. J.*, 112, 469, 1950.

IX. LUMINOSITY EFFECTS

There are several conspicuous deviations from the mean for individual stars plotted in Figures 4, 5, and 6. In Figure 5, BD+15°4733 deviates from a curve terminating at C-6-K at $C_p = +1^m.51$. The BD star is a known main-sequence object, whereas C-6-K is HD 96373, an Ma star, almost certainly a giant. The apparent lack of agreement between the magnitudes of these two stars is therefore caused by the well-known differences between the distribution of radiation in main-sequence and giant stars. In Figure 5 may also be noted a certain amount of scatter among the blue stars, too large to be attributed to observational error. Chief among the stars affected are C-12-C and C-4-A; these deviations may well be an expression of the fine structure found in color-magnitude arrays by Eggen.[16] Some of the scatter in Figure 6 may be due to such luminosity effects or, less probably, to the effects of space reddening. The effect of space reddening would be to

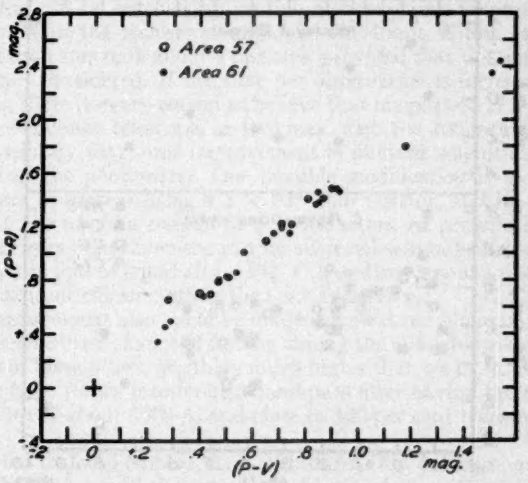

FIG. 6.—Relationship between the *R* system of magnitudes and the *P*, *V* system of Stebbins, Whitford, and Johnson's measurements of Selected Areas 57 and 61.

make a star appear brighter in the red than would be expected from its brightness in the blue; thus *R* will be abnormally small for a reddened star, and $(P-R)$ will be too large. The present data, however, do not show any clear-cut evidence for the presence of space reddening, as distinguished from other scatter-causing effects.

An additional cause for scatter in the curves of Figures 4, 5, and 6 may be the presence of binary stars among those observed. It is entirely possible for the spectrum of a red companion to escape detection by spectroscopy in the blue region of the spectrum, and yet to affect the red magnitude by a noticeable amount. Stars like YZ Cas or α CrB, for example, might be expected to appear abnormally bright in the red, thus falling high on $(P-R)$ versus $(P-V)$ plots. All the effects just discussed will be enhanced by employing $(P-I)$ instead of $(P-R)$.

X. VARIABLES

Throughout the course of the work, several stars were observed a great many times. In some cases, notably NPS 2r and 1r, C-12-A, and 61-80, the deviations of the measure-

[16] *Ap. J.*, 111, 65, 81, 1950.

ments from the mean were unusually large. It is probable that these stars are variable to an extent somewhat more than average for a star not definitely recognized as a variable. Extensive measurements at this observatory of the A-type eclipsing variable α CrB indicate that this star is an intrinsic variable with an amplitude of about 0.02 mag., even though A-type stars generally are recognized as among the most constant of all types. Other extensive measurements made here, particularly for the purpose of checking the constancy of comparison stars, indicate that probably none of these stars stay constant to better than 1 per cent of their light. This fact has a bearing on the establishment of standards. It is clear that a standard may not meet a ± 1 per cent tolerance unless it is based on more than one star, regardless of how good or extensive the work devoted to the determination of the standard. Furthermore, a group of, say, four or five stars intended to establish a standard magnitude precise to 1 per cent must be investigated to be certain

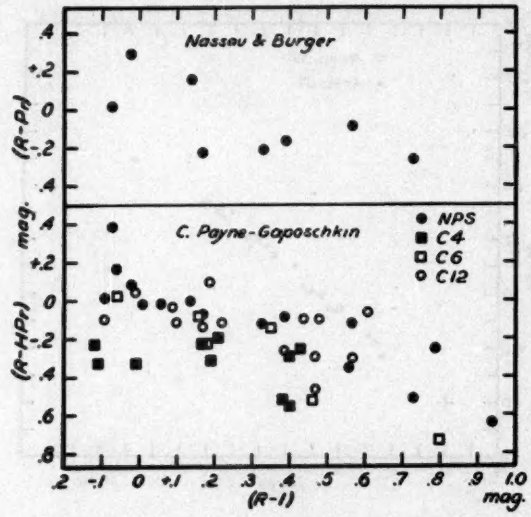

FIG. 7.—Relationships between the *R, I* system and other red magnitude systems. *HPr* are red magnitudes on the Harvard system; *Pr* is the designation of the Nassau-Burger system.

that it does not contain a star having an amplitude of variation large enough to vitiate the entire standard.

In Figure 6, one star at $(P-V) = +0.28$ deviates by a large amount from the others. This star, 57-40, may be another variable, although in this case the evidence is insufficient to be certain of the discordance.[17]

XI. OTHER RED MAGNITUDE SYSTEMS

Two other red magnitude systems are available for comparison with the present data, that of Nassau and Burger[18] and that of C.P. and S. Gaposchkin.[19] In Figure 7 we have

[17] In a recent paper (*Ap. J.*, **112**, 240, 1950) H. L. Johnson mentions the difficulty of setting the fine sensitivity control without making an occasional error of ½ mag. We have also found this to be true. Star 57-40 is off by +0.20 mag., and this large deviation may be from a shunt error. The difference, if real, cannot be due to an error in our observations, since our magnitude depends upon consistent measurements made on four nights.

[18] *Ap. J.*, **103**, 25, 1946.

[19] *Harvard Ann.*, Vol. **89**, Nos. 5 and 8, 1935.

plotted the differences between our red magnitudes and those from these two systems against our ($R-I$) as an independent variable, for all stars in common. The zero points of the three systems seem to be nearly in agreement, so far as one can tell. With the exception of C 4, the Nassau-Burger and Gaposchkin systems are to the blue of ours, in agreement with statements made by these authors. C 4, however, seems to be on the same color as our R system, but with a zero displacement of nearly 0.3 mag.

XII. LIMITING MAGNITUDE

The faintest stars for which measurements were attempted with the 100-inch telescope are 57-36 and 61-63. One measurement of the 16.58-mag. star 57-63 was made, and this single measurement deviated from the others of Figure 6 by only 0.02 mag. The measurements with the 100-inch telescope were made by ordinary methods, and no attempt was made to extend the range by resort to extraordinary means. It is evident that magnitude 16.5 photographic can be reached by routine methods with present equipment, in a reasonable time. With the technique employed at Mount Wilson (and at Lick), the measurement of each star took about 4 minutes, provided that the time for transfer to a distant area is not considered. If the time per observation is increased to some 30–45 minutes per star, there is every reason to believe that magnitude 17.5 can be reached in practice with the 100-inch telescope, or 19.0 mag. with the 200-inch telescope.

There is a possibility that some improvement in limiting magnitude can be achieved by modification of the photometer. One possible modification is to increase the grid resistance. We are at present using a 5×10^{13} ohm resistor, and H. L. Johnson is experimenting with the use of a resistor of 1×10^{14} ohms. At present, however, it seems unlikely that any great improvement can be achieved without refrigeration to a lower temperature, such as that of liquid air (−192° C.), or discovery of a photoelectric surface having higher quantum efficiency than the *CsO-Ag* surface.

Significant improvement also could be made if a good red filter could replace the one we used. There seems little chance of finding among the available glass or gelatin filters, or combinations of these filters, anything much better than we have. But possibly in the future we might hope for an interference band-pass filter having the characteristics we wish: a band width of about 1000 A, and close to 100 per cent transmission.*

We are indebted to Joel Stebbins, A. E. Whitford, Olin J. Eggen, and H. L. Johnson for extensive help, advice, and the use of unpublished data, without which the value of the work reported here would be greatly reduced. Dr. W. Baade's interest in the work has been a constant stimulation. Without the facilities of the Mount Wilson and Palomar Observatories, placed at our disposal through the kindness of Dr. I. S. Bowen, the faint sequences in Areas 57 and 61 would have been impossible to set up. The electronic equipment with which this work was done was designed and built with the aid of a contract with the Office of Naval Research.

*Note Added in Proof.—Such a filter has since been produced in the laboratory at Mount Hamilton. Details will be published in a forthcoming note in the *Publications of the Astronomical Society of the Pacific*.

THE COLOR-MAGNITUDE ARRAY FOR STARS IN THE GLOBULAR CLUSTER M 15*

ARCHIBALD BROWN
Yerkes and McDonald Observatories
Received October 9, 1950

ABSTRACT

The paper gives photovisual and photographic magnitudes for a number of stars in the globular cluster M 15, as measured from direct photographs taken at the McDonald Observatory. The photographs were calibrated by means of a sequence of stars in the field whose magnitudes had been determined with a photoelectric photometer.

It was possible to recognize a number of foreground stars in the photographs from their proper motion and to eliminate these stars from the color-magnitude diagram. The resulting diagram shows a well-defined "red-giant" sequence extending from absolute magnitude −0.6 on the photovisual scale (color index approximately 0.65) to absolute magnitude −2.8 (color index 1.4). In addition, there are a few scattered stars on the blue side of this "red-giant" sequence.

I

The distinction drawn by Baade[1] between two types of stellar population in our own galaxy and in extragalactic systems has revived interest in the color-magnitude diagrams of globular clusters, as representative of the characteristics of type II populations. One difficulty in drawing up a color-magnitude diagram for a globular cluster arises from the presence of field stars. A way of distinguishing them would be from their spectra, but they are rather faint for this. The proper motions of these stars may be used more readily, since they are generally larger than those of the cluster stars and can be determined differentially with respect to the cluster. This method has been applied to the globular cluster M 15 ($\alpha = 21^h28^m$, $\delta = 11°57'$). It has proved possible to recognize a number of field stars, which, from their position alone, might have been taken to be cluster members. The effectiveness of the method depends rather critically on the accuracy with which the proper motions can be determined. Fortunately, first-epoch plates were available at the Yerkes Observatory which gave a large scale (approximately 10″/mm) and intervals of 35–48 years between the first- and second-epoch plates. As a result, the mean-square error of a (relative) proper motion derived from one pair of plates was small (~0″.002 per annum), and it was this fact which made the method of practical value. Details of the plates used in determining the proper motion are given in Section IV, and the effectiveness of this method of picking out field stars is discussed in a later section.

The observational material for the magnitude and color determinations was obtained at the McDonald Observatory during September and October, 1949. I took a series of direct photographs at the Cassegrain focus of the 82-inch reflector and later selected a number of plates for measurement with a Schilt-type photometer at the Yerkes Observatory. To calibrate these photographs, I made photoelectric observations of a star sequence in the field of the cluster. Yellow and blue filters were inserted to provide color determinations. The observed photoelectric colors were transferred to the International System by means of observations of the North Polar Sequence. These observations were also used for connecting the "yellow" magnitude system of the photoelectric photometer to the photovisual system of the NPS. Finally, the zero point of the calibration sequence was fixed by photoelectric comparisons with the NPS. Details of the photoelectric observations are given in Section II, details of the photographic photometry in Section III.

* *Contributions from the McDonald Observatory, University of Texas*, No. 198.

[1] *Ap. J.*, **100**, 137, 1944; *Mt. W. Contr.*, No. 696.

II

The photoelectric observations were made with a photometer designed by Dr. W. A. Hiltner and briefly described by him.[2] The receiver is a 1P21 photomultiplier tube, whose output is fed through a d.c. amplifier to a Brown recorder. In the observations for colors, a Corning No. 3385 filter was used for the yellow region and a Corning No. 5850 filter for the blue. A diaphragm of 2 mm diameter was used; this gave an area of the sky of approximately 14″ in diameter.

Table 1 lists the stars in the field of the cluster which were observed photoelectrically. The numbers preceded by "K" refer to stars in Küstner's catalogue[3] of M 15; the numbers preceded by "B" refer to a supplementary list drawn up during the present investi-

TABLE 1

LIST OF STARS OBSERVED WITH PHOTOELECTRIC PHOTOMETER

Star	Magnitude		Star	Magnitude	
	m_{pv}	m_{pg}		m_{pv}	m_{pg}
K 1118	10.43	10.81	K 7	12.92	13.58
B 7	10.64	11.39	K 1115	13.48	13.98
B 3	11.19	12.17	K 40	13.89	14.61
B 27	12.09	13.60	K 22	14.50	15.24
K 32	12.23	12.77	K 17	15.02	15.62
K 160	12.91	13.54	K 92	15.26	15.90

gation (Table 6). The Küstner catalogue covers an area of 20′ × 20′, centered on the cluster, and the B numbers refer to stars outside that area. It turned out that the four brightest stars in the sequence were not required for the cluster stars; the remaining stars, from K 32 to K 92, lie between 4½′ and 8½′ from the center of the cluster.

The effect of changes in the zenith distance on the observed color indices was determined from a series of observations on a red star (B 27) and a bluer star (K 1115) at different altitudes. For each star the observed color index, c, was plotted against sec z (z is the zenith distance), and a straight line was drawn through the plotted points. The equations of these lines were

$$c_1 = 1.86 + 0.17\,(\sec z - 1)\,, \tag{1}$$

$$c_2 = 0.38 + 0.22\,(\sec z - 1)\,, \tag{2}$$

for B 27 and K 1115, respectively.[4] Then, for any other star, the correction to the zenith was obtained by an interpolation between equations (1) and (2). More explicitly, for an observed color index c at zenith distance z, the corresponding color index at the zenith, c_0, was computed by making

$$\frac{1.86 - c_0}{c_0 - 0.38} = \frac{c_1 - c}{c - c_2}\,, \tag{3}$$

where c_1 and c_2 were computed from equations (1) and (2) for the appropriate value of z.

[2] *Ap. J.*, **108**, 56, 1948.

[3] *Veröff. Sternw. Bonn*, No. 15, 1921.

[4] In the reduction, an additional place was retained; the magnitudes and colors were rounded off to two decimal places subsequently.

This allowed all the observed colors to be corrected to the zenith, and the next step was to relate these corrected colors to the International System. This was done by observing a number of stars in the North Polar Sequence and in the supplementary sequences. Table 2 shows the stars observed, the date of observation, the corrected color, c_0, and the International color c', as given by Seares.[5] From the last two columns of Table 2, c_0 was plotted against c' (Fig. 1). It appeared that a linear relation between c_0 and c' would be consistent with the observations; so a straight line was drawn, and this was used to transfer from c_0 to the International System c'. These observations of NPS stars were also used to obtain a correction to allow for the difference in effective wave length between the magnitudes obtained with the yellow filter photoelectrically and the

TABLE 2

OBSERVATIONS FOR COLOR ON STARS OF NORTH POLAR SEQUENCE

Star	Date and Time of Observation		Observed Color c_0	International Color c'
	October 1949	U.T.		
NPS 5	26	8^h42^m	−0.28	+0.03
9	26	7 34	−0.04	+0.14
13	21	7 24	0.00	+0.22
14	21	6 30	+0.20	+0.40
16	25	10 35	+0.11	+0.34
16	27	1 38	+0.14	+0.34
16	27	2 16	+0.12	+0.34
17	25	11 39	+0.46	+0.57
18	25	11 56	+0.15	+0.40
5r	26	7 14	+1.98	+1.50
9r	21	7 48	+1.15	+1.00
10r	22	7 00	+0.32	+0.54
11r	26	6 06	+1.31	+1.17
11r	26	6 48	+1.30	+1.17
11r	27	6 20	+1.34	+1.17
6s	22	7 13	+0.63	+0.68
H.A. 48, 345	26	8 12	+2.01	+1.63

photovisual scale defined by the NPS. To a first approximation, the correction should be a linear function of the color index of the stars involved.[6] Thus, for a comparison of two stars in the NPS, the difference between (*a*) their observed magnitude difference and (*b*) their magnitude difference on the photovisual scale should be proportional to the difference in their color indices. It was apparent that the correction required was relatively small and somewhat difficult to determine with the observations available, but the best value appeared to be

$$\Delta(\delta m) = -0.10\,\Delta c', \tag{4}$$

where $\Delta c'$ is the difference in color index c' of the stars compared; δm is the observed difference in magnitude; and $\Delta(\delta m)$ is the correction to be applied to the observed magnitude difference to obtain the difference on the photovisual scale. The effect of this correction was small, but it was included in deriving the photovisual magnitudes in Table 1.

[5] *Ap. J.*, **101**, 15, 1945; *Mt. W. Contr.*, No. 701.

[6] See B. Strömgren, *Handb. d. exper. Phys.*, **26**, 394, 1937.

(The sign of the correction indicates that the effective wave length of the photoelectric yellow magnitudes was slightly less than the effective wave length of the photovisual system. It was computed to be about 5500 A, as compared with 5615 A for the photovisual system.)

To establish the zero point of the calibration sequence, comparisons were made between three stars in the sequence and NPS stars. The comparisons were as follows:

1949 Oct. 11, 12	NPS 14 against K 1118	1949 Oct. 26	NPS 11r against K 7
		27	NPS 11r against B 27

Although the comparisons were made with the cluster at approximately the same altitude as the pole, the zenith distances were not exactly the same, and a correction for extinction

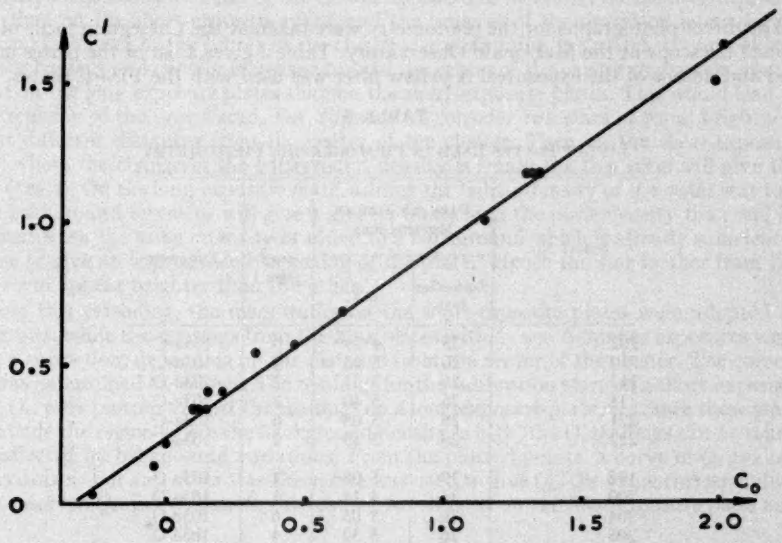

FIG. 1.—Graph of color index on International System (c') against c_o, observed color index (reduced to zenith).

was required. The amount of this correction was obtained from the observations on B 27 and K 1115, mentioned earlier. The difference in magnitude due to extinction was taken as

$$\delta m = 0.2\ (\sec\ z_2 - \sec\ z_1)\,, \qquad (5)$$

where z_2 and z_1 represent the two zenith distances ($z_2 > z_1$). Equation (5) is for a comparison using the readings with the yellow filter. The "yellow" readings were used because the extinction coefficient in the yellow region was effectively independent of color, whereas with the blue filter the extinction was different for a red star and a blue star. (The difference in the slopes of the lines in eqs. [1] and [2] arose from this difference in extinction in the blue region.) This was probably a combination of two effects: (1) the interval of wave length which contributed to the readings with the blue filter was greater than for the reading with the yellow filter; (2) the extinction coefficient changes more rapidly with wave length in the blue region than in the yellow. It was found that an

ultraviolet screen used with the blue filter, while reducing the wave-length interval, cut the intensity of the transmitted radiation too much.

Thus, essentially, a sequence of photovisual magnitudes and colors was determined. The photographic magnitudes were derived from these data. One reason for giving this preference to the photovisual magnitudes has been mentioned above. Another was that the proper motions were measured from plates taken with a yellow filter and the limiting magnitude for the proper motions (approximately 15.0) was essentially on the photovisual scale. In the photometry, I tried to include all the stars whose proper motion had been measured. This happened to give a suitable limiting magnitude for the photoelectric work; although fainter stars would have given sufficiently large deflections, it was becoming difficult to see them in the guiding eyepiece of the photometer, and they would have required off-set guiding.

III

The direct photographs for the photometry were taken at the Cassegrain focus of the 82-inch telescope at the McDonald Observatory. Table 3 gives a list of the plates measured and details of the exposures. A yellow filter was used with the 103*a*-C plates. The

TABLE 3

LIST OF PLATES USED IN PHOTOGRAPHIC PHOTOMETRY

Serial No. CC	Date and Time at Mid-exposure		Exposure (Min.)	Emulsion
	September 1950	U.T.		
202	25	$4^h 59^m$	6	103*a*-C
210	26	5 05	4	103*a*-C
212	26	5 37	2	103*a*-C
213	26	5 40	2	103*a*-C
221	28	5 08	6	103*a*-C
222	28	5 15	2	103*a*-C
192	19	5 08	1	103*a*-O
200	25	4 14	1	103*a*-O
204	26	3 05	6	103*a*-O
205	26	3 32	4	103*a*-O
206	26	3 39	1½	103*a*-O
216	27	5 36	4	103*a*-O

plates were measured in a Schilt-type photometer, designed by F. E. Ross and described by him.[7] For the most part, the measurement and reduction followed the procedure recommended by Ross. However, it was thought advisable to take two readings on each star, as a check on the centering, and two or more readings on the background. Measurements were made over a range of about 2 mag. on each plate; in particular, the very faintest stars on each plate were left out. More precisely, if

$$Q = \frac{\text{Galvanometer deflection with star centered in beam}}{\text{Galvanometer deflection for plate background}},$$

then the upper limit in the reduction was $Q = 0.85$. On some plates the limit was lower, since it depended on the readings for the calibration stars.

[7] *Ap. J.*, **84**, 241, 1936.

In his description Ross considered the possibility of magnitude errors due to irregularities in the background density on the plate and concluded that using the ratio Q as a measure of the magnitude gave consistent results over a wide range in background density. In the present investigation the results from the "yellow" plates were consistent, but there were discrepancies in the results for "blue" plates with different exposure times, and these discrepancies were attributed to variations in the background density. If we take readings on a number of stars which are within the working range on two plates, we should expect to have a functional relation of some kind between the two sets of readings (since each set is a function of magnitude). Hence, if we plot Q_1, the reading on one plate, against Q_2, the reading for the same star on the other plate, the points should lie along a curve. When blue plates with 1-minute and with 4-minute exposures were compared in this way, a curve relating Q_1 to Q_2 could be drawn for the calibration stars, but stars toward the center of the cluster deviated from this curve. The deviations were such that a star near the center of the cluster appeared to be fainter on the long-exposure plate than on the short-exposure plate, and the amount of the deviation increased on approaching closer to the center of the cluster. On examining the plates, it was evident that the background density increased toward the center of the cluster to a much greater extent on the long-exposure plates than on the short-exposure plates. This would lead to a discrepancy of the type found. For, suppose we consider two stars of equal brightness but at different distances from the center of the cluster. Then on the short-exposure plate, where the change in the background density is small, the two stars will give the same Q ratio. On the long-exposure plate, adding the light-intensity of the outer star to a small background intensity will give a greater increase in the plate density than will be obtained when the same intensity is added to a background which is already sufficiently intense to give an appreciable blackening of the plate.[8] Hence the star farther from the center will appear brighter than the other.

From this reasoning, the magnitudes on the short-exposure plates were adopted as they stood, while the readings from the blue plates with 4- and 6-minute exposures were given a correction, depending on the distance from the center of the cluster. The correction was determined as follows: The readings for the calibration stars on a short-exposure plate, Q_s, were plotted against the readings on a long-exposure plate, Q_l. Since these stars are outside the region where the background density is high, the Q_l readings can be taken as unaffected by background variations. From the plotted points, a curve of Q_l against Q_s was drawn. For any other star this curve was used to give Q_l', the value corresponding to its observed Q_s. Let Q_l denote the reading for the star on the long-exposure plate and let

$$\Delta Q = Q_l' - Q_l .$$

Then ΔQ was plotted against r, the distance of the star from the center of the cluster. A curve $\Delta Q(r)$ against r was drawn through the points plotted in this way, and $\Delta Q(r)$ was used as the correction required to reduce the observed Q_l to the magnitude system of the short-exposure plate. (In practice, grouped means were used, and a curve was drawn through them by eye.) For one plate, the stars were divided into groups according to magnitude, but there was no obvious dependence of $\Delta Q(r)$ on magnitude. The need for a correction disappeared at about 5′ from the center of the cluster; at 50″ from the center it was equivalent to 0.1 mag., and at smaller distances from the center it increased so rapidly that it seemed advisable to discard the observations or give them very low weight.

From an intercomparison of the magnitudes obtained from different plates, the mean-square error of a determination from a single plate was 0.03 mag. Thus for the mean of three plates, the mean-square error is slightly less than 0.02 mag. However, this is an

[8] Cf. Fig. 1 of Ross's paper (*op. cit.*) and the discussion.

internal error; it represents the accuracy of the interpolation between the magnitudes determined for the calibration stars and does not allow for any errors in the photoelectric determinations. It would be more realistic to think of the mean-square error for a determination from a single plate as approximately 0.04 mag. and the mean-square error of the values in the list of cluster stars (Table 5) as 0.03 mag. This would give a mean-square error in the colors of 0.04 mag. The real danger is, of course, of systematic errors in the magnitude systems; the discussion above indicates that the accidental errors are unimportant. Possible sources of systematic errors are considered later (Sec. IX), but the available evidence is that the magnitude scales are trustworthy.

IV

The plates used for the proper-motion determinations were taken with the 40-inch refractor at the Yerkes Observatory. Table 4 lists these plates. Overlapping of images in the central portion of the cluster was avoided by making only one exposure per plate. Two of the first-epoch plates were taken by G. W. Ritchey (Pls. F.Ry 8 and 11); the

TABLE 4

PLATES USED IN PROPER-MOTION DETERMINATIONS
(Plate Scale: 10".655 per Mm)

PAIR	PLATE NO.	EPOCH	EXPOSURE (MIN.)	SIZE (INCHES)	INTERVAL (YEARS)	REFERENCE STARS	
						No.	$\bar{m}_{pv}$
1.....	F.Ry 8	1900.680	120	5×4	48.059	19	14.2
	F 722a	1948.739	20	10×8			
2.....	F.Ry 11	1900.713	200	5×4	48.117	21	14.5
	F 733	1948.830	30	10×8			
3.....	F 55	1908.516	120	10×8	40.352	22	13.6
	F 748	1948.868	15	10×8			
4.....	F 197	1913.587	120	10×8	35.265	22	13.6
	F 740	1948.852	20	10×8			

other two, by E. E. Barnard. The second-epoch plates were taken by the author, on Eastman 103*a*–C plates. The quality of the images was improved by reducing the aperture from 40 to 24 inches. Both sets of plates were taken through a yellow filter; accordingly, the appearance of the images corresponds to photovisual brightness. Because of the number of stars near the center of the cluster, the differential method of measuring proper motions could not be used; instead, the positions of the stars were measured on each plate separately. (The second-epoch plates were taken direct instead of through the glass.)

The measurements were made on a Gaertner measuring machine at the Yerkes Observatory. Each plate was oriented from positions given in Küstner's catalogue[3] so that the co-ordinates measured corresponded to right ascension and declination for the epoch 1900. As the machine is a single-screw machine, each co-ordinate had to be measured independently. Two readings were made for each co-ordinate, with the plate rotated through 180° between the readings. The difference between the co-ordinates of a star on

corresponding plates had still to be corrected for the usual errors of centering, orientation, etc.[9] This was done by means of linear correction formulae:

$$T\mu_x = q\,(\Delta x + ax + by + c)\,,$$

$$T\mu_y = q\,(\Delta y + dx + ey + f)\,,$$

where the notation used follows that of Smart,[9] i.e., where x and y denote the co-ordinates of the star; Δx and Δy denote the difference in the co-ordinates on corresponding plates; T is the interval between the plates; μ_x and μ_y are the proper motions in the x- and y-directions; q denotes a constant to adjust the units; and a, b, c, d, e, and f are the plate constants for the pair of plates under discussion. If T is in years, μ_x and μ_y in seconds of arc per annum, and x, y, Δx, and Δy in millimeters, then q is the plate scale in seconds of arc per millimeter. The constants a, b, c, d, e, and f were evaluated for each pair of plates from reference stars which, from their position or proper motion (from a preliminary reduction), appeared to be field stars. Table 4 gives the number of reference stars and their mean apparent magnitude for each pair of plates. Denote the annual proper motions thus obtained by μ_x' and μ_y'; these are, of course, proper motions relative to the mean motion of the reference stars. These relative motions would be sufficient for the purpose of this investigation in sorting out field stars from cluster members; but, for comparison with other observations, it is desirable to allow for the parallactic motion of the reference stars and so convert from relative to absolute motions.

For this purpose, Binnendijk's mean parallaxes were used.[10] The galactic latitude of M 15 is $-28°$. Interpolating for this latitude from Table 10 of Binnendijk's paper, we obtain

$$\log \bar{p}_m = -2.562 - 0.115\,(m_{pg} - 12)\,, \tag{6}$$

where $\bar{p}_m$ is the mean parallax for stars of photographic magnitude m_{pg} at galactic latitude 28°. The mean proper motion of the reference stars is given by

$$\mu_x'' = P\bar{p}_m \frac{V_0}{\kappa}\,, \tag{7}$$

$$\mu_y'' = P'\bar{p}_m \frac{V_0}{\kappa}\,, \tag{8}$$

in seconds of arc per annum, where μ_x'' is the mean proper motion in the x-direction (R.A.), μ_y'' is the mean proper motion in the y-direction (Dec.), V_0 is the amount of the solar motion relative to the reference stars, in km/sec, $\kappa = 4.74$ (km/sec), and P and P' are coefficients tabulated by van Rhijn and Bok[11] (they depend on the position of the star relative to the solar apex). Equations (7) and (8) make no allowance for galactic-rotation effects; since the mean motion of the cluster is of interest in a determination of the galactic rotation for the system of globular clusters, systematic corrections will not be introduced at this stage. For M 15, $P = 0.68$, $P' = -0.393$, and V_0 was taken to be 19.5 km/sec. For the pair of plates with the faintest reference stars (pair 2 of Table 4), $m_{pg} = 15.2$ for the reference stars, and this gives $\bar{p}_m = 0''.00118$. If we insert these values in equations (7) and (8), we obtain

$$\mu_x'' = +0''.0033\,, \qquad \mu_y'' = -0''.0019\,.$$

[9] For a discussion of the various errors see W. M. Smart, *Spherical Astronomy* (4th ed.; Cambridge: At the University Press, 1944), p. 287.

[10] *B.A.N.*, Vol. **10**, No. 362, 1943.

[11] *Groningen Pub.*, No. 45, Tables 11 and 12, 1931.

The absolute proper motion (μ_x, μ_y) is then

$$\mu_x = \mu_x' + \mu_x'', \qquad \mu_y = \mu_y' + \mu_y''.$$

The other pairs of plates were reduced to the same reference system.

V

Some discussion of the errors of the proper motions will now be made. There was a risk of systematic errors entering at the measuring stage, owing to slight displacements of the plate in the course of a long series of measurements. To guard against this, check measurements were made on a star in each corner of the plate at intervals of 30-40 minutes. For Plate F 55 two independent series of measurements were made of the x-co-ordinates. A comparison of the two series showed occasional traces of systematic differences, but the amounts were small and the mean-square error of a single measurement came out at 3.2 μ. A similar check for F 197 gave a mean-square error of 3.0 μ. If we take the displacement of a star between the two epochs as the difference between two independent measurements, each with a mean-square error of 3.2 μ, then the mean-square error of the displacement should be $(3.2)\sqrt{2} = 4.5\ \mu$. In practice, this mean-square error came out at 7.5 μ. Probably this increase in the mean-square error arises from setting on a slightly different portion of the image on the two plates. If the image is slightly distorted, either by guiding or by proximity to another star, an additional error is liable to be introduced. In general, too, the images on the second-epoch plates were smaller than the images on the first-epoch plates, so the measuring conditions were not quite identical. Thus the errors in the determination could not be made negligible by repeating the measurements several times, since there was an appreciable contribution added when different plates were compared. Similarly, when the proper motions from different pairs of plates were compared, there was evidence of occasional systematic differences in different parts of the field, and these increased the effective mean-square error of the determinations to 0".0024 p.a. for μ_x' and 0".0018 p.a. for μ_y'. (These values are for stars within the region covered by the cluster. For stars near the edge of the plates, the mean-square error increases to about 0".003 p.a.)

As regards systematic errors in the absolute proper motions, there are two bright stars in the field which provide some check. The star K 1018 = BD+11°4578 is included in the Yale catalogue[12] for the zone +10° to +15°, and its annual proper motion is given there as

$$\mu_x = -0".086 \pm 0".008 \text{ (p.e.)}, \qquad \mu_y = -0".122 \pm 0".006 \text{ (p.e.)}.$$

The value found in the present investigation is

$$\mu_x = -0".104, \qquad \mu_y = -0".138.$$

The determination from the Yerkes plates is not a good one, since the star is heavily overexposed. We estimate $\pm 0".003$ or $\pm 0".004$ as the probable error attached to the Yerkes values. Therefore, the two determinations are not significantly different.

The other star is BD+11°4571 = B 3 of Table 6. Van Maanen[13] has given a proper motion and parallax for this star; his values are

$$\mu_x = +0".202 \pm 0".009 \text{ (p.e.)}, \qquad \mu_y = -0".457 \pm 0".005 \text{ (p.e.)},$$

which correspond to a position angle of 156°. The values obtained in the present investigation are

$$\mu_x = +0".142, \qquad \mu_y = -0".456,$$

[12] *Trans. Yale Obs.*, Vol. 19, 1948.

[13] *Pub. A.S.P.*, 41, 114, 1929, and *Mt. W. Contr.*, No. 391, 1929.

which give a position angle of 163°. Luyten and Ebbighausen[14] found a position angle of 164° from a comparison of plates taken with the 24-inch reflector at Yerkes. Thus the Yerkes measures are in agreement, but they differ appreciably from van Maanen's determination. Van Maanen's time interval may have been too short; his value of μ_x was obtained while determining the parallax, and it is unlikely that the series of plates extended over more than ten years.

The checks provided by these brighter stars are inconclusive. A better check can be obtained from the mean motion of the cluster given by Gamaley,[15] who has derived the mean motion of a number of globular clusters from plates taken with the 13-inch astrographic telescope at Poulkovo. For M 15, he gives

$$\mu'_x = -0''.0037\,, \qquad \mu'_y = +0''.0015\,,$$

relative to reference stars of magnitude 14–14.5 (pg). In converting to absolute motions he uses secular parallaxes derived by Deutsch,[16] which are slightly larger than Binnendijk's. Hence, to compare his results with the present investigation, we must start from the relative motions and convert to absolute motions, as in Section IV. For $m_{pg} = 14.2$, equation (6) gives

$$\overline{\left(\frac{h}{\rho}\right)} = \frac{V_0}{\kappa}\,\bar{p}_m = 0''.0063\,,$$

and

$$\mu_x = -0''.0037 + 0''.0043 = +0''.0006$$

$$\mu_y = +0''.0015 - 0''.0025 = -0''.0010\,.$$

If we take $\overline{(h/\rho)} = 0''.0080$, which is the value Gamaley uses, then

$$\mu_x = -0''.0037 + 0''.0054 = +0''.0017\,,$$

$$\mu_y = +0''.0015 - 0''.0031 = -0''.0016\,.$$

The present investigation gives

$$\mu_x = +0''.0038\,, \qquad \mu_y = -0''.0015\,.$$

In general, Deutsch's mean parallaxes should be more reliable than Binnendijk's, since the proper motions from which they were derived had a longer time base. However, in the region around M 15, the mean parallaxes of the reference stars are likely to be smaller than the average for their galactic latitude, since the region seems to be practically clear of obscuration. So in this instance Binnendijk's values are probably more appropriate.

As regards the merits of the two determinations of the relative motion of the cluster, there is not much to choose between them. The Poulkovo determinations may have a slight advantage, in that the reference stars are distributed over a larger area and therefore the orientation of the co-ordinate axes will be determined more accurately. For separating cluster stars from field stars, the Yerkes plates will be superior, since the plate scale is six times larger, but they cover rather a small field for a determination of the mean motion of the cluster relative to a fundamental system. The precision of the latter determination depends mainly on the precision with which the mean motion of the reference stars is known. In this respect the very small probable errors quoted by Gamaley

[14] *A.J.*, **45**, 188, 1936. I am indebted to Dr. G. P. Kuiper for drawing my attention to this paper.

[15] *Bull. Obs. Poulkovo*, **17**, No. 6, 27, 1948.

[16] *Poulkovo Bull.*, Vol. **17**, No. 3, 1947.

may be misleading. They apply to the mean motion of the cluster *relative to the reference stars;* by using twenty to twenty-five members of the cluster to determine this relative motion, the error attached to it can be made negligibly small. Despite this, the error attached to the absolute motion remains of the order of 0".001 per annum, for the mean motion of the reference stars is subject to errors of this order. For example, for the pair of plates F.Ry 11 and F 733 (Table 4), the peculiar motions of the reference stars have a standard deviation of 0".004 per annum in either co-ordinate. Using twenty reference stars gives a standard deviation of approximately 0".001 in either co-ordinate for the mean motion of the reference stars. If we assume an error of equal amount attached to the determination of the mean motion of the Poulkovo reference stars, then the two determinations of $\bar{\mu}_x$ and $\bar{\mu}_y$ are in satisfactory agreement.

An estimate of the errors attached to $\bar{\mu}_x$ and $\bar{\mu}_y$ is obviously required when comparing different determinations of $\bar{\mu}_x$ and $\bar{\mu}_y$. These errors will also be of importance if values of $\bar{\mu}_x$ and $\bar{\mu}_y$ for different clusters are used in determining the motion of the system of globular clusters relative to the Milky Way system, e.g., for M 15, a change in $\bar{\mu}_x$ from 0".001 p.a. to 0".004 p.a. corresponds to a change in linear speed from 60 to 240 km/sec. Clearly, the uncertainties in the determination of $\bar{\mu}_x$ and $\bar{\mu}_y$ will have a strong influence on the precision of the solution for the motion of the globular clusters.

VI

The determination of μ_x and μ_y allowed a preliminary sorting of the stars into cluster stars and field stars, and a more precise criterion was obtained as follows: First of all, the mean motion of the cluster was evaluated from fifty-four of the cluster stars which had well-determined proper motions. This gave

$$\bar{\mu}_x = +0''.0038\,, \qquad \bar{\mu}_y = -0''.0015$$

as the mean motion of the cluster. The dispersion in each component was also computed; this gave

$$\sigma_x = 0''.0015\,, \qquad \sigma_y = 0''.001$$

as the standard deviation of the distribution of μ_x and μ_y respectively. Limiting values of μ_x and μ_y for inclusion as cluster members were taken at

$$\bar{\mu}_x \pm 2.5\sigma_x \quad \text{and} \quad \bar{\mu}_y \pm 2.5\sigma_y\,,$$

i.e., for a star to be classified as a member of the cluster, its proper motion had to satisfy the criterion

$$\begin{aligned} +0''.0001 \leq \mu_x \leq +0''.0075\,, \\ -0''.0012 \leq \mu_y \leq +0''.0042\,. \end{aligned} \tag{9}$$

In drawing up a list of cluster members, one additional criterion was used, namely, that the star should lie within 5′ of the center of the cluster. Outside this region the ratio of field stars to cluster stars began to increase rapidly; hence all stars outside this zone were omitted in order to keep the color-magnitude diagram as free from field stars as possible. This left more than one hundred and fifty stars available for the diagram, a number which seemed sufficient to show the main characteristics of the population.

Table 5 was drawn up on the basis of these two criteria—proper motion and position—and without reference to the brightness or color of the star. Figure 2 shows a plot of photovisual magnitude against color for the stars in Table 5. Two subsidiary tables were compiled to complete the presentation of the results. Table 6 gives a list of field stars, and Table 7 gives a list of intermediate cases in which there is some doubt to which category the star should be assigned. In Table 6 the stars included in Küstner's catalogue are given first, with the magnitudes and proper motions found in the present investigation. The second part of the table gives the positions, magnitudes, and proper motions of some

TABLE 5

LIST OF CLUSTER MEMBERS

(Criteria: Proper Motion and Distance from Center)

STAR K	MAGNITUDE		COLOR	PROPER MOTION (UNIT: 0".0001 P.A.)			NO. OF PAIRS OF PLATES
					μ_y		
	m_{pg}	m_{pv}	c'	μ_x +	+	−	
47.....	15.01	14.22	+0.79	37	.....	10	2
69.....	15.27	14.53	+0.74	65	0	.....	2
73.....	14.19	13.78	+0.41	20	.....	10	4
77.....	14.81	13.87	+0.94	30	.....	23	4
87.....	14.78	13.87	+0.91	54	.....	16	4
89.....	15.27	14.56	+0.71	33	3	.....	1
114.....	14.89	13.93	+0.96	62	1	.....	4
129.....	15.18	14.34	+0.84	22	.....	28	2
136.....	15.59	15.01	+0.58	55	.....	15	1
141.....	15.70	15.02	+0.68	22	.....	6	1
144.....	14.32	13.06	+1.26	20	.....	18	4
146.....	14.60	13.60	+1.00	50	.....	7	4
152.....	15.92	15.28	+0.64	35	.....	21	1
158.....	14.92	14.28	+0.64	67	.....	6	2
169.....	14.63	13.54	+1.09	32	.....	11	4
179.....	15.68	15.07	+0.61	49	.....	15	1
185.....	15.28	14.57	+0.71	64	.....	23	1
193.....	15.84	15.13	+0.71	51	.....	8	1
202.....	15.81	15.19	+0.62	20	.....	28	1
205.....	15.81	15.10	+0.71	60	.....	35	1
224.....	14.51	13.44	+1.07	18	.....	28	4
238.....	14.46	13.29	+1.17	27	.....	5	4
240.....	14.12	12.81	+1.31	30	.....	23	4
254.....	14.48	13.35	+1.13	42	.....	10	4
255.....	14.80	13.85	+0.95	26	.....	16	4
260.....	14.55	14.16	+0.39	39	.....	32	4
272.....	14.56	13.52	+1.04	29	.....	2	4
280.....	15.41	14.62	+0.79	60	.....	26	1
284.....	15.54	14.85	+0.69	40	.....	17	1
286.....	15.53	14.80	+0.73	42	.....	15	1
288.....	14.68	13.75	+0.93	35	.....	8	4
290.....	14.36	13.31	+1.05	44	.....	20	4
293.....	15.59	14.74	+0.85	42	5	.....	1
296.....	15.34	14.67	+0.67	35	1	.....	1
305.....	15.52	14.93	+0.59	35	.....	12	1
306.....	15.31	14.64	+0.67	11	.....	23	1
309.....	15.60	15.01	+0.59	49	.....	41	1
319.....	14.53	13.49	+1.04	12	.....	12	4
323.....	15.30	14.63	+0.67	14	0	.....	2
328.....	14.79	13.77	+1.02	42	.....	11	4
341.....	14.19	12.83	+1.36	27	.....	25	4
343*.....	13.83	12.61	+1.22	26	.....	8	2
344.....	15.58	14.81	+0.77	35	10	.....	1
346.....	14.85	14.07	+0.78	26	.....	13	3
354.....	15.33	14.57	+0.76	35	.....	20	2
357.....	15.23	14.70	+0.53	20	.....	6	1
361.....	14.68	13.96	+0.72	36	.....	5	2
366.....	15.22	14.38	+0.84	22	.....	10	1
373†.....	14.15:§	12.90:	+1.25	33	.....	15	4
375.....	15.43	14.70	+0.73	28	2	.....	2

* Double.
† Not included in color-magnitude diagram; photometric data poor.
§ : = Observation of low weight.

TABLE 5—*Continued*

Star K	Magnitude m_{pg}	Magnitude m_{pv}	Color c'	Proper Motion (Unit: 0".0001 p.a.) μ_x +	μ_y +	μ_y −	No. of Pairs of Plates
383*.....	14.57	13.94	+0.63	41	.....	17	2
386.....	14.12	12.69	+1.43	18	.....	38	4
387.....	14.54	13.50	+1.04	21	.....	14	4
391.....	15.12	14.59	+0.53	17	1	.....	1
393.....	14.40	13.28	+1.12	45	.....	23	4
401.....	15.01	14.24	+0.77	45	.....	25	2
403.....	15.10	14.39	+0.71	34	.....	10	2
404†.....	15.53:	14.76	+0.77	37	.....	28	1
406.....	14.66	13.83	+0.83	31	.....	26	3
421*.....	13.77	12.54	+1.23	12	.....	25	4
422.....	15.18	14.41	+0.77	28	5	.....	2
427.....	14.89	14.03	+0.86	38	.....	25	4
431.....	14.26	13.06	+1.20	30	.....	24	4
435.....	14.59	13.53	+1.06	45	.....	20	4
436.....	15.07	14.36	+0.71	44	.....	28	2
442.....	14.63	13.86	+0.77	52	.....	9	2
447.....	13.85	13.09	+0.76	48	.....	12	4
449.....	15.04	14.38	+0.66	43	7	.....	2
450.....	14.76	13.80	+0.96	33	4	.....	4
458†.....	14.95:	14.65	+0.30	13	.....	6	1
459†.....	14.55:	14.14	+0.41	49	.....	23	3
462.....	14.13	12.77	+1.36	44	.....	4	4
476.....	15.39	14.70	+0.69	35	.....	19	1
479*†....	13.76:	12.43	+1.33	36	.....	29	3
481.....	14.78	13.91	+0.87	66	4	.....	2
482.....	15.11	14.49	+0.62	37	.....	19	1
487†.....	14.81:	14.06	+0.75	30	.....	7	1
488.....	14.43	13.48	+0.95	42	.....	10	4
490.....	13.78	12.71	+1.07	56	.....	14	4
497.....	14.42	13.13	+1.29	45	.....	2	4
501†.....	15.63:	14.88:	+0.75	49	.....	19	1
506.....	15.51	14.80	+0.71	20	10	.....	1
508.....	14.64	13.74	+0.90	44	.....	24	4
511.....	14.25	13.08	+1.17	36	.....	21	4
514.....	14.52	14.48	+0.04	62	.....	23	1
519†.....	14.58	13.81:	+0.77	11	.....	1	3
531.....	14.07	12.89	+1.18	17	.....	13	4
532†.....	15.22:	14.68	+0.54	24	.....	1	1
534*.....	13.99	13.08	+0.91	62	.....	7	1
535†.....	15.43:	14.64	+0.79	17	.....	8	1
559.....	14.19	14.98	−0.79	24	.....	21	1
565†.....	14.86:	14.11:	+0.75	6	6	.....	1
566†.....	14.62:	13.88	+0.74	38	.....	18	4
567.....	14.16	13.15	+1.01	25	.....	15	4
569.....	14.91	13.99	+0.92	66	.....	16	2
572.....	14.70	13.82	+0.88	29	.....	9	4
578.....	14.77	14.03	+0.74	22	.....	3	1
583.....	14.19	12.74	+1.45	37	.....	2	4
584.....	14.97	14.27	+0.70	50	.....	5	2
585.....	15.12	14.54	+0.58	41	.....	15	2

TABLE 5—*Continued*

Star K	Magnitude m_{pg}	Magnitude m_{pv}	Color c'	Proper Motion (Unit: 0".0001 p.a.) μ_x +	μ_y +	μ_y −	No. of Pairs of Plates
589.....	14.56	13.52	+1.04	56	.....	12	4
591.....	15.32	14.63	+0.69	13	.....	17	1
592.....	14.94	14.11	+0.83	60	.....	41	3
596.....	14.98	14.24	+0.74	45	.....	12	2
601.....	14.07	13.03	+1.04	19	.....	23	4
607.....	15.04	14.24	+0.80	62	.....	5	2
618†.....	14.45:	13.57:	+0.88	57	.....	36	2
619.....	15.04	14.47	+0.57	26	.....	15	2
625†.....	14.93:	14.55:	+0.38	35	.....	28	1
631.....	15.43	14.79	+0.64	22	.....	23	1
634*.....	13.95	12.86	+1.09	46	.....	7	4
635†.....	.....	13.76:	.....	26	.....	1	2
638.....	15.31	14.79	+0.52	33	.....	15	1
647.....	14.58	13.61	+0.97	48	.....	17	4
648.....	13.39:	14.06:	−0.67	35	.....	39	1
669.....	15.24	14.61	+0.63	46	.....	12	1
670.....	14.20	13.02	+1.18	32	.....	23	4
672.....	14.71	13.90	+0.81	72	.....	17	4
673.....	14.07	13.03	+1.04	57	.....	5	4
677.....	15.61	15.06	+0.55	29	.....	12	1
684.....	14.94	14.29	+0.65	31	.....	17	1
691.....	15.53	14.83	+0.70	42	.....	12	1
694†.....	.....	14.72	.....	44	.....	1	1
702.....	14.15	12.89	+1.26	38	.....	30	4
706.....	14.23	12.90	+1.33	32	.....	27	4
709.....	14.66	13.68	+0.98	64	.....	24	4
731.....	15.18	14.35	+0.83	30	.....	19	2
733†.....	14.24:	13.21	+1.03	42	.....	23	3
734†.....	14.35:	13.24	+1.11	50	.....	29	3
736.....	14.76	13.98	+0.78	32	4	.....	4
739†.....	15.46:	14.72	+0.74	20	12	.....	1
749.....	14.49	13.53	+0.96	60	.....	20	4
753.....	15.46	14.68	+0.78	51	.....	1	1
757.....	14.25	12.76	+1.49	32	.....	32	4
764.....	14.81	13.81	+1.00	62	.....	14	4
768.....	.....	.....	.....	49	1	.....	1
775.....	15.41	14.84	+0.57	64	12	.....	1
797.....	15.54	14.81	+0.73	26	.....	21	1
803†.....	15.00:	14.43	+0.57	53	.....	3	1
806.....	15.36	14.55	+0.81	24	.....	12	1
809.....	15.24	14.71	+0.53	24	.....	19	1
810.....	15.28	14.51	+0.77	42	.....	35	2
812.....	15.43	14.94	+0.49	46	.....	30	1
825.....	14.09	12.65	+1.44	31	.....	32	4
848.....	15.28	14.53	+0.75	13	.....	3	1
851.....	15.27	14.80	+0.47	20	.....	15	1
853.....	14.13	12.80	+1.33	56	.....	26	4
863.....	14.68	13.93	+0.75	35	.....	35	2
865.....	15.42	14.84	+0.58	17	.....	6	1
866.....	15.47	14.77	+0.70	4	.....	30	1

TABLE 5—*Continued*

Star K	Magnitude m_{pg}	Magnitude m_{pv}	Color c'	Proper Motion (Unit: 0".0001 p.a.) μ_x +	μ_y +	μ_y −	No. of Pairs of Plates
884.....	14.85	14.12	+0.73	29	.....	27	2
902.....	15.62	14.86	+0.76	51	.....	12	1
918.....	15.01	14.13	+0.88	21	.....	41	2
919.....	14.65	13.64	+1.01	37	2	.....	4
925.....	15.42	14.67	+0.75	43	.....	16	2
926.....	15.70	15.23	+0.47	57	.....	6	1
928.....	14.84	13.92	+0.92	22	.....	35	4
930†.....	15.07:	14.08	+0.99	33	.....	8	1
932.....	14.98	14.15	+0.83	7	.....	8	2
934.....	15.27	14.50	+0.77	37	.....	35	1
936.....	15.07	14.28	+0.79	3	.....	8	2
943.....	15.08	14.36	+0.72	2	.....	12	2
947.....	15.15	14.34	+0.81	32	.....	13	2
954.....	15.16	14.37	+0.79	44	.....	3	2
956.....	15.39	14.59	+0.80	24	.....	3	1
961.....	15.06	14.17	+0.89	43	.....	5	3
969.....	14.52	13.50	+1.02	62	.....	24	4
979.....	14.93	14.32	+0.61	32	5	.....	2
990.....	14.84	13.86	+0.98	34	.....	5	2
993.....	14.94	14.06	+0.88	33	.....	7	4
996.....	14.16	14.54	−0.38	17	.....	12	2
1006.....	15.09	14.22	+0.87	9	.....	12	2
1010.....	15.69	15.00	+0.69	42	.....	12	1
1014.....	15.51	14.76	+0.75	73	.....	33	1
1029.....	14.62	13.56	+1.06	15	.....	31	4
1033.....	15.30	14.46	+0.84	20	.....	5	2
1040.....	14.56	13.44	+1.12	44	0	.....	4
1043.....	15.85	15.11	+0.74	33	.....	12	1
1054.....	15.09	14.26	+0.83	59	.....	32	3
1056.....	15.53	14.79	+0.74	29	.....	17	1
1069.....	15.39	14.64	+0.75	60	.....	10	1
1073.....	15.08	14.22	+0.86	28	.....	4	2
1079.....	15.01	14.18	+0.83	49	.....	8	3
1082.....	15.05	15.10	−0.05	2	.....	35	1

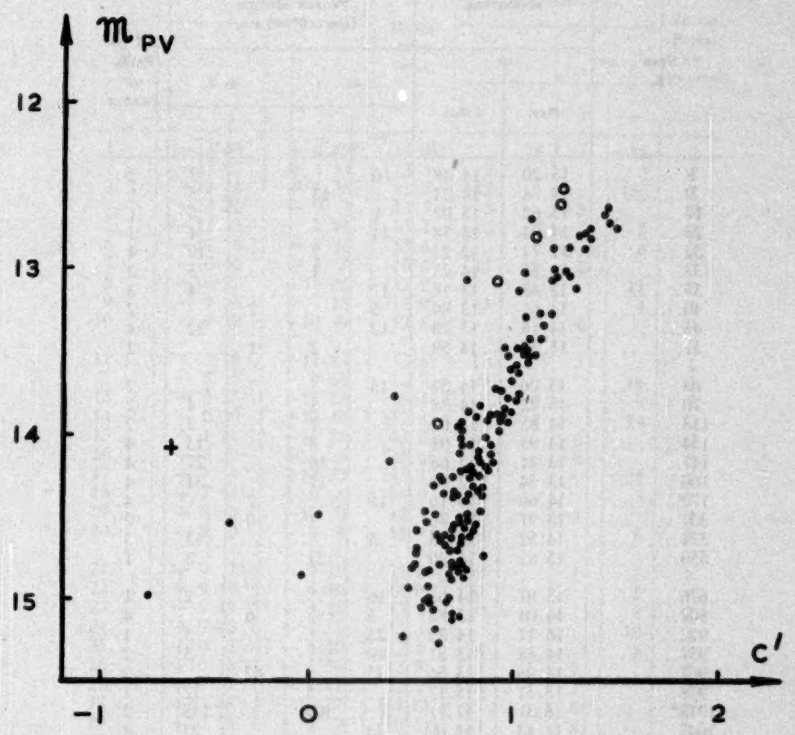

FIG. 2.—Color-magnitude diagram for cluster stars. (Apparent magnitude m_{pv} plotted against color index c').

TABLE 6

LIST OF FIELD STARS

a) KÜSTNER STARS

STAR K	MAGNITUDE		PROPER MOTION (UNIT: 0".001 P.A.)				NO. OF PAIRS OF PLATES
			μ_x		μ_y		
	m_{pg}	m_{pv}	+	−	+	−	
8	15.20	14.48	10	.....	.....	2	2
9	14.78	14.23	.....	13	.....	5	1
17	15.62	15.02	1	.....	.....	5	1
23	14.04	13.58	14	.....	.....	4	3
32	12.77	12.23	.....	7	.....	19	4
33	14.55	14.23	.....	1	.....	5	2
35	13.48:	13.16	17	.....	.....	4	3
40	14.61	13.89	5	.....	2	.....	2
45	14.15	13.70	12	.....	.....	22	4
57	15.35	14.59	.....	2	1	.....	2
63	15.06	14.52	13	.....	7	.....	2
70	15.22	14.38	.....	1	.....	4	2
113	14.85	14.61	.....	7	.....	2	2
134	14.95	14.08	.....	8	.....	13	4
147	13.21:	12.66	.....	10	.....	27	4
160	13.54	12.91	.....	17	.....	31	4
172	14.60	14.16	15	.....	7	.....	4
307	13.97	13.76	.....	1	0	.....	2
371	14.52	14.35	5	.....	.....	13	3
550	15.82	15.20	.....	21	.....	3	1
676	15.07	14.65	16	.....	.....	2	1
802	14.04	13.82	3	.....	6	.....	4
922	16.17	14.82	23	.....	.....	3	1
957	14.88	13.81	10	.....	.....	3	2
967	14.95	13.56	25	.....	62	.....	2
978	15.51	15.17	.....	5	.....	12	1
1018*	(8.3)	(7.7)	.....	104	.....	138	2
1047	14.43	14.00	23	.....	.....	23	4
1089	13.93	13.34	.....	37	.....	66	2
1095	.....	12.58	13	.....	.....	4	2
1096	14.45	14.13	0	.....	.....	7	2
1115	13.98	13.48	4	.....	3	.....	2
1118	10.81	10.43	19	.....	9	.....	2
1130	13.77	13.14	.....	7	.....	27	2
1134	13.97	14.14	9	.....	2	.....	2

* HD 204712 = BD+11°4578. The magnitudes for this star have been taken from the *Henry Draper Catalogue*.

TABLE 6—*Continued*

b) ADDITIONAL STARS

Star B	Position X	Position Y	Magnitude m_{pv}	Proper Motion (Unit: 0".001 p.a.) μ_x +	μ_x −	μ_y +	μ_y −	No. of Pairs of Plates
1	−13′ 46″	+ 6′ 49″	(14.0)*	.....	18	.....	18	2
2	−13 12	+ 4 53	13.3	2	.....	.....	5	2
3	−12 44	+ 1 36	11.2	142	.....	.....	456	2
4	−12 26	+ 9 7	13.5:	2	.....	5	.....	2
5	−12 13	− 0 44	13.4	.....	3	.....	3	2
6	−11 16	+ 0 54	13.4	.....	7	.....	6	2
7	−10 56	+ 4 3	10.6	36	.....	2	.....	2
8	−10 12	+12 34	(13.2)	.....	17	.....	11	2
9	− 9 44	+ 9 13	(13.9)	3	.....	.....	4	1
10	− 9 20	+10 29	12.8:	.....	12	4	.....	2
11	− 5 18	+11 43	(13.6)	17	.....	3	.....	1
12	− 5 5	− 9 44	12.7	9	.....	.....	10	2
13	− 3 25	−11 23	13.1:	.....	4	.....	9	2
14	− 0 20	+12 19	(12.8)	.....	2	.....	14	2
15	+ 1 41	−11 23	13.3:	10	.....	6	.....	2
16	+ 6 51	+12 3	(13.6)	19	.....	0	.....	2
17	+ 7 4	+12 30	(13.3)	19	.....	.....	25	2
18	+ 7 41	+10 8	13.9	6	.....	.....	5	1
19	+ 8 48	−11 0	12.4	35	.....	4	.....	2
20	+ 9 0	− 3 9	13.7	4	.....	.....	6	2
21	+ 9 7	− 9 29	13.6	13	.....	7	.....	2
22	+ 9 10	− 4 46	14.0	11	.....	.....	5	1
23	+ 9 19	+ 3 25	13.2	10	.....	.....	8	2
24	+ 9 42	+ 7 5	13.3	.....	7	.....	10	2
25	+10 3	− 4 40	12.4	14	.....	.....	5	2
26	+10 16	− 5 54	13.5:	15	.....	2	.....	2
27	+10 32	− 2 41	12.1	13	.....	2	.....	2
28	+10 48	−10 27	(11.6)	27	.....	6	.....	2
29	+10 58	+10 9	(10.4)	31	.....	8	.....	2
30	+11 11	+ 1 19	13.7	13	.....	.....	2	2
31	+13 10	−11 9	(13.1)	0	.....	.....	34	2
32	+14 44	− 8 53	12.3:	22	.....	.....	4	1
33	+14 48	− 7 46	11.9:	.....	3	.....	23	1

* Magnitudes in parentheses are visual estimates.

additional stars which were outside the area covered by Küstner's catalogue. The positions have been expressed in the same system of co-ordinates as in Küstner's lists. Only photovisual magnitudes are given, and these have been rounded off to 0.1 mag., since the values are less accurate than those in Table 5. In some instances visual estimates are given, where the star was too bright for the photometric work or too far from the center of the cluster to be measured on the McDonald plates.

TABLE 7

LIST OF STARS WHICH MAY BE MEMBERS OF CLUSTER

	Star* K	Magnitude		Color c'	Proper Motion (Unit: 0".001 p.a.)		No. of Pairs of Plates
		m_{pg}	m_{pv}		μ_x	μ_y	
a)	235.....	15.06	14.51	+0.55	+7	−1	2
	277†.....	15.06	14.38	+0.68	+2	0	1
	428.....	15.45	14.72	+0.73	+3	−3	1
	474.....	14.33	13.80	+0.53	+6	−1	1
	475.....	15.29:‡	14.63	+0.66	+5	−2	1
	539.....	14.08:	13.11:	+0.97	+4	−4	2
	570.....	14.24:	12.77:	+1.47	+4	−2	2
	661.....	14.86:	14.19:	+0.67	+6	0	1
	681.....	15.52:	14.68	+0.84	+5	−2	1
	693.....	15.64:	15.02:	+0.62	+4	−4	1
	718.....	14.87	14.74	+0.13	+6	+1	1
	735.....	14.91:	14.05	+0.86	+3	−4	1
	912.....	15.18	14.49	+0.69	+7	+1	1
b)	66.....	15.17	14.43	+0.74	0	0	2
	95.....	15.57	14.88	+0.69	+4	+3	1
	151.....	15.80	15.13	+0.67	+5	+2	1
	154.....	15.60	14.86	+0.74	+5	+1	1
	470.....	15.05:	14.41	+0.64	+8	−2	2
	560.....	15.29	14.57	+0.72	+8	+1	2
	582.....	15.08	14.58	+0.50	+8	0	2
	642.....	14.65:	13.96	+0.69	+3	−5	1
	701.....	14.92	14.44	+0.48	+2	−4	1
	846.....	14.95	14.06	+0.89	+8	0	2
	875.....	14.95	14.17	+0.78	−1	−3	2
	879.....	15.15	14.24	+0.91	+8	0	2
	994.....	14.82	13.94	+0.88	+8	0	4
	1030.....	15.07	14.17	+0.90	−1	−1	2
c)	7.....	13.58	12.92	+0.66	+4	−2	4
	21.....	15.62	15.08	+0.54	+1	0	1
	22.....	15.24	14.50	+0.74	+6	0	1
	27.....	15.71	15.18	+0.53	+5	−2	1
	28.....	14.66	13.78	+0.88	+1	−4	3
	29.....	15.06	14.25	+0.81	+1	−4	2
	49.....	15.27	14.81	+0.46	+2	−4	1
	553.....	15.66	14.95	+0.71	+4	−3	1
	813.....	15.57	15.05	+0.52	+6	−4	1
	1084.....	15.30	14.45	+0.85	0	−3	2
	1137.....	13.99	13.26	+0.73	+6	−2	2

* Group (*a*), Proper motion within permissible limits but determination below normal weight. Position: $r \leq 5'$. Group (*b*), Proper motion just outside limit. Position: $r \leq 5'$. Group (*c*), Proper motion within limits or just outside them. Position: outside circle of radius $r = 5'$.

† Double.

‡ : = Observation of low weight.

Table 7 has been subdivided into three groups: (*a*) stars which lie within 5′ of the center of the cluster and whose proper motion satisfies criterion (9) but is not as well determined as usual; (*b*) stars which satisfy the criterion as to position but whose proper motion is slightly outside the permissible limits; and (*c*) stars whose proper motion is within the permissible limits or just outside them but which lie more than 5′ from the center of the cluster.

VII

It is quite likely that a number of the stars in Table 7 are actually cluster members, since the criteria used to test for inclusion in Table 5 tend to err on the safe side. The proper-motion criterion was derived from stars which could be measured on all four pairs of plates. Where the proper motions are determined from fewer plates, the values will have a greater scatter and the criterion can be expected to reject some stars which are actually members of the cluster. However, there were enough stars available to justify this risk. Similarly, the limitation to a circle of radius 5′ is liable to reject a few members of the cluster. For example, there are cluster-type variables outside this circle whose magnitude and period indicate that they are members of the cluster. On the other hand, from counts of stars down to the fifteenth magnitude, the star density does not begin

TABLE 8

COUNTS OF STARS IN SUCCESSIVE RINGS
(Limiting Magnitude = 15.2 Approximately)

Sector	1	2	3	4	5	6	7	8	9	10	11	12	Total	Relative Areas
Zone														
$3\frac{1}{3}' < r \leq 5'$	6	5	4	4	1	1	3	4	3	2	1	2	36	5
$5' < r \leq 6\frac{2}{3}'$	2	1	3	1	0	2	3	1	2	5	3	2	25	7
$6\frac{2}{3}' < r \leq 8\frac{1}{3}'$	2	3	0	5	0	3	5	5	3	0	3	3	32	9
$8\frac{1}{3}' < r \leq 10'$	1	5	2	2	3	3	1	1	2	4	2	2	28	11

to increase markedly until the counts come inside this circle. Table 8 gives the results of counts on one of the McDonald plates (CC 201). Sector 1 corresponds to position angles between 0° and 30°, sector 2 to position angles between 30° and 60°, and so on. A similar effect can be seen on considering the number of stars rejected by the proper-motion criterion in different zones. For the stars measured in pairs 3 and 4 (Table 4)—roughly, stars down to $m_{pv} = 14$—the proper-motion criterion rejected 36 out of 38 stars, for which $r > 8\frac{1}{3}'$, 15 out of 17 stars,[17] for which $5' < r \leq 8\frac{1}{3}'$, and 6 stars for which $r \leq 5'$. For the fainter stars between $m_{pv} = 14$ and $m_{pv} = 15$, 6 out of 13 stars in the zone $5' < r \leq 8\frac{1}{3}'$ had proper motions within the acceptable limits. However, the evidence from the brighter stars suggested that it would be more prudent to omit all the stars more than 5′ from the center of the cluster, since there was a high proportion of field stars beyond this limit.

It is reasonable to find a greater fraction of the stars having proper motions within the acceptance limits as we proceed to fainter magnitudes, even in a region of the plate where we know there is an appreciable proportion of field stars. The proper-motion criterion becomes less sensitive as we go to fainter stars, and, unless more accurate proper motions could be obtained, this method of recognizing field stars would not be of much help in dealing with sixteenth- or seventeenth-magnitude stars. For field stars of magnitude 13.5 (pv), the peculiar motions have a scatter characterized by a standard deviation of approximately 0″.010 p.a. in each co-ordinate. The proper-motion criteria (9) have half-widths of 0″.0037 and 0″.0027 p.a.; hence, even if we neglect the relative motion of cluster

[17] In addition to the 15 stars rejected, there was 1 boundary case.

and field stars, only 6 per cent of the field stars would be expected to have proper motions within the acceptable limits. As we go to fainter stars, the peculiar motions become smaller, and a greater fraction of the field stars will have proper motions within the permissible limits. For $m_{pv} = 15.0$, the standard deviation of the peculiar motions of the field stars will be about 0".005 p.a., and in that case 22 per cent of the field stars can be expected to have proper motions within the permissible limits.[18] Thus the proper-motion criterion is of most value in ridding the color-magnitude diagram of the brighter field stars but is liable to admit an increasing percentage of field stars on going to fainter magnitudes. Since the half-widths of the proper-motion criteria depend on the accuracy with which the proper motions can be measured, it is the accuracy of the proper motions which determines to what magnitudes measurements should be made.

VIII

Now that we have discussed the criteria used in compiling Table 5, we can examine the corresponding color-magnitude diagram, Figure 2. In the diagram each filled circle corresponds to a cluster star, the open circles represent double stars, and the cross at the left-hand side represents a planetary nebula.[19] The main feature of the diagram is the "red-giant" sequence, which runs from $m_{pv} = 12.75$ (color index 1.4) to $m_{pv} = 13.8$ (color index 0.9) and then drops more steeply toward $m_{pv} = 15.0$ (color index 0.65). This feature was pointed out by Shapley[20] as early as 1916; Figure 2 indicates that there is an appreciable scatter in magnitude for a given color. As the cluster is moderately rich in variables and is free from obscuration, its distance modulus is well determined; it is given by Mrs. Hogg[21] as 15.63. With this value, the brightest stars in the cluster are of absolute magnitude $M_{pv} = -3$ ($M_{pg} = -1.6$) and the color-magnitude diagram goes down to $M_{pv} = -0.5$ ($M_{pg} = 0$). In their photoelectric work on the colors of globular clusters, Stebbins and Whitford[22] obtained zero color excess for M 15; and counts of nebulae in the surrounding region by Baade[23] and Mayall[24] confirm that the region is clear of obscuration. Hence the observed colors need not be corrected for reddening in associating the colors with spectral type. This would indicate that the red-giant sequence ranges from spectral type G0 to K5 or thereabouts, although it should be noted that the usual relation between color and spectral type does not take account of differences between type I and type II populations.

In addition to the red-giant sequence, there is a number of outlying stars toward the blue side of the diagram. Two of these outliers, namely, K 447 ($c' = 0.76$, $m_{pv} = 13.09$) and K 490 ($c' = 1.07$, $m_{pv} = 12.71$), may be double stars. Their images are not visibly elongated, but both lie close to the center of the cluster, in regions where the star density is high. Of the others, it is possible that one or two may be field stars, since the proper-motion criterion is not foolproof. However, there is evidence from other sources[25] that blue stars of absolute magnitude $M_{pg} = -1$ do occur in globular clusters. (After all, if a planetary nebula can occur in a type II population, it should not be too hard to accept these early-type stars!) Figure 2 shows one star, K 559, with a negative color index of

[18] Computed as before, neglecting relative motion of field stars and cluster. This corresponds to the most unfavorable case.

[19] Radial-velocity measurements indicate that this object is a member of the cluster (cf. A. H. Joy, *Ap. J.*, **110**, 105, 1949). It appears as K 648 in Table 5. Both the photometric and the positional measurements are below normal weight because of the presence of other stars close to it, but, in view of the radial-velocity evidence, it was included in Table 5.

[20] *Mt. W. Comm.*, No. 34, 1916, and *Proc. Nat. Acad. Sci.*, **2**, 525, 1916.

[21] *Pub. David Dunlap Obs.*, Vol. 1, No. 20, Table 1, 1947.

[22] *Ap. J.*, **84**, 132, 1936; *Mt. W. Contr.*, No. 547.

[23] Quoted by Stebbins and Whitford (*ibid.*, Table 5).

[24] *Ap. J.*, **104**, 290, 1946.

[25] See, e.g., D. M. Popper, *Ap. J.*, **105**, 204, 1947.

unusual size ($c' = -0.79$, $m_{pv} = 14.98$). The actual value should not be stressed too much, since the photographic magnitude measured from the McDonald plates may require a color correction for the bluest stars. As the mirrors in the McDonald telescope have aluminized surfaces and the Eastman O plates record down to about 2800 A, there will be a contribution from the ultraviolet wave lengths below 3300 A which would not be obtained with a silvered mirror. Thus the tendency would be to obtain color indices which are too small (algebraically) in the case of the bluest objects in the field. However, K 559 stands out as an exceptionally blue object, and it would be of considerable interest to obtain a spectrum of it.

IX

Some comments on the methods employed in this investigation may be of use to anyone contemplating or engaged on similar work. The effectiveness of the proper-motion criterion has been discussed in Section VII. With mean-square errors of 0".002 per annum in the proper motions, it would hardly be worth the labor involved to attempt to apply this criterion to fainter stars. As it is, the use of the proper motions has cleaned up the upper part of the color-magnitude diagram considerably. It is only necessary to add, say, the field stars within 5′ of the center[26] to Figure 2 to see the difference, and outside this circle there is an increasing proportion of field stars, some of which would probably be taken as members of the cluster from visual inspection of the photographs.

For the magnitudes, the main difficulty is to take account of the background, and this will apply to any method of photometry. Near the center of the cluster, visual estimates would have an advantage, in that there is a number of stars which can be recognized individually on the plates but which had to be left out in using a photometer because the background was too irregular to give a reliable comparison reading. Of course, it is hard to say how far the human eye allows for the background in a case like this. For a Schilt-type photometer, it is usually advisable to work with plates of comparatively low contrast, in order to get images which are not too dense over as wide a range as possible. It was evident, however, that, where the star density is high and the stars are crowded together, a sharp contrast would offer some advantages. It would reduce the range of magnitude for which a given plate could be used, but it would also reduce the effect of faint background stars in the photometry. Some of the most troublesome fluctuations in the background are those due to faint stars which are just on the threshold of visibility on the plate, and it would be advantageous to make the threshold transition as abrupt as possible.

The fainter members of the cluster are also important in selecting a sequence of stars for photoelectric observation. For example, an inspection of the Yerkes photographs suggested that the star K 147, which is 2½′ from the center of the cluster, was sufficiently isolated to be included in the photoelectric program; but when it was examined visually with the McDonald telescope, two or three fainter stars were visible so close to it that it would have been very difficult to isolate it in the photometer. It would obviously be an advantage to have the calibration sequence closer to the center of the cluster, but the presence of the faint stars in the background means that any photoelectric observations within 3′ of the center would be rather unreliable. The best procedure would be to select stars at about 5′–7′ from the center for the calibration sequence and to have them distributed more uniformly round the cluster than the sequence in Table 1. This would reduce the risk of systematic errors due to differences between the images in different parts of the field in the photographic photometry.

Differences of this kind are the most likely source of systematic errors in the magnitudes. To some extent, the selection of the plates for photometry should help to eliminate them. In the present case, plates with soft, round images were used in preference to

[26] K 63, 113, 134, 147, 160, 371, 676, 802, 922, 1047 (Table 6).

plates on which the images were sharper but less regular. The cluster stars which provided the data for Figure 2 lie within a circle of diameter 3½ inches on the McDonald plates, and the images in this area appeared quite uniform. On some of the plates the cluster was displaced by about an inch from the center of the plate without revealing any systematic differences. In the same way, using plates taken on different nights should reduce the risk of systematic errors.

In the present work the scale of photographic magnitudes is more suspect than the photovisual scale. In the first place, the photoelectric comparisons with the NPS were "yellow" comparisons, and the photographic scale was obtained as a kind of derivative, via the photovisual scale and a calibration of the colors. Then, in the photometric work, the background density gave more trouble when measuring the "blue" plates. A comparison can be made with the magnitudes given by Shapley[27] from his observations at Mount Wilson. Shapley established his magnitude scale by photographing the NPS on the same plates as M 15, so it is of interest to compare his results with those from transferring the magnitude scales photoelectrically. Unfortunately, Shapley does not give positions for the stars he observed, but it is possible to identify those used as comparison stars in studying variables in the cluster.[28] Table 9 gives Shapley's designation of these stars, followed by their Küstner number and a comparison of the photographic and photovisual magnitudes. It will be seen that the photographic magnitudes are in good agreement but that there appears to be a systematic difference of about 0.2 mag. over most of the visual scale. However, the fact that my derived scale, the photographic scale, agrees with the Mount Wilson scale gives me some confidence that both my scales are substantially correct.

TABLE 9

COMPARISON OF MAGNITUDES

Star	Magnitudes			
	Photographic		Photovisual	
	Shapley	Brown	Shapley	Brown
a=K 341.....	14.14	14.19	12.82	12.83
b 1047.....	14.51	14.43	13.72	14.00
c 146.....	14.58	14.60	13.40	13.60
d 255.....	14.81	14.80	13.63	13.85
e 114.....	14.76	14.89	13.70	13.93
f 846.....	14.98	14.95	13.94	14.06
g 63.....	15.01	15.06	14.26	14.52
h 69.....	15.23	15.27	14.30	14.53
k 1014.....	15.49	15.51	14.79	14.76
l 677.....	15.68	15.61	15.00	15.06

In concluding, I should like to express my appreciation for the facilities put at my disposal at the Yerkes Observatory and at the McDonald Observatory and for the help I have received from the staff of both observatories, in particular to Dr. G. P. Kuiper and Dr. W. A. Hiltner. The work was carried out during my tenure of a Commonwealth Fund Fellowship at the University of Chicago.

[27] *Ap. J.*, 49, 40, Table 5, 1919.

[28] *Harvard Ann.*, Vol. 78, Part 3, 1919.

PHOTOELECTRIC STUDIES. V. MAGNITUDES AND COLORS OF CLASSICAL CEPHEID VARIABLE STARS*

OLIN J. EGGEN
Lick Observatory, University of California
Received September 25, 1950

ABSTRACT

Magnitudes and colors, totaling 594 observations, have been determined for 32 classical cepheids. These variables can be divided into three types, A, B, and C, on the basis of the relations between the period, the color amplitude, and the light-amplitude. The cepheids of these three types are characterized by the light-curves of δ Cephei, type A; η Aquilae, type B; and ζ Geminorum, type C. A very close relation is also shown to exist between the amplitude of the radial-velocity variation and the amplitude of the light-variation. The existence of relations between the period and the color at maxium and minimum light, as well as a relation between period and luminosity of a cepheid, makes these variables powerful tools for sounding the interstellar medium. The use of these relations is demonstrated. The period-magnitude relation, as obtained from the cepheids in the Magellanic Clouds, is discussed, and a method of determining the zero point of this relation from physical companions of galactic cepheids is demonstrated. The color–minimum-luminosity array of the classical cepheids of types A and B, obtained by combining the period-color and period-luminosity relations, is shown to be very similar to the color-luminosity array obtained from the brightest stars in globular clusters.

I. INTRODUCTION

Since June, 1948, the principal program with the photometer on the 12-inch refractor of the Lick Observatory has been the determination of magnitudes and colors of stars in clusters. In addition, however, several subsidiary programs have been carried along, one of which concerns the determination of light- and color-curves of cepheid variables.

The original cepheid program called for observations to be made at times of maximum and minimum brightness, but it was extended later to cover as much of the complete cycles of variations as was possible. No attempt was made to compute the phase of any cepheid in advance of observation, but each star was observed on several consecutive nights, which cover one or more periods, during the long and nearly uninterrupted runs permitted by the Mount Hamilton sky during the summer and fall observing season.

The present contribution, a first report of the results from this program, contains 594 observations of both magnitudes and colors of 32 cepheids. Observations of cluster-type variables have been excluded; the stars reported on here belong to the group often referred to as "classical" cepheids. The color system and magnitude convention used for the colors, C_p, and magnitudes, Pg_p, of the cepheids are those described in Paper I of this series.[1] The variables were observed in the same manner as that described for the cluster stars in Paper I.

Early in the program it became apparent that the present sample of classical cepheids could be divided into three groups. Since this separation is closely analogous to that found to exist by S. I. Bailey[2] in the cluster-type cepheids, the stars of these groups have been labeled with capital letters A, B, and C to correspond to Bailey's types *a*, *b*, and *c*.

II. CEPHEIDS OF TYPES A AND B

LIGHT-ELEMENTS

Table 1 contains 420 observations of the magnitude and color of 24 cepheids. The light-elements for all stars, with the exception of X Cygni, have been taken from the

* *Contributions from the Lick Observatory*, Ser. II, No. 32.

[1] *Ap. J.*, 111, 65, 1950.

[2] *Harvard Ann.*, 38, 98, 1902.

TABLE 1

MAGNITUDES AND COLORS OF CEPHEIDS OF TYPES A AND B

DATE	JD	PHASE	P_{gp}	C_p
	DT Cygni $21^h05^m.4$ $+30°48'.0$ (Fig. 1) Max. = JD2424605.651 $+2^d.949911E$, log P = 0.40			
1948 Aug. 8	2432772.872	0.052	$5^m.88$	$+0^m.395$
25	89.880	.857	6.06	+ .43
27	91.889	.661	6.30	+ .50
28	92.885	.060	5.88	+ .39
1949 June 25	3093.917	.516	6.33	+ .53
26	94.920	.917	6.04	+ .43
27	95.908	.312	6.12	+ .46
28	96.903	.710	6.31	+ .48
30	98.897	.508	6.36	+ .54
Aug. 7	3136.754	.656	6.31	+ .50
25	54.851	.898	6.05	+ .42
Sept. 19	79.689	0.837	6.12	+0.44
	SZ Tauri $4^h34^m.3$ $+18°26'.7$ (Fig. 2) Max. = JD2423619.49 $+3^d.149130E$, log P = 0.50			
1948 Sept. 29	2432824.990	0.188	7.28	+0.75
Oct. 6	32.038	.426	7.48	+ .83
7	32.949	.716	7.16	+ .67
16	41.875	.550	7.45	+ .77
23	48.910	.784	7.04	+ .64
Nov. 4	60.806	.562	7.40	+ .76
8	64.912	.865	6.96	+ .63
29	85.799	0.498	7.46	+0.79
	SS Scuti $18^h41^m.0$ $-07°47'.0$ (Fig. 3) Max. = JD2428538.55 $+3^d.671253E$, log P = 0.56			
1949 June 19	2433087.882	0.177	8.73	+0.78
21	89.864	.717	9.68	+ .94
22	90.856	.987	8.50	+ .68
23	91.908	.274	8.89	+ .84
24	92.820	.522	9.20	+ .89
25	93.809	.791	9.04	+ .87
26	94.814	.065	8.57	+ .73
27	95.814	.338	8.99	+ .91
28	96.785	.602	9.12	+ .88
30	98.818	.156	8.72	+ .77
July 18	116.770	.046	8.52	+ .715
25	23.750	.947	8.51	+ .69
27	25.741	0.489	9.22	+0.95

TABLE 1—*Continued*

Date	JD	Phase	P_{Sp}	C_p
	SU Cygni 19^h42^m8 $+29°08'.5$ (Fig. 4) Max. = JD2421278.503 $+3^d845507E$, log P = 0.58			
1949 June 23	2433091.910	0.002	6^m82	$+0^m32$
24	92.944	.271	7.18	+ .47
25	93.948	.532	7.47	+ .56
26	94.943	.791	7.54	+ .55
27	95.944	.052	6.69	+ .33
28	96.930	.308	7.23	+ .48
30	98.938	.830	7.55	+ .53
July 27	125.906	.843	7.50	+ .50
28	26.912	.105	6.82	+ .36
Aug. 23	52.798	.836	7.50	+ .52
24	53.816	.101	6.79	+ .33
25	54.788	.354	7.29	+ .50
30	59.750	0.644	7.52	+0.57
	Y Lacertae 22^h06^m9 $+50°47'.9$ (Fig. 5) Max. = JD2418424.295 $+4^d323844E$, log P = 0.64			
1949 June 25	2433093.934	0.731	10.05	+0.76
26	94.934	.962	9.09	+ .47
27	95.920	.190	9.55	+ .63
28	96.917	.421	9.90	+ .715
30	98.908	.881	9.36	+ .53
July 4	102.941	.814	9.74	+ .64
5	03.944	.046	9.20	+ .54
24	22.920	.435	9.93	+ .73
27	25.872	.117	9.43	+ .57
28	26.858	.345	9.83	+ .68
Aug. 22	51.799	.114	9.40	+ .56
23	52.872	.362	9.83	+ .70
24	55.913	.603	10.05	+ .75
25	54.868	.823	9.59	+ .60
29	58.767	.725	10.03	+ .75
30	59.788	0.961	9.09	+0.475
	T Vulpeculae 20^h49^m3 $+28°03'.6$ (Fig. 6) Max. = JD2419372.151 $+4^d435578E$, log P = 0.65			
1948 July 25	2432758.774	0.011	5.68	+0.70
Aug. 4	68.778	.266	6.20	+ .63
6	70.875	.739	6.68	+ .69
7	71.889	.968	5.79	+ .66
8	72.868	.188	6.05	+ .41
9	73.799	.398	6.41	+ .57
1949 July 4	3102.804	.572	6.61	+ .52
5	03.849	.808	6.56	+ .635
Aug. 4	33.726	.544	6.60	+ .50
17	46.771	.485	6.52	+ .38
24	53.878	.087	5.79	+ .53
25	54.854	.307	6.23	+ .67
29	58.757	.187	6.09	+ .39
30	59.757	.412	6.49	+ .50
Sept. 19	79.698	0.908	6.08	+0.60

TABLE 1—*Continued*

DATE	JD	PHASE	P_{E_p}	C_p
	V350 Sagittarii 18^h42^m3 $-20°42'.2$ (Fig. 7) Max. = JD2425885.014 $+5^d15424E$, log $P=0.71$			
1949 June 24	2433092.872	0.433	8m33	+0m88
25	93.858	.624	8.56	+ .955
26	94.860	.818	8.23	+ .82
27	95.854	.011	7.49	+ .635
28	96.840	.203	7.87	+ .77
30	98.854	.593	8.51	+ .94
Aug. 16	145.719	.686	8.55	+ .96
17	46.729	.882	7.77	+ .66
18	47.743	.079	7.66	+ .66
19	48.746	.273	8.03	+ .79
23	52.698	.040	7.51	+ .63
24	53.708	.236	7.97	+ .79
25	54.705	0.429	8.30	+0.88
	δ Cephei 22^h27^m3 $+58°09'.5$ (Fig. 8) Max. = JD2427999.148 $+5^d366306E$, log $P=0.73$			
1948 Aug. 4	2432768.774	0.810	4.91	+0.69
9	73.847	.755	5.00	+ .73
10	74.993	.969	4.05	+ .50
15	79.990	.900	4.42	+ .58
1949 Aug. 7	3136.882	.406	4.58	+ .65
8	37.837	.584	4.89	+ .74
16	45.806	.069	3.92	+ .40
17	46.830	.260	4.30	+ .55
18	47.802	.441	4.66	+ .68
19	48.854	.637	4.95	+ .74
22	51.812	.188	4.16	+ .49
23	52.854	.382	4.54	+ .64
24	53.802	.559	4.84	+ .72
25	54.892	.762	5.00	+ .72
29	58.792	.489	4.75	+ .70
30	59.826	.682	4.96	+ .74
Sept. 18	78.774	.213	4.22	+ .52
19	79.753	.395	4.56	+ .64
20	80.736	0.578	4.89	+0.73
	BG Lacertae 21^h58^m4 $+43°12'.2$ (Fig. 9) Max. = JD2426213.548 $+5^d331908E$, log $P=0.73$			
1949 June 25	2433093.941	0.419	9.70	+0.90
26	94.927	.604	9.87	+ .94
27	95.913	.788	9.76	+ .88
28	96.910	.975	9.04	+ .65
30	98.906	.350	9.60	+ .87
July 4	102.934	.105	9.16	+ .715
5	03.938	.294	9.48	+ .85
24	22.872	.845	9.58	+ .81
25	23.868	.031	8.99	+ .67
27	25.861	.405	9.67	+ .88
28	26.851	.591	9.82	+ .92
Aug. 22	51.795	.269	9.45	+ .80
23	52.865	.470	9.69	+ .90
25	54.875	.847	9.49	+ .78
29	58.774	.578	9.80	+ .91
30	59.792	.769	9.79	+ .89
Sept. 19	79.722	.507	9.72	+ .91
20	80.708	0.692	9.91	+0.96

TABLE 1—*Continued*

Date	JD	Phase	P_{g_p}	C_p
	Y Sagittarii $18^h18^m.4$ $-18°53'.2$ (Fig. 10) Max. = JD2425503.22 $+5^d.77335E$, log P=0.76			
1949 June 15	2433083.872	0.042	5m.87	+0m.56
24	92.847	.597	6.84	+ .91
25	93.835	.768	6.88	+ .93
26	94.833	.941	6.06	+ .635
27	95.830	.113	5.98	+ .62
28	96.812	.284	6.32	+ .76
July 18	116.795	.745	6.90	+ .93
24	22.765	.779	6.86	+ .91
25	23.766	.952	6.00	+ .63
27	25.760	.298	6.34	+ .77
28	26.750	.469	6.61	+ .85
Aug. 17	46.708	.926	6.11	+ .715
18	47.717	.101	5.96	+ .59
19	48.728	.276	6.28	+ .73
22	51.690	.789	6.81	+ .89
24	53.730	.142	5.99	+ .63
25	54.724	0.314	6.35	+0.77
	FM Aquilae $19^h06^m.9$ $+11°28'.2$ (Fig. 11) Max. = JD2425870.347 $+6^d.11423E$, log P=0.79			
1948 Aug. 9	2432773.762	0.073	8.79	+0.96
24	88.823	.537	9.64	+1.29
25	89.833	.702	9.77	+1.31
26	90.812	.862	9.28	+1.10
27	91.799	.023	8.73	+0.93
28	92.802	.188	9.05	+1.08
1949 June 23	3091.879	.102	8.90	+1.01
24	92.908	.271	9.28	+1.115
25	93.891	.432	9.49	+1.23
26	94.887	.594	9.76	+1.30
27	95.867	.755	9.71	+1.24
28	96.861	.917	8.89	+0.96
30	98.863	.245	9.24	+1.13
Aug. 23	3152.738	.056	8.75	+0.96
24	53.740	.220	9.10	+1.09
25	54.736	0.383	9.34	+1.14
	X Vulpeculae $19^h55^m.4$ $+26°52'.3$ (Fig. 12) Max. = JD2420636.231 $+6^d.31938E$, log P=0.80			
1949 June 25	2433093.962	0.353	10.11	+1.30
26	94.955	.510	10.33	+1.38
27	95.955	.669	10.52	+1.41
28	96.941	.825	10.32	+1.30
30	98.938	.140	9.69	+1.13
July 3	101.962	.619	10.46	+1.40
4	02.955	.776	10.51	+1.40
5	03.957	.935	9.71	+1.12
24	22.823	.920	9.83	+1.16
25	23.917	.093	9.53	+1.05
27	25.913	.409	10.12	+1.31
28	26.924	.569	10.44	+1.39
Aug. 24	53.823	.826	10.36	+1.32
25	54.809	0.982	9.40	+1.01

TABLE 1—*Continued*

DATE	JD	PHASE	P_{g_p}	C_p
	RR Lacertae $22^h39^m.5$ $+56°10'.2$ (Fig. 13) Max. = JD2419434.272 $+6^d.417492E$, log P = 0.81			
1948 Aug. 7	2432771.944	0.331	10m.02	+0m.93
8	72.977	.492	9.40	+ .73
9	73.846	.627	8.84	+ .55
10	74.983	.804	9.25	+ .73
13	77.882	.256	10.06	+ .95
14	78.986	.428	9.76	+ .84
15	79.979	.583	8.81	+ .55
24	88.927	.977	9.60	+ .83
26	90.906	.286	10.04	+ .96
27	91.955	.449	9.67	+ .81
1949 June 30	3098.930	.283	10.05	+ .95
July 24	122.910	.020	9.64	+ .86
25	23.882	.171	9.98	+ .96
27	25.882	.483	9.44	+ .715
28	26.868	.637	8.85	+ .58
Aug. 2	31.892	.420	9.86	+ .86
3	32.906	.578	8.86	+ .55
22	51.830	.526	9.03	+ .65
23	52.882	.690	8.88	+ .61
24	53.944	.856	9.36	+ .75
25	54.903	.005	9.60	+ .84
29	58.806	.613	8.83	+ .56
30	59.819	0.771	9.15	+0.71
	XX Sagittarii $18^h21^m.8$ $-16°49'.6$ (Fig. 14) Max. = JD2419189.730 $+6^d.424264E$, log P = 0.81			
1949 June 24	2433092.872	0.161	9.36	+0.89
25	93.854	.314	9.60	+1.00
26	94.854	.470	9.88	+1.06
27	95.847	.624	10.12	+1.17
28	96.830	.777	10.14	+1.12
30	98.847	.091	9.15	+0.84
July 25	123.785	.973	9.10	+0.80
27	25.776	.283	9.58	+1.00
Aug. 16	45.715	.387	9.60	+0.99
17	46.722	.543	9.98	+1.12
19	48.740	.858	9.85	+1.01
22	57.701	.318	9.60	+1.00
23	52.694	.473	9.81	+1.06
24	53.701	.630	10.11	+1.17
25	54.704	0.786	10.09	+1.09
	U Sagittarii $18^h28^m.9$ $-19°09'.8$ (Fig. 15) Max. = JD2420600.325 $+6^d.744917E$, log P = 0.83			
1949 June 26	2433094.855	0.436	7.57	+1.02
27	95.840	.582	7.88	+1.12
28	96.826	.727	8.02	+1.14
30	98.840	.027	7.20	+0.83
July 21	119.785	.133	6.93	+0.75
25	23.781	.725	8.03	+1.14
27	25.769	.020	7.24	+0.83
28	26.764	.167	7.03	+0.79
Aug. 16	45.707	.976	7.44	+0.875
17	46.719	.126	6.90	+0.74
18	47.726	.275	7.23	+0.86
19	48.736	.425	7.43	+0.95
22	51.694	.863	7.89	+1.035
23	52.696	.012	7.26	+0.84
24	53.700	.161	6.97	+0.79
25	54.698	0.309	7.29	+0.90

TABLE 1—*Continued*

Date	JD	Phase	P_{g_p}	C_p
	U Aquilae $19^h26^m.7$ $-07°09'.0$ (Fig. 16) Max. = JD2410170.173 $+7^d.023838E$, log $P = 0.85$			
1948 July 29	2432762.740	0.556	7m.71	+1m.04
31	64.753	.842	7.51	+0.92
Aug. 1	65.750	.984	6.78	+0.715
2	66.821	.137	6.93	+0.82
7	71.746	.828	7.56	+0.92
8	72.781	.985	6.76	+0.72
9	73.769	.126	6.89	+0.79
1949 June 19	3087.927	.854	7.42	+0.89
23	91.917	.422	7.48	+0.96
24	92.913	.563	7.68	+1.035
25	93.899	.704	7.84	+1.08
26	94.910	.848	7.49	+0.95
27	95.896	.988	6.74	+0.715
28	96.882	.128	6.93	+0.78
30	98.892	.415	7.45	+0.97
July 3	101.839	.834	7.57	+0.96
Aug. 22	51.736	.938	6.98	+0.75
23	52.771	.086	6.78	+0.715
24	53.774	.228	7.12	+0.875
29	58.715	0.932	7.05	+0.76
	η Aquilae $19^h49^m.9$ $+00°52'.4$ (Fig. 17) Max. = JD2414826.26 $+7^d.176678E$, log $P = 0.86$			
1948 Aug. 10	2432774.858	0.962	4.70	+0.71
13	77.802	.372	4.41	+ .68
14	78.792	.510	4.63	+ .72
25	89.840	.050	4.22	+ .58
26	90.836	.188	4.04	+ .54
27	91.840	.328	4.39	+ .68
28	92.830	.466	4.43	+ .70
Oct. 16	841.658	.270	4.21	+ .61
1949 July 4	3102.828	.661	4.94	+ .89
5	03.821	.800	5.14	+ .90
18	16.852	.615	4.82	+ .85
Aug. 2	31.803	.699	4.95	+ .88
3	32.733	.828	5.10	+ .875
4	33.750	.970	4.69	+ .68
5	34.792	.115	3.94	+ .50
7	36.803	.395	4.40	+ .69
8	37.758	.528	4.67	+ .77
23	52.774	.621	4.83	+ .84
24	53.778	.761	5.04	+ .89
25	54.796	.903	4.98	+ .82
29	58.708	.448	4.43	+ .67
30	59.729	.590	4.76	+ .82
Sept. 18	78.680	.231	4.11	+ .58
19	79.678	.370	4.39	+ .70
20	80.677	.509	4.64	+ .77
Oct. 10	200.655	.293	4.38	+ .63
16	06.660	0.129	3.96	+0.52

TABLE 1—*Continued*

Date	JD	Phase	P_{g_p}	C_p
	RX Camelopardalis 4^h00^m8 $+58°31'.6$ (Fig. 18) Max. = JD2420359.798 $+7^d.911848E$, log $P = 0.90$			
1948 Aug. 24	2432789.003	0.961	8m.14	+0m.91
26	90.969	.210	8.29	+0.99
27	92.031	.344	8.70	+1.09
Sept. 2	97.955	.093	8.30	+0.93
Nov. 4	860.785	.034	8.00	+0.89
8	64.958	.561	8.97	+1.23
26	82.899	.829	8.74	+1.10
27	83.875	.952	8.22	+0.94
29	85.919	.211	8.31	+0.99
Dec. 1	87.889	.460	8.83	+1.19
1949 Jan. 27	944.840	.658	9.22	+1.28
30	47.705	.020	8.00	+0.875
Aug. 24	3153.983	.092	8.22	+0.94
25	54.950	.214	8.32	+1.00
29	58.920	.716	9.23	+1.23
Sept. 18	78.917	.243	8.40	+0.98
19	80.000	.380	8.71	+1.14
20	80.972	.503	8.92	+1.20
30	90.920	.760	9.17	+1.22
Oct. 16	206.801	.768	9.09	+1.195
26	16.843	.037	8.04	+0.89
Nov. 12	33.688	.166	8.40	+1.02
17	38.712	0.801	9.06	+1.17
	Z Lacertae 22^h38^m9 $+56°34'.0$ (Fig. 19) Max. = JD2418475.819 $+10^d.885824E$, log $P = 1.04$			
1948 Aug. 7	2432771.930	0.278	9.39	+1.07
8	72.958	.372	9.70	+1.17
9	73.823	.452	9.82	+1.20
10	74.972	.557	9.99	+1.26
12	76.965	.740	9.41	+0.98
13	77.958	.832	9.16	+0.90
14	78.948	.922	8.90	+0.86
15	79.976	.017	8.49	+0.75
24	88.917	.838	8.19	+0.94
26	90.903	.021	8.48	+0.75
27	91.951	.118	9.01	+0.96
28	92.930	.207	9.18	+1.02
1949 June 30	3098.927	.317	9.59	+1.12
July 24	122.906	.519	9.97	+1.26
25	23.878	.609	9.96	+1.19
27	25.878	.792	9.30	+0.93
28	26.865	.883	9.16	+0.89
Aug. 2	31.885	.344	9.66	+1.15
3	32.899	.437	9.80	+1.20
22	51.826	.176	9.04	+0.97
23	52.878	.273	9.31	+1.07
24	53.941	.370	9.68	+1.15
25	54.896	.458	9.82	+1.21
29	58.799	.817	9.20	+0.90
30	59.816	.910	8.95	+0.86
Sept. 18	78.781	.652	9.77	+1.11
19	79.750	.741	9.38	+0.98
20	80.729	.831	9.20	+0.91
Nov. 17	238.628	0.150	9.02	+0.97

TABLE 1—*Continued*

Date	JD	Phase	P_{fp}	C_p
	TT Aquilae $19^h05^m.7$ $+01°13'.1$ (Fig. 20) Max. = JD2420097.90 $+13^d.475475E$, log $P = 1.14$			
1949 June 19	2433087.909	0.402	$8^m.44$	$+1^m.32$
22	90.892	.619	8.87	+1.43
23	91.855	.689	8.93	+1.38
24	92.896	.764	8.64	+1.26
25	93.882	.836	8.35	+1.17
26	94.899	.910	8.19	+1.12
27	95.875	.981	7.16	+0.83
28	96.870	.053	7.38	+0.88
July 3	101.828	.414	8.50	+1.335
Aug. 16	45.760	.608	8.92	+1.41
17	46.742	.679	8.87	+1.37
19	48.758	.826	8.35	+1.17
23	52.719	.114	7.54	+0.98
24	53.729	.187	7.81	+1.09
25	54.726	0.759	8.00	+1.18
	RW Cassiopeiae $1^h33^m.9$ $+57°30'.3$ (Fig. 21) Max. = JD2421354.222 $+14^d.801043E$, log $P = 1.17$			
1949 Aug. 22	2433151.927	0.086	9.84	+1.08
23	52.913	.153	10.05	+1.16
24	53.962	.224	10.30	+1.23
25	54.920	.288	10.45	+1.25
29	58.882	.556	11.01	+1.37
30	59.882	.624	10.82	+1.29
Sept. 18	78.795	.901	9.43	+0.79
19	79.792	.969	9.60	+0.91
20	80.795	.036	9.76	+1.02
Oct. 16	206.722	.788	10.32	+1.09
Nov. 12	33.656	.608	10.88	+1.33
17	38.660	0.946	9.50	+0.89
	X Cygni $20^h41^m.4$ $+35°24'.3$ (Fig. 22) Max. = JD2421511.892 $+16^d.385680E$, log $P = 1.21$			
1948 July 24	2432757.930	0.333	9.29	+1.08
25	58.781	.385	7.45	+1.14
Aug. 2	66.882	.880	7.55	+1.07
4	68.771	.995	6.69	+0.72
7	71.882	.185	6.90	+0.88
8	72.865	.245	7.04	+0.96
9	73.795	.302	7.18	+1.04
10	74.854	.366	7.39	+1.12
12	76.983	.496	7.75	+1.25
1949 June 25	3093.906	.838	7.78	+1.12
27	95.908	.960	7.41	+0.96
28	96.899	.020	6.37	+0.70
30	98.965	.146	6.78	+0.83
July 21	119.837	.420	7.50	+1.19
24	22.833	.603	7.95	+1.33
25	23.934	.670	8.05	+1.34
27	25.927	.792	7.90	+1.20
28	26.938	.854	7.61	+1.09
Aug. 2	31.764	.148	6.83	+0.86
3	32.920	.219	6.99	+0.93
4	33.951	.281	7.14	+1.00
22	51.719	.366	7.42	+1.11
23	52.823	.433	7.61	+1.195
24	53.865	.497	7.76	+1.23
25	54.837	.556	7.87	+1.27
Sept. 19	79.667	0.072	6.54	+0.75

TABLE 1—*Continued*

DATE	JD	PHASE	P_{gp}	C_p
	SZ Aquilae 19^h02^m1 $+01°13'.7$ (Fig. 23) Max. = JD2420258.765 $+17^d137939E$, log $P = 1.23$			
1949 June 19	2433087.903	0^p581	10^m52	$+1^m57$
21	89.929	.699	10.62	+1.55
22	90.885	.755	10.57	+1.515
23	91.847	.811	10.32	+1.37
24	92.890	.872	10.13	+1.32
25	93.875	.930	10.00	+1.265
26	94.892	.989	8.68	+0.88
27	95.872	.046	8.90	+0.95
28	96.868	.104	9.06	+1.02
July 3	101.833	.394	10.01	+1.44
Aug. 16	45.757	.957	9.43	+1.04
17	46.740	.014	8.70	+1.88
18	47.750	.073	8.96	+0.97
19	48.753	.132	9.16	+1.08
23	52.710	.363	9.88	+1.39
24	53.722	.422	10.05	+1.435
25	54.719	0.480	10.22	+1.49
	WZ Sagittarii 18^h14^m0 $-19°05'.8$ (Fig. 24) Max. = JD2424625.350 $+21^d849708E$, log $P = 1.34$			
1949 June 24	2433092.854	0.534	9.78	+1.51
25	93.840	.579	9.80	+1.53
26	94.840	.625	9.87	+1.54
27	95.833	.670	9.83	+1.49
28	96.819	.715	9.75	+1.45
30	98.837	.808	9.56	+1.33
July 18	116.799	.630	9.84	+1.53
25	23.771	.949	9.52	+1.03
28	26.760	.086	8.38	+1.00
Aug. 16	45.704	.953	8.36	+0.90
17	46.753	.001	8.11	+0.875
18	47.764	.047	8.25	+0.93
19	48.774	.093	8.40	+1.00
22	51.733	.229	8.89	+1.265
23	52.726	.274	9.02	+1.29
24	53.733	.320	9.13	+1.33
25	54.730	0.366	9.30	+1.39

General Catalogue of Variable Stars.[3] The additional terms, involving functions of E, the epoch, have been omitted. The elements given, in this reference, for X Cygni seem to be erroneous, and they have been replaced with those given by H. Schneller.[4] The phases, in fractions of the period, in Table 1 are geocentric and the positions are for 1950.

The magnitudes and colors in Table 1 are plotted in Figures 1–24, and free-hand curves are drawn through the observations; solid curves refer to light-variation, broken curves to color variation. Inspection of these figures shows that, with the exception of RR Lacertae, the maxima all occur within 0^p1 of the predicted time. The elements

[3] By Parenago and Kukarkin (Moscow, 1948).

[4] *Kl. Veröff. Berlin-Babelsberg*, No. 22, 1941.

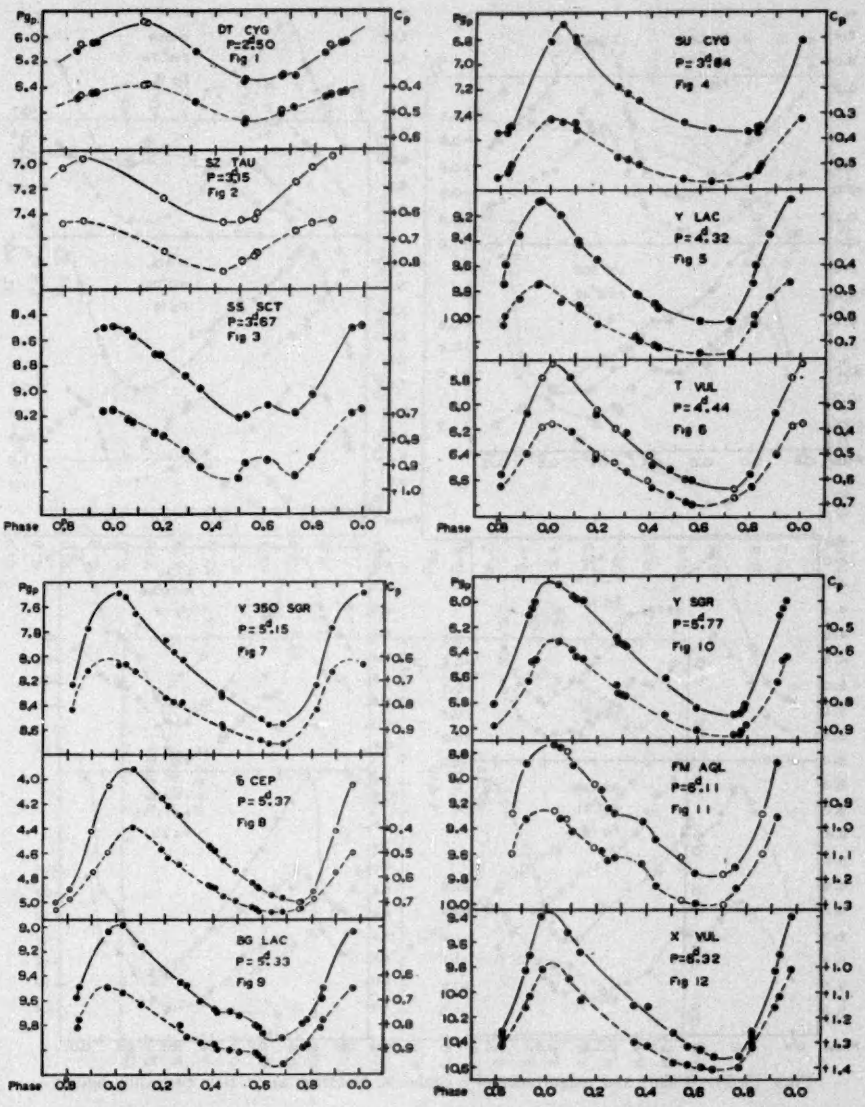

FIGS. 1–12.—Colors and magnitudes of 12 cepheids. The open circles represent observations made in 1948; the filled circles, observations made in 1949. The solid curves indicate the light-variation, the broken curves the color variation.

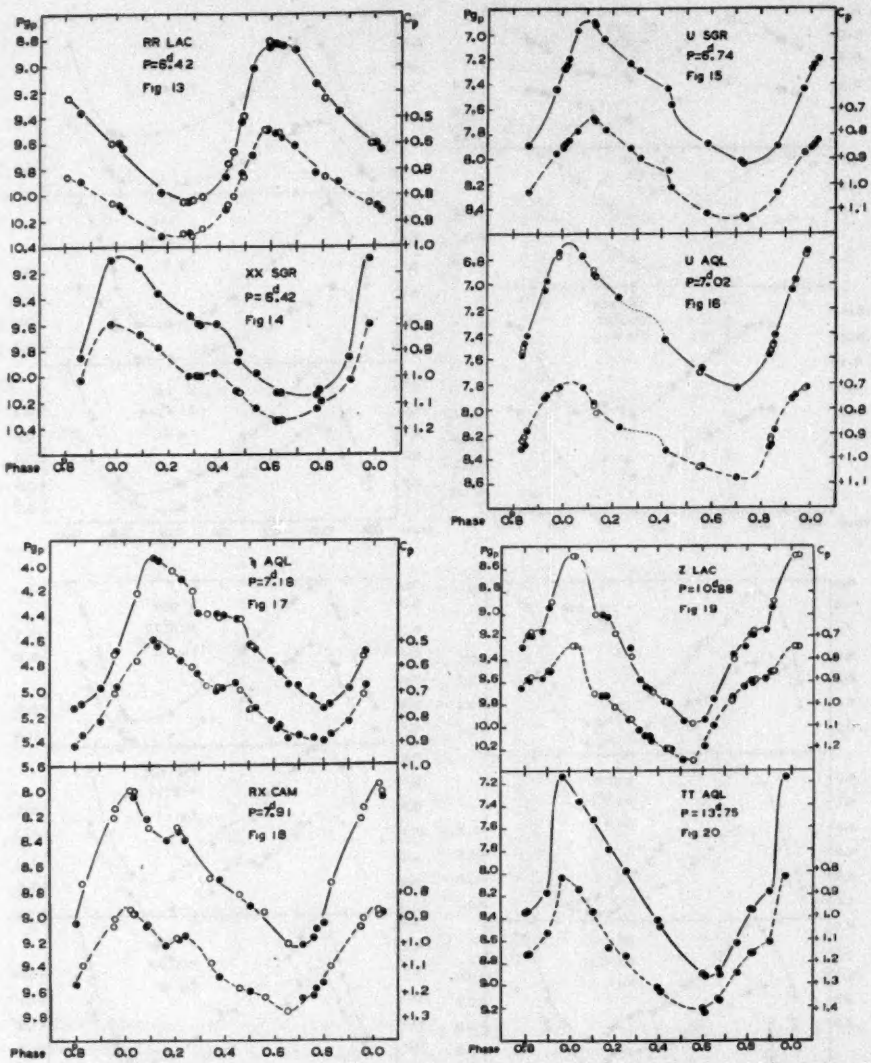

FIGS. 13–20.—Colors and magnitudes of 8 cepheids. Notation same as in preceding figures

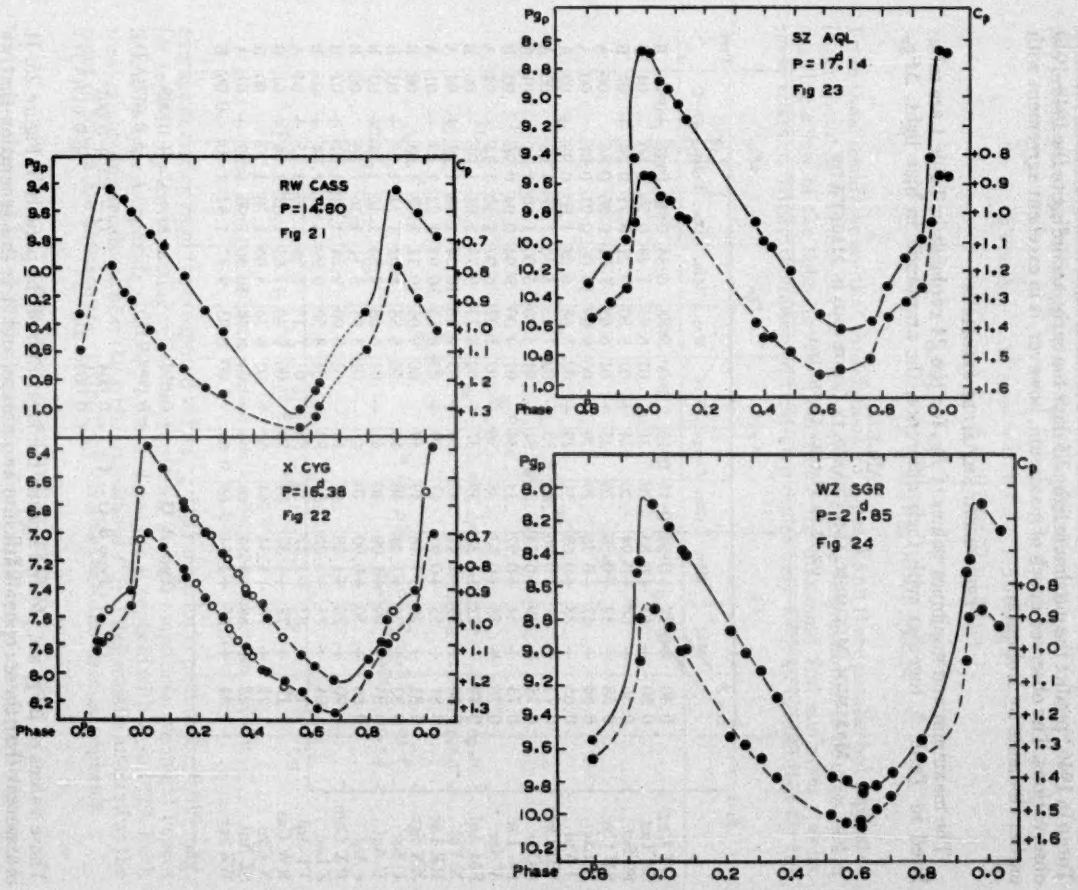

FIGS. 21–24.—Colors and magnitudes of 4 cepheids. Notation same as in preceding figures

given in the catalogue for RR Lacertae, which are the results of observations made in Torun in 1946,[5] predict the maximum light 2.5 days too early, according to the 1948–1949 observations. The observed epoch of maximum, however, is in excellent agreement with earlier elements by Robinson.[6]

PERIOD–LIGHT-AMPLITUDE RELATIONS

The maximum and minimum values of Pg_p for the 24 cepheids in Table 1 are tabulated in Table 2, together with their difference, the amplitude in blue light, ΔPg_p.

TABLE 2

MAXIMUM, MINIMUM, AND CHANGE IN COLOR AND IN MAGNITUDE OF 24 CLASSICAL CEPHEIDS

STAR	LOG P	C_p		ΔC_p			Pg_p		ΔPg_p			TYPE
		Max.	Min.	Obs.	Comp.	O−C	Max.	Min.	Obs.	Comp.	O−C	
DT Cyg	0.40	+0^m.39	+0^m.54	0^m.15	0^m.15	0^m.00	5^m.88	6^m.34	0^m.46	0^m.45	+0^m.01	B
SZ Tau	0.50	+ .63	+0.83	.20	.21	− .01	6.93	7.49	0.56	0.60	− .04	B
SS Sct	0.56	+ .68	+0.94	.26	.24	+ .02	8.50	9.21	0.71	0.70	+ .01	B
SU Cyg	0.58	+ .32	+0.58	.26	.25	+ .01	6.68	7.54	0.86	0.86	.00	A
Y Lac	0.64	+ .47	+0.76	.29	.29	.00	9.09	10.06	0.97	0.97	.00	A
T Vul	0.65	+ .38	+0.69	.31	.29	+ .02	5.68	6.68	1.00	0.98	+ .02	A
V350 Sgr	0.71	+ .61	+0.96	.35	.33	+ .02	7.48	8.56	1.08	1.08	.00	A
δ Cep	0.73	+ .39	+0.74	.35	.34	+ .01	3.90	5.00	1.10	1.11	− .01	A
BG Lac	0.73	+ .64	+0.97	.33	.34	− .01	9.00	9.94	0.94	0.96	− .02	B
Y Sgr	0.76	+ .55	+0.93	.38	.36	+ .02	5.82	6.92	1.10	1.14	− .04	A
FM Aql	0.79	+ .92	+1.31	.39	.37	+ .02	8.73	9.78	1.05	1.05	.00	B
X Vul	0.80	+ .99	+1.41	.42	.39	+ .03	9.36	10.54	1.18	1.22	+ .04	A
RR Lac	0.81	+ .55	+0.97	.42	.39	+ .03	8.83	10.05	1.22	1.23	− .01	A
XX Sgr	0.81	+ .79	+1.18	.39	.39	.00	9.06	10.14	1.08	1.08	.00	B
U Sgr	0.83	+ .74	+1.14	.40	.40	.00	6.88	8.02	1.14	1.11	+ .03	B
U Aql	0.85	+ .69	+1.09	.40	.41	− .01	6.68	7.84	1.16	1.14	+ .02	B
η Aql	0.86	+ .50	+0.90	.40	.41	− .01	3.94	5.11	1.16	1.16	.00	B
RX Cam	0.90	+ .86	+1.28	.42	.44	− .02	8.00	9.24	1.24	1.22	+ .02	B
Z Lac	1.04	+ .75	+1.26	.51	.52	− .01	8.50	9.99	1.49	1.44	+ .05	B
TT Aql	1.14	+ .83	+1.42	.59	.58	+ .01	7.15	8.94	1.79	1.75	+ .04	A
RW Cas	1.17	+ .78	+1.37	.59	.59	.00	9.40	11.03	1.63	1.64	− .01	B
X Cyg	1.21	+ .70	+1.34	.64	.62	+ .02	6.36	8.06	1.70	1.70	.00	B
SZ Aql	1.23	+ .88	+1.56	.68	.64	+ .04	8.70	10.60	1.90	1.89	+ .01	A
WZ Sgr	1.34	+0.85	+1.54	0.69	0.69	0.00	8.03	9.87	1.84	1.90	−0.06	B

Type A, $\overline{O-C}$:	+ 0.019 ± 0.009(A.D.)	$\overline{O-C}$: + 0.005 ± 0.017(A.D.)
Type B, $\overline{O-C}$:	− 0.004 ± 0.009(A.D.)	$\overline{O-C}$: + 0.001 ± 0.019(A.D.)

These values of ΔPg_p are plotted against the logarithm of the periods in Figure 25. It is apparent that these cepheids fall into two groups, and it is this separation that we will use as a criterion for classifying them into types A and B; the open circles indicate

[5] *Bull. Astr. Obs. Torun*, No. 1, 1946.

[6] *Harvard Ann.*, **90**, 60, 1933. An unpublished investigation, by G. Reaves, Lick Observatory Fellow, indicates that the elements given by Robinson probably are as good as can be obtained from the existing observations. The elements given in the *General Catalogue of Variable Stars* may contain a misprint of $P = 6.416492$ days, which may be 6.417492 days; but the Torun publication, from which these elements were taken, was not available to check this possibility.

type A, the filled circles type B. A least-squares solution for the observations of these two groups gave the following period–light-amplitude relations:

$$\text{Type A:} \quad \Delta P g_p = -0^m.037 + 1.568 \log P \pm 0.013 \pm 0.018 \text{ (p.e.)}, \tag{1}$$

$$\text{Type B:} \quad \Delta P g_p = -0^m.172 + 1.550 \log P \pm 0.007 \pm 0.008 \text{ (p.e.)}. \tag{2}$$

From these results we see that the relations for types A and B are parallel but separated in zero point by 0.13 mag. In view of the fact that some judgment had to be exercised in drawing a few of the light-curves to determine the maximum and minimum epochs, these relations satisfy the observed light-amplitudes very well, as is indicated by the

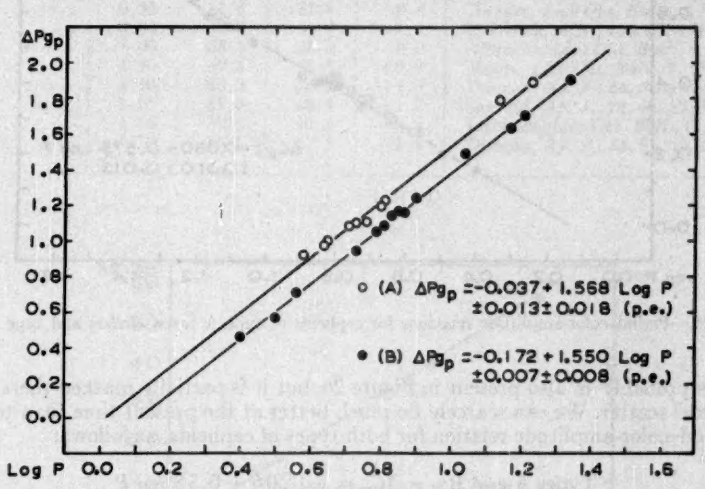

FIG. 25.—Period–light-amplitude relations for cepheids of types A and B

average deviation from the computed values, ±0.017 mag. for type A and ±0.019 mag. for type B. By extrapolating relations (1) and (2) to zero amplitude, we might expect to find no type A cepheids with $P < 1^d.06$, and no type B cepheid with $P < 1^d.29$. Both these minimum periods are near the arbitrary value of $P = 1$ day usually adopted as the point of separation between the cluster-type variables and the classical cepheids.

PERIOD–COLOR-AMPLITUDE RELATION

The maximum and minimum values of C_p and their difference, ΔC_p, are also tabulated in Table 2. The resulting period-color-amplitude relation is shown in Figure 26, where, as in Figure 25, the open circles indicate type A cepheids, the filled circles those of type B. Since Figure 25 shows a separation of the two types in the period–light-amplitude relations, we might expect to find a similar separation in Figure 26. The average ratio of light-amplitude to color-amplitude, however, is only 2.7, and, since relations (1) and (2) are separated by only 0.14 mag., the maximum separation to be expected in the period–color-amplitude relations would be ~0.05 mag., which easily could be masked by the

errors of observation. A least-squares solution for the period–color-range relation for only the type B stars gave

$$\text{Type B:} \quad \Delta C_p = -0^m.080 + 0.575 \log P \pm 0.010 \pm 0.010 \text{ (p.e.)}. \tag{3}$$

This relation satisfies the color-amplitudes of the type B stars very well, with an average deviation of ± 0.009 mag. between the computed and the observed values, but it leaves a systematic difference, O−C, of $+0.019 \pm 0.009$ (A.D.) mag. for the stars of type A. We can conclude that the separation shown in Figure 25 between the two types of

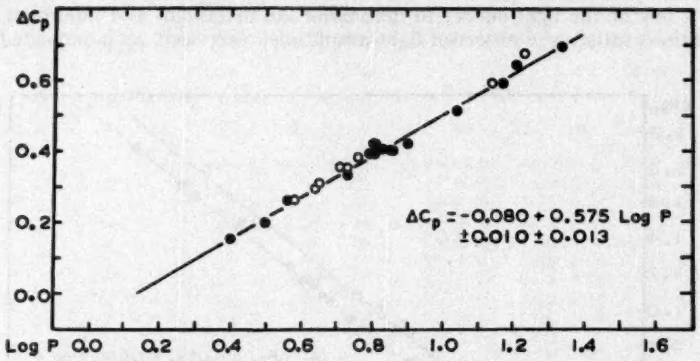

FIG. 26.—Period–color-amplitude relations for cepheids of type A (*open circles*) and type B (*filled circles*).

cepheids probably is also present in Figure 26, but it is partially masked there by observational scatter. We can scarcely do much better at the present time than to adopt one period–color-amplitude relation for both types of cepheids, as follows:

$$\text{Types A and B:} \quad \Delta C_p = -0^m.06 + 0.58 \log P \pm 0.01 \pm 0.01 . \tag{4}$$

From relation (3) we would expect no cepheids of type B with $P < 1^d.38$, a value which agrees well enough with the value $P < 1^d.29$, found from relation (2).

RELATION BETWEEN VELOCITY- AND LIGHT-AMPLITUDES

There are available, in the literature, complete velocity-curves for nine stars of Table 2 in addition to the extensive material obtained by A. H. Joy.[7] Since, in general, these nine velocity-curves were derived from more observations than those given by Joy, we shall treat them separately. Table 3 contains the light-amplitudes from Table 2 for these nine stars, together with their observed velocity-amplitudes; and Figure 27 is the correlation diagram between $\Delta P g_p$ and ΔV. The straight line corresponds to the following least-squares solution:

$$\Delta V \text{ (km/sec)} = +3.64 + 31.67 \Delta P g_p \pm 1.26 \pm 1.21 \text{ (p.e.)}. \tag{5}$$

[7] *Ap. J.*, **86**, 363, 1937.

That this expression represents satisfactorily the observed values can be seen from the average deviation of the computed values, ±1.3 km/sec. Since the constant term exceeds its probable error only by a factor of 3, perhaps it could be omitted; in this case $\Delta V = 35.91\ (\pm 1.05)\ \Delta Pg_p$. From material that has a much larger scatter, Robinson obtained $\Delta V = 33.9\ \Delta Pg$. Table 4 contains the 15 stars common to Table 2 and Joy's list of radial velocities. The computed ΔV's in Table 4 were obtained from expression (5). The system-

TABLE 3

COMPARISON OF LIGHT-AMPLITUDE AND VELOCITY-AMPLITUDE

Star	ΔPg_p (Mag.)	ΔV(Obs.) (Km/Sec)	ΔV(Comp.) (Km/Sec)	O−C (Km/Sec)	Authority for ΔV
DT Cyg	0.46	17.0	18.2	−1.2	Sanford, *Ap. J.*, **72**, 40, 1930
SZ Tau	0.56	21.8	21.4	+0.4	Haynes, *Lick Obs. Bull.*, **6**, 85, 1913
SU Cyg	0.86	30.0	31.9	−1.9	Hellerich, *A.N.*, **210**, 67, 1919
T Vul	1.00	35.3	35.3	0.0	Albrecht, *Lick Obs. Bull.*, **4**, 137, 1907
δ Cep	1.10	39.4	38.5	+0.9	Moore, *Lick Obs. Bull.*, **7**, 153, 1913
Y Sgr	1.10	40.0	38.5	+1.5	Duncan, *Ap. J.*, **56**, 340, 1922
U Aql	1.16	41.6	40.4	+1.2	Sanford, *Ap. J.*, **72**, 46, 1930
η Aql	1.16	39.5	40.4	−0.9	Jacobsen, *Lick Obs. Bull.*, **12**, 153, 1923
X Cyg	1.70	56.1	57.5	−1.4	Duncan, *Ap. J.*, **53**, 95, 1921

± 1.3(A.D.)

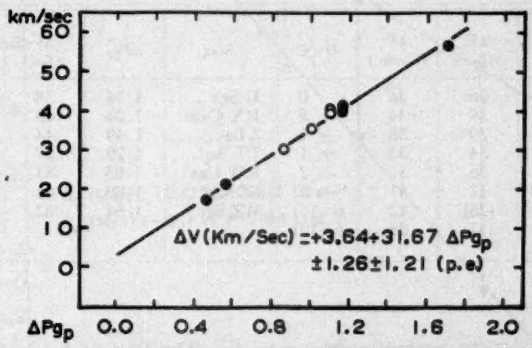

FIG. 27.—Relation between velocity and light-amplitude for cepheids of type A (*open circles*) and type B (*filled circles*).

atic difference is negligible, −0.2 km/sec, and the average deviation of the computed from the observed values is only ±3.0 km/sec, if RR Lacertae and XX Sagittarii are omitted. Even if these two stars are included, the dispersion is not much larger than would be expected from the mean residual of a single plate from the smoothed velocity-curves, which Joy gives as 3 km/sec. A reinvestigation of the velocity-curves of RR Lacertae and XX Sagittarii would be of interest.

ASYMMETRY OF LIGHT-CURVES

From the light-curves of Figures 1–24 we see that the stars referred to here as of type A could be called the "δ Cephei type" because, like δ Cephei, there are no secondary

fluctuations in the light-variation. Also, the group referred to as type B could be called the "η Aquilae type" because they all show "bumps" or stillstands in their light-curves. The one exception to this may be SZ Aquilae, a type A cepheid with a stillstand on the rising branch of the light-curve. An interesting feature of the bumps on the type B light-curves is the progression of their position with period. This progression is illustrated in the accompanying tabulation.

Period (Days)	Bump Phase	Stars
3.67	$+0^p6$	SS Sct
5.33	+ .5	BG Lac
6.1–7.1	+ .35	FM Aql, XX Sgr, U Sgr
10.88	.0	Z Lac
13.75	− .15	TT Aql
14.8–16.4	−0.2	RW Cas, X Cyg

Previous investigators, especially E. Hertzsprung,[8] Kukarkin and Parenago,[9] and Campbell and Jacchia,[10] have divided the cepheids into period groups and have found a predominating form of light-curve within each group, but, since the groups overlap, the

TABLE 4

COMPARISON OF LIGHT-AMPLITUDE IN PHOTOGRAPHIC MAGNITUDE AND VELOCITY-AMPLITUDE IN KM/SEC FOR STARS OBSERVED BY JOY

Star	ΔP_{g_p}	ΔV (Obs.)	ΔV (Comp.)	O−C	Star	ΔP_{g_p}	ΔV (Obs.)	ΔV (Comp.)	O−C
SS Sct	0.71	26	26	0	U Sgr	1.14	38	40	−2
Y Lac	0.97	39	34	+ 5	RX Cam	1.24	48	42	+5
V350 Sgr	1.08	39	38	+ 1	Z Lac	1.49	44	51	−7
BG Lac	0.94	34	33	+ 1	TT Aql	1.79	52	60	−8
FM Aql	1.05	35	37	− 2	RW Cas	1.63	53	55	−2
X Vul	1.18	47	41	+ 6	SZ Aql	1.90	64	64	0
RR Lac	1.22	(26)	42	(−16)	WZ Sgr	1.84	62	62	0
XX Sgr	1.08	(57)	38	(+19)					

$\overline{O-C}$: − 0.2
± 3.0(A.D.)

separation is by no means complete. This matter will be discussed more fully below; but, when we separate the groups of cepheids according to light-amplitude, we also automatically sort them by form of light-curve and, although the number of stars plotted in Figure 25 is small, from the figures we can surmise that the grouping by period is the result of the fact that the relative abundances of type A and type B cepheids vary with the period.

INTERSTELLAR ABSORPTION

We have already discussed the relation between the color-amplitude and the period. The use of the range in color in this relation instead of the maximum, mean, or minimum color practically eliminates the effects of interstellar absorption on these observations. From relation (3), however, we might expect the maximum or minimum

[8] *B.A.N.*, **3**, 15, 1926.

[9] *A.J., Soviet Union*, **14**, 182, 1937.

[10] *The Story of Variable Stars* (Philadelphia: Blakiston Co., 1941).

colors of the cepheids, freed of interstellar absorption, to show similar correlations with the period. Figure 28 shows a plot of the maximum and minimum colors against the logarithm of the period, for the five stars SU Cygni, T Vulpeculae, δ Cephei, η Aquilae, and X Cygni, which, of the stars in Table 2, are probably least affected by interstellar reddening. The relations between the maximum and minimum color for these stars and the log periods are:

$$C_p\,(\text{max.}) = -0^m.036 + 0.613 \log P\,, \tag{6}$$

$$C_p\,(\text{min.}) = -0^m.112 + 1.194 \log P\,; \tag{7}$$

$$\Delta C_p = -0.076 + 0.581 \log P\,,$$

$$\Delta C_p = -0.080 + 0.575 \log P\,. \tag{3}$$

The difference, ΔC_p, is in excellent agreement with expression (3), derived above from all 24 stars, reddened and unreddened, in Table 2. Table 5 lists the stars of Table 2, to-

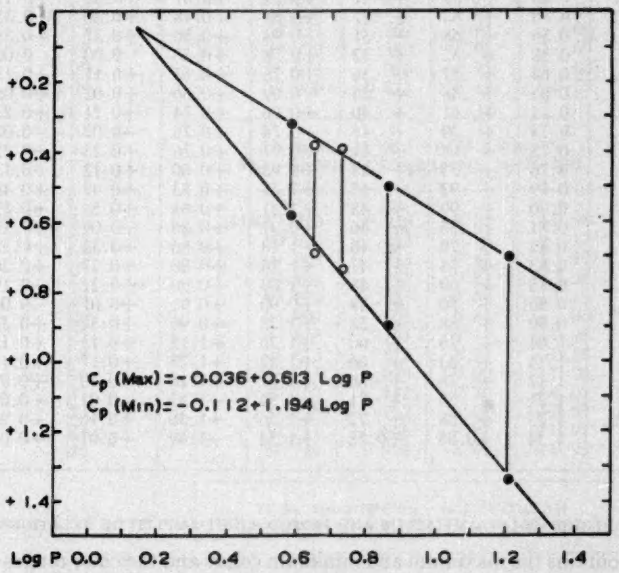

FIG. 28.—Relation between colors of unreddened cepheids at maximum and minimum light and the period for type A (*open circles*) and type B (*filled circles*).

gether with the values of the color excess, E, determined from the observed colors at both maximum and minimum and from the normal colors determined from expressions (6) and (7). The fact that δ Cephei, the nearest cepheid of the group, shows an excess of -0.02 probably means that the other four stars of Figure 28 are slightly reddened. In view of the fact, however, that Figure 26 indicates a small difference in the color range for type A and type B cepheids of the same period, which we cannot allow for at the present time, it appears reasonable to adopt expressions (6) and (7) as given, for computing the normal colors; the error can hardly exceed 0.02–0.03 mag.

III. CEPHEIDS OF TYPE C

LIGHT-ELEMENTS

As in the case of the types A and B discussed above, the elements for the type C cepheids were all taken from the Russian catalogue.[3] The term in E^2, given in that reference, was not used in computing the phases of the observations of ζ Geminorum. The arrangement of Table 6 and Figures 29–34 is the same as that of Table 1 and Figures 1–24.

TABLE 5

COLOR EXCESS FOR CEPHEIDS OF TYPES A AND B

STAR	LOG P	C_p(MAX.)		C_p(MIN.)		E		
		Obs.	Comp.	Obs.	Comp.	Max.	Min.	Mean
DT Cyg	0.40	+0^{m}39	+0^{m}21	+0^{m}54	+0^{m}37	+0^{m}18	+0^{m}17	+0^{m}175
SZ Tau	0.50	+ .63	+ .27	+0.83	+0.48	+0.36	+0.35	+0.355
SS Sct	0.56	+ .68	+ .31	+0.94	+0.56	+0.37	+0.38	+0.375
SU Cyg	0.58	+ .32	+ .32	+0.58	+0.58	0.00	0.00	0.00
Y Lac	0.64	+ .47	+ .36	+0.76	+0.65	+0.11	+0.11	+0.11
T Vul	0.65	+ .38	+ .36	+0.69	+0.66	+0.02	+0.03	+0.025
V350 Sgr	0.71	+ .61	+ .40	+0.96	+0.74	+0.21	+0.22	+0.215
δ Cep	0.73	+ .39	+ .41	+0.74	+0.76	−0.02	−0.02	−0.02
BG Lac	0.73	+ .64	+ .41	+0.97	+0.76	+0.23	+0.21	+0.22
Y Sgr	0.76	+ .55	+ .43	+0.93	+0.80	+0.12	+0.13	+0.125
FM Aql	0.79	+ .92	+ .45	+1.31	+0.83	+0.47	+0.48	+0.475
X Vul	0.80	+ .99	+ .45	+1.41	+0.84	+0.54	+0.57	+0.555
RR Lac	0.81	+ .55	+ .46	+0.97	+0.86	+0.09	+0.11	+0.10
XX Sgr	0.81	+ .79	+ .46	+1.18	+0.86	+0.33	+0.32	+0.325
U Sgr	0.83	+ .74	+ .47	+1.14	+0.88	+0.27	+0.26	+0.265
U Aql	0.85	+ .69	+ .48	+1.09	+0.90	+0.21	+0.19	+0.20
η Aql	0.86	+ .50	+ .49	+0.90	+0.91	+0.01	−0.01	0.00
RX Cam	0.90	+ .86	+ .52	+1.28	+0.96	+0.34	+0.32	+0.33
Z Lac	1.04	+ .75	+ .60	+1.26	+1.13	+0.15	+0.13	+0.14
TT Aql	1.14	+ .83	+ .66	+1.42	+1.25	+0.17	+0.17	+0.17
RW Cas	1.17	+ .78	+ .68	+1.37	+1.28	+0.10	+0.09	+0.095
X Cyg	1.21	+ .70	+ .71	+1.34	+1.33	−0.01	+0.01	0.00
SZ Aql	1.23	+ .88	+ .72	+1.56	+1.36	+0.16	+0.20	+0.18
WZ Sgr	1.34	+0.85	+0.78	+1.54	+1.49	+0.07	+0.05	+0.06

PERIOD–COLOR-AMPLITUDE AND PERIOD–LIGHT-AMPLITUDE RELATIONS

Table 7 contains the maximum and minimum colors and the color ranges observed for the six type C cepheids. These color ranges are plotted against the logarithms of the periods in Figure 35; the broken line in the figure represents the period–color-amplitude relation (3) found above for the cepheids of types A and B. An excellent fit to the observations is obtained from the expression:

$$\text{Type C:} \quad \Delta C_p = -0^m.242 + 0.560 \log P \pm 0.006 \pm 0.004 \text{ (p.e.)}. \tag{8}$$

For comparison we have:

$$\text{Types A and B:} \quad \Delta C_p = -0^m.080 + 0.575 \log P \pm 0.010 \pm 0.010 \text{ (p.e.)}, \tag{3}$$

TABLE 6

MAGNITUDES AND COLORS OF CEPHEIDS OF TYPE C

DATE	JD	PHASE	P_{g_p}	C_p
	FF Aquilae 18h56m0 +17°17′5 (Fig. 29) Max. = JD2424703.115 +4d471361E, log P = 0.65			
1948 July 29	2432762.719	0.495	6.16	+0.68
31	64.736	.946	5.78	+ .62
Aug. 1	65.717	.165	6.05	+ .67
2	66.806	.409	6.16	+ .71
4	68.715	.836	5.65	+ .59
6	70.778	.297	6.14	+ .72
7	71.731	.510	6.11	+ .67
8	72.771	.743	5.72	+ .60
9	73.760	.964	5.77	+ .60
10	74.823	.202	6.06	+ .71
1949 July 4	102.815	.553	6.06	+ .67
5	03.811	.778	5.69	+ .59
Aug. 3	32.708	.241	6.09	+ .69
5	34.771	.702	5.81	+ .60
7	36.729	.140	6.03	+ .69
29	58.674	.048	5.91	+ .635
30	59.680	0.273	6.12	+0.71
	FN Aquilae 19h10m3 +03°28′2 (Fig. 30) Max. = JD2430812.87 +9d48224E, log P = 0.98			
1949 June 19	2433087.910	0.926	8.83	+0.93
22	90.900	.242	9.54	+1.17
23	91.862	.343	9.83	+1.195
24	92.903	.453	9.83	+1.20
25	93.890	.557	9.58	+1.13
26	94.904	.664	9.34	+1.06
27	95.878	.767	9.11	+0.98
28	96.875	.872	8.83	+0.88
Aug. 16	145.767	.028	9.00	+0.98
17	46.750	.132	9.20	+1.07
23	52.725	.762	9.08	+0.99
24	53.731	.868	8.87	+0.91
25	54.729	0.973	8.91	+0.95
	YZ Sagittarii 18h46m6 −16°47′0 (Fig. 31) Max. = JD2419741.43 +9d55345E, log P = 0.98			
1949 June 24	2433092.878	0.553	8.65	+1.05
25	93.861	.655	8.27	+0.96
26	94.865	.760	7.87	+0.84
28	96.845	.968	7.56	+0.75
30	98.858	.178	7.99	+0.91
July 25	123.790	.788	7.82	+0.82
27	25.781	.997	7.56	+0.75
Aug. 16	45.726	.084	7.80	+0.80
17	46.733	.190	8.02	+0.92
18	47.746	.296	8.22	+0.985
19	48.750	.401	8.47	+1.04
23	52.705	.815	7.69	+0.77
25	54.712	0.025	7.60	+0.76

TABLE 6—*Continued*

Date	JD	Phase	P_{g_p}	C_p
	ζ Geminorum 7^h01^m2 +20°38′8 (Fig. 32) Max. = JD2410639.801 +10^d153527E, log P = 1.01			
1948 Oct. 16	2432841.971	0.646	4.33	+0.60
23	48.955	.334	4.86	+ .84
Nov. 4	60.958	.516	4.53	+ .69
8	65.035	.918	4.60	+ .72
26	82.875	.675	4.31	+ .61
27	83.863	.772	4.34	+ .62
29	85.881	.971	4.67	+ .74
Dec. 1	87.870	.167	5.06	+ .90
1949 Oct. 26	3217.017	.584	4.40	+ .62
Nov. 12	33.930	.249	4.99	+ .89
17	38.951	0.744	4.32	+0.59
	T Monocerotis 6^h22^m5 +07°07′0 (Fig. 33) Max. = JD2428193.08 +27^d018E, log P = 1.43			
1948 Sept. 14	2432809.996	0.883	7.52	+1.12
18	13.979	.030	6.27	+0.80
19	14.970	.067	6.34	+0.83
25	21.010	.291	7.13	+1.19
26	22.003	.327	7.25	+1.21
29	25.008	.439	7.51	+1.26
Oct. 6	31.990	.697	7.82	+1.34
7	33.021	.735	7.82	+1.32
16	41.964	.066	6.37	+0.81
23	48.938	.324	7.28	+1.21
Nov. 4	60.972	.770	7.76	+1.24
8	65.014	.919	7.15	+1.02
26	82.835	.579	7.75	+1.34
27	83.962	.621	7.79	+1.355
29	85.899	.692	7.82	+1.33
Dec. 1	87.844	.764	7.79	+1.265
1949 Oct. 26	3216.979	.946	6.80	+0.875
Nov. 17	38.889	0.757	7.80	+1.265
	SV Vulpeculae 19^h49^m5 +27°19′9 (Fig. 34) Max. = JD2429025.37 +45^d145E, log P = 1.65			
1948 July 28	2432761.740	0.764	9.12	+1.41
31	64.781	.831	8.23	+1.12
Aug. 1	65.764	.853	7.85	+0.98
2	66.840	.877	7.68	+0.94
4	68.740	.919	7.66	+0.96
6	70.847	.965	7.78	+1.02
7	71.792	.986	7.81	+1.04
8	72.844	.010	7.90	+1.08
9	73.788	.031	7.98	+1.14
10	74.844	.054	8.10	+1.22
12	76.927	.100	8.18	+1.28
13	77.830	.120	8.33	+1.34
14	78.816	.142	8.18	+1.33
15	79.826	.164	8.27	+1.35
16	80.820	.186	8.23	+1.35
20	84.771	0.274	8.53	+1.46

TABLE 6—*Continued*

DATE	JD	PHASE	P_{fp}	C_p
	SV Vulpeculae 19h49m5 +27°19'9 (Fig. 34) Max = JD2429025.37 + 45d145E, log P = 1.65			
Sept. 2	2432797.807	0.563	9.28	+1.60
14	809.719	.826	8.06	+1.14
27	22.804	.110	8.15	+1.30
Oct. 16	41.662	.534	9.07	+1.58
23	48.699	.690	9.28	+1.60
Nov. 4	60.597	.954	7.61	+1.01
1949 June 24	3092.948	.100	8.22	+1.26
25	93.955	.123	8.17	+1.29
26	94.948	.145	8.30	+1.36
27	95.948	.167	8.30	+1.345
28	96.936	.189	8.35	+1.38
30	98.944	.233	8.54	+1.40
July 3	101.958	.300	8.69	+1.50
4	02.948	.322	8.72	+1.515
5	03.951	.344	8.77	+1.52
25	23.910	.786	8.87	+1.29
27	25.910	.830	8.03	+1.06
28	26.917	.853	7.77	+0.97
Aug. 2	31.753	.960	7.83	+1.02
3	32.715	.981	7.85	+1.03
4	33.781	.005	7.96	+1.06
5	34.913	.030	7.95	+1.10
7	3136.736	.070	8.13	+1.195
8	37.764	.093	8.27	+1.24
23	52.812	.426	8.84	+1.51
24	53.826	.449	8.93	+1.515
25	54.802	0.470	8.98	+1.53

which shows that the period–color-amplitude relation for the type C cepheids has the same slope as that for types A and B but is displaced 0.16 mag. from the latter.

From a plot of the light-amplitudes of the type C stars in Figure 36 it appears that, although these amplitudes could be roughly fitted with two linear relations indicated by broken lines, both parallel to the period–light-amplitude relations (6) and (7) for the type A and type B stars, individual deviations would be somewhat larger than those found for the latter cases. The constant ratio of 2.7 between light- and color-amplitudes, found for types A and B, is not valid for those of type C; this ratio varies from 2.4 for ζ Geminorum to 3.5 for YZ Sagittarii.

RELATION BETWEEN VELOCITY- AND LIGHT-AMPLITUDES

In Table 8 the observed radial-velocity amplitudes of the stars in Table 7 are compared with those computed from expression (5). The velocity-amplitudes of FF Aquilae, T Monocerotis, and SV Vulpeculae were kindly provided by Dr. R. F. Sanford in advance of publication and are preliminary values. With the exception of SV Vulpeculae, the agreement is good, and relation (3) apparently holds for type C as well as for types A and B—at least up to periods of 27 days.

ASYMMETRY OF LIGHT-CURVES

The four light-curves in Figures 29, 30, 31, and 32 differ in form from the curves of types A and B of corresponding periods. Like those of type A, the type C curves are free

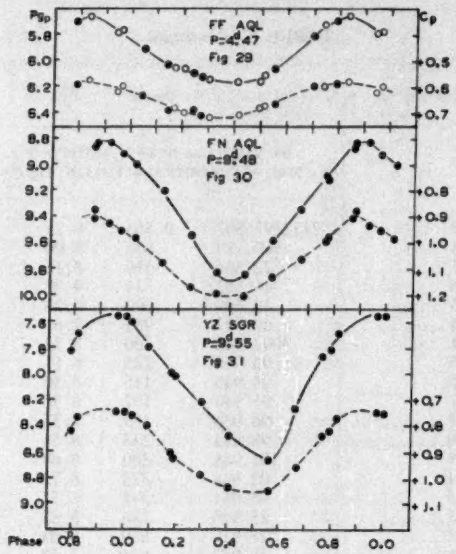

FIGS. 29–31.—Light- and color-curves of cepheids of type C. The open circles indicate observations made in 1948; the filled circles, observations made in 1949.

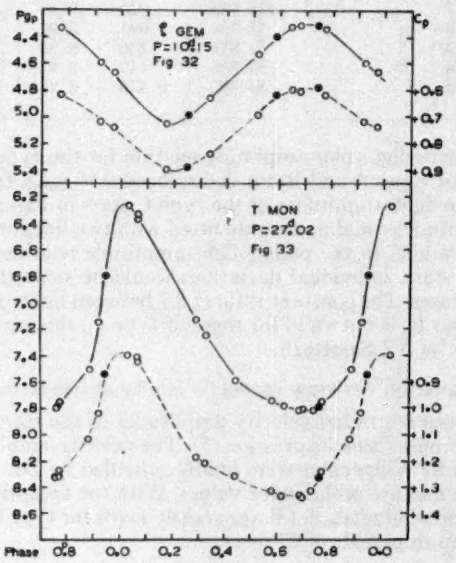

FIGS. 32–33.—Light- and color-curves of cepheids of type C. The open circles indicate observations made in 1948; the filled circles, observations made in 1949.

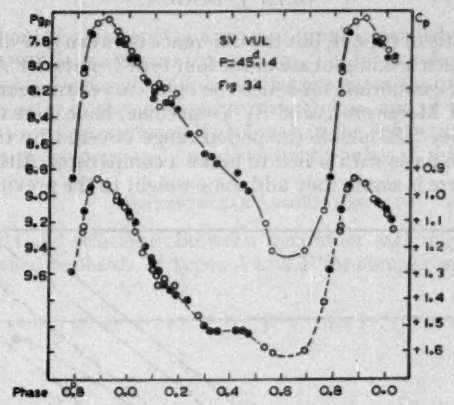

FIG. 34.—Light- and color-curves of cepheids of type C. The open circles indicate observations made in 1948; the filled circles, observations made in 1949.

TABLE 7

MAXIMUM, MINIMUM, AND CHANGE IN COLOR AND IN MAGNITUDE OF SIX CEPHEIDS OF TYPE C

STAR	LOG P	C_p		ΔC_p			Pg_p		ΔPg_p
		Max.	Min.	Obs.	Comp.	O−C	Max.	Min.	
FF Aql.....	0.65	+0.59	+0.71	0.12	0.12	0.00	5.66	6.17	0.51
FN Aql.....	0.98	+ .89	+1.20	.31	.31	.00	8.82	9.90	1.08
YZ Sgr.....	0.98	+ .74	+1.05	.31	.31	.00	7.55	8.65	1.10
ζ Gem.....	1.01	+ .59	+0.91	.32	.32	.00	4.30	5.06	0.76
T Mon.....	1.43	+ .80	+1.37	.57	.56	+ .01	6.26	7.82	1.56
SV Vul.....	1.65	+0.96	+1.64	0.68	0.68	0.00	7.65	9.48	1.83

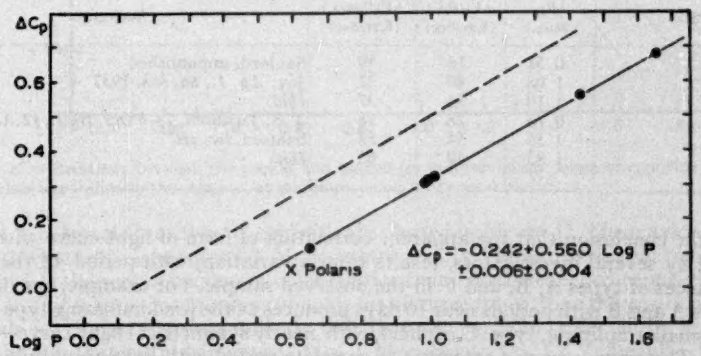

FIG. 35.—Period–color-amplitude relation for cepheids of type C. The broken line represents the relation valid for variables of types A and B.

of bumps characteristic of type B, but the difference between rate of increase and rate of decrease of light is much less in the case of the four type C stars, FF Aquilae, FN Aquilae, YZ Sagittarii, and ζ Geminorum, for which the light-curves are nearly symmetrical. The longer-period stars, T Monocerotis and SV Vulpeculae, have more unsymmetrical light-curves; but, since they fall outside the period range covered by the cepheids of types A and B, we have no basis with which to make a comparison. Although the number of type C stars given here is small, they add some weight to the previous discussion, which

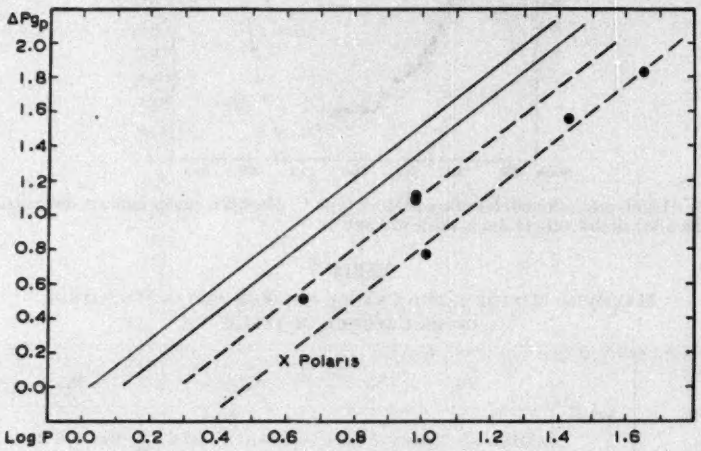

FIG. 36.—Relation between the period and light-amplitudes of the cepheids of type C. The continuous lines represent the relations found for the variables of types A and B; the broken lines possible ones for type C.

TABLE 8

COMPARISON OF LIGHT-AMPLITUDE AND VELOCITY-AMPLITUDE FOR CEPHEIDS OF TYPE C

Star	ΔP_{g_p} (Mag.)	ΔV(Obs.) (Km/Sec)	ΔV(Comp.) (Km/Sec)	Authority
FF Aql	0.51	16	19	Sanford, unpublished
FN Aql	1.08	40	37	Joy, *Ap. J.*, **86**, 363, 1937
YZ Sgr	1.10	34	37	*Ibid.*
ζ Gem	0.76	28	28	T. S. Jacobsen, *Lick Obs. Bull.*, **12**, 138, 1926
T Mon	1.56	54	53	Sanford, *loc. cit.*
SV Vul	1.83	49	62	*Ibid.*

led to the conclusion that the apparent correlation of form of light-curve with period, studied by several investigators, results from a variation, with period, of the relative abundances of types A, B, and C in the observed sample. For example, the deficiency of types A and B with periods near 10 days produces as the predominating type the relatively small-amplitude, type C cepheid, with nearly symmetrical light-curve—ζ Geminorum. The many previous attempts to correlate period with light-amplitude have invariably shown a break at periods near 10 days, but we can now see that the break probably results from a relative deficiency of type A and type B cepheids with periods close to 10 days.

Some mention should be made of the apparent break in the light-curve of SV Vulpeculae that occurs at 10–12 days after maximum light. The four cycles covered by the photoelectric observations in 1948 and 1949 show a large scatter at this point, as can be seen in Figure 34. The scatter in the color-curve is much less, and, if it is real, it is partially masked by observational inaccuracies. This break in the light-curve probably is real, for it appears in nearly every previously published light-curve of this star.

INTERSTELLAR ABSORPTION

Figure 37 repeats the relations (between maximum and minimum colors and the periods) of unreddened cepheids of types A and B for comparison. The maximum and

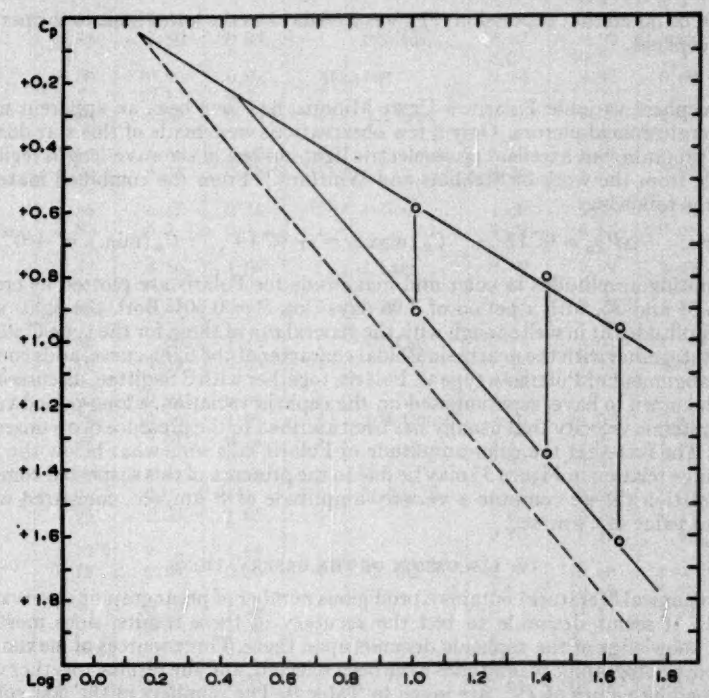

FIG. 37.—Relations between the period and maximum and minimum colors of cepheids of type C. The broken line indicates the relation, at minimum color, for types A and B.

minimum colors of three type C cepheids are plotted in Figure 37. The maximum colors of the three stars ζ Geminorum, T Monocerotis, and SV Vulpeculae appear to fit relation (6), which is the period–maximum-color relation found for unreddened cepheids of types A and B. If it is true that relation (6) holds for all three types, then the positions of these cepheids in Figure 37 would indicate that they are negligibly affected by absorption. Also, the fact that the maximum colors of T Monocerotis and SV Vulpeculae, like those of δ Cephei in Figure 28, fall 0.02 or 0.03 mag. above the period–maximum-color relation probably means that some of the stars used in determining this relation are slightly reddened. The minimum colors of these three type C stars fall above the period–mini-

mum-color relation derived for types A and B, as we would expect from a comparison of relations (3) and (8). Combining relations (6) and (8), we find relation (9) for the period–minimum-color relation as follows:

$$\text{Types A, B, and C:} \quad C_p\,(\text{max.}) = -0^m.04 + 0.61 \log P\,, \tag{6}$$

$$\text{Type C:} \quad \Delta C_p = -0^m.24 + 0.56 \log P\,; \tag{8}$$

$$\text{Type C:} \quad C_p\,(\text{min.}) = -0^m.28 + 1.17 \log P\,, \tag{9}$$

$$\text{Types A and B:} \quad C_p\,(\text{min.}) = -0^m.11 + 1.19 \log P\,. \tag{7}$$

It should be noted that expression (8) gives 2.68 days as the lower limit to the period of a type C cepheid.

POLARIS

The cepheid variable Polaris, α Ursae Minoris, has long been an apparent misfit in the general cepheid picture. Only a few observations were made of this star during the present program, but excellent photoelectric light-curves, in six wave-length regions, are available from the work of Stebbins and Whitford.[11] From the combined material we derive the following:

$$\text{Polaris:} \quad \Delta P g_p = 0^m.15\,, \quad C_p\,(\text{max.}) = +0^m.49\,, \quad C_p\,(\text{min.}) = +0^m.55\,.$$

The resulting amplitudes in color and magnitude for Polaris are plotted as crosses in Figures 35 and 36, with a period of 3.96 days ($\log P = 0.60$). Both the light- and the color-amplitudes fit in well enough with the general run of those for the type C stars, and this fact, together with the nearly sinusoidal character of the light-curve, adds confidence to the assignment of Polaris to type C. Polaris, together with S Sagittae, discussed below, are both known to have, superimposed on the cepheid variation, a long-period variation in the systemic velocity that usually has been ascribed to the presence of an unseen companion. The fact that the color-amplitude of Polaris falls somewhat below the period–color-range relation in Figure 35 may be due to the presence of this suspected companion. From relation (5) we compute a velocity-amplitude of 8 km/sec, compared with the observed value of 6 km/sec.

IV. DISCUSSION OF THE OBSERVATIONS

Astronomical literature contains a prodigious number of photographic observations of cepheids. It seems desirable to test the accuracy of these results, since most of our present knowledge of the cepheids depends upon them. Three sources of maximum and minimum photographic magnitudes have been selected, and the results, together with the corresponding values of Pg_p, are given in Table 9. The numbers in the last column of the table refer to the following sources: (1) Tables 2 and 7. (2) *General Catalogue of Variable Stars*.[3] This catalogue contains maximum and minimum magnitudes taken from what the compilers considered the most reliable light-curves available. When visual magnitudes are given in this reference, they have been omitted from Table 9. (3) L. V. Robinson.[6] From a large number of plates taken at the Harvard College Observatory, with scales ranging from 390″ to 1300″ per millimeter, Robinson has determined light-curves for 106 cepheids brighter than magnitude 12. The stated mean error of a single observation is 0.06 mag., and, since each light-curve consists of at least 200 observations and many of them of several fold more, the magnitude range should be quite accurately determined. (4) C. P. and S. Gaposchkin.[12] They have published light-curves for several

[11] *Ap. J.*, 103, 108, 1946. [12] *Harvard Ann.*, Vol. 115, Nos. 12, 23, and 24, 1950.

TABLE 9

COMPARISON OF PHOTOGRAPHIC AND PHOTOELECTRIC AMPLITUDES

Star	P_g(Max.)	P_g(Min.)	ΔP_g	Source	Star	P_g(Max.)	P_g(Min.)	ΔP_g	Source
SZ Tau	6.93	7.49	0.56	1	U Aql	6.68	7.84	1.16	1
	6.9	7.5	0.6	2		6.91	7.65	0.74	3
	6.66	7.26	0.60	3		6.71	7.50	0.79	4
SS Sct	8.50	9.21	0.71	1	η Aql	3.94	5.11	1.16	1
	8.8	9.6	0.8	2		3.82	4.54	0.72	4
	8.05	8.87	0.82	3					
	9.52	9.93	0.41	4	RX Cam	8.00	9.24	1.24	1
						8.0	9.4	1.4	2
SU Cyg	6.68	7.54	0.86	1					
	6.85	7.80	0.95	3	FN Aql	8.82	9.90	1.08	1
						8.8	10.0	1.2	2
Y Lac	9.09	10.06	0.97	1		9.32	9.92	0.60	4
	9.3	10.1	0.7	2					
	8.30	8.84	0.54	3	YZ Sgr	7.55	8.65	1.10	1
						7.8	8.6	0.8	2
T Vul	5.68	6.68	1.00	1		7.62	8.41	0.79	3
	5.96	6.84	0.88	3		8.25	9.07	0.82	4
FF Aql	5.66	6.17	0.51	1	ζ Gem	4.30	5.06	0.76	1
	5.8	6.2	0.4	2		4.20	4.85	0.65	3
V350 Sgr	7.48	8.56	1.08	1	Z Lac	8.50	9.99	1.49	1
	7.6	8.6	1.00	2		8.6	9.9	1.3	2
	8.37	8.83	0.46	4		8.43	9.79	1.36	3
δ Cep	3.90	5.00	1.10	1	TT Lac	7.15	8.94	1.79	1
	3.90	4.55	0.65	3		7.43	9.11	1.68	3
						8.01	9.21	1.20	4
BG Lac	9.00	9.94	0.94	1					
	9.35	10.36	1.01	2	RW Cas	9.40	11.03	1.63	1
	8.89	9.61	0.72	3		9.7	11.4	1.7	2
						9.49	10.67	1.18	3
Y Sgr	5.82	6.92	1.10	1					
	5.9	7.0	1.1	2	X Cyg	6.36	8.06	1.70	1
	5.95	7.00	1.05	4		7.0	8.2	1.2	2
						6.70	8.12	1.42	3
FM Aql	8.73	9.78	1.05	1					
	8.78	9.34	0.56	4	SZ Aql	8.70	10.60	1.90	1
						7.93	10.49	2.56	3
X Vul	9.36	10.54	1.18	1		9.25	11.17	1.92	4
	9.5	10.5	1.00	2					
	8.84	9.53	0.69	3	WZ Sgr	8.03	9.87	1.84	1
						8.2	10.0	1.8	2
RR Lac	8.83	10.05	1.22	1		7.91	10.08	2.17	3
	9.0	10.2	1.2	2		9.10	10.37	1.27	4
	8.71	9.86	1.15	3					
					T Mon	6.26	7.82	1.56	1
XX Sgr	9.06	10.14	1.08	1		6.45	8.08	1.63	3
	9.0	10.5	1.5	2					
	8.88	10.04	1.16	3	SV Vul	7.65	9.48	1.83	1
	9.44	10.50	1.06	4		7.7	9.5	1.8	2
U Sgr	6.88	8.02	1.14	1					
	7.3	8.5	1.2	2					
	7.33	8.49	1.16	3					
	6.99	8.40	1.41	4					

of the cepheids in Tables 2 and 7, based on Harvard patrol plates. They have estimated the probable error of the normal places used in determining their light-curves as 0.02 mag.,[13] so that the light-amplitudes should be very accurate.

An inspection of Table 9, however, is discouraging. For example, the amplitude of δ Cephei, derived photographically, is nearly a half-magnitude less than the photoelectric amplitude, ΔPg_p. Although Robinson states that the images of this star were overexposed on the Harvard plates, he nevertheless thought that perhaps the photographic amplitude was smaller than the visual amplitude found earlier by Stebbins,[14] because of intrinsic changes in the star. The relatively stunted photographic curves, moreover, are not confined to the bright stars, since the light-amplitude of the ninth-magnitude star FN Aquilae, determined by the Gaposchkins, is little more than half that found for the range in Pg_p, although the light-amplitude given in the Russian catalogue (see n. 2) exceeds the Pg_p value by 0.1 mag. The Harvard value for the magnitude at minimum light differs from Pg_p by only 0.02 mag., but the magnitude at maximum differs by 0.5 mag.

Perversely enough, one of the better agreements between the Pg and Pg_p amplitudes for the stars in Table 9 is for Y Sagittarii, the one star in the table for which a variation in light-amplitude has come to be accepted.[15] A systematic comparison of zero points for the magnitudes given in Table 9 is impossible, since the difference $Pg_p - Pg$ for the values of Pg given by the Gaposchkins ranges from -0.1 to $+1.1$ mag.; a comparison with references 2 or 3 is only slightly better.

We can agree with Mrs. Gaposchkin's conclusion that "the interest and flexibility of the study of variable stars have resulted in a vast accumulation of material of many kinds and quality, and this material must be sifted before an effective use can be made of it. The critical must be separated from the uncritical, the responsible from the irresponsible."[16]

FORM OF THE PERIOD-LUMINOSITY RELATION

With the possible exception of the Russell-Hertzsprung diagram, astrophysical literature probably contains more references to this correlation of observational data than to any other single subject. Since the period-luminosity relation, as we now know it, is based mainly on photographic observations of the cepheids in the Magellanic Clouds, the results of the comparison in the foregoing subsection indicate that perhaps many previous formulations of the relation should not be taken too seriously. Some reasons why this relation should be examined more closely are given below.

In the preceding discussion of the colors of the cepheids of types A, B, and C, it was shown that the differences in the period–color-range relations probably are caused by a differencé, from type to type for a given period, in the minimum colors, since the period–maximum-color relation appears to be the same for all types. If this inference is true, then it would seem best to use magnitudes of maximum light in the formulation of period-luminosity relations, since the use of median or mean magnitudes may lead to spurious discontinuities caused by variations in the relative abundances of the different types of variables. We have evidence that such discontinuities are present in the period-luminosity relation that was formerly derived from the cepheids in the Small Magellanic Cloud. For example, from a rediscussion of the Harvard observations of those cepheids, B. W. Kukarkin[17] has shown that a break exists in the slope of the period-luminosity relation for periods near 10 days. It is probably not a coincidence that this discontinuity in the period-luminosity relation corresponds to a radical change in the form of the mean light-curve, described above. Also the cause is undoubtedly the same, that is to say, a sudden change in the relative abundance of cepheids of types A and B compared to those

[13] *A.J.*, **52**, 218, 1947.

[14] *Ap. J.*, **27**, 188, 1908.

[15] Cf. P. ten Bruggencate, *Harvard Circ.*, No. 351.

[16] *Proc. Amer. Phil. Soc.*, **81**, 192, 1939.

[17] *A.J. Soviet Union*, **14**, 127, 1937.

of type C. We conclude that either the type C cepheids should be eliminated from the period-luminosity relation, or, since the colors indicate that stars of all three types form a homogeneous group at maximum light, magnitudes at maximum, instead of the mean or median, should be used. We shall show the result of such a procedure when applied to a representative set of photographic data.

Shapley and Mrs. Nail[18] have given maximum and minimum *Pg* magnitudes of selected cepheids in the Large and Small Magellanic Clouds. We have plotted the resulting light-amplitudes in Figure 38. The solid lines drawn in the figure have the same slope as that of relations (1) and (2) but have seven times the separation between them, to allow for the larger accidental errors in the photographic magnitudes. The few stars indicated by crosses will be discussed in more detail below. The filled circles probably represent stars of types A and B and perhaps some of type C, whereas the open circles indicate, besides stars of type C, those stars whose observed amplitudes are stunted because of various observational difficulties.

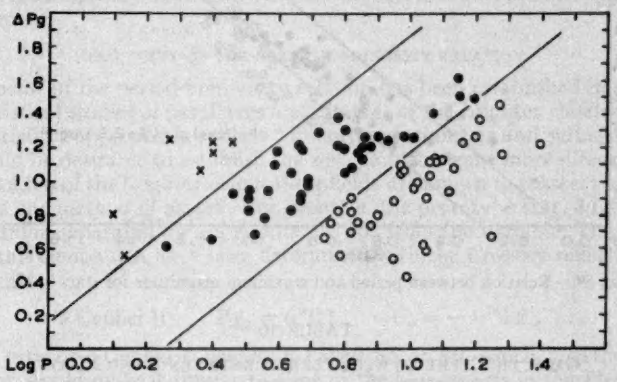

FIG. 38.—Relation between period and photographic amplitude for selected cepheids in the Magellanic Clouds (Shapley and Mrs. Nail).

Figure 39 is a correlation diagram between the periods and magnitudes at maximum; the crosses and filled and open circles indicate corresponding stars from Figure 38. The lines drawn in Figure 39 divide the stars into nearly the same three groups as in Figure 38. The mean relation between period and magnitude at maximum for the stars indicated by filled circles is

$$\text{Probable types A and B:} \qquad Pg\,(\text{max.}) = 17^{m}.2 - 2.9 \log P\,. \qquad (10)$$

The fact that some stars (indicated by open circles) fall below the general run of filled circles in Figures 38 and 39 is puzzling. If the open circles represent stars whose observed amplitudes are stunted by the presence of companion or field stars, we should expect them to fall high, or too bright, in Figure 39. Perhaps stars of types A and B obey a different period-magnitude relation than do those of type C, but more accurate observational data are needed before this possibility can be investigated.

The stars marked in Figures 38 and 39 by crosses present another difficulty that can be overcome only with more accurate data. These stars for which $P < 3$ days are a representative sample of a much larger group known to exist in the Small Magellanic Cloud. Shapley[19] has pointed out that the period distribution of cepheids in the Small Cloud

[18] *Proc. Amer. Phil. Soc.*, **92**, 310, 1948.

[19] Cf. *Proc. Nat. Acad. Sci.*, **26**, 105, 1940.

is different from that for the known galactic cepheids, in that the maximum frequency is near $P = 2$ days instead of 4.8 days. A peculiar feature of these short-period cepheids is their large light-amplitudes; the mean amplitude of 100 stars with periods between 1 and 2 days is 0.8 mag., with a range from 0.5 to 1.8 mag. It is impossible to ascribe all these large amplitudes to observational error. The difficulty arises from the fact that, from the discussion of the cepheids of types A and B, we would expect stars in the 1–2-day period range to have very small light-amplitudes. Sixteen galactic cepheids with periods between 1 and 2 days are given in Table 10. The periods and light-amplitudes

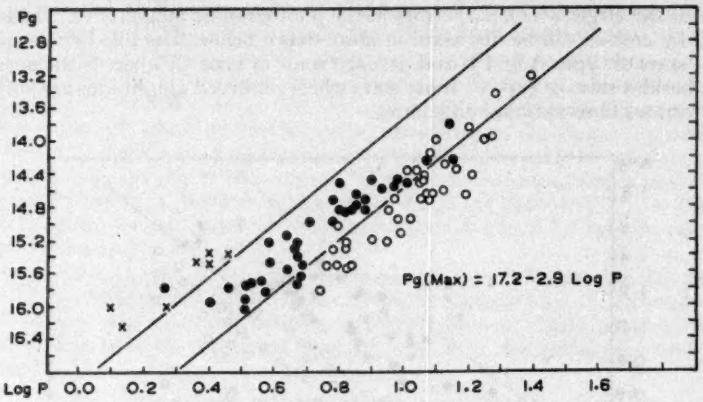

FIG. 39.—Relation between period and maximum magnitude for stars in Fig. 38

TABLE 10

GALACTIC CEPHEIDS WITH PERIODS BETWEEN 1 AND 2 DAYS

Star	Period (Days)	ΔP_g	Star	Period (Days)	ΔP_g
DE CrA	1.01	1^m1	KZ Cen	1.52	0^m6
BQ CrA	1.13	1.3	VW Mon	1.53	1.0
CE Her	1.20	1.2	SW Tau	1.58	1.6
V527 Sgr	1.26	0.7	DU Ara	1.64	1.3
BL Her	1.31	1.4	VZ Aql	1.67	1.4
VX Cap	1.33	1.7	SU Cas	1.95	0.4
XX Vir	1.35	1.7	GR Nor	1.96	0.5
HQ CrA	1.42	1.2	V477 Oph	1.97	1.3

for these stars have been taken from the *General Catalogue of Variable Stars*.[3] One star, UW Leonis, has been omitted, since unpublished photoelectric results indicate that it probably is a long-period red variable. The stars SU Cassiopeiae and GR Normae and perhaps KZ Centauri, with their relatively small ranges, may be cepheids of types A or B, but the remaining stars in Table 10 probably are the galactic counterparts of the short-period, large-range variables in the Small Magellanic Cloud. Some of the stars in Table 10 heretofore have been assigned for various reasons to the class of cluster-type variables. For example, Joy[20] has pointed out that the high-galactic-latitude stars SW Tauri and XX Virginis have spectra more like those of the cluster-type cepheids than

[20] *Ap. J.*, 110, 110, 1949.

like the classical variety, such as SU Cassiopeiae and DT Cygni. He places SW Tauri and XX Virginis in his group 1, which contains those variables in globular clusters whose periods range from 1.4 to 2.8 days and whose light-amplitudes range from 0.9 to 1.8 mag. More recently, Joy[21] has included CE Herculis, $P = 1.2$ days, in this group because of its high velocity and its spectral similarity to the cluster-type variables. We might conclude that, with the exception of the three small-amplitude stars mentioned above, the cepheids in Table 10 are all of the cluster type. If this deduction is true, then there is no need to account for the variables of abnormally large light-amplitudes and of short periods by relations (1) and (2) found for the classical cepheids of types A and B. Moreover, it is tempting to regard those stars in the Small Cloud having large amplitudes and short periods as cluster-type variables. Shapley and Mrs. Nail[18] have commented on the "great rarity, or complete absence, of cluster-type variables in the [Magellanic] Clouds," but it is possible that this rarity is only a matter of definition and that, by analogy with variables in our own galaxy, the large-amplitude, short-period stars in the Small Cloud, which distort the frequency distribution of periods, are, in reality, cluster-type variables of Joy's group 1.

ZERO POINT OF THE PERIOD-LUMINOSITY RELATION

The zero point of the period-luminosity relation has been established in the past by means of statistical studies of parallaxes and motions of the brighter classical cepheids. Since the statistical approach is subject to many uncertainties and serious systematic errors, it would be desirable to establish the zero point by some more direct procedure. The fact that a few of the brighter classical cepheids are known to possess physical companions offers one method of attack. For example, the prototype star, δ Cephei, has a fainter companion separated by approximately 40″ from the variable. The magnitude and color of this companion have been determined with the Crossley reflector with the following results:

$$\delta \text{ Cephei B:} \qquad Pg_p = 6^{m}.01 , \qquad C_p = -0^{m}.12 .$$

The spectral type of δ Cephei B usually is called B8 or B9, which, together with the observed color, would make it similar to some of the blue-dwarfs in the Pleiades.[22] Dr. G. H. Herbig kindly made a comparison of the spectrum of δ Cephei B with the spectra of several Pleiades stars, and he found a satisfactory match with stars of corresponding color. The similarity of δ Cephei B to Pleiades stars of corresponding spectral type is confirmed by unpublished six-color observations made at this observatory by Dr. Stebbins. If the companion to δ Cephei is a blue-dwarf, we find from Paper IV[23] of this series, for $C_p = -0^{m}12$, that $M = +0^{m}55$; thus $m - M = 6^{m}01 - 0^{m}55 = +5^{m}46$. If we apply this modulus to the magnitude of the variable at maximum light, $Pg_p = 3^{m}.90$, we obtain $M = -1^{m}.56$. Relation (10) then gives for the modulus of the Magellanic Clouds, $m - M = +16^{m}6$, which may be compared to the most recent value given by Shapley,[24] $+17^{m}32$. On the other hand, if we adopt Shapley's most recent period–median-magnitude relation,

$$Pg \text{ (median)} = 17^{m}.04 - 1.74 \log P ,$$

we find from the median absolute magnitude of δ Cephei a modulus of +16.78 mag., or a correction of −0.54 mag. to Shapley's modulus, or a correction or +0.54 mag. to the luminosities of the cepheids. From some of the same material used by Shapley, Kukarkin[17] has derived

$$Pg \text{ (median)} = 16^{m}.87 - 1.28 \log P \qquad (\log P < 0.96) ,$$

[21] *Pub. A.S.P.*, **62**, 60, 1950.
[22] *Ap. J.*, **111**, 81, 1950.
[23] *Ap. J.*, **112**, 141, 1950.
[24] *Proc. Nat. Acad. Sci.*, **26**, 541, 1940.

from which we find a modulus of +16.95 mag. The results from δ Cephei alone must be considered provisional, especially since δ Cephei B falls on the color-luminosity array at a place where small changes in C_p correspond to large changes in luminosity. Also there is some suggestion that the star may be a spectroscopic binary; but, when five or six other cepheid companions suitable for this purpose have been observed, an accurate zero point for the period-luminosity relation should be available. It is interesting to note that, since this important relation was found by Miss Levitt and developed by Shapley, several corrections to the zero point have been suggested, ranging from 0 to +1 mag.

INTERSTELLAR ABSORPTION

The existence of relations between the period and luminosity and between the period and maximum and minimum colors of the cepheids makes them objects of great value in sounding the interstellar medium. Since only the *selective* absorption is measured by the colors of the variables, to obtain the *total* absorption we must know the ratio $\chi = A(pg)/E_{int}$ between these two quantities. Two determinations, by photoelectric methods, of this ratio are available. In Paper II of this series a value of $\chi = 4.7$ was found from a highly reddened A star in the Pleiades. A. E. Whitford,[25] from an extension of the interstellar absorption-curve into the infrared, has confirmed the earlier result of Stebbins and Whitford[26] that $A(pg)/E_1 = 9.0$. F. H. Seares[27] has shown that $C_{int} = +1.90C_1 +$ const., of $\chi = 9.0/1.90 = 4.7$. We will adopt $\chi = 4.75$, a value in agreement with H. C. van de Hulst's[28] conclusion that "$A(Pg)/E = 4.5$ to 5.0 appears now to be the best theoretical extrapolation of Stebbins's [six] color measurements." As discussed above, neither the form nor the zero point of the period-luminosity relation has as yet been determined with satisfactory precision, but for the present purpose we shall adopt the form of the relation given by Shapley and the preliminary zero point indicated by δ Cephei B. Using the mean of relations (1) and (2) between the magnitude ranges and periods of types A and B cepheids, we finally obtain the following period-luminosity relation:

$$M\,(\text{max.}) = +0^{m}.31 - 2.52 \log P\,. \qquad (11)$$

Individual distances derived from relation (11) will not be precise until more data are available for the zero point and form of this relation, but we can place some confidence in the resulting relative distances of the cepheids.

Table 11 contains the cepheids of types A, B, and C from Tables 2 and 7, with their distances computed from relation (11) and with $\chi = 4.75$. An inspection of this table shows at once the spotty nature of the absorbing material. For example, WZ, Y, and U Sagittarii, which fall within a 3° square, show large differences in absorption; WZ is in a relatively clear area, on the border of a large dark region in which Y and U fall. As expected, the relatively near cepheid, SZ Tauri, shows a large amount of reddening, since it lies in the Taurus dark cloud. RR and Z Lacertae are separated by less than a degree and appear to be at nearly the same distance. X Vulpeculae is the most highly reddened star in Table 11, but it is only 2° south of SV Vulpeculae, which, although about twice the distance of X, shows no appreciable absorption. Photographs of this region show that SV Vulpeculae lies in a bright star-cloud on the edge of the dark region in which X is involved. In regard to the distances given in Table 11, we repeat that they probably indicate only the correct order of magnitude, but we anticipate that only small corrections to the values of E will be necessary when definitive period–maximum- and period–minimum-color relations are established. Also, it remains to be determined whether all three types of cepheids follow the same period-luminosity relation.

[25] *Ap. J.*, **107**, 102, 1948.

[26] *Ap. J.*, **90**, 209, 1939; **91**, 20, 1940. [27] *Ap. J.*, **98**, 261, 1943.

[28] *Centennial Symposia* ("Harvard Observatory Monographs," No. 7 [1948]).

Some mention should be made of the absorption at the pole as derived from colors of Polaris given in Section III above. From relations (6) and (9) we compute for α UMi normal colors of C_p (max.) = +0^{m}33 and C_p (min.) = +0^{m}42, as compared to the observed values of +0.49 and +0.55 mag., respectively. The two values give a mean E = +0^{m}14, or A = 0^{m}66 if we ignore the possible effects of the suspected spectroscopic companion. The distance to Polaris computed from relation (11) is only 42 parsecs, or a parallax of 0".024. It may be significant that, from a combination of long-period spectroscopic elements and the astrometric results, B. P. Gerasimovič[29] found π =

TABLE 11

ABSORPTION AND DISTANCES OF 30 GALACTIC CEPHEIDS

Star	l	b	E	A_{P_g}	r(Kpc)	Star	l	b	E	A_{P_g}	r(Kpc)
SZ Aql....	3°3	− 3°8	+0.18	0.86	1.34	RR Lac...	73°4	− 2°1	+0.10	0.48	1.04
TT Aql....	3.7	− 4.6	+0.17	0.81	0.60	Z Lac.....	73.5	− 1.7	+0.14	0.66	1.07
FN Aql....	6.3	− 4.4	+0.325	1.54	0.77	RW Cas..	96.8	− 4.1	+0.095	0.45	1.31
η Aql.....	8.8	−14.5	0.00	0.00	0.14	RX Cam..	113.5	+ 5.6	+0.33	1.57	0.48
FM Aql...	12.0	− 0.5	+0.475	2.26	0.43	SZ Tau....	147.4	−17.3	+0.355	1.69	0.17
FF Aql....	16.8	+ 5.1	+0.235	1.12	0.15	ζ Gem....	163.4	+13.4	0.00	0.00	0.20
X Vul.....	31.6	− 2.4	+0.555	2.64	0.48	T Mon....	171.3	− 1.1	−0.03	0.00	0.81
SV Vul....	31.7	− 0.8	−0.01	0.00	1.26	WZ Sgr...	339.8	− 2.8	+0.06	0.28	1.46
SU Cyg...	32.4	+ 1.5	0.00	0.00	0.37	Y Sgr.....	340.5	− 3.7	+0.125	0.59	0.23
T Vul.....	40.0	−11.5	+0.025	0.12	0.28	U Sgr.....	341.4	− 5.9	+0.265	1.26	0.30
DT Cyg...	44.5	−11.6	+0.175	0.79	0.20	V350 Sgr..	341.4	− 9.4	+0.215	1.02	0.39
X Cyg.....	44.7	− 5.1	0.00	0.00	0.66	XX Sgr...	342.7	− 3.4	+0.325	1.54	0.71
BG Lac...	60.9	− 9.7	+0.22	1.04	0.79	YZ Sgr....	345.4	− 8.6	+0.175	0.83	0.60
Y Lac.....	66.5	− 4.3	+0.11	0.52	0.94	SS Sct....	352.9	− 3.3	+0.375	1.78	0.37
δ Cep.....	72.9	+ 0.4	−0.02	0.00	0.12	U Aql.....	358.7	−13.1	+0.20	0.95	0.32

0".024. Even though we assign up to 0.04 mag. of the reddening found for Polaris to the effects of the spectroscopic companion, it is surprising to find 0.10-mag. reddening in the relatively short distance of 40 parsecs.

SPECTRAL TYPES

Recent studies of spectra of the brightest cepheids have been made by O. Struve[30] and A. Code.[31] The latter has described the spectra as follows: "It is found that the general features of the cepheid spectra match those of standard supergiants well. The hydrogen lines, as pointed out by Struve, are abnormally strong at maximum, and the cyanogen band near λ 4215 is found to be abnormally weak at minimum." Table 12 contains Code's assignments of spectral types and luminosity classes at maximum and minimum light for nine of the cepheids contained in Tables 2 and 7, and, for comparison, the computed values of spectral types obtained from the normal colors in Table 5 and the relation between color and spectral type shown in Figure 40. Table 13 lists the values of C_p for some of the brighter supergiants, and the color–spectral-type correlation for these supergiants is illustrated in Figure 40. Although we might expect these stars to show some effect of interstellar reddening, apparently only α Aquarii shows a significant deviation from a linear relation, and a change of spectral type of one subclass would remove the discrepancy. The systematic character of the residuals in Table 12 is shown graphically in Figure 41, where the maximum and minimum colors and spectral types are plotted. The full line in Figure 41 represents the color–spectral-type relation of Figure 40. For cepheids in the period range of 5–8 days, the colors and spectral types at both

[29] *Ap. J.*, **84**, 229, 1936.

[30] *Observatory*, **65**, 257, 1944.

[31] *Ap. J.*, **106**, 309, 1947.

maximum and minimum light satisfy the same relationship that holds for the supergiants of luminosity class I*b*. The two stars with periods less than 5 days—DT Cygni and SZ Tauri—give a large systematic difference from both maximum and minimum spectral types, but one of these stars—DT Cygni—is classified as of luminosity classes I–II, whereas the stars in Figure 41 are all of class I*b*, so a luminosity effect may be present. The stars with periods longer than 5 days satisfy the relation of Figure 41 very well at

TABLE 12

SPECTRAL TYPES OF BRIGHT CEPHEIDS ACCORDING TO CODE

STAR	MAX. SP.			MIN. SP.		
	Obs.	Comp.	O−C	Obs.	Comp.	O−C
DT Cyg	F5.5	F2	+3	F7	F5	+2
SZ Tau	F6	F3	+3	F9	F6	+3
δ Cep	F5	F5	0	G2	G1	+1
η Aql	F6	F6	0	G4	G3	+1
ζ Gem	F7	F8	−1	G3	G3	0
Z Lac	F6	F8	−2	G6	G6	0
X Cyg	F7	G0	−3	G8	G9	−1
T Mon	F7	G1	−4	K1	K0	+1
SV Vul	F7	G3	−6	(K0)	.....	.....

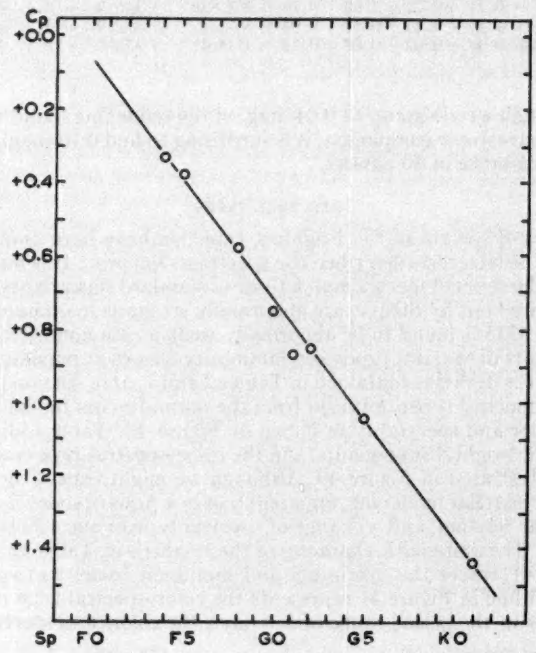

FIG. 40.—The color-spectral-type relation for standard stars of luminosity class I*b*

minimum light, but the constancy of spectral type at maximum light, suggested by Code, is not confirmed by the colors. Figure 41 bears out Struve's conclusion that "at minimum light the Cepheids belong to Morgan's luminosity class *Ib* . . . [and] . . . almost identically resemble the spectra of standard stars."

It is interesting that the mean color of Polaris, computed from relations (6) and (9), is +0.39 mag., which corresponds to a spectral type of F5, whereas the mean observed color, +0.52 mag., corresponds to type F7. Stebbins[32] has inferred, from a six-color study of Polaris, that the spectral type varies between cF6 and cF7. The spectral type is given as cF7 by the Mount Wilson observers and as F7 *Ib* on the Yerkes system.

TABLE 13

COLORS AND SPECTRAL TYPES OF STANDARD SUPERGIANTS

Star	Sp.	C_p	Star	Sp.	C_p
41 Cyg	F4 *Ib*	0^m33	α Aqr	G1 *Ib*	0^m89
α Per	F5 *Ib*	.38	β Dra	G2 *Ib*	0.87
γ Cyg	F8 *Ib*	.58	9 Peg	G5 *Ib*	1.04
β Aqr	G0 *Ib*	0.75	ζ Cep	K1 *Ib*	1.44

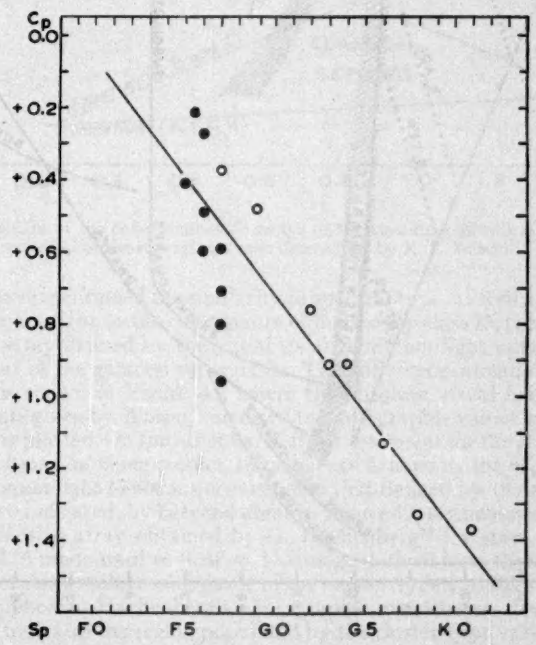

FIG. 41.—The color-spectral-type relation for the cepheids classified by Code. The filled circles represent the cepheids at maximum light, the open circles minimum light. The straight line is the color-spectral-type relation for the standard stars given in Fig. 40.

[32] *Ap. J.*, **103**, 108, 1946.

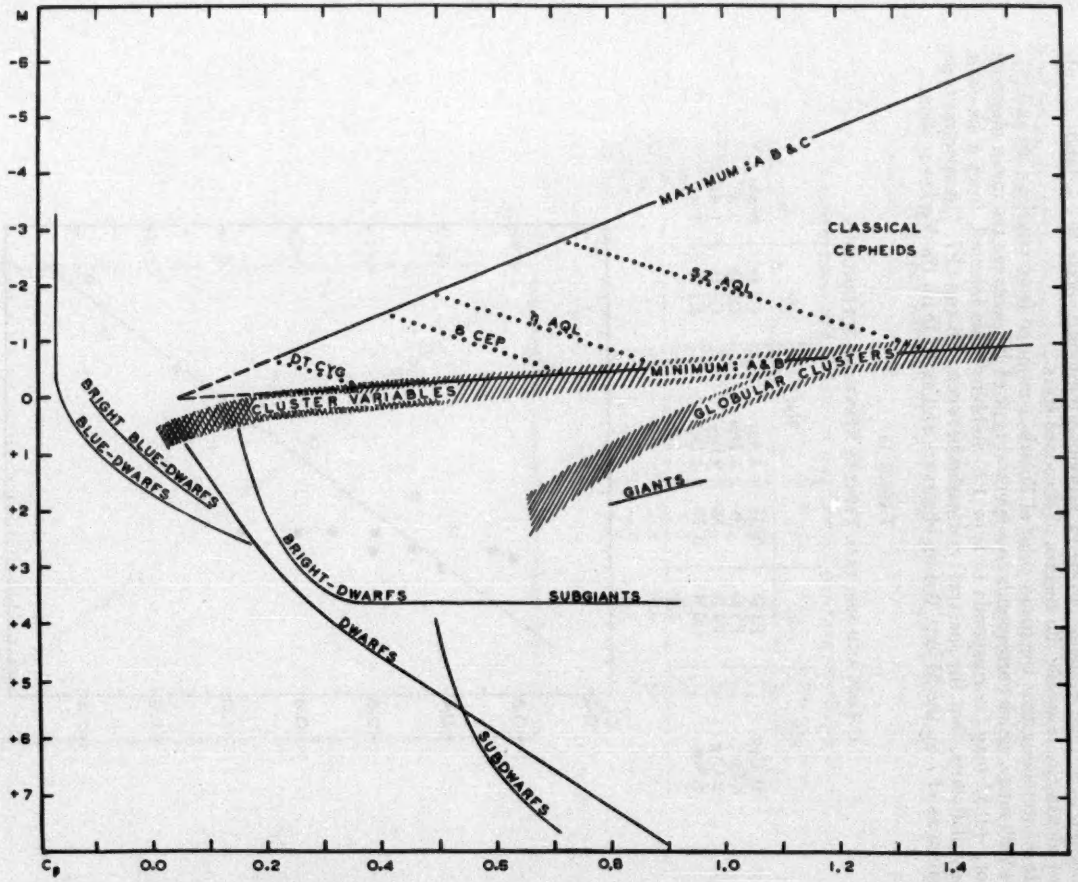

FIG. 42.—The color-luminosity array for stars near the sun, classical cepheids, and globular clusters. The dotted lines indicate the course of variation of the cepheids. The hatched areas are taken from Hachenberg's observations of M 92; the cross-hatched region represents that part of the array populated by cluster-type variables.

COLOR-LUMINOSITY ARRAY

If we combine relations (6) and (7), between period and color, and relation (11), between period and luminosity, we obtain relations between luminosity and colors of the cepheids at maximum and at minimum light. The resulting sequences in the color-luminosity array have been plotted in Figure 42; the array sequences given by stars near the sun, taken from Paper IV[23] of this series, are also shown in the figure. The small, 0.1-mag., difference between the light-amplitudes of cepheids of types A and B has been neglected in the figure. Also, the sequence of type C cepheids at minimum light has been omitted for two reasons: (1) we do not know whether the variables of type C obey the same period-luminosity relation as those of types A and B, and (2) the relation between light-amplitude and period is ill defined for variables of type C. The light- and color-variations for four representative cepheids—DT Cygni, δ Cephei, η Aquilae, and SZ Aquilae—are indicated by dotted lines in the figure. The relation of the color to the light-variation is actually a closed loop, but it would be impracticable to portray this phenomenon on the small scale of Figure 42.

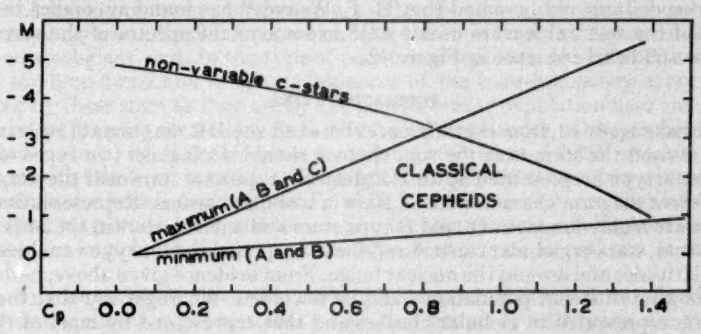

FIG. 43.—Comparison of the color-luminosity arrays of the classical cepheids and the nonvariable supergiants. The luminosities of the supergiants were determined by R. E. Wilson.

Although we have mentioned the similarity in spectral type, as well as in color, of the cepheids at minimum light to the supergiants of luminosity class *Ib*, the sequence in the color-luminosity array defined by the variables at minimum light appears to be quite different from that of the galactic supergiants. This difference, already pointed out by R. E. Wilson,[34] is shown in Figure 43, where the absolute visual magnitudes of the galactic supergiants given by Wilson, corrected to photographic values by the C_p's taken from Figure 40, are plotted. On the other hand, if our zero point for the period-luminosity relation is within $\frac{1}{2}$ mag. of being correct, the sequence defined by the type A and type B cepheids at minimum light looks suspiciously like that defined by the stars in globular clusters.[35] We have indicated, by hatched areas in Figure 42, a schematic representation of the color-luminosity array obtained by O. Hachenberg[36] for stars in the globular cluster Messier 92. A modulus of $m - M = 15.0$ mag., derived from the assumption that the mean photographic absolute magnitude of the cluster-type variables in the cluster is zero, has been applied to Hachenberg's photographic magnitudes. The cross-hatched area in Figure 42 indicates the region populated by the cluster-type variables. A similar color-luminosity array would be obtained by transforming Baade's[35] schematic representation of the HR diagram of globular clusters to photographic magnitudes and colors.

[33] *Ap. J.*, **112**, 141, 1950.

[34] *Ap. J.*, **93**, 212, 1941.

[35] W. Baade, *Ap. J.*, **100**, 137, 1944.

[36] *Zs. f. Ap.*, **18**, 72, 1939.

Even when we consider the possible errors in the assumed zero points of both the array determined for the globular cluster and that for the cepheids at minimum light, the correspondence in luminosity and color of the cepheids at minimum to the brightest stars in globular clusters is striking. This correspondence in position in the array is supported by spectroscopic considerations. We have already quoted Code's remark that the spectra of cepheids at minimum are almost perfectly matched by those of galactic supergiants of luminosity class I*b*, except for the fact that the spectral feature near λ 4215 is found to be abnormally weak in the cepheids. D. M. Popper[37] has found that the stars in the globular clusters Messier 3 and 13 with "color indices principally between +0.9 and +1.6 mag., are of spectral type G5–K0 and luminosity class I*b*. They are peculiar in that the *CN* absorption shortward from λ 4215 is weak."

Another striking feature of Figure 42 is the splitting of the globular cluster array near $M_{P_g} = 0$ and $C_p = +1$ and the run of one sequence toward lower luminosities. The downward direction of this latter sequence is very suggestive of a junction with the subdwarf sequence. It was shown in Paper IV that the subdwarf sequence was populated mainly, but not wholly, by high-velocity stars, that is to say, stars not native to the solar neighborhood. It should be noted that H. F. Weaver[38] has found anomalies in the intensities of the spectral feature near λ 4215 in some of the spectra of the stars which define the subdwarf sequence in Figure 42.

POPULATION TYPES

Baade has suggested, from the differences between the HR diagrams of stars in globular clusters and the stars near the sun, that we should distinguish two types of stellar populations: type I represented by an HR diagram typical of stars near the sun, type II by a different diagram characteristic of stars in globular clusters. Representative of the first type are highly luminous O- and B-type stars and open clusters in the Milky Way; of the second, stars in globular clusters and the short-period cluster-type variables in high galactic latitudes and around the nuclear bulge. From evidence given above, perhaps the criteria of kind of stellar population could be reworded. We might say that the stellar population represented in globular clusters and that represented by most of the stars near the sun differ mainly in relative abundance of stars populating the various sequences of *the* color-luminosity array or HR diagram. Baade's division into two types may represent the extremes of populations thus far observed; but, using more refined criteria, we are able to distinguish several other population types, or perhaps subtypes. For example, in Papers I and II of this series it was shown that a sequence of the color-luminosity array, termed the "blue-dwarf sequence," was heavily populated by Pleiades stars but not at all by Hyades stars. On the other hand, the dwarf sequence, for stars of type F and later, is populated in common by both clusters. Both clusters contain A-type stars, but those in the Pleiades populate the blue-dwarf sequence, while those in the Hyades populate the dwarf sequence. It is interesting in this connection to examine the results obtained by Struve[39] concerning the spectra of these cluster stars:

> If we compare critically, the main [dwarf] sequences of the two clusters, we find that at F9 and F8 the spectra are almost identically the same; even a somewhat superficial study fails to reveal systematic differences between the two groups. At the other end of the main sequence, where the two clusters overlap, namely at A1, the difference is most conspicuous and is definitely systematic in character. The Hyades are all much richer in the metallic lines, including not only FeI and FeII, but also CaI, SrII, and probably MgII and SiII. At the same time, the lines of H and probably those of CaII are much weaker in the Hyades than in the Pleiades. This effect is somewhat obscured in the case of the Pleiades, because of the large rotational velocities which

[37] *Ap. J.*, **105**, 204, 1947.

[38] *Pub. A.S.P.*, **62**, 50, 1950.

[39] *Stellar Evolution* (Princeton: Princeton University Press, 1950), p. 56.

are frequently found in that cluster but even allowing for the rotational broadening, it is a most conspicuous phenomena and one that cannot be attributed to observational effects. It is closely connected with the well-known tendency of the Hyades to possess members which W. W. Morgan described as having metallic-line spectra. It is, of course, also known that these metallic-line spectra are not present in the Pleiades.[40]

We see, then, that, when Pleiades and Hyades stars populate a sequence of the color-luminosity array in common, the spectra are similar, just as the cepheids at minimum light and the brightest stars in globular clusters populate the same sequence and show the same spectral peculiarities. Baade explains the absence of cluster-type cepheids in populations of type I by the fact that "since the short-period cepheids are localized in a well-defined, narrow strip of the HR plane, they can be expected in considerable number only in stellar populations which possess a high density in this particular region of the HR plane. This condition is fulfilled by the HR distribution of the stars in globular clusters. It is not fulfilled by the stars in the solar neighborhood . . . because their distribution exhibits the Hertzsprung gap."[35] This feature of the color-luminosity array will be discussed at more length in a future paper of this series dealing with the cluster-type variables. A similar argument, furthermore, can be offered as an explanation for the fact that no Algol-type eclipsing binaries, which were shown in Paper IV to consist of a blue-dwarf and a subgiant, exist in the type of population represented by the Hyades stars, because the blue-dwarf and subgiant sequences of the color-luminosity array are not populated by these stars as they are by the general stellar population near the sun.

If we adopt Baade's corrections to E. Hubble's[41] magnitudes of the cepheids in the Andromeda nebula, relation (11) gives a modulus $m - M = +22^m3$, which is in good agreement with Baade's[35] value of +22.4 mag. The brightest stars in the central region of the nebula, for which Baade gives $Pg = 21.3$ and $C = +1.3$, are then of absolute photographic magnitude −1.0, and they fall on the same sequence in Figure 42 as do the brightest stars in globular clusters and the type A and type B cepheids at minimum light.

To summarize the above discussion, although it appears that the more refined criteria used for distinguishing types of stellar population permit several types, the two large divisions given by Baade probably should be maintained, but the purity of any one type may be largely a matter of definition.

ANOMALOUS CEPHEIDS

1. *S Sagittae.*—The magnitudes and colors of S Sagittae are contained in Table 14 and plotted in Figure 44. The table and figure are arranged in the same manner as Table 1 and Figures 1–24. The observed ranges in C_p and Pg_p are 0.38 and 1.15 mag., respectively, as compared with the values 0.45 and 1.25 mag. computed from relations (3) and (2). Also, from Figure 44 we find Pg_p (max.) $= 5^m73$, Pg_p (min.) $= 6^m58$, C_p (max.) $= 0^m53$, C_p (min.) $= 0^m91$. S Sagittae is known to possess, in addition to the cepheid variation, a 676-day variation in systemic velocity.[42] It appears that S Sagittae is a type B cepheid, and the observed color and magnitude amplitudes are reduced by the presence of a spectroscopic companion. It should be noted that the position of the bump in the light-curve of this variable, a quarter-period after maximum light, fits into the progression of the phase of the bumps with period noted in Section II above. From the

[40] The absence of metallic-line stars in the Pleiades was first pointed out by H. Weaver (*Pub. A.S.P.*, 58, 247, 1946). This deficiency, however, probably applies only to those metallic-line stars showing large differences between the metallic- and hydrogen-line classifications. Weaver has recently suggested (*A.J.*, 55, 82, 1950) that nine metallic-line stars exist in the Pleiades.

[41] *Ap. J.*, 69, 104, 1929.

[42] Aldrich, *Pub. Obs. U. Michigan*, Vol. 4, 1932; and unpublished results obtained by J. H. Moore at this observatory.

TABLE 14

MAGNITUDES AND COLORS OF S SAGITTAE AND Y OPHIUCHI

DATE	JD	PHASE	P_{Bp}	C_p
	S Sagittae 19^h53^m8 $+16°30'.0$ (Fig. 44) Max. = JD2429091.48 $+8^d.3821723E$, log $P = 0.92$			
1948 Aug. 8	2432772.788	$0^p.183$	5.94	+0.63
9	73.778	.301	6.07	+ .67
15	79.816	.021	5.75	+ .55
16	80.792	.138	5.98	+ .61
20	84.767	.612	6.82	+ .91
25	89.863	.220	5.87	+ .60
26	90.840	.337	6.28	+ .74
27	91.844	.456	6.54	+ .84
1949 July 4	3102.809	.555	6.74	+ .89
5	03.816	.675	6.87	+ .92
18	16.844	.229	5.86	+ .61
Aug. 2	31.795	.013	5.74	+ .54
3	32.740	.126	5.96	+ .61
4	33.752	.246	5.91	+ .60
5	34.782	.369	6.35	+ .76
7	36.778	.607	6.80	+ .90
8	37.755	.724	6.85	+ .87
23	52.783	.517	6.65	+ .86
24	53.785	.636	6.82	+ .91
25	54.799	.757	6.68	+ .82
29	58.700	.223	5.88	+ .60
30	59.722	.345	6.31	+ .75
Sept. 18	78.680	.606	6.79	+ .90
19	79.674	.725	6.83	+ .87
20	80.674	.844	6.40	+ .715
Oct. 10	200.661	.229	5.88	+ .60
16	06.667	0.945	5.85	+0.57
	Y Ophiuchi 17^h50^m0 $-06°08'.2$ (Fig. 45) Max. = JD2408694.86 $+17^d.11884E$, log $P = 1.23$			
1948 Aug. 7	2432771.694	0.452	7.57	+1.29
8	72.708	.512	7.64	+1.32
9	73.705	.570	7.67	+1.31
12	76.708	.745	7.53	+1.25
14	78.728	.863	7.30	+1.15
16	80.719	.980	6.95	+1.07
1949 May 22	3059.930	.290	7.36	+1.23
23	60.938	.349	7.42	+1.24
24	61.919	.406	7.47	+1.265
25	62.924	.465	7.58	+1.31
26	63.906	.522	7.65	+1.32
June 1	69.889	.872	7.27	+1.14
15	83.854	.687	7.66	+1.28
19	87.852	.921	7.10	+1.11
21	89.837	.037	6.92	+1.07
22	90.835	.095	7.01	+1.10
23	91.809	.152	7.15	+1.16
24	92.816	.211	7.17	+1.16
25	93.788	.268	7.31	+1.22
26	94.785	.326	7.39	+1.24
27	95.792	.385	7.43	+1.23
28	96.781	.442	7.56	+1.29
30	98.771	0.559	7.68	+1.31

TABLE 14—*Continued*

Date	JD	Phase	Pg_p	C_p
	Y Ophiuchi 17h50m0 −06°08'.2 (Fig. 45) Max. = JD2408694.86 +17d11884E, log P = 1.23			
July 3.....	101.875	0d735	7.58	+1.26
4.....	02.792	.794	7.46	+1.22
5.....	03.799	.852	7.32	+1.18
Aug. 2.....	31.722	.484	7.61	+1.32
3.....	32.701	.541	7.64	+1.31
23.....	52.674	.707	7.63	+1.27
24.....	53.684	.766	7.50	+1.23
25.....	54.677	.824	7.39	+1.20
29.....	58.663	.057	6.95	+1.07
30.....	59.670	0.116	7.07	+1.14

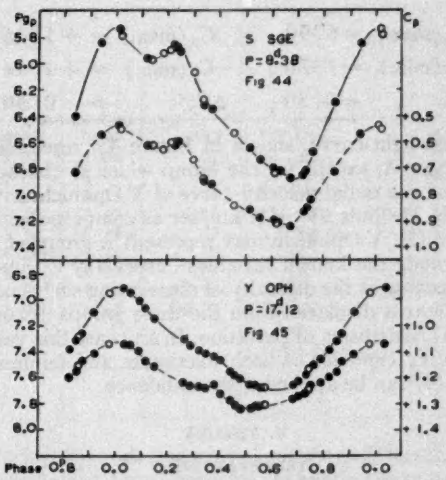

FIGS. 44 and 45.—Colors and magnitudes of S Sge and Y Oph. The broken curves represent the color variation, the full curves the light-variation. The open circles indicate observations made in 1948, the filled circles in 1949.

assumption that S Sagittae is a type B cepheid, we can compute the color and magnitude of the companion necessary to cause the observed diminution of the light- and color-curves. The best results are obtained from:

S Sge A: Pg_p (max.) = $5^m.79$ C_p (max.) = $+0^m.56$,

Pg_p (min.) = $7^m.04$ C_p (min.) = $+1^m.01$,

S Sge B: Pg_p = $8^m.9 \pm 0.1$, C_p = $+0^m.0 \pm 0.1$ } estimated uncertainty.

We conclude that, if the departure of S Sagittae from the period–color-amplitude and period–light-amplitude relations is interpreted as due to the presence of a companion star, that star is probably of late B or early A type. From relation (5) we can predict a radial-velocity amplitude, ΔV, of 43.2 km/sec from $\Delta Pg_p = 1^m.25$. From spectra taken with the Mills spectrograph of the Lick Observatory, T. S. Jacobsen[43] has obtained $V =$ 41.2 km/sec, which agrees tolerably well with the computed value. Aldrich, from spectra covering several cycles of the 8-day period, has given $\Delta V = 30.2$ km/sec for the cepheid variation freed of the effects of the long-period motion. He also found a second variation in the systemic velocity with one-half the pulsation period and with an amplitude of $\Delta V \sim 10$ km/sec. From a large amount of material gathered by J. H. Moore, plus the published observations, G. H. Herbig has recently found $\Delta V = 36.0$ km/sec for the radial-velocity amplitude, in the pulsation period freed of the long-period variation. The residual, O − C, from the value computed by expression (5) then becomes −7 km/sec, a value greatly exceeding any other in Table 3. Either (*a*) the long-period variation represents some phenomena other than, or in addition to, orbital motion, or (*b*) the relations (2), (3), and (5) are not valid for S Sagittae; the effects of the first alternative could cause the second.

2. *Y Ophiuchi.*—Table 14 and Figure 45 contain the results obtained for Y Ophiuchi. The magnitudes and colors, at maximum and minimum light, and their ranges are:

$$\begin{aligned} Pg_p\,(\text{max.}) &= 6^m.90\,, & C_p\,(\text{max.}) &= +1^m.06\,, \\ Pg_p\,(\text{min.}) &= 7^m.70\,, & C_p\,(\text{min.}) &= +1^m.36\,, \\ \Delta Pg_p &= 0.80\,, & \Delta C_p &= 0.30\,. \end{aligned}$$

The nearly symmetrical light-curve, shown in Figure 45, resembles those of type C rather than those of type A, except for the bump which is characteristic of type B. S. Albrecht[44] determined the radial-velocity-curve of Y Ophiuchi with a low, one-prism dispersion spectrograph. He finds $\Delta V = 17$ km/sec as compared with $\Delta V = 29$ km/sec computed from relation (5). Y Ophiuchi may represent a group of cepheids which are sparsely represented among the known variables—especially with periods shorter than that of Y Ophiuchi—because of the difficulty of discovering such small amplitudes. It is also possible that this star is displaced from the three groups discussed above because of some abnormality in constitution or pulsation. In any case this variable demonstrates the necessity of observing cepheids at both maximum and minimum light before expressions (6), (7), and (9) can be applied with confidence.

V. THEORY

TEMPERATURES

In recent years the pulsation theory of cepheid variation has come to be generally accepted. At least two astronomers, F. Hoyle and R. A. Lyttleton, however, regard it as a "vague alternative hypothesis"[45] to the older, binary theory. Since, in the words of these theorists, the binary hypothesis "is of such surpassing intractability, as far as details are concerned, that it is scarcely possible to extract from the theory more than general indications of the kind of temperature ranges likely to occur,"[45] we shall not consider it here.

From considerations of black-body radiation and with $C_p = +0.49$ (G0) and $T =$ 6000° for the sun, we find

$$T = \frac{7200}{C_p + 0.71}\,. \tag{12}$$

[43] *Lick Obs. Bull.*, 13, No. 393, 112, 1927.

[44] *Lick Obs. Bull.*, 4, No. 118, 130, 1907.

[45] *Observatory*, 69, 65, 1949.

Differentiating Stefan's law, we have

$$\Delta P_{\text{bol}} = -2.17\frac{\Delta R}{R} - 4.35\frac{\Delta T}{T}. \tag{13}$$

Since at both maximum and minimum light the cepheids have, according to the pulsation theory, intermediate radii, ΔR is small, and the bolometric ranges, ΔP_{bol}, must be given substantially by ΔT. If we substitute in equation (13) expression (12) for T, the range in bolometric magnitude should be closely predictable from

$$\Delta P_{\text{bol}} = 4.35\frac{\Delta C_p}{\bar{C}_p + 0.71}. \tag{14}$$

This expression shows that the bolometric ranges can be computed directly from the color ranges. As a first step in comparing computed bolometric ranges with observation, we shall compare ΔP_{bol} with ΔPg_p, and we should expect the former to be considerably smaller than the latter. Table 15 shows the result of the comparison for cepheids of types

TABLE 15

COMPARISON OF COMPUTED BOLOMETRIC AMPLITUDES AND OBSERVED PHOTOGRAPHIC AMPLITUDES

Type A				Type B			
Star	ΔPg_p	ΔP_{bol}	O−C	Star	ΔPg_p	ΔP_{bol}	O−C
SU Cyg	0m86	0m97	−0m11	DT Cyg	0m46	0m65	−0m19
Y Lac	0.97	1.04	− .07	SZ Tau	0.56	0.80	− .24
T Vul	1.00	1.07	− .07	SS Sct	0.71	0.96	− .25
V350 Sgr	1.08	1.15	− .07	BG Lac	0.94	1.14	− .20
δ Cep	1.10	1.20	− .10	FM Aql	1.05	1.22	− .17
Y Sgr	1.10	1.22	− .12	XX Sgr	1.08	1.24	− .16
X Vul	1.18	1.28	− .10	U Sgr	1.14	1.26	− .12
RR Lac	1.22	1.27	− .05	U Aql	1.16	1.25	− .09
TT Aql	1.79	1.54	+ .25	η Aql	1.16	1.24	− .08
SZ Aql	1.90	1.63	+0.27	RX Cam	1.24	1.29	− .05
				Z Lac	1.49	1.41	+ .08
				RW Cas	1.63	1.52	+ .11
				X Cyg	1.70	1.57	+ .13
				WZ Sgr	1.84	1.65	+0.19

A and B. Despite the fact that one range is bolometric and the other photographic, we see that, contrary to expectation, the amplitudes are nearly the same, and even the systematic run of the residuals could be explained by the omission of the small term in $\Delta R/R$. Pettit and Nicholson,[46] however, have found that the bolometric ranges of δ Cephei and η Aquilae are 0.58 and 0.55 mag., respectively; these values are just half the observed ranges in Pg_p and the bolometric ranges computed from expression (14). The discrepancy suggests a closer examination of the results predicted from pulsation theory, especially those relating to the changes in radii.

From relations (12), (6), and (7), we find:

$$\text{Types A and B} \begin{cases} T\,(\text{max.}) = \dfrac{7200}{0.61\log P + 0.67}, \\ T\,(\text{min.}) = \dfrac{7200}{1.19\log P + 0.60}. \end{cases} \tag{15}$$

[46] *Ap. J.*, **78**, 320, 1933.

The computed temperature of δ Cephei, for example, then ranges from 6450° K at maximum to 4900° K at minimum. Since Stebbins[47] has found 6500° K and 4920° K as maximum and minimum temperatures from a much longer color base line, the discrepancy in the bolometric ranges computed with omission of the $\Delta R/R$ term is not attributable to the shorter-base-line color system used here.

From the assumption of black-body radiation, Hertzsprung[48] has computed bolometric corrections, $P_{bol} - P_v$, as a function of black-body temperature. For the extreme temperatures of δ Cephei found above—6450° K and 4900° K—the corrections are −0.03 and −0.22 mag., respectively. The observed amplitude of δ Cephei is $\Delta P v_p = 0^m.75$, so $\Delta P_{bol} = 0^m.75 - 0^m.19 = 0^m.56$, compared to 0.58 mag. found by Pettit and Nicholson. We are left with the possibility that the term in $\Delta R/R$ in expression (13) is not negligible but that it may account for approximately 50 per cent of the observed light-range. If this surmise is correct, the computed value of $\Delta R/R$ for δ Cephei from expression (13) and the observed bolometric amplitude becomes 0.18.

OVERTONE PULSATIONS

M. Schwarzschild[49] has suggested that the cluster-type variables of Bailey's subclass *c* in Messier 3 are pulsating in the second mode with respect to the stars of subclasses *a* and *b*, which are pulsating in the fundamental mode. The separation of the subclass *c* stars from those of subclasses *a* and *b*, in the period-density relation, corresponds to a change in period by a factor of 0.63. It is interesting to note that the period–color-amplitude relation (3) for type B cepheids is displaced from that of type C, relation (8), by an amount corresponding to a factor of 0.51 in the period, which, if interpreted as a ratio of the first overtone to the fundamental period of a pulsating standard-model star, corresponds to a ratio of specific heats, γ, of 1.40.[50] This suggestion that the cepheids of type C may be pulsating in the first overtone may offer an explanation for the fact that the best-documented period variations are found among these stars, notably ζ Geminorum and FF Aquilae. Another explanation of the separation of relations (3) and (8) is offered by the work of Miller,[51] who has shown that the ratio of periods of the standard model having $\gamma = 1.43$ and polytropic indices 2 and 3, is $P_3/P_2 = 0.58$. The separation between the cepheids of types A and B and those of type C, therefore, may be an effect of overtone pulsations or of central density corresponding to different polytropic indices. The interpretation of the still smaller separation between types A and B is more obscure, but a natural point of departure for future theoretical work would be further study of anharmonic pulsations.

The writer is greatly indebted to Miss Beverly Ann Turner for her aid in preparing the material in this paper for publication.

[47] *Ap. J.*, **101**, 47, 1945.

[48] *Zs. f. wiss. Phot.*, **4**, 49, 1906.

[49] *Harvard Circ.*, No. 437, 1940.

[50] M. Schwarzschild, *Ap. J.*, **94**, 245, 1941.

[51] *M.N.*, **90**, 59, 1929.

STELLAR POPULATIONS AND COLLISIONS OF GALAXIES

LYMAN SPITZER, JR., AND WALTER BAADE*
Princeton University Observatory
and
Mount Wilson and Palomar Observatories
Received October 2, 1950

ABSTRACT

Dense clusters of galaxies, such as the Coma and Corona clusters, contain large numbers of S0 galaxies, which are highly flattened but show no obscuration or spiral structure and presumably contain stars only of population type II. It is suggested that collisions between galaxies sweep any interstellar matter out of the galaxies in such clusters and thereby prevent the appearance of any type I systems. In the Coma cluster each galaxy will collide with at least twenty other galaxies during 3×10^9 years if the galactic motions within the cluster are largely radial. An analysis of galactic collisions shows that two galaxies will interpenetrate freely with relatively little effect on the velocities and positions of the stars in each galaxy but that interstellar matter will be swept completely out of the two galaxies and left in intergalactic space, provided that the initial density is not much lower than 0.1 *H* atoms per cubic centimeter. Thus highly flattened systems, which might otherwise retain interstellar matter and develop into normal spirals, become pure type II systems.

I. INTRODUCTION

The existence of broad differences between stars of population types I and II[1] seems fairly well established. In particular, the highly luminous stars of population I, such as main-sequence O and B stars, supergiant stars of types F–M, and classical cepheids, are found almost entirely in spiral arms of late-type spiral galaxies and in irregular galaxies, such as the Magellanic Clouds. In elliptical galaxies and outside the spiral arms in spiral galaxies only stars of population II are found, with a sharp cutoff in the luminosity function at M_v equal to about -2.5 mag.

Theory indicates and observation confirms that the presence of dense interstellar matter is both a necessary and a sufficient condition for the appearance of population type I. The stars as bright as absolute magnitude -5, which are so characteristic of type I, cannot have been shining at this present rate for anything like 3×10^9 years, and theories have been advanced[2] which may explain the formation of supergiant stars from the interstellar matter. The cutoff in the luminosity function in type II systems is consistent[3] with the belief that all these stars were formed some 3×10^9 years ago; and the observed absence of much interstellar matter in these systems, in accord with theoretical expectations,[4] accounts naturally for the absence of young stars.

While the correlation between dense interstellar matter and type I stars is extremely good, the correlation between the degree of flattening and the presence of strong obscuration produced by interstellar grains is broken by one striking exception. It is well known that in the very dense clusters of galaxies, such as the Coma and Corona clusters, most of the members seem to belong to the early galactic classes, and Hubble assigns[5] the major-

* Visiting professor at Princeton University during March, 1950, when most of this paper was written.

[1] W. Baade, *Ap. J.*, **100**, 137, 1944.

[2] F. Hoyle and R. A. Lyttleton, *Proc. Cambridge Phil. Soc.*, **35**, 405, 1939, and **36**, 424, 1940; F. L. Whipple, *Ap. J.*, **104**, 1, 1946; L. Spitzer, Jr., *Centennial Symposia* ("Harvard Obs. Monographs," No. 7 [1948]).

[3] H. N. Russell, *Pub. A.S.P.*, **60**, 202, 1948.

[4] L. Spitzer, Jr., *Ap. J.*, **95**, 329, 1942.

[5] Informal communication to W. Baade.

ity of the members now to the class S0. This class, which in a way is a continuation of the E galaxies, where the intensity distribution from the center outward is smooth, is characterized by the segregation of a central lens of high density from an outer disk of much lower density, no spiral structure appearing. A closer study of the S0 members of the Coma and Corona clusters shows the following interesting features:

1. As far as flattening (angular momentum) is concerned, the S0 galaxies exhibit the full range from relatively small to very high flattening (see Fig. 1).

2. With increasing flattening, the central lens shrinks in dimensions, a feature analogous to the shrinking of the central lens in the series of spirals Sa, Sb, Sc (see Fig. 1).

3. None of the S0 galaxies shows spiral structure or exhibits any signs of obscuration, although quite a number of the galaxies are seen edge-on. This absence of obscuration is particularly striking in highly flattened systems seen edgewise, because, without exception, the small central nuclei are visible (see Fig. 1).

These three features strongly suggest that the galaxies classed together as S0 by Hubble represent actually a series of forms paralleling the series of normal spirals, Sa, Sb, Sc. But the galaxies of the S0 series contain no obscuring matter and presumably are therefore unable to develop spiral structure. That their stellar composition is the same as that of the E galaxies (pure type II) follows from the fact that, according to unpublished measures of Stebbins and Whitford, E and S0 galaxies have identical color indices.

It is the purpose of the present paper to point out that collisions between galaxies may explain the lack of type I systems in the denser clusters. In less massive or less dense systems, such as the Virgo and Hercules clusters, collisions are less frequent, corresponding with the observed fact that many spirals are observed in these aggregations. The relatively high frequency of collisions between galaxies within a dense cluster has already been pointed out,[6] but the detailed processes occurring in such collisions do not seem to have been considered. In Section II below, the collisional frequency is reinvestigated, and it is shown that a typical galaxy in the Coma cluster will have passed through some twenty to five hundred galaxies during 3×10^9 years, if it has been moving nearly radially in the cluster. Section III investigates a typical collision. Encounters between stars are negligible, but each stellar system will be distorted somewhat by the gravitational field of the other. The chief effect is that, if gas is present in the two galaxies, it will be swept out of both by the collision and left behind in intergalactic space. While further details of this process remain to be worked out, one may apparently conclude that interstellar matter cannot be present in any appreciable amount in many of the galaxies in the Coma cluster. As a tentative hypothesis, one may infer that this lack of interstellar matter is the reason why the highly flattened S0 galaxies show no obscuration or spiral structure and, presumably, represent pure population type II.

II. FREQUENCY OF COLLISIONS

If a galaxy is assumed to move in a straight line through the cluster at a very great velocity, passing at a distance r from the cluster center, the average number of collisions that this galaxy will suffer with other galaxies during a single passage through the cluster will equal simply $\sigma N(r)$, where σ is the collisional cross-section in square parsecs and $N(r)$ is the number of galaxies in a cylinder 1 square parsec in cross-section passing r parsecs from the cluster center. For an actual galaxy, moving at a velocity about the average, the actual number of collisions per passage through the cluster will exceed $\sigma N(r)$ by $2^{1/2}$ because of the velocity of the other galaxies. The curvature of the galaxy's path will also modify the actual number of collisions somewhat, but the difference will not be large, provided that the orbit is not nearly circular and provided that r is set equal to the actual distance of closest approach.

[6] F. Zwicky, *Ap. J.*, **86**, 217, 1937.

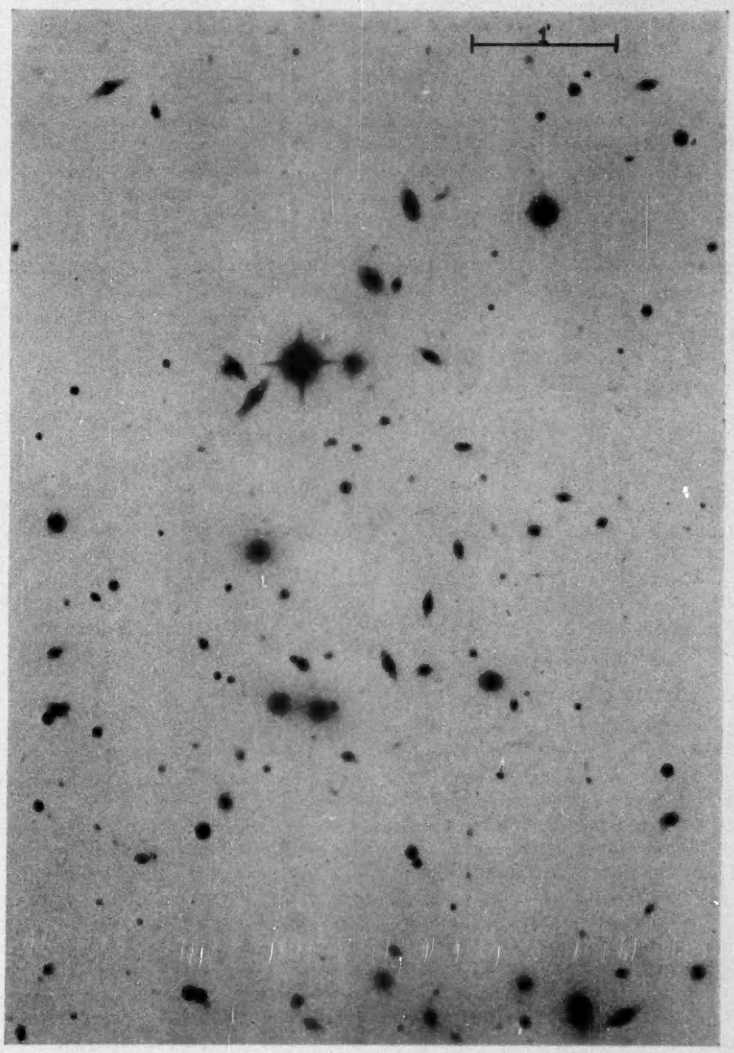

FIG. 1.—Central region of the Corona Borealis cluster, photographed with the Hale 200-inch telescope.

The appropriate value of σ is somewhat uncertain. The interstellar matter and spiral arms in a flattened galaxy may lie anywhere from 1000 out to 20,000 parsecs from the galactic center. We shall here take 2000 and 5000 parsecs as typical distances. With these values, a "collision" will occur if the centers of two galaxies pass within 4000 or 10,000 parsecs, respectively, from each other. The effective collisional cross-section for the average galaxy should lie somewhere between the two limiting values computed in this way.

Values of $N(r)$ may be obtained from nebular counts by Zwicky[6] and by Omer, Page, and Wilson.[7] We shall here use the latter counts. These are based on blue and red plates obtained with the 48-inch Schmidt telescope and consequently have a lower limiting magnitude (19.2) than the earlier counts. These later counts yield about 790 galaxies in the Coma cluster, with about half within a cylinder 40′ from the center. To obtain $N(r)$ from the counts of galaxies per square degree, the distance of the cluster must be known. According to unpublished velocity measures by Humason,[8] the mean radial velocity of the Coma cluster is 6570 km/sec, corresponding to a distance of 1.25×10^7 parsecs. This adopted value of the distance has been used to obtain the values of $N(r)$ given in Table 1.

To find the total number of collisions within 3×10^9 years, we must compute the number of times that a typical galaxy traverses the cluster. The radius of 40′, containing

TABLE 1

NUMBER OF COLLISIONS PER GALAXY IN 3×10^9 YEARS

Collision Distance (Parsecs)	Distance of Closest Approach to Center of Coma Cluster						
	2′	5′	10′	20′	40′	60′	80′
10,000	490	260	140	51	27	13	5
4,000	79	42	22	8.2	4.3	2.1	0.8
$10^9 \times N(r)(\mathrm{pc}^{-2})$	5.7	3.0	1.6	0.6	0.3	0.15	0.06

about half the galaxies (in projection), corresponds to a distance of some 150 kiloparsecs. If the root-mean-square (r.m.s.) velocity is taken to be 1700 km/sec, corresponding to the observed r.m.s. radial velocity of 1000 km/sec,[8] the time for a single passage through a diameter of 280 kiloparsecs is 1.7×10^8 years. Hence the values of $\sigma N(r)$ must be multiplied by about 18 times $2^{1/2}$ to find the total number of collisions per galaxy within the presently accepted "age of the universe." The numbers of collisions computed in this way are given in Table 1 for the two values of the collision distance.

It should be emphasized that these computations are very preliminary and are designed to give only the order of magnitude. In particular, the values obtained for large distances of closest approach are not very reliable, since, for these, one should presumably consider nearly circular orbits about the center. More precise computations should also take into account a number of other effects neglected here.

One may infer from Table 1 that, if the galaxies move nearly radially, passing within 10′ of the cluster center, the number of collisions during 3×10^9 years is at least 20 and probably nearer to 150. Even if only 10 per cent of the galaxies had interstellar matter originally, these would be mostly swept clean by collisions in 3×10^9 years. For galaxies moving in nearly circular orbits far out in the cluster, the number of collisions is much smaller, and it is doubtful whether the interstellar matter would be swept out of many

[7] Unpublished.

[8] Private communication to W. Baade.

such spirals in the Coma cluster. It is difficult to see how a cluster of galaxies could be formed in such a way as to leave galaxies moving in these large, nearly circular orbits.[9]

III. DYNAMICS OF GALACTIC COLLISIONS

While the details of a collision between two galaxies are naturally very complicated, several results can be established immediately. In the first place, encounters between individual stars are almost entirely negligible. In general, the velocity with which two galaxies collide must be at least several hundred kilometers per second, about equal to the escape velocity from either galaxy. At such high velocities two stars must pass within several stellar radii to deflect each other appreciably. In the Coma cluster, the r.m.s. relative velocity of the galaxies is 2400 km/sec (equal to $2^{1/2}$ times the r.m.s. individual galactic velocity of 1700 km/sec). At this very great velocity, two stars in different galaxies would have to collide physically to be deflected several degrees, and even one such collision is unlikely when one galaxy passes through another. Hence the only force which must be considered on a star during the collision is the smoothed gravitational force produced by both galaxies.

In the second place, it is evident that, while stellar systems may interpenetrate one another with relatively little mutual disturbance, the effect on any interstellar matter present will be catastrophic. Even if the interstellar density is as low as 0.1 H atom/cm^3, a single neutral H atom will move less than 0.1 parsec, on the average, before it collides with a similar atom. At the relative velocity of 2400 km/sec under consideration, corresponding to about 7600 electron volts (e.v.) of energy for each H atom, relative to the center of gravity of the two systems, both atoms are likely to be ionized, and the gas, even if neutral originally, will rapidly become ionized. The high proton velocities will then reduce the interaction cross-section somewhat; according to the equations previously given,[10] the time of relaxation of the protons, for a kinetic energy of 7600 e.v. and a proton density of 0.1 cm^{-3}, is about 7.5×10^4 years. During this time the protons will travel about 180 parsecs relative to one another, somewhat less than the thickness of the interstellar gas in a typical galaxy. Heavier atoms will be more highly charged and will be slowed down more rapidly. These estimates consider only the interactions with protons. While there can be no large-scale separation of electric charges, it is readily shown that the electrons will be stopped almost at once. Interaction with electrons will then tend to slow down the protons and other positive ions.

A small grain, 3×10^{-5} cm in radius, will lose about half its initial energy in a distance of 30 parsecs, if the proton density is 0.1 cm^{-3}. This estimate neglects the electrical charge on the grain, which may considerably reduce the distance traveled. Evidently, densities as low as 10^{-2} H atoms/cm^3 and probably less than this value would be required for two gaseous masses several hundred parsecs thick to pass through each other.

The subsequent motions of the gas will depend on the temperature. If the gas retained the temperature of 60,000,000° produced by the collision, the resultant expansion would be so vigorous that little gas could be left in either galaxy. However, cooling may be appreciable in the 10^5–10^7 years required for the galaxies to pass through each other. In this case the gas would have a low velocity relative to the center of gravity of the two systems, while the galaxies will be moving away in opposite directions at velocities greater than the escape velocity from either galaxy separately. It is possible that some gas might fall back into each galaxy, but it seems likely that most of it will be left in intergalactic space. We conclude that any interstellar gas will be swept out of two colliding galaxies (or, more accurately, out of those sections of the galaxies which interpene-

[9] This point has been discussed by several authors, including E. von der Pahlen (*Zs. f. Ap.*, **24**, 68, 1947) and G. Gamow and G. Keller (informal communication), in connection with the motion of stars in globular clusters and spherical galaxies, respectively.

[10] L. Spitzer, Jr., *Ap. J.*, **93**, 369, 1941.

trate one another), provided that the gas densities are at all comparable to those in the solar neighborhood.

The ultimate fate of the gas swept out is difficult to predict. When two field galaxies collide, some of the gas might condense to form an irregular galaxy. This suggestion is consistent with the fact that irregular galaxies have mostly pure type I population. In a dense cluster of galaxies other possibilities are present. Some gas might escape from the cluster, though much loss of matter in this way seems unlikely in view of the velocities in excess of 2400 km/sec that would be required.

Some of the gas swept out might be expected to form new galaxies. If such a formation had occurred long ago and if the new galaxies had lost their interstellar matter in subsequent collisions, such systems would probably be indistinguishable from the original galaxies. Finally, the gases swept out of different galaxies might collide, cool off, and collect at the center of the cluster. The passage of galaxies through the cluster center might then sweep out any remaining gas in such systems. Some interstellar matter might still remain at the center of the cluster. It seems more likely that any central core of gas, with no net angular momentum to impede contraction and condensation, would have condensed into stars long ago.

It remains to consider the effect of collisions on the stars themselves. Zwicky has suggested that the collisions would sweep individual stars out of a galaxy, as well as interstellar matter, but, in view of the negligible interaction between specific stars, this seems unlikely. There will be, as he suggests, a tendency for the internal energy of the galaxies to increase at the expense of the kinetic energy of the galaxies as a whole. While this effect may be appreciable for collisions between field galaxies, whose relative velocities are not very large, it is certainly less important for collisions between cluster galaxies, whose relative velocities are great.

Let us consider in more detail a collision between two galaxies moving with a relative velocity V of 2400 km/sec. This velocity is so much greater than the velocity of an individual star relative to the center of its own galaxy that we may compute the perturbations of each galaxy on the other as if the stars in each system were at rest relative to one another. Let us consider a particular star in galaxy 1, with a distance a_1 from the center of galaxy 1; let a_2 be the distance of closest approach of galaxy 2 to the star in question. We assume that the masses M_1 and M_2 of each galaxy are effectively concentrated at the galactic centers. Then it is readily shown that Δv, the change of velocity of the particular star under consideration, is given by

$$\Delta v = \frac{2GM_2}{a_2 V} = \frac{2\, v_{c2}^2\,(a_2)}{V}, \tag{1}$$

where $v_{c2}(a_2)$ is the circular velocity around M_2 at the distance a_2. The velocity change, Δv, will be directed toward the point of closest approach of M_2. Values of v_{c2} are observed[11] to range up to about 100 km/sec for a dwarf galaxy, such as M 33, and up to about 300 km/sec for a giant galaxy, such as M 31. We shall use here an intermediate value of 200 km/sec. The value of Δv is then 33 km/sec.

Other parts of galaxy 1 will also be accelerated. On these assumptions, the velocity changes will all be parallel and will decrease proportionally to $1/a_2$. Let Δv_R be the velocity change of a star relative to the galactic center, i.e., Δv_R equals Δv for the star under consideration minus Δv for the center of galaxy 1. We shall compute the r.m.s. Δv_R for stars moving in the same plane with the same value of a_1. Two simplifying assumptions will be made: first, that the relative motion of the two galaxies is perpendicular to the orbits of the star under consideration and, second, that the distance of closest approach of the two galactic centers is $2a_1$. Thus the distance a_2 of closest approach of the

[11] H. W. Babcock, *Lick Obs. Bull.*, 19, 41, 1939 (No. 498); N. U. Mayall and L. H. Aller, *Ap. J.*, 95, 24, 1942.

center of galaxy 2 varies from a_1 for a star on one side of galaxy 1 to $3a_1$ for a star on the other side. Then Δv_R will vary from 17 km/sec on one side to 6 km/sec on the other side. Most of the stars will have intermediate values of Δv_R, and it may be shown that the r.m.s. value of Δv_R is in the neighborhood of 8 km/sec.

It is evident that these computations are very crude; they give too high a value for the r.m.s. Δv_R. First, the mass of a galaxy is not concentrated at its center. Let us denote by $M_2(a_2)$ the mass of galaxy 2 lying within a sphere of radius a_2 about the galactic center. Then the increase of $M_2(a_2)$ with increasing a_2 will prevent Δv from falling off as rapidly with increasing distance as equation (1) would predict. As a result, the differential change of velocity between different regions of galaxy 1 will be less than was found in the previous simplified computations. Second, a change in the values of a_1 or a_2 is likely to decrease the r.m.s. Δv_R; for example, with a fixed a_1, an increase of a_2 will evidently decrease Δv_R, while a decrease of a_2 will decrease $M_2(a_2)$ and may also decrease the r.m.s. Δv_R. Finally, if the direction of relative motion of the two galaxies is not perpendicular to the orbital plane of the stars under consideration, Δv_R will again be decreased. While detailed computations are desirable for more definite results, it would appear that the r.m.s. Δv_R computed above is too great by at least a factor of 2 and possibly much more. We shall tentatively take 3 km/sec as a final average value.

The effect of such velocity increments is apparently small. In successive collisions the mean-square velocities will add, but 100 collisions, each with a value of Δv_R of 3 km/sec, will produce an increase of only 900 km^2/sec^2 in the mean-square velocities of the stars in the galaxy. In an elliptical galaxy, where random velocities are already some 200 km/sec, the internal energy will increase by about 2 per cent. Such an increase would have a completely negligible effect on the size and shape of the galaxy. In a highly flattened system each collision will yield velocity increments of about 1.7 km/sec perpendicular to the galactic plane, and 100 such collisions would increase the mean-square velocities in this direction by some 300 km^2/sec^2. This change, also, is probably below the limit of detection.

We may conclude that collisions between galaxies in a dense cluster, where the random galactic velocities are as great as 1700 km/sec, have a relatively small effect on the distribution of the stars already present in the galaxies.

EXACT SOURCE FUNCTIONS BY AN EXTENSION OF CHANDRASEKHAR'S LIMITING PROCESS

VLADIMIR KOURGANOFF
Institut d'Astrophysique de Paris
Received November 15, 1950

ABSTRACT

Chandrasekhar discovered that solutions in the nth approximation given by the method of discrete beams for the *emergent intensity* can be transformed in such a way that equations of an infinite degree are avoided and their limits, as $n \to \infty$, obtained explicitly.

In this paper Chandrasekhar's limiting process is extended to functions describing the *internal state* of the atmosphere. In particular, we show how, by a suitable interpretation of the constants of integration, the solutions in the nth approximation for the source functions $\mathfrak{Z}(\tau)$ can also be transformed into a form suitable for effecting the passage to infinite approximation. Two examples of obtaining the exact $\mathfrak{Z}(\tau)$ by this method are given: (i) for the problem of isotropic scattering in a gray atmosphere and (ii) for a problem of line formation in a nongray atmosphere.

1. *Introduction.*—Chandrasekhar's recent treatise[1] on radiative transfer illustrates the power of the method of discrete ordinates, which represents the radiation field in $2n$ terms of n discrete beams. This method gives approximate solutions in an nth approximation (or "n-solutions," as we shall call them) when all integrals with respect to $\mu = \cos\vartheta$, in the interval $(-1, +1)$, are evaluated by some numerical quadrature formula of the general type[2]

$$\int_{-1}^{+1} f(\mu)\, d\mu = \sum_{i=1}^{n} a_i f(\mu_i)\,. \tag{1}$$

Thus, for instance, Chandrasekhar found that, in the problem of conservative isotropic scattering in a gray atmosphere, the "law of darkening" $I(0, \mu)$ and the source function $J(\tau)$ are given by the following elegant formulae (we have added a suffix n to the usual notation in order to distinguish n-solutions from the rigorous ones):

$$I_n(0, \mu) = \tfrac{3}{4}F\,\frac{(\mu+\mu_1)(\mu+\mu_2)\dots(\mu+\mu_n)}{(\mu+x_1)(\mu+x_2)\dots(\mu+x_{n-1})} \qquad (x_a = k_a^{-1}) \tag{2}$$

and[3]

$$J_n(\tau) = \tfrac{3}{4}F(\Sigma\mu_j - \Sigma x_a) - \tfrac{3}{16}F^2\sum_{a=1}^{n-1}\frac{e^{-\tau/x_a}}{x_a T_n'(x_a)\, I_n(0, x_a)} + \tfrac{3}{4}F\tau \tag{3}$$

where the x_a's are the positive zeros of the "characteristic function"

$$T_n(\mu) = 1 + \mu^2\Sigma\,\frac{a_j}{\mu_j^2 - \mu^2} = \frac{1}{3}\,\frac{(x_1^2-\mu^2)(x_2^2-\mu^2)\dots(x_{n-1}^2-\mu^2)}{(\mu_1^2-\mu^2)(\mu_2^2-\mu^2)\dots(\mu_n^2-\mu^2)}\,. \tag{4}$$

Chandrasekhar investigated whether exact solutions could be derived from the corresponding n-solutions by a limiting process in which n becomes infinite.

If the function $f(\mu)$ in equation (1) were continuous, we could expect that, by making n larger and larger, i.e., by making the division (μ_j) finer and finer, the representation

[1] S. Chandrasekhar, *Radiative Transfer* (Oxford: Clarendon Press, 1950), referred to hereafter as "*R.T.*"

[2] For more details see, e.g., *R.T.*, §§ 20–26, and Wick, *Zs. f. Phys.*, 120, 702, 1943.

[3] This form of $J_n(\tau)$ results from a transformation of Chandrasekhar's expression (*R.T.*, p. 78) for L_n. All other symbols have their usual meanings, j running from 1 to n and a from 1 to $(n-1)$.

(1) would become exact in the limit. When, however, we try to apply this idea to the n-solutions, several difficulties arise even when the question of the validity of the limiting process itself is not considered and it is taken for granted that the n-solutions tend to the exact solutions as $n \to \infty$. Thus it is not obvious what the form of the limit of $I_n(0, \mu)$ and $J_n(\tau)$ given by equations (2) and (3) will be as $n \to \infty$, since in the limit the x_n's depend on the solution of an algebraic equation of infinite degree. However, Chandrasekhar discovered that an exact relation involving $I(0, \mu)$ can be derived by the limiting process from equation (2) by introducing the characteristic function $T_n(\mu)$ itself instead of its zeros. On comparing equations (2) and (4), we find that a simple relationship can be established between $I_n(0, \mu)$ and $T_n(\mu)$, namely,

$$I_n(0, \mu)\, I_n(0, -\mu) = \tfrac{3}{16} F^2 \frac{1}{T_n(\mu)}. \tag{5}$$

In this formula the roots $\pm x_n$ no longer appear explicitly.

When, however, we try to perform the limiting process on equation (5), a difficulty of an entirely different kind arises. Although it is obvious that the formal limit of $T_n(\mu)$ is the integral

$$T(\mu) = 1 + \mu^2 \int_0^1 \frac{dz}{z^2 - \mu^2}, \tag{6}$$

this integral cannot be defined without special precautions for real values of μ lying between -1 and $+1$. The same difficulty also arises in the case of the function $I_n(0, -\mu)$ even when the analysis is restricted to real values of μ lying between 0 and 1. This difficulty can fortunately be overcome by a method which has been well known in analysis since the time of Cauchy. We avoid the singularities on the real axis by changing to a complex variable which can lie anywhere in the complex plane except in certain forbidden regions and on certain lines ("cuts"). This explains why Chandrasekhar was led to associate with the physical function $I_n(0, \mu)/I_n(0, 0)$, defined for real μ in the interval $(0, 1)$, the function

$$H_n(\mu) = \sqrt{3}\, \frac{(\mu_1 + \mu)(\mu_2 + \mu) \dots (\mu_n + \mu)}{(x_1 + \mu)(x_2 + \mu) \dots (x_{n-1} + \mu)}, \tag{7}$$

defined in the complex μ-plane; since the x's are real $H_n(\mu)$ as a function of the complex variable μ has singularities between -1 and 0 on the real axis and is regular in the rest of the μ-plane. For real values of μ such that $0 \leqslant \mu \leqslant 1$, it reduces to $I_n(0, \mu)/I_n(0, 0)$. Since (*R.T.*, p. 77)

$$I_n(0, \mu) = \frac{\sqrt{3}}{4} F H_n(\mu), \tag{8}$$

we can write

$$I(0, \mu) = \frac{\sqrt{3}}{4} F H(\mu) \qquad (0 \leqslant \mu \leqslant 1), \tag{9}$$

where $H(\mu)$ is the limit of $H_n(\mu)$ as $n \to \infty$, assuming that this limit exists.

On the other hand, it is easy to show that, when μ is complex, the integral (6) represents a many-valued function of μ. This can be made one-valued if we insert a cut in the μ-plane between -1 and $+1$ and choose a certain branch of the function—for example, that branch which is real when μ lies on the real axis outside the cut.

By elementary integration and the classical formula

$$\log \mu = \log \rho e^{i\theta} = \log_e \rho + i(\theta + 2k\pi), \tag{10}$$

we have

$$\begin{aligned} T(\mu) &= 1 + \tfrac{1}{2}\mu \left[\int_0^1 \frac{dz}{z - \mu} - \int_0^1 \frac{dz}{z + \mu} \right] \\ &= 1 + \tfrac{1}{2}\mu \left[\log(1 - \mu) - \log(-\mu) \right] - \tfrac{1}{2}\mu \left[\log(1 + \mu) - \log \mu \right]. \end{aligned} \tag{11}$$

Letting (cf. Fig. 1 for the meanings of ρ', ρ'', θ', and θ'')

$$\mu = -u + iv = \rho e^{i\theta}, \qquad -\mu = +u - iv = \rho e^{i(\theta+\pi)}, \tag{12}$$

and

$$\mu + 1 = \rho' e^{i\theta'}, \qquad 1 - \mu = \rho'' e^{i\theta''}, \tag{13}$$

we get, for one branch, the formula

$$T(\mu) = 1 + \tfrac{1}{2}\mu \log_e \left|\frac{1-\mu}{1+\mu}\right| + \tfrac{1}{2}\mu(\theta'' - \theta' + \pi) i, \tag{14}$$

where $|1 - \mu|$ and $|1 + \mu|$ are the moduli of $(1 - \mu)$ and $(1 + \mu)$ and θ'' and θ' are their respective arguments. (Note that, in Fig. 1, θ'' is given by a negative rotation, so that $\theta'' = -|\theta''|$.)

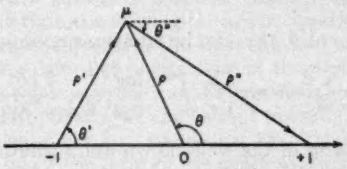

FIG. 1.—The complex μ-plane

Since $\theta'' - \theta' = -\pi$ when μ lies on the real axis outside the interval $(-1, +1)$, equation (14) represents the branch which is real on these parts of the axis. An equivalent form is

$$T(\mu) = 1 - \tfrac{1}{2}\mu \log \frac{\mu+1}{\mu-1} \qquad \text{(plane cut from } -1 \text{ to } +1), \tag{15}$$

where $\log \mu$ denotes the principal branch:

$$\log \mu = \log \rho e^{i\theta} = \log_e \rho + i\theta \qquad (-\pi \leqslant \theta \leqslant \pi). \tag{16}$$

From equations (4) and (7) we have Chandrasekhar's identity,

$$H_n(\mu) H_n(-\mu) = \frac{1}{T_n(\mu)}, \tag{17}$$

in which μ is still a complex variable. As $n \to \infty$, this becomes

$$H(\mu) H(-\mu) = \frac{1}{T(\mu)} \qquad \text{(plane cut from } -1 \text{ to } +1), \tag{18}$$

where, as in equation (9),

$$H(\mu) = \lim_{n\to\infty} H_n(\mu), \tag{19}$$

and $T(\mu)$ is the function now given by equation (14).

It must again be stressed that, although relation (18) is not valid on the strip $(-1, +1)$ of the real axis, $H(\mu)$ has no singularity for any real value of μ lying between 0 and 1 (cf. eq. [7]).

We have now resolved the two major difficulties in the limiting process: that of the dependence on an algebraic equation of infinite degree and that of the impossibility of defining some of the limiting functions for certain real values of μ. We have shown how these difficulties can be overcome by the introduction of $T_n(\mu)$, the complex variable μ, and the function $H(\mu)$.

In *R.T.*, § 39.1, the further difficulty of the dependence of $H_n(\mu)$ on only half the zeros of $T_n(\mu)$ has been solved by Chandrasekhar by an application of Cauchy's theorem. Thus, using the relation

$$-\log(a+\mu) = \frac{1}{2\pi i}\int_{-i\infty}^{+i\infty} \frac{\mu}{w^2-\mu^2}\log(a^2-w^2)\,dw \begin{cases} \Re(a) > 0 \\ \Re(\mu) > 0 \end{cases}, \tag{20}$$

he found

$$\log H_n(\mu) = \frac{1}{2\pi i}\int_{-i\infty}^{+i\infty} \frac{dw}{w^2-\mu^2}\,\mu \log T_n(w). \tag{21}$$

Letting $n \to \infty$, we have the exact solution,

$$I(0,\mu) = \frac{\sqrt{3}}{4} F \exp\left[\frac{1}{2\pi i}\int_{-i\infty}^{+i\infty} \frac{dw}{w^2-\mu^2}\,\mu \log T(w)\right]. \tag{22}$$

By the substitution[4] $w = i\cot\theta$, this can be transformed into the real integral,

$$I(0,\mu) = \frac{\sqrt{3}}{4} F \exp\left[\frac{\mu}{\pi}\int_0^{\pi/2} \frac{\log(1-\theta\cot\theta)}{\cos^2\theta+\mu^2\sin^2\theta}\,d\theta\right]. \tag{23}$$

This is simply an elegant form of the well-known exact solution of Wiener-Hopf:

$$I(0,\mu) = \frac{\sqrt{3}}{4} F(1+\mu) \exp\left[\frac{\mu}{\pi}\int_0^{\pi/2} \frac{\log[\sin^2\theta/(1-\theta\cot\theta)]}{\cos^2\theta+\mu^2\sin^2\theta}\,d\theta\right], \tag{24}$$

the derivation of which involves much more transcendental mathematics than do the transformations used by Chandrasekhar for establishing equation (21).

Chandrasekhar applied a similar treatment to the functions $I_n(0,\mu)$ obtained in several more difficult problems and derived exact solutions for $I(0,\mu)$ in a direct and elegant way by the limiting process.[5] Chandrasekhar did not attempt to apply his limiting process to functions describing the internal state of a stellar atmosphere, such as $J(\tau)$. After this short review of the spirit of Chandrasekhar's method, we shall investigate whether the method cannot be extended to obtain the exact solutions for the source functions as well; in this way we can preserve the symmetry of Chandrasekhar's work.

Of course, as in Chandrasekhar's derivation of exact solutions for the $I(0,\mu)$ functions, the method we shall describe will have some deep relations with the methods based on Fourier and Laplace transforms; and, as in Chandrasekhar's case, it will give the known exact solutions of the elementary problems. The method has nevertheless two great advantages from the point of view of astrophysical research. First, it involves only the classical theorems of "higher mathematics," such as Cauchy's residue theorem, and it avoids all the complications connected with the theory of Laplace transforms. Also, by its simplicity, it makes possible the treatment of very complex problems. This is apparent from Chandrasekhar's applications of the method to various $I_n(0,\mu)$ functions. We shall illustrate the proposed extension of Chandrasekhar's limiting process by considering two problems.

The first, discussed in § 2, is that of isotropic conservative scattering in a gray at-

[4] I am indebted to Dr. I. Busbridge for the transformation of eq. (22) into eq. (23).

[5] For the complex problems it is not practicable to base the whole argument on the limiting process, since the constants appearing in the solutions cannot be easily expressed in a form suitable for a direct passage to the limit of infinite approximation. In these cases Chandrasekhar treats the exact values of these constants as indeterminate parameters and computes them by substituting the solutions obtained by the limiting process (but keeping the explicit values of the constants unspecified) into the rigorous equations obtained from the principles of invariance. A very good example of this method is provided by Chandrasekhar's treatment of the problem of the diffuse reflection on Rayleigh scattering (*R.T.*, pp. 254–259). I am very much indebted to Professor Chandrasekhar for this remark and several other suggestions concerning my comments on his work.

mosphere. The simplicity of the problem makes the exposition of the method particularly easy. In this case the result is simply Mark's well-known exact solution for $J(\tau)$; but the calculations are much more elementary.

The second problem, considered in § 3, is that of the theory of line formation in a nongray atmosphere (Milne-Eddington model). This choice was inspired by recent investigations of Dr. Menzel and Dr. Sen on the same subject by a different method.[6] The exact source function $\mathfrak{J}(\tau)$ for the Milne-Eddington model obtained in this section completes Chandrasekhar's exact solution for the corresponding $I(0, \mu)$. In an unpublished investigation of the same problem, we have derived the exact formula for $J(\tau)$ by the Laplace transform method. This, of course, gives the same result but at a "higher cost."

In this paper, only formal difficulties connected with the limiting process are considered and solved. If we now turn to the mathematical justification of the process itself, we at once meet several difficulties, and these have not, as yet, been entirely overcome. Chandrasekhar attempted a sketch of a proof,[7] though he did not consider it to be entirely rigorous. We think that, considering the a_i's in equation (1) to be the intervals $\Delta\mu_i$ in the usual formula giving an integral as the limit of a sum, some light can be thrown on this delicate problem, and a complete justification of the process does not appear impossible. Because, however, a rigorous proof would involve analysis outside the scope of what is reasonably needed in astrophysics, we shall adopt toward the limiting process the same attitude as that of Chandrasekhar, by considering that the main purpose is to provide an algorithm for writing down the form of the exact solutions.

2. *Application of the "limiting process" to the determination of the exact source function in the case of isotropic scattering in a gray atmosphere.*—In this section we shall consider the conservative case ($\varpi_0 = 1$), since the nonconservative case can be considered as a special case of the problem studied in the following section.

Adopting Chandrasekhar's notation, but for the addition of the suffix n to distinguish the n-solutions from the exact ones, we start from the results established in *R.T.*, § 25. It is shown there that $J_n(\tau)$ is given by

$$J_n(\tau) = \tfrac{3}{4}F\left(\tau + Q + \sum_{a=1}^{n-1} L_a e^{-k_a\tau}\right), \tag{25}$$

where k_a is the reciprocal of x_a and Q and L_a are the constants of integration; further,

$$I_n(0, \mu) = \tfrac{3}{4}F\left(\mu + Q + \sum_{a=1}^{n-1} \frac{L_a}{1 + k_a\mu}\right). \tag{26}$$

Introducing Chandrasekhar's function $H_n(\mu)$ (cf. eq. [8]), we can rewrite equation (26) in the form

$$\frac{H_n(\mu)}{\sqrt{3}} = \mu + Q + \sum_{a=1}^{n-1} \frac{L_a x_a}{\mu + x_a}, \tag{27}$$

where μ may now be treated as a complex variable. From equation (27) it is at once seen that $x_a L_a$ *is the residue* of $H_n(\mu)/\sqrt{3}$ *at the pole* $\mu = -x_a$. Our extension of Chandrasekhar's method is based entirely on this simple remark.

In order to obtain the quantity $L_a e^{-k_a\tau}$ appearing in $J_n(\tau)$, we multiply equation (27) by $e^{\tau/\mu}/(-\mu)$, so that we produce $L_a e^{-\tau/x_a} = L_a e^{-\tau k_a}$ when $\mu = -x_a$. This gives us the function

$$\phi(\mu) = \frac{H_n(\mu)\, e^{\tau/\mu}}{-\mu\sqrt{3}} = -\frac{\mu + Q}{\mu}\, e^{\tau/\mu} - \sum_{a=1}^{n-1} \frac{x_a}{\mu}\, \frac{L_a e^{\tau/\mu}}{\mu + x_a}; \tag{28}$$

[6] I am very much indebted to Drs. Menzel and Sen for allowing me to see a copy of their paper in advance of publication.

[7] *Ap. J.*, **105**, 189, 1942.

and if we exclude the singular point $\mu = 0$ by means of a very small circle, this has only the $(n-1)$ poles $\mu = -x_a (a = 1, 2, \ldots, n-1)$ in the rest of the complex μ-plane.

The quantity $L_a e^{-k_a \tau}$ must, by construction, be the residue of $\phi(\mu)$ at $\mu = -x_a$, and this is readily verified because the residue is the limit, as $\mu \to -x_a$, of $(\mu + x_a)\,\phi(\mu)$. We can therefore interpret $\Sigma L_a \exp(-k_a \tau)$ in equation (25) as the sum of the residues of $\phi(\mu)$ at the poles $(-x_1, -x_2, \ldots, -x_{n-1})$, which are known to lie on the real axis between -1 and 0 (cf. *R.T.*, § 25).[8]

By Cauchy's residue theorem, we can now express $\Sigma L_a \exp(-k_a \tau)$ as a complex integral along a contour C inclosing all the poles $(-x_a)$ and excluding the circle of very small radius ϵ about the singular point $\mu = 0$. Obviously, ϵ must be smaller than x_1. We could, for instance, take $\epsilon = \mu_1$, since we know[8] that $-x_1$ always lies to the left of $-\mu_1$. This gives us

$$\sum_{a=1}^{n-1} L_a e^{-k_a \tau} = \frac{1}{2\pi i} \int_C \phi(\mu)\, d\mu . \tag{29}$$

A suitable form for the contour C would be one starting from $\mu = -\epsilon$ and inclosing the interval $(-1, -\epsilon)$ of the real axis.

Now we know that the function $H_n(\mu)$ gives, by the limiting process, the function $H(\mu)$, which is not defined on the real axis between -1 and 0 and which therefore requires a cut along this interval. We therefore insert the cut and eliminate $H_n(\mu)$ from equation (28) by means of Chandrasekhar's identity (17) and rewrite $\phi(\mu)$ in the form

$$\phi(\mu) = -\frac{e^{\tau/\mu}}{\mu H_n(-\mu) T_n(\mu) \sqrt{3}} . \tag{30}$$

We also make C pass just above the cut, around $\mu = -1$, and back to $\mu = -\epsilon$ just below the cut. Since, as $n \to \infty$, the point $(-x_1)$ (the nearest pole to the origin) tends to zero, ϵ will also tend to zero.

We now apply the limiting process $(n \to \infty)$ to $T_n(\mu)$; it then becomes $T(\mu)$, given by equation (14). From this expression for $T(\mu)$ we see that, above the cut, where $\theta' = 0$, $\theta'' = 0$, and $\mu = -u + i0$, $T(\mu)$ takes the value

$$T_A(\mu) = 1 - \tfrac{1}{2} u \log\left(\frac{1+u}{1-u}\right) - \tfrac{1}{2}\pi u i . \tag{31}$$

After passing counterclockwise around $\mu = -1$, θ' becomes 2π while $\theta'' = 0$; $T(\mu)$ therefore takes the value

$$T_B(\mu) = 1 - \tfrac{1}{2} u \log\left(\frac{1+u}{1-u}\right) + \tfrac{1}{2}\pi u i . \tag{32}$$

below the cut. In this way we obtain from equation (29), with $\mu = -u$,

$$\lim_{n\to\infty} \sum_{a=1}^{n-1} L_a e^{-k_a \tau} = \lim_{\epsilon \to 0} -\frac{1}{2\pi i} \int_\epsilon^1 \frac{e^{-\tau/u}}{uH(u)\sqrt{3}} \left[\frac{1}{T_A(\mu)} - \frac{1}{T_B(\mu)}\right] du . \tag{33}$$

Substituting, now, from equations (31) and (32), we have

$$\lim_{n\to\infty} \sum_{a=1}^{n-1} L_a e^{-k_a \tau} = -\frac{1}{2\sqrt{3}} \int_0^1 \frac{e^{-\tau/u}}{H(u) Z(u)}\, du , \tag{34}$$

[8] A more detailed analysis has been given in the paper by V. Kourganoff and Ch. Pecker, *Ann. d'ap.*, 12, 247, 1949.

where $Z(u)$ is given by

$$Z(u) = \left(1 - \tfrac{1}{2}u \log \frac{1+u}{1-u}\right)^2 + \tfrac{1}{4}\pi^2 u^2 \tag{35}$$

$$= (1 - u \tanh^{-1} u)^2 + \tfrac{1}{4}\pi^2 u^2 .$$

From equation (35) and the known exact value of $I(0, 0)$, we find the relation $H(0)$ $Z(0) = 1$, and we conclude that the integral (34) behaves like

$$\int_0^1 e^{-\tau/u} du = E_2(\tau) ; \tag{36}$$

it is known from the theory of the $E_n(\tau)$-functions (cf. *R.T.*, Appendix I) that this exists for $\tau \geqslant 0$. Thus the integral (34) exists for $\tau \geqslant 0$.

We have still to apply the limiting process to the integration constant Q. In the n-solution it is usually expressed[8] by

$$Q_n = q_n(\infty) = \Sigma \mu_j - \Sigma x_n , \tag{37}$$

and this is not at all suitable for our present purpose, since, as $n \to \infty$, it gives Q in terms of the roots of a characteristic equation of infinite degree.

The difficulty can be overcome if we first evaluate $\Sigma a_j I_n(0, \mu_j)\mu_j^2$; for this is a quantity to which the limiting process is readily applied and it is, moreover, simply related to Q. On using the identities given in *R.T.*, § 25, we find that

$$\tfrac{1}{2}FQ = \Sigma a_j I_n(0, \mu_j)\, \mu_j^2 . \tag{38}$$

Hence the limiting process gives

$$Q = \frac{2}{F}\int_0^1 I(0, \mu)\, \mu^2 d\mu = \frac{\sqrt{3}}{2}\int_0^1 H(\mu)\, \mu^2 d\mu = \frac{\alpha_2}{\alpha_1}, \tag{39}$$

where α_2 and $\alpha_1 = 2/\sqrt{3}$ are the "moments" of the $H(\mu)$-functions (α_2 is given by Chandrasekhar in *R.T.*, Table XXXIII, as 0.820352). (In more complex problems the constants cannot be so easily expressed in terms of the "moments" of $H_n(\mu)$; this leads to the modification of the method described in n. 5.)

From equations (25), (34), and (39) we see that $J(\tau)$, obtained as limit $J_n(\tau)$ as $n \to \infty$, is given by the real expression

$$J(\tau) = \tfrac{3}{4}F\left[\tau + \frac{\alpha_2}{\alpha_1} - \frac{1}{2\sqrt{3}}\int_0^1 \frac{e^{-\tau/u}}{H(u)\, Z(u)}\, du\right]. \tag{40}$$

In this formula for $J(\tau)$, all quantities can be computed with any desired accuracy (cf. eq. [35] and the theory of the H-functions given in *R.T.*, §§ 38 and 42).

The exact solution in the form (40) was obtained by Mark[9] with the Laplace transform method, i.e., a method involving much more "advanced" mathematics than what we have used. The following observations on the foregoing method may be made:

(i) In the treatment we have given, the "construction" of the function $\phi(\mu)$ (eq. [28]) resulted in a very obvious way from our desire to represent $L_n e^{-k_n \tau}$ in a manner suitable for the application of Chandrasekhar's process. It should be noticed, however, that $I_n(0, \mu)$, defined by equation (26), is also the Laplace transform,

$$\mathfrak{L}\{J_n(\tau)\} = s\int_0^\infty J_n(\tau)\, e^{-\tau s} d\tau ; \tag{41}$$

[8] *Phys. Rev.*, **72**, 558, 1947.

so we might equally have applied the "inversion theorem" for Laplace transforms to expression (26) to find $J_n(\tau)$. Such a method would be superior to Mark's method because the singularities of $I_n(0, \mu)$ can be found more simply than those of $I(0, \mu) = (\sqrt{3}/4)\, FH(\mu)$; but it would be more complicated than the method we have described. Moreover, a treatment such as this would involve the use of the variable s, which would finally have to be eliminated; it would not then be possible to separate the function $(Q + \mu)$ from $\Sigma L_a \exp(-k_a\tau)$; also the straight line in the s-plane parallel to the imaginary axis which appears in the "inversion theorem" would have to be completed on the left by a fairly complicated and rather artificial contour, several parts of which would contribute nothing to the final result.

(ii) When looking for a suitable representation of L_a, we found the following interesting formula:

$$L_a = -\frac{1}{\sqrt{3}} \frac{1}{x_a H_n(x_a) T_n'(x_a)}, \tag{42}$$

in which $T_n'(\mu)$ is the derivative of $T_n(\mu)$ defined by equation (4). This form for L_a did not prove useful because, on writing $L_a \exp(-\tau/x_a)$ as

$$\left[-\frac{1}{\sqrt{3}} \frac{e^{-\tau/\mu}}{\mu H_n(\mu) T_n'(\mu)}\right]_{\mu = x_a}, \tag{43}$$

we found that, on applying the "limiting process," the integral involving $\mu T'(\mu)$ does not converge; for, after some simple reductions, we find

$$\mu T'(\mu) = 2\mu^2 \int_0^1 \frac{z^2 dz}{(z^2 - \mu^2)^2}, \tag{44}$$

and, contrary to $T(\mu)$, this integral does not have a Cauchy principal value.

(iii) The complex integral (22) and the corresponding real integral (23) give the exact solution for $H(\mu)$. Similarly, though Ambarzumian's integral equation[10]

$$\frac{1}{H(\mu)} = \frac{1}{2} \int_0^1 \frac{xH(x)}{x + \mu}\, dx \tag{45}$$

does not give $H(\mu)$ explicitly in terms of known functions, we can consider that it does give the exact solution for $H(\mu)$, since from either equation (22) or equation (45) a table of the function can be computed with any desired accuracy—more easily, in fact, by iteration of equation (45) than by numerical quadrature applied to equation (23) or equation (24).

Now consider Milne's integral equation,

$$J(\tau) = \frac{1}{2} \int_0^\infty J(t) E_1(|t - \tau|)\, dt. \tag{46}$$

This equation represents the exact solution for $J(\tau)$ in the same way as equation (45) represents the exact solution for $H(\mu)$; and we could, in principle, construct a table of values for $J(\tau)$ by iterating equation (46). But this "exact solution" for $J(\tau)$ is not similar to the solution given by equation (45), since a practical method of iterating equation (46) has not been devised. Moreover, a solution of the type of equation (40), though less explicit than equation (23), allows us to avoid the iteration of equation (46) if $H(\mu)$ has already been computed. Finally, several properties of $J(\tau)$, such as the fact that the exponential integrals ought to appear in an expansion of $J(\tau)$, are much more obvious from equation (40) than from equation (46). We may also note in this connection that the method we have described could be modified more or less along the same

[10] *A.J.U.S.S.R.*, 19, 36, 1942; where H is called ψ.

lines as that indicated in the footnote.[11] We could stop the analysis at formula (33) (or even earlier), deducing from that the form of the exact $q(\tau)$, namely,

$$q(\tau) = \int_0^1 \psi(u)\, e^{-\tau/u} du\,, \tag{46'}$$

and then try to determine $\psi(u)$ by substituting this form for $q(\tau)$ in Milne's equation. This would lead to an alternative proof of a result established earlier by Menzel and Sen.[11]

3. *Exact $\mathfrak{J}(\tau)$-function for the Milne-Eddington model in the theory of line formation.*— We consider a nongray atmosphere and start from Chandrasekhar's n-solution derived in § 84 of *R.T.*; references to equations in this section of *Radiative Transfer* will be prefixed by "*R.T.*"

The notation is Chandrasekhar's, but for brevity the following quantities are introduced and the suffix n is inserted to distinguish the n-solutions:

$$B^{(0)} = a\,; \qquad \frac{\lambda B^{(1)}}{1+\epsilon\eta} = b\,; \qquad \varpi_0 = 1-\lambda\,; \qquad \text{and} \qquad \bar{I} = \frac{1}{2}\int_{-1}^{+1} I\, d\mu\,. \tag{47}$$

From Chandrasekhar's formula equation (eq. *R.T.* [27]) for $I_n(t, \mu_i)$, the following expression for $\bar{I}_n(t)$ is easily derived:

$$\bar{I}_n(t) = \tfrac{1}{2}\Sigma a_i I_n(t, \mu_i) = a + bt + \frac{b}{\varpi_0}\sum_{\alpha=1}^{n} L_\alpha e^{-k_\alpha t}\,, \tag{48}$$

where the k_α's are the positive roots of the characteristic equation (eq. *R.T.* [28]):

$$T_n(\varpi_0, \mu) = 1 - \varpi_0 \mu^2 \sum_{j=1}^{n} \frac{a_j}{\mu^2 - \mu_j^2} = 0\,. \tag{49}$$

From the equation of transfer (eq. *R.T.* [24]) we see immediately that the source function $\mathfrak{J}_n(t)$ in the nth approximation is given by

$$\mathfrak{J}_n(t) = \varpi_0 \bar{I}_n(t) + \lambda(a + bt)\,. \tag{50}$$

Hence, by equation (48) and introducing the further abbreviation

$$l_\alpha = bL_\alpha\,, \tag{51}$$

we have

$$\mathfrak{J}_n(t) = a + bt + \sum_{\alpha=1}^{n} l_\alpha e^{-k_\alpha t}\,. \tag{52}$$

By computing the corresponding $I_n(0, \mu)$, we obtain

$$I_n(0, \mu) = \int_0^\infty \mathfrak{J}_n(t)\, e^{-t/\mu} \frac{dt}{\mu} = a + b\mu + \sum_{\alpha=1}^{n} \frac{l_\alpha}{1 + k_\alpha \mu}\,; \tag{53}$$

and this is precisely Chandrasekhar's expression (eq. *R.T.* [31]).

Now, as in § 2, we note that, according to equation (53), $x_\alpha l_\alpha$ is the residue at $\mu = -x_\alpha = -1/k_\alpha$ of the function $I_n(0, \mu)$. But Chandrasekhar has found that $I_n(0, \mu)$ is given by (cf. eqs. *R.T.* [47] and [64])

$$I_n(0, \mu) = H_n(\varpi_0, \mu)(a + b\mu + bq_n)\sqrt{\lambda}\,, \tag{54}$$

[11] D. Menzel and H. Sen, *Ap. J.*, **110**, 1, 1949; see also I. W. Busbridge, *Ap. J.*, **111**, 654, 1950.

where the exact $H(\varpi_0, \mu)$ satisfies Ambarzumian's integral equation[12]

$$H(\varpi_0,\mu) = 1 + \tfrac{1}{2}\varpi_0\mu H(\varpi_0,\mu)\int_0^1 \frac{H(\varpi_0,\mu')}{\mu+\mu'}\,d\mu'. \tag{55}$$

On the other hand, according to equation *R.T.* (64), q_n is given by

$$q_n = \frac{\varpi_0}{2\sqrt{\lambda}}\sum_{j=1}^{n} a_j\mu_j H_n(\varpi_0, \mu_j). \tag{56}$$

For the same reason as in § 2, we introduce the function $\Phi(\varpi_0, \mu)$, defined by

$$\Phi(\varpi_0, \mu) = -\left[a + b\mu + \sum_{\alpha=1}^{n}\frac{l_\alpha x_\alpha}{\mu + x_\alpha}\right]\frac{e^{t/\mu}}{\mu}. \tag{57}$$

Using equations (53) and (54), we can rewrite this in the form

$$\Phi(\varpi_0, \mu) = -H_n(\varpi_0, \mu)(a + b\mu + bq_n)\frac{e^{t/\mu}}{\mu}\sqrt{\lambda}. \tag{58}$$

As in § 2, we transform this, by means of Chandrasekhar's identity (*R.T.*, p. 114),

$$\frac{1}{H_n(\varpi_0, \mu)\,H_n(\varpi_0, -\mu)} = T_n(\varpi_0, \mu), \tag{59}$$

into

$$\Phi(\varpi_0, \mu) = -\frac{(a + b\mu + bq_n)\,e^{t/\mu}\sqrt{\lambda}}{\mu H_n(\varpi_0, -\mu)\,T_n(\varpi_0, \mu)}. \tag{60}$$

Isolating the point $\mu = 0$ from the rest of the μ-plane, we see from equation (57) that $\Phi(\varpi_0, \mu)$ has no singularity other than the n poles $(-x_1, -x_2, \ldots, -x_n)$, which are known to lie on the real axis between -1 and 0, with the exception of one (say, $-x_n$), which lies to the left of $-\mu_n$ and can be less than -1.

FIG. 2.—The contour of integration C

From equation (57) we easily find that $\Sigma l_\alpha \exp(-k_\alpha l)$ represents the sum of the residues of $\Phi(\varpi_0, \mu)$ at its poles. Hence

$$\Sigma l_\alpha e^{-t/x_\alpha} = \frac{1}{2\pi i}\int_C \Phi(\varpi_0, \mu)\,d\mu, \tag{61}$$

where C represents the contour shown in Figure 2. It starts from $(-\epsilon)$ on the real axis and incloses all the n poles, and it can be deformed into two closed contours γ and Γ (see Fig. 2). By the limiting process, $T_n(\varpi_0, \mu)$ will be transformed into

$$T(\varpi_0, \mu) = 1 - \varpi_0\mu^2\int_0^1 \frac{dz}{\mu^2 - z^2} = \lambda + \varpi_0 T(\mu), \tag{62}$$

where $T(\mu)$ is the function (6) already studied in § 1. Because $T_n(\varpi_0, \mu)$ has $2n$ poles $(\pm\mu_j)$ between -1 and $+1$, we can expect that it will not be possible to define $T(\varpi_0, \mu)$

[12] *Op. cit.*, p. 34.

between -1 and $+1$ as a real integral but that it will have to be defined as a complex integral in the μ-plane cut from -1 to $+1$. On the other hand, the isolated zero, $(-x_n)$ of $T_n(\varpi_0, \mu)$ on the left of $(-\mu_n)$, can be expected to remain as a distinct feature even in $T(\varpi_0, \mu)$. It is, in fact, well known that the equation $T(\varpi_0, \mu) = 0$ has exactly two real roots $\pm x$, one on the left of -1 and the other on the right of $+1$. From equations (62) and (14) we see immediately that the zero $(-x)$ on the left of (-1), which alone interests us, corresponds with the notation of equation (13) to

$$u = x\,, \qquad \mu = -x, \qquad \theta' = \pi\,, \qquad \text{and} \qquad \theta'' = 0\,; \tag{63}$$

this gives us the equation defining x, namely,

$$0 = \lambda + \varpi_0 T(-x) = \lambda + \varpi_0 \left(1 - \tfrac{1}{2} x \log \frac{x+1}{x-1}\right) = 1 - \tfrac{1}{2}\varpi_0 x \log \frac{x+1}{x-1}. \tag{64}$$

A table of $k = 1/x$ as a function of ϖ_0 is given by Chandrasekhar in *R.T.*, page 19.

Since, by the limiting process, equation (61) will introduce a contour integral around $(-x)$ (corresponding to the integral around $-x_n$) and since $T(\varpi_0, \mu)$ will appear in the denominator of $\Phi(\varpi_0, \mu)$, the isolated zero of $T(\varpi_0, \mu)$ will act as an isolated pole of $\Phi(\varpi_0, \mu)$. Hence, applying again the Cauchy residue theorem, this time to the part γ of C around $-x_n \to -x$, we at once find that this part of the integral (61) is simply the residue of $\Phi(\varpi_0, \mu)$ at $\mu = -x$, that is,

$$\frac{(a - bx + bq)\, e^{-\tau/k}\sqrt{\lambda}}{xH(\varpi_0, x)} \times \lim_{\mu \to -x} \frac{\mu + x}{T(\varpi_0, \mu)}. \tag{65}$$

The latter limit, i.e., the residue of $1/T(\varpi_0, \mu)$ at $\mu = -x$, is easy to compute if we use expressions (62) and (14), which, near $\mu = -x$, give

$$T(\varpi_0, \mu) = 1 - \tfrac{1}{2}\varpi_0 u \log \frac{u+1}{u-1} \qquad (\mu \to -u)\,. \tag{66}$$

From equations (64) and (66) it is now easy to find, by expanding near $u = x$, that

$$\lim_{\mu \to -x} \frac{\mu + x}{T(\varpi_0, \mu)} = \left[\frac{1}{\partial T(\varpi_0, \mu)/\partial \mu}\right]_{\mu = -x} = \left(\frac{1}{x} - \frac{\varpi_0 x}{x^2 - 1}\right)^{-1}. \tag{67}$$

Thus the part of the integral representing equation (61) relative to the circle γ around $\mu = -x$ is given by

$$C e^{-\tau/k}\,, \tag{68}$$

where

$$C = \frac{(a - bx + bq)(x^2 - 1)\sqrt{\lambda}}{(x^2\lambda - 1) H(\varpi_0, x)} \tag{69}$$

and q represents the limit of q_n as $n \to \infty$, namely,

$$q = \frac{\varpi_0 a_1}{2\sqrt{\lambda}} = \frac{\varpi_0}{2\sqrt{\lambda}} \int_0^1 H(\varpi_0, \mu)\, \mu\, d\mu\,. \tag{70}$$

In equation (69) $H(\varpi_0, x)$ is not given by the usual tables of the $H(\varpi_0, \mu)$ functions because $x > 1$, but they can easily be computed from Chandrasekhar's formula (*R.T.*, p. 107, eq. [13]),

$$\frac{1}{H(x)} = \tfrac{1}{2}\varpi_0 \int_0^1 \frac{z H(z)}{z + x}\, dz + \sqrt{\lambda}\,. \tag{71}$$

The computation of the part of C inclosing the interval $(-1, -\epsilon)$ of the real axis is entirely similar to the computation described in § 2. As before, $\epsilon \to 0$ as $n \to \infty$, and we find that

$$\frac{1}{2\pi i}\int_\Gamma \Phi(\varpi_0, \mu)\, d\mu \to -\frac{1}{2\pi i}\int_0^1 \frac{(a-bu+bq)\sqrt{\lambda}}{uH(\varpi_0, u)}\left[\frac{1}{T_A(\varpi_0, \mu)} - \frac{1}{T_B(\varpi_0, \mu)}\right] e^{-t/u}\, du\,. \tag{72}$$

Since, by equation (62),

$$T_A(\varpi_0, \mu) = \lambda + \varpi_0 T_A(\mu) \quad \text{and} \quad T_B(\varpi_0, \mu) = \lambda + \varpi_0 T_B(\mu)\,, \tag{73}$$

where $T_A(\mu)$ and $T_B(\mu)$ are given by equations (31) and (32), we have, finally,

$$\mathfrak{J}(t) = a + bt + Ce^{-kt} - \sqrt{\lambda}\,\frac{\varpi_0}{2}\int_0^1 \frac{(a-bu+bq)\, e^{-t/u}}{H(\varpi_0, u)\, Z(\varpi_0, u)}\, du\,, \tag{74}$$

where C is given by equations (69), (70), and (71) and Table XXXIII of *R.T.*, page 328; k is given by Chandrasekhar's table (*R.T.*, p. 19); $H(\varpi_0, u)$ is given by equation (55) or by Table XI of *R.T.*, page 125; and

$$\begin{aligned} Z(\varpi_0, u) &= \left(1 - \tfrac{1}{2}\varpi_0 u \log\frac{1+u}{1-u}\right)^2 + \tfrac{1}{4}\varpi_0^2\pi^2u^2 \\ &= (1 - \varpi_0 u \tanh^{-1} u)^2 + \tfrac{1}{4}\varpi_0^2\pi^2u^2\,. \end{aligned} \tag{75}$$

We may now make the following observations:

(i) The exact solution (74) is also that of an integral equation of Milne's, corresponding to equation (50), namely,

$$\mathfrak{J}(t) = \lambda(a+bt) + \tfrac{1}{2}\varpi_0\int_0^\infty \mathfrak{J}(\tau) E_1(|\tau - t|)\, d\tau\,. \tag{76}$$

(ii) Equation (76) can be rewritten in the form

$$\mathfrak{J}(t) = a\mathfrak{J}_a(t) + b\mathfrak{J}_b(t)\,, \tag{77}$$

were $\mathfrak{J}_a$ and $\mathfrak{J}_b$ are, respectively, the solutions of the more elementary equations:

$$\mathfrak{J}_a(t) = \lambda + \tfrac{1}{2}\varpi_0\int_0^\infty \mathfrak{J}_a(\tau) E_1(|t-\tau|)\, d\tau \tag{78}$$

and

$$\mathfrak{J}_b(t) = \lambda t + \tfrac{1}{2}\varpi_0\int_0^\infty \mathfrak{J}_b(\tau) E_1(|t-\tau|)\, d\tau\,. \tag{79}$$

A treatment of these equations by the method of Laplace transforms shows that

$$\mathfrak{J}_b(t) = \int_0^t \mathfrak{J}_a(x)\, dx + q\mathfrak{J}_a(t)\,, \tag{80}$$

where q is a constant. But it easily follows from equations (78) and (80) that the corresponding "laws of darkening" are given by

$$I_a(0, \mu) = H(\varpi_0, \mu)\sqrt{\lambda} \tag{81}$$

and

$$I_b(0, \mu) = \mu I_a(0, \mu) + q I_a(0, \mu)\,. \tag{82}$$

Hence

$$I(0, \mu) = (a + bq + b\mu)\, H(\varpi_0, \mu)\, \sqrt{\lambda}\,; \tag{83}$$

by comparison with formula (54) for $I_a(0, \mu)$ we see that in this case the "limiting process" has given Chandrasekhar the right result.

By separating the parts of equation (74) respectively proportional to a and to b, we can find the exact solutions of the problems expressed by equations (78) and (79).

From equations (77) and (80) we also have

$$\mathfrak{J}(t) = a\mathfrak{J}_a(t) + b\left[q\,\mathfrak{J}_a(t) + \int_0^t \mathfrak{J}_a(x)\, dx\right]. \tag{84}$$

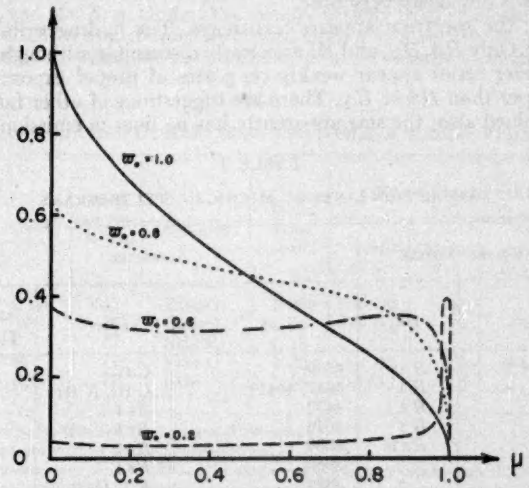

FIG. 3.—The behavior of the function $\varpi_0^{-2} H^{-1}(\varpi_0, \mu)\, Z^{-1}(\varpi_0, \mu)$

By identifying the coefficients of a, we get

$$\mathfrak{J}_a(t) = 1 + C_1 e^{-kt} - \sqrt{\lambda}\,\frac{\varpi_0}{2}\int_0^1 \frac{e^{-t/u}\, du}{H(\varpi_0, u)\, Z(\varpi_0, u)}, \tag{85}$$

where

$$C_1 = \frac{(x^2 - 1)\sqrt{\lambda}}{H(\varpi_0, x)(\lambda x^2 - 1)}. \tag{86}$$

(iii) We have studied the integrand in equations (74) and (85) numerically and we have found that the function $1/[H(\varpi_0, u)\, Z(\varpi_0, u)]$ behaves in a more complicated fashion for values of ϖ_0 which are less than 0.6 than for $\varpi_0 = 1$. Figure 3 gives the variations of this function divided by ϖ_0^2. It shows that the "singularity" at $\mu = 1$ is much "stronger" than that at $\mu = 0$.

It is a pleasure to express my gratitude to Dr. I. W. Busbridge for many valuable suggestions and assistance with the translation of the manuscript.

NOTES

A PECULIAR O STAR AT HIGH GALACTIC LATITUDE*

The star BD+28°4211, $\alpha = 21^h49^m$, $\delta = +28°38'$ (1950), $l = 50°.2$, $b = -19°.9$ (Lund), has an unusual spectrum on objective-prism plates taken with the Burrell Schmidt telescope of the Warner and Swasey Observatory. The change of intensity of the continuous spectrum from the ultraviolet (3600 A) to the sensitivity limit of the II*a*-O plate (5000 A) is very gradual. The maximum intensity is in the neighborhood of 4100 A. The star is obviously very blue.

At first sight, the spectrum appears featureless. The hydrogen lines are extremely weak and diffuse. Only *Hβ*, *Hγ*, and *Hδ* are clearly discernible, although some later members of the Balmer series appear weakly on plates of proper exposure. *He* II 4686 is visible and sharper than *Hβ* or *Hγ*. There are suggestions of other faint lines. The *Hα* region was examined also; the star apparently has no lines in emission.

TABLE 1

ABSORPTION LINES ON MICHIGAN SPECTROGRAMS

Clearly Visible		Suspected		
λ	Ion	λ	Ion	No. of Plates*
4861	*H* I	4659	*C* IV	2
4340	*H* I	4647, 4641†	*C* III, *N* III	2
4101	*H* I	4472	*He* I	2
3970	*H* I	4026	*He* I	2
4686	*He* II	4009	*He* I	2
		3965	*He* I	1
		3889	*H* I, *He* I	1
		4089, 4116	*Si* IV	1
		4481	Mg II	2

* The total number of good plates is four.
† These lines appear as a blend.

Slit spectra of higher dispersion have been obtained with the 37.5-inch telescope and two-prism spectrograph of the University of Michigan at Ann Arbor through the kind co-operation of Dr. Dean B. McLaughlin. On these plates the extreme blueness of the continuous spectrum is at once evident when the plates are compared with other O stars. The left-hand part of Table 1 lists the lines which are clearly visible on all four spectrograms of good quality, while the right-hand part gives those which are suspected on several of the plates. The λ 4686 line of *He* II is the strongest and sharpest feature in the spectrum with this dispersion, and it is stronger in this star than in 10 Lacertae (O9 V). However, λ 4541 of *He* II is not observed. The hydrogen lines are very shallow and wide, but the wings are not so extensive, nor are the central intensities so great, as those in the white dwarf o^2 Eridani. On some of the plates of BD+28°4211, structure is suspected in *Hβ* and *Hγ*. On a panchromatic plate, which was somewhat weakly exposed except in the

* This star was found during the course of a study supported in part by grant No. 1121 from the Penrose Fund of the American Philosophical Society.

photographic region, *Ha* appears as a faint, but fairly sharp, absorption line, although the dispersion in this region is low (355 A/mm).

The slit spectrograms have been measured for radial velocity, but the results, presented in Table 2, are not very accordant. To what extent the observed velocity differences represent real stellar phenomena is difficult to say.

Through the kindness of the late Dr. Frank S. Hogg, four spectrograms of BD+28°4211 were secured at the David Dunlap Observatory during the summer of 1950. The one-prism spectrograph with the 12-inch camera gives a dispersion of 66 A/mm at $H\gamma$. Dr. Hogg gave us permission to quote his description of the spectrum and the David Dunlap Observatory radial-velocity measures as follows:

> The lines are few, and very poorly defined. *He* II 4686 is the strongest line. The hydrogen lines are broad and shallow and possibly complex. A few early-type lines are probably present but are too poor for velocity measurement. The plates have been measured by Dr. J. F. Heard, Miss Ruth J. Northcott, and Mr. A. A. Griffin. The average velocity from all measures (*H* and *He* II) is −03 ± 8 km/sec. The measures from *He* II 4686 alone give a velocity of +26 ± 6 km/sec. These few measures do not eliminate the possibility that the velocity is variable.

TABLE 2

JOURNAL OF MICHIGAN OBSERVATIONS AND TABLE OF RADIAL VELOCITIES

Date (U.T.)	Obs.*	Disp. at $H\gamma$ (A/mm)	Emulsion	Total Exposure	Radial Velocity (Km/sec)				Remarks§
					4686 *He* II†	Mean *H* I‡	4659 *C* IV	4481 *Mg* II	
1949 Oct. 27.1...	C,W	142	103*a*-O	1h20m	+ 29	−13	.....	.....	
1949 Oct. 28.0...	M	77	103*a*-O	4 06	+ 31	−34	−96	+42	Haze
1950 July 22.3...	C	77	103*a*-F3	4 18	.....	.....	.....	.....	1
1950 July 23.2...	W	77	103*a*-O	4 20	− 13	− 1	+45	−81	2
1950 July 25.3...	C,W	77	103*a*-F	5 56	+112	− 5	.....	.....	3

* C, Donald H. Clements; M, Miss Marilyn J. Mears; W, Weston.

† λ 4686 is the strongest and sharpest feature in the spectrum.

‡ The lines $H\gamma$ and $H\delta$ were given weight 2; $H\beta$ and *He* weight 1. The hydrogen lines are very shallow and wide.

§ 1, underexposed; 2, scattered clouds; 3, correctly exposed for the photographic region; remainder of plate weak.

There is thus general agreement in the means of the radial-velocity measurements from the two observatories if the one very large measure of λ 4686 is excluded. The effect of solar motion should amount to about −13 km/sec. Taken as a whole, the star does not give evidence in this component of being a high-velocity star. No information on its proper motion is available.

Dr. W. W. Morgan has obtained spectrograms at the Yerkes Observatory of BD+28°4211 and another star in the same part of the sky. He has generously prepared the following paragraphs for inclusion in this note:

> The spectrum of BD+28°4211 resembles that of no other star in the Yerkes files. The type is probably Op; the spectrum contains faint, rather broad, lines of hydrogen and a strong line near λ 4686 which appears to be due to *He* II. No other lines are seen with certainty on low-dispersion plates between 3900 A and 4900 A; in particular, the other *He* II lines must be far weaker than λ 4686.
>
> The near-by star BD+28°4177 makes an interesting comparison possible; it has about the same apparent photographic magnitude and a spectral type of B0.5 III; this corresponds to an absolute photographic magnitude of around −4.7 and an apparent distance modulus of about 14.6. Since there is no appreciable absorption due to the interstellar band near λ 4430, it is unlikely that the total amount of interstellar absorption in the light-path is greater than 1 mag.; the true distance modulus is therefore near 13.5, and the distance of BD+28°4177 is approximately 5 kiloparsecs.

Now, if BD+28°4211 were as bright as a main-sequence O star, its photographic absolute magnitude and distance would be similar to those of BD+28°4177; and, since the stars are located in the same region of the sky, the light-paths can be assumed to be similar. In spite of these considerations, however, we find that, while there is a strong interstellar K line in BD+28°4177, none can be seen on low-dispersion plates in BD+28°4211. This indicates rather definitely that BD+28°4211 is very much nearer than 5 kiloparsecs and that it is a subluminous O star.

The star 16 Pegasi is only 3° distant at galactic latitude −22°. Published spectroscopic parallaxes of 16 Pegasi place it only 200 parsecs away. Although interstellar H and K lines of *Ca* II are visible on Michigan plates of 16 Pegasi, no interstellar lines can be seen on the Michigan spectrograms of BD+28°4211 with similar contrast and dispersion. Dr. Morgan's conclusions as to the probable distance and luminosity of this star are therefore strengthened.

The apparent photographic magnitude of BD+28°4211 is 9.93 ± 0.06. Its color index on the International System is −0.53. Photometric studies of faint B and A stars surrounding this star made at the Warner and Swasey Observatory show that the absorption in this direction corresponds to a maximum color excess of 0.15 mag., which is reached at a distance of 800 parsecs. We should expect the interstellar reddening and absorption to be small in a region with this galactic longitude and latitude. If we adopt the figure quoted above, the star must be intrinsically at least as blue as −0.65 mag. on the International scale of color. One should be cautious in adopting these figures, however, inasmuch as the International color system is not defined for stars as blue as this; the stars in the North Polar Sequence are all redder than −0.2 mag. More revealing information is given by comparison of the color of BD+28°4211 with the colors of other very blue stars when all are measured in the same color system. Dr. Harris reports on photoelectric observations of this nature in a following note in this issue of the *Journal*.

The available information on this star calls to mind other very blue objects of similar nature, but none appears to be identical. In spectrum and color it is not a typical white dwarf. Its spectrum differs in many respects from that of a typical O star. We seem to be closer to the truth when we assume that the star is a subdwarf, perhaps lying in the blue extension of Baade's population II.[1] Its position at a moderate distance (of the order of 250 parsecs) from the galactic plane can then be reasonably explained. The intensities of the *He* II lines λ 4686 and λ 4541 appear to be quite different in the O8 star reported by Popper[2] in the globular cluster M 3. Perhaps it is more nearly similar to the nuclei of certain planetaries, such as NGC 246, which Aller has suggested are also members of the same population group.[3] A careful examination of long-exposure Schmidt plates does not reveal any nebulosity associated with the star. Some of the stars listed by Humason and Zwicky[4] and perhaps HD 124448, noted by Popper,[5] may be related to BD+28°4211.

The authors wish to thank their colleagues at their own and other institutions for the interest they have shown in this unusual star.

DONALD A. MACRAE
ROBERT FLEISCHER
EDWIN B. WESTON

CASE INSTITUTE OF TECHNOLOGY, EAST CLEVELAND, OHIO
RENSSELAER POLYTECHNIC INSTITUTE, TROY, NEW YORK
UNIVERSITY OF MICHIGAN, ANN ARBOR, MICHIGAN
December 4, 1950

[1] *Mt. W. Contr.*, No. 696; *Ap. J.*, **100**, 137, 1944.
[2] *McDonald Obs. Contr.*, No. 131; *Ap. J.*, **105**, 204, 1947.
[3] *Pub. Goethe Link Obs.*, No. 1; *Ap.J.* **108**, 462, 1948.
[4] *Mt. W. Contr.*, No. 724; *Ap. J.*, **105**, 85, 1947.
[5] *Pub. A.S.P.*, **59**, 320, 1947.

THE COLOR OF BD+28°4211

The peculiar O-type star, BD+28°4211, described in the previous note in this issue of the *Journal*,[1] was observed by Dr. Kuiper and the writer with the photoelectric photometer attached to the 82-inch McDonald reflector. The first observations, obtained while determining a magnitude sequence in the surrounding region, indicated that the star was abnormally blue, and it was decided to compare its color directly with the star HD 14633. The latter star has a C_1 color of -0.30 mag.[2] and a V−I color of -2.55 mag.,[3] being the bluest star observed in either list. Recently Johnson[4] has published its color on the International System, $CI = -0.46$ mag. and at the same time found τ Canis Majoris to be 0.02 mag. bluer.

The observations at the McDonald Observatory were made with a 1P21 cell behind a blue (C 5850) and a yellow (C 3385) filter. The scale of the resulting color, C, derived from a comparison with stars whose CI range is from 0.0 to 1.0, was found to be equal to $CI/0.74$. The observed difference in color between the star under examination and the comparison star, corrected for extinction, was found to be

$$\Delta C = C\,(\text{BD}+28°4211) - C\,(\text{HD } 14633) = -0^{m}.21,$$

or, expressing the result on the CI scale,

$$\Delta CI = -0^{m}.16.$$

Adopting Johnson's color for HD 14633, the CI color of BD+28°4211 becomes -0.62 mag. This reduction to CI is justified only to the extent that one can consider a color extrapolated 0.6 mag. beyond the range defined by the NPS as still being on the International System.

Schilt and Jackson,[5] using similar filters, have listed several stars that appear to be nearly as blue as this. Four of their stars, which appear to be at least a tenth of a magnitude bluer than τ Canis Majoris on the CI scale, are BS Nos. 2222, 3165, 4199, and 4730. The second star is the bright O5f star, ζ Puppis, while the first is a fifth-magnitude B2 star with an observed C_1 color of -0.27 mag.

All these stars with large negative color indices undoubtedly deviate from black bodies in the sense that they have ultraviolet excesses that affect the measures through the "blue" filter. Gascoigne's[6] discussion of the Mount Stromlo and Greenwich gradients appears to confirm this; their bluest O-type stars have definitely redder gradients than those observed for the unreddened B0–B2 stars. Therefore, it is possible that colors obtained for these stars from the yellow and blue regions of the spectrum (as opposed to the yellow and near-ultraviolet regions) would not be abnormally blue. Until the question of the colors of these stars is settled, any conclusions regarding intrinsic colors and derived total interstellar absorptions must be considered as uncertain.

DANIEL L. HARRIS III

WARNER AND SWASEY OBSERVATORY
CASE INSTITUTE OF TECHNOLOGY
EAST CLEVELAND, OHIO
December 4, 1950

[1] MacRae, Fleischer, and Weston, *Ap. J.*, **113**, 432, 1951.
[2] Stebbins, Huffer, and Whitford, *Ap. J.*, **91**, 20, 1940.
[3] Stebbins and Whitford, *Ap. J.*, **102**, 318, 1945.
[4] *Ap. J.*, **112**, 240, 1950. [5] *A.J.*, **55**, 9, 1949. [6] *M.N.*, **110**, 15, 1950.

LINES OF NEUTRAL OXYGEN IN THE INFRARED SPECTRA OF Be STARS*

Anomalies in the behavior of the *O* I lines at λ 7774 and λ 8446 in the spectra of Be stars have been pointed out by Merrill,[1] Swings,[2] Hiltner,[3] and, most recently, Keenan and Hynek.[4] As a result of the latter investigation, it was thought desirable to investigate these anomalies for a number of the brighter Be stars.

Spectrograms of twenty-five Be stars brighter than magnitude 5.3 were obtained with the two-prism spectrograph attached to the 69-inch reflector of the Perkins Observatory, giving a dispersion of about 250 A/mm at λ 7700. At this dispersion, the three lines at λλ 7771.90, 7774.18, and 7775.40, arising from the $3^5S^\circ - 3^5P$ transition, are blended into

TABLE 1

LIST OF OBSERVATIONS

Star	Date of Spectrogram	*O* I 7774*	*O* I 8446*	*Hα**	*Hβ**	Remarks
o Cas	Jan. 9, 1950	A	O	E	A	
γ Cas	Dec. 3, 1949	O	O	EE	E	Paschen emission
φ Per	Dec. 3, 1949	E	EEE	EEE	E	Paschen emission, *Ca* II emission
HD 20336	Dec. 8, 1949	O	E	EE	E	
ψ Per	Dec. 8, 1949	O	EEE	EEE	E	*Ca* II emission
17 Tau	Dec. 30, 1949	A	O	AA	A	
23 Tau	Dec. 30, 1949	O	(E)	EE	A	Weak double emission at *Hβ*
28 Tau	Dec. 3, 1949	AA	A	EE	A	Very weak double emission at *Hβ*
48 Per	Jan. 8, 1950	O	E	EE	E	*Ca* II emission
11 Cam	Jan. 17, 1950	O	E	EE	E	Paschen emission
25 Ori	Feb. 21, 1950	O	O	AA	A	
ζ Tau	Dec. 3, 1949	AA	EE	EE	A	Very weak double emission at *Hβ*
ω Ori	Jan. 8, 1950	O	O	E	A	Weak double emission at *Hβ*
HD 41335	Jan. 9, 1950	E	EE	EE	E	Paschen emission, *Ca* II emission
17 Lep	Jan. 17, 1950	AA	O	E	A	
β Mon A	Dec. 1, 1949	O	EEE	EEE	E	Paschen emission, *Ca* II emission
14 Com	Apr. 17, 1950	A	(A)	AAA	A	
κ Dra	Apr. 17, 1950	E	EE	EE	E	Paschen emission, *Ca* II emission
θ CrB	Apr. 27, 1950	A	A	AAA	A	
48 Lib	June 6, 1950	AAA	A	EE	A	Weak double emission at *Hβ*
χ Oph	June 13, 1950	x	EEE	EEE	E	Paschen emission
P Cyg	Aug. 5, 1950	AA	EEE	EEE	E	
HD 217050	Nov. 24, 1949	AA	EEE	EEE	E	*Ca* II emission
o And	Dec. 30, 1949	AAA	A	A	A	
β Psc	Jan. 9, 1950	O	(E)	EE	E	

* The letters in these columns have the following meanings: A, absorption; E, emission; O, not visible; x, plate overexposed. *Hβ* symbols do not designate intensities but only whether the line is essentially in emission or absorption.

one line, as are also the lines at λ 8446.35 and λ 8446.76, which arise from the $3^3S^\circ - 3^3P$ transition. Table 1 lists the characteristics of the *O* I lines in the stars investigated.

Figure 1 illustrates the behavior of the oxygen lines in the spectra of five of the more interesting Be stars, all of them being absorption shell stars. It will be seen that both lines are in emission in φ Persei; both are in absorption in 48 Librae and 28 Tauri

* This and the following note are *Contributions from the Perkins Observatory*, No. 29.

[1] *Mt. W. Contr.*, No. 486; *Ap. J.*, **79**, 183, 1934.

[2] *Pub. A.S.P.*, **56**, 238, 1944.

[3] *Ap. J.*, **105**, 212, 1947.

[4] *Ap. J.*, **111**, 1, 1950.

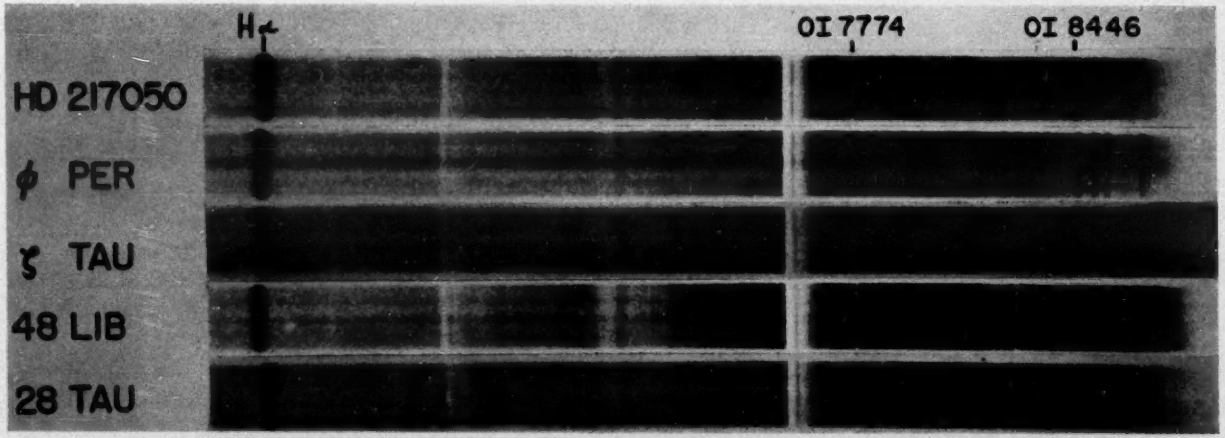

FIG. 1.—The behavior of the infrared *O* I lines in the spectra of five of the more interesting Be stars

(Pleione); and λ 7774 is in absorption, while λ 8446 is in emission, in HD 217050 and ζ Tauri. The spectrograms illustrate the well-known tendency of λ 8446 to go into emission more readily than λ 7774. This has been explained by Bowen[5] as a resonance phenomenon. The *O* I transition $2^3P_2-3^3D^\circ$ gives rise to a line of wave length 1025.766 A, while Lyman-β is of wave length 1025.717 A. Whenever Lyman-β is in emission, the 3^3D° state of *O* I will thus become overpopulated, and subsequent cascading will lead to λ 8446 emission. If this mechanism is correct, a correlation between Balmer and λ 8446 emission should exist, and this is, in fact, observed. The best correlation is perhaps that of *Hβ* and λ 8446 emission. The majority of the stars investigated also show strong *Hα* emission when λ 8446 is strong in emission. Exceptions to the latter are 28 Tauri, as was pointed out by Hiltner,[3] and 48 Librae, both of which have *Hα* fairly strong in emission with λ 8446 in absorption; in both, however, *Hβ* is mainly an absorption line. The most reasonable explanation seems to be that given by Keenan and Hynek:[4] that the Lyman series is behaving similarly to the Balmer series, without strong emission in Lyman-β.

The behavior of λ 7774 in Be stars is a partial result of the metastability of its lower level. It should be relatively stronger in absorption in the shell stars, in which the equatorial ring of gas lies between the star and the observer, than in the "pole-on"[6] stars, in which the axis of rotation is approximately directed toward the observer. Of four pole-on stars investigated, λ 7774 is an emission line in two and is not visible in the remaining two. As Figure 1 illustrates, however, the shell stars do not all follow the expected behavior. It is true that λ 7774 is a very strong absorption line in certain shell stars, such as 28 Tauri, 48 Librae, ζ Tauri, and HD 217050—stronger, in fact, than in the B5 supergiant, 67 Ophiuchi. This must be due to the metastability of the line, since all four of these stars have well-developed absorption-shell spectra. On the other hand, λ 7774 is not visible in β Monocerotis A and ψ Persei and is an emission line in φ Persei.[7] The absorption-shell spectra of these stars are not so well developed as are those of the afore-mentioned four, so that one might conclude that a large shell relative to the size of the star is involved, the line being filled in with emission from those areas of the shell which are not projected in front of the star. This picture appears to be too simple, however, since the hydrogen emission should be more pronounced in the stars with larger shells and the observations do not bear this out.

ARNE SLETTEBAK

PERKINS OBSERVATORY
December 1, 1950

LINES OF NEUTRAL OXYGEN IN THE INFRARED SPECTRA OF PECULIAR A STARS

In the course of an investigation of the behavior of the infrared *O* I lines in stellar atmospheres by Keenan and Hynek,[1] it was noticed by these investigators and by A. J. Deutsch that these lines are very weak or absent in the spectra of several of the brighter peculiar A stars. In an effort to establish whether or not this weakness is characteristic of the peculiar A stars in general, spectrograms of twenty stars of this class were obtained with the 69-inch telescope of the Perkins Observatory. The grating spectrograph, giving a scale of about 48 A/mm, was used for a few of the brighter stars; the remaining spectrograms were taken with the two-prism spectrograph, giving a scale of about 250 A/mm at λ 7700.

[5] *Pub. A.S.P.*, **59**, 196, 1947. [6] *Ap. J.*, **110**, 498, 1949.

[7] Spectrograms of φ Persei taken by J. A. Hynek on November 22, 1950, show very sharp and deep hydrogen absorption cores, indicating a thicker shell in front of the star. At this phase, the emission characteristics of the *O* I 7774 line illustrated in Fig. 1 disappear: the line appears to be mainly in absorption.

[1] *Ap. J.*, **111**, 1, 1950.

Figure 1 illustrates the anomalous weakness of the *O* I lines at λ 7774 and λ 8446 in the spectra of three of the brighter peculiar A stars, with the standard A5 main-sequence star, β Arietis, shown for comparison, all taken with the grating spectrograph. Of the few stars which could be obtained on the higher dispersion, all show both oxygen lines to be weak or absent. These spectrograms also suggest a weakening of the nitrogen lines between P12 and P13, but this observation is uncertain because of the intrinsic weakness of these lines in stars near the main sequence. A series of spectrograms of the spectrum variable α Andromedae was taken to determine whether any variation in the strength of the oxygen lines exists; no variation was detected.

While the prism spectrograms obtained are of insufficient dispersion to give much information about the λ 8446 line of *O* I, the λ 7774 line can be studied. Table 1 lists

TABLE 1

LIST OF OBSERVATIONS—PRISM SPECTROGRAMS

Star	Spectral Type	Peculiar Features*	Intensity of *O* I 7774	Remarks*
α And	B9p	*Mn*, λ 4137	2	Spectrum variable
γ Ari S	A0p	*Cr*, *Eu*, *Si*	0	Spectrum variable
ι Cas	A5p	*Sr*, *Cr*	0	Spectrum variable
56 Tau	A0p	*Si*	1	
17 Com	A2p	*Cr*, *Eu*	2	Spectrum variable
21 Com	A3p	*Sr*, *Cr*	0	Spectrum variable
ε UMa	A0p	*Cr*, *Eu*	0	Spectrum variable
α^2 CVn	A0p	*Si*, *Cr*, *Eu*	0	Spectrum variable
78 Vir	A2p	*Sr*, *Cr*, *Eu*	0	Spectrum variable
81 UMa	A0p	*Si*	2	
84 UMa	A0p	*Sr*, *Si*	0	
α Dra	A0p	*Si*	2	
HD 124224	A0p	*Si*	1	
π Boo A	A0	*Mn*, λ 4137	3	Spectrum variable
β CrB	F0p	*Cr*, *Eu*	0	
χ Ser	A0p	*Sr*, *Cr*	1	Spectrum variable
45 Her	A0p	*Cr*	2	Spectrum variable
21 Aql	B8	*He*	3	Spectrum variable
κ Psc	A2p	*Sr*	0	

* Spectrum variables and their peculiar features from Deutsch's "First Catalogue of Spectrum Variables," *Ap. J.*, **105**, 298, 1947.

approximate intensities of this line as estimated from prism spectrograms of nineteen stars. Since, according to Deutsch,[2] the peculiar A stars lie slightly above the main sequence, intensity comparisons were made with class IV standard stars on the Morgan-Keenan-Kellman system[3] when possible. Intensity 3 in the table corresponds to the normal intensity of λ 7774 in the spectrum of the appropriate standard star used for the comparison. It will be seen that *O* I 7774 appears to be weak or absent in all but two of the peculiar A stars considered. No explanation for this anomalous weakness exists at present.

I am indebted to Dr. J. A. Hynek for permission to reproduce the spectrogram of β Arietis shown in Figure 1.

ARNE SLETTEBAK

PERKINS OBSERVATORY
December 1, 1950

[2] *Ap. J.*, **105**, 283, 1947.

[3] *An Atlas of Stellar Spectra* (Chicago: University of Chicago Press, 1943).

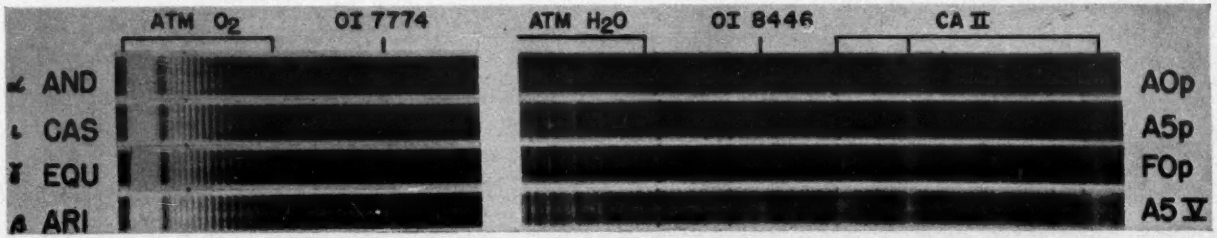

FIG. 1.—The anomalous weakness of the infrared *O* I lines in the spectra of three bright peculiar A stars. The main-sequence standard A5 star, β Arietis, is shown for comparison.

ZETA AURIGAE: PHOTOELECTRIC OBSERVATIONS OF THE PARTIAL PHASE AT EGRESS ON SEPTEMBER 20, 1950

Photoelectric magnitude observations of ζ Aurigae during the recent eclipse were carried out with the pulse-counting photoelectric photometer attached to the 15-inch Huggins refractor of the Cambridge Observatories. Measurements were made alternately with the filters Wratten 5 (Y) and Wratten 39 (B), which, combined with the sensitivity of the 931A multiplier tube, give results near to the International photovisual and photographic scales, respectively. (A description of instrument and method has been given by Yates in *M.N.*, **108**, 476, 1948.)

The stars ρ Aurigae, λ Aurigae, and BD $+40°1240$ were used as comparison stars. Most individual observations are the means, reduced to λ Aurigae as standard, of comparisons with each of two comparison stars, with the exception of the night of September 20, when only λ Aurigae was used. The 54 observations are distributed as follows: August 10–11, 1950: 2 B, 2 Y; August 13–14: 3 Y; September 12–13: 6 B, 9 Y; September 19–20: 6 B, 5 Y; October 5–6: 5 B, 4 Y; and October 13–14: 6 B, 6 Y.

The combination of the first, fifth, and sixth group determined the total light of the system, giving for the mean magnitude difference ($\zeta - \lambda$) Aurigae in the blue -0.25 mag. (2), and in the yellow -0.86 mag. (1). The second and the third sets, obtained during total eclipse, give for ($\zeta - \lambda$) $+0.64$ mag. (1) in B and -0.73 mag. ($\frac{1}{2}$) in Y. The partial phase is represented by the observations on the fourth date, which give $+0.47$ mag. (2) in B and -0.75 mag. (3) in Y. The bracketed figures are quotients of mean deviations, expressed in 0.01 mag., by the square root of the number of observations.

The above observations of the partial phase were obtained during 40 minutes of clear sky in an otherwise completely cloudy and rainy night. The mean observing epoch was September 20.113, 1950 (JD. 2433544.613). The observations did not show a systematic trend during the short interval.

These results demonstrate that on September 20.113, 1950, the system of ζ Aurigae had reached, in blue, 19 per cent of its total light (0.89 mag. = 1.0). The less accurate yellow values give 15 per cent (0.13 mag. = 1.0) in confirmation.

The calculation of the phases for this egress was based on the combination of recent sets of elements: Pettit's revision (*Pub. A.S.P.*, **60**, 102, 1948) of Christie's elements (*Ap. J.*, **92**, 394, 1940) sets the beginning of the 1947 eclipse at JD 2432533.65 (period 972.07, duration of totality 36.80, and duration of the whole eclipse 39.50 days). Kron (see Welsh, *J.R.A.S. Canada*, **43**, 222, 1949) gives the mid-eclipse in 1947–1948 at JD 2432553.5; with Pettit's above data, this leads to JD 2432533.75 for the beginning of the eclipse. Adopting the mean, JD 2432533.70, the prediction of the 1950 eclipse becomes: beginning and end of the partial phase JD 2433543.92 (September 19.42, 1950) and JD 2433545.27 (September 20.77, 1950) respectively.

This prediction thus sets the epoch of the Cambridge observations as 0.51 of the partial phase, while the observed magnitudes indicate an epoch of 0.19 (assuming an approximately linear increase of magnitude; see Kopal's curve in *Ap. J.*, **103**, 315, 1946). It therefore appears that the egress partial phase took place about 0.32 of its duration, i.e., *0.43 day later* than predicted.

This interesting behavior should be compared with the observations both by Pettit and by Kron during the ingress partial phase of the 1947–1948 eclipse, which were the basis of the above prediction. Using four-color photometry and comparing with Christie's 1939 elements, Pettit (*loc. cit.*) then found "indications that the eclipse occurred about *half a day early*," a conclusion confirmed by Kron's observations (*loc. cit.*).

Prediction from Christie's original elements, but with the mean of Christie and Roach (see Kopal, *op. cit.*, p. 312) for the epoch of mid-primary minimum, sets the Cambridge observation to an epoch corresponding to an eclipse only 0.14 day early, a difference near to the limit of observational accuracy. The indications, therefore, are that the 1947 eclipse was anomalous.

ARTHUR BEER
MICHAEL W. OVENDEN

THE OBSERVATORIES,
CAMBRIDGE UNIVERSITY, ENGLAND
October 19, 1950

CALCULATED TRANSITION PROBABILITIES FOR THE C_2 SWAN BANDS

In a recent note[1] in this *Journal*, Tawde and Patel pointed out differences between the transition probabilities calculated by them for bands of the Swan system of C_2 and values previously computed by McKellar and Buscombe.[2] The note may have left the impression that the differences could not be readily reconciled. We are glad, in the present brief communication, to be able to clear up completely the apparent discrepancies. On checking over both sets of calculations, three points have come to light:

1. A numerical error in McKellar and Buscombe's calculations for the 2, 0 band requires that the transition probability be changed from 0.034 to 0.067.

2. A similar error by Tawde and Patel requires their value for the 5, 4 band to be changed from 0.554 to 0.233.

3. The remaining differences are not large, and calculation shows that they are completely accounted for by the different values of Δr_e used by the two sets of authors (Δr_e is the difference in equilibrium internuclear distance for the upper and lower vibrational states concerned). Tawde and Patel used $\Delta r_e = 0.046$ A, while McKellar and Buscombe used 0.047 A. The latest laboratory data by Phillips[3] favor the former value.

Therefore, with the two changes given in 1 and 2 above, both the values of McKellar and Buscombe and of Patel, as shown in Table 1 of the note[1] by Tawde and Patel, may be taken as substantially correct, it being borne in mind that the one column is calculated for $\Delta r_e = 0.047$ and the other for $\Delta r_e = 0.046$ A. Incidentally, the differences remaining between the two sets of figures then serve to illustrate the considerable sensitivity of the calculated transition probabilities to the quantity Δr_e.

One of us (N. R. T.) wishes to thank Mr. B. B. Laud for checking his calculations.

ANDREW MCKELLAR
N. R. TAWDE

DOMINION ASTROPHYSICAL OBSERVATORY
VICTORIA, B.C.
AND
INSTITUTE OF SCIENCE
BOMBAY, INDIA
October 28, 1950

[1] *Ap. J.*, **112**, 210, 1950.

[2] *Pub. Dom. Ap. Obs. Victoria*, **7**, 361, 1948.

[3] *Ap. J.*, **108**, 434, 1948.

FILMS

AL JOURNAL

...ciences may now ...ble roll of positive ...ameled metal ...approximately one-...ge frame, which is ...ding preserving ...ge survey binding. ...ed to those sub-...ation, and the ...distributed only ...ecember year, after ...December issue.

...ld be addressed to

...OFILMS

...ange, mass.

POP

ASTRO

A ...

fifty-ninth ...

to the ...

of Astron...

sciences.

Publishe...

...sept. July ...

Yearly sub...

Domestic ...

$4.25; For...

dollars).

...

POPULAR ...

...

NORTHFIELD, ...

THE OBSERVATORY

FOUNDED 1877

* * *

...presenting current developments in Astron... ...

...correspondence. Notes on discoveries and ... ...

...scientific books. The papers read at the Meet... ...

...ety of the Royal Astronomical Society are ...

...also fully reported.

* * *

...subscription for 6 issues, post free, ...

should be sent to

... Editors, ROYAL OBSERVATO...

Greenwich, London S.E., 10

ASTROPHYSICAL MONOGRAPHS

Sponsored by the Editors of the Astrophysical Journal

PRINCIPLES OF STELLAR DYNAMICS

By S. CHANDRASEKHAR

"In this monograph the dynamical methods of investigating the ... motions, and star clusters are developed from A ... [illegible] should exert a profound influence on the future ... galactic dynamics. I can recommend its study unreservedly ... and to those who already have a passing acquaintance with ... can profit from reading it."—Bertil J. Bok, in *Science* ...

SPECTRA OF LONG-PERIOD VARIABLE STARS

By PAUL W. MERRILL

"This monograph is devoted largely to the observational side ... discussion of the physical significance of various spectral ... introduction and a historical chapter are inserted for the ... are a specialist in stellar spectra. . . . For one desiring an ... knowledge of the spectra of long-period variable stars, ... astronomer, physicist, or chemist, this present monograph ... Miller in *Astronomical Society of the Pacific* ... Peter ...

THE MASSES OF THE STARS. WITH ... CATALOGUE OF DYNAMICAL P...

By HENRY NORRIS RUSSELL and CHARLOTTE E. ...

"Astrophysicists will be grateful to the ... authors for an ... of available knowledge. . . . We may be permitted to congratulate ... on this magnificent outgrowth from an idea which ... years ago."—Frederick A. S. Emmerson, *The Observatory* ...

THE DISTRIBUTION OF THE ST...

By BART J. BOK

"... an extremely important contribution to the field of ... to both students and research workers in the field ... and variety of researches carried out in this field ... and discussed critically in this study with clarity and ...

THE UNIVERSITY OF CHICAGO ...